PB81-152324

REPORT NO.
UCB/EERC-80/39
OCTOBER 1980

EARTHQUAKE ENGINEERING RESEARCH CENTER

DYNAMIC RESPONSE OF EMBANKMENT CONCRETE-GRAVITY AND ARCH DAMS INCLUDING HYDRODYNAMIC INTERACTION

by
JOHN F. HALL
ANIL K. CHOPRA

A Report on Research Conducted under
Grants ATA74-20554 and ENV76-80073
from the National Science Foundation.

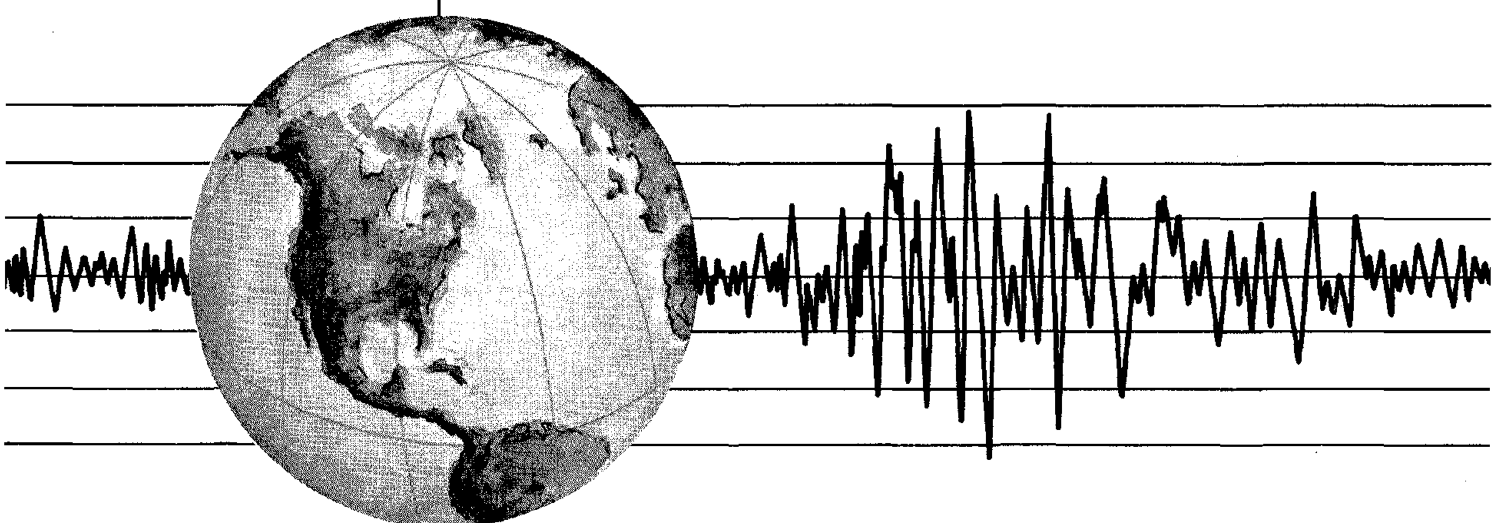

COLLEGE OF ENGINEERING
UNIVERSITY OF CALIFORNIA · Berkeley, California

REPRODUCED BY
NATIONAL TECHNICAL
INFORMATION SERVICE
U.S. DEPARTMENT OF COMMERCE
SPRINGFIELD, VA 22161

DISCLAIMER

Any opinions, findings, and conclusions or recommendations expressed in this publication are those of the authors and do not necessarily reflect the views of the National Science Foundation or the Earthquake Engineering Research Center, University of California, Berkeley.

For sale by the National Technical Information Service, U.S. Department of Commerce, Springfield, Virginia 22161.

See back of report for up to date listing of EERC reports.

50272-101

REPORT DOCUMENTATION PAGE

1. REPORT NO. NSF/RA-80 0298

2.

3. Recipient's Accession No. PB81 152324

4. Title and Subtitle
Dynamic Response of Embankment Concrete-Gravity and Arch Dams Including Hydrodynamic Interaction

5. Report Date
October, 1980

6.

7. Author(s)
John F. Hall and Anil K. Chopra

8. Performing Organization Rept. No.
UCB/EERC-80/39

9. Performing Organization Name and Address
Earthquake Engineering Research Center
University of California, Berkeley
Richmond Field Station
47th Street & Hoffman Boulevard
Richmond, Calif. 94804

10. Project/Task/Work Unit No.

11. Contract(C) or Grant(G) No.
(C)
(G)

12. Sponsoring Organization Name and Address
National Science Foundation
1800 G. Street, N.W.
Washington, D.C. 20550

13. Type of Report & Period Covered

14.

15. Supplementary Notes

16. Abstract (Limit: 200 words)
An analysis procedure in the frequency domain is developed for determining the earthquake response of a dam including hydrodynamic interaction and water compressibility effects. Linear responses of idealized, two-dimensional gravity dams and three-dimensional dams, including arch dams, can be obtained. The dam and fluid domain are treated as substructures and modeled with finite elements. The only geometric restriction is that an infinite fluid domain must maintain a uniform cross-section beyond some point in the upstream direction. For such an infinite uniform region, a finite element discretization within the cross-section combined with a continuum representation in the infinite direction provides for a proper transmission of pressure waves. The fluid domain model approximately accounts for fluid-foundation interaction through a damping boundary condition applied along the reservoir floor and sides. The dam foundation is assumed rigid.

Hydrodynamic effects are shown to be equivalent to an added mass and added load in the frequency domain equations of motion of the dam.

Hydrodynamic effects on the dam response are investigated for acceleration responses to harmonic ground motions. Complex frequency response functions for acceleration at the dam crest are presented for two-dimensional concrete gravity and earth dams and for a three-dimensional arch dam. Several reservoir shapes are included for the concrete gravity dams. Water compressibility and fluid-foundation interaction significantly influence the response of concrete gravity dams and are even more important for the arch dam. One effect is a greatly increased importance for the vertical component of ground motion. Hydrodynamic effects on the responses of earth dams are shown to be minor.

18. Availability Statement:
Release Unlimited

19. Security Class (This Report)

20. Security Class (This Page)

21. No. of Pages
246

22. Price

(See ANSI-Z39.18) See Instructions on Reverse OPTIONAL FORM 272 (4-77) (Formerly NTIS-35) Department of Commerce

DYNAMIC RESPONSE OF EMBANKMENT, CONCRETE-GRAVITY AND ARCH DAMS INCLUDING HYDRODYNAMIC INTERACTION

by

John F. Hall

Anil K. Chopra

A Report on Research Conducted Under
Grants ATA74-20554 and ENV76-80073
from the National Science Foundation

Report No. UCB/EERC-80/39
Earthquake Engineering Research Center
University of California
Berkeley, California

October 1980

i a

ABSTRACT

An analysis procedure in the frequency domain is developed for determining the earthquake response of a dam including hydrodynamic interaction and water compressibility effects. Linear responses of idealized, two-dimensional gravity dams and three-dimensional dams, including arch dams, can be obtained. The dam and fluid domain are treated as substructures and modeled with finite elements. The only geometric restriction is that an infinite fluid domain must maintain a uniform cross-section beyond some point in the upstream direction. For such an infinite uniform region, a finite element discretization within the cross-section combined with a continuum representation in the infinite direction provides for a proper transmission of pressure waves. The fluid domain model approximately accounts for fluid-foundation interaction through a damping boundary condition applied along the reservoir floor and sides. The dam foundation is assumed rigid.

Hydrodynamic effects are shown to be equivalent to an added mass and added load in the frequency domain equations of motion of the dam. When water compressibility is considered, the added mass and added load vary with excitation frequency, and factors influencing the dam response include resonances of the added load and the radiation damping associated with the imaginary component of the added mass. If fluid-foundation interaction is neglected, this damping occurs only for infinite fluid domains, but occcurs for both infinite and finite fluid domains if fluid-foundation interaction is included.

Fluid-foundation interaction also reduces resonances of the added load which can be very large if the foundation beneath the water is assumed rigid.

Hydrodynamic effects on the dam response are investigated for acceleration responses to harmonic ground motions. Complex frequency response functions for acceleration at the dam crest are presented for two-dimensional concrete gravity and earth dams and for a three-dimensional arch dam. Several reservoir shapes are included for the concrete gravity dams. Water compressibility and fluid-foundation interaction significantly influence the response of concrete gravity dams and are even more important for the arch dam. One effect is a greatly increased importance for the vertical component of ground motion. Hydrodynamic effects on the responses of earth dams are shown to be minor.

ACKNOWLEDGEMENT

This research investigation was supported by the National Science Foundation under Grants ATA74-20554 and ENV76-80073. The authors are grateful for this support.

This report also constitutes John F. Hall's doctoral dissertation which has been submitted to the University of California, Berkeley. The dissertation committee consisted of Professors A. K. Chopra (Chairman), R. W. Clough and B. A. Bolt. Appreciation is expressed to Professors Clough and Bolt for reviewing the manuscript.

TABLE OF CONTENTS

Preceding page blank

1. INTRODUCTION

1.1 Objectives

The impounded water may significantly influence the dynamic response of dams subjected to earthquake ground motions. Present analysis capabilities for dam response considering hydrodynamic interaction are limited because portions of the analysis dealing with the fluid domain are inefficient except for a few, simple geometries. An objective of this work is the development of an analysis procedure which can efficiently handle an arbitrary fluid domain geometry, either finite or infinite, and either two or three-dimensional. This procedure will then be used to further the study of hydrodynamic effects on the dynamic response of two-dimensional gravity dams and three-dimensional arch dams.

1.2 Background

The earthquake response of a linearly, elastic dam can be determined by standard techniques if the reservoir is empty and the foundation rigid. The finite element method is well suited for this problem resulting in discretized equations of motion in which displacements of the dam are the unknowns. Two-dimensional idealizations are often adequate for concrete and earth gravity dams while arch dams require three-dimensional analyses. Solutions of the equations of motion can be attained directly through step-by-step integrations in the time domain. The modal superposition technique can be used to advantage by including only a few of the lower dam modes. Such an analysis is possible with standard structural, finite element computer programs. The program ADAP (1) contains features pertinent to arch dam analysis such as special shell elements and mesh generation capabilities. Alternatively, the frequency domain version of the equations of motion can be solved and the resulting frequency responses of the dam converted to the time domain by Fourier transform procedures. The frequency responses generated by this method are useful for identifying aspects of structural response behavior.

If water is present in the reservoir, it should be included in the analysis. This problem is an interactive one; dam motions are affected by the hydrodynamic pressures, and these pressures are generated in part by the dam motions. Further, water compressibility influences the earthquake response of dams (2,3). Successful analyses have been performed by the method of substructures in which effects of the fluid are included in the equation of motion of the dam by addition of hydrodynamic forces which act on the upstream dam face. These hydrodynamic terms are computed from solutions to the wave equation over the fluid domain substructure subjected to appropriate boundary conditions.

The substructure method can be implemented in either the time domain (4,5) or frequency domain (3,6,7). Explicit mathematical expressions for the hydrodynamic terms can be employed for simple fluid domain geometries. For compressible water, such analyses are most conveniently carried out in the frequency domain, and the resulting hydrodynamic terms are frequency dependent. Two-dimensional concrete gravity dam-fluid systems have been successfully treated using an infinite fluid domain of constant depth (7). More recently, the method has been applied to arch dam-fluid systems where the infinite reservoir is defined by a cylindrical dam face of constant radius, a horizontal floor, and vertical, radial banks enclosing a central angle of 90° (3). Both these analyses efficiently use free vibration mode shapes of the dam without water as generalized coordinates.

For irregular fluid domain geometries, numerical discretization techniques are required. Both finite difference (4,5) and finite element (6) discretization techniques have been used, although finite elements are better suited to irregular geometries. For compressible water and an infinite fluid domain, time domain procedures require very long meshes so that pressure waves reflecting from the upstream boundary do not return to the dam during the period of analysis. "Quiet" boundaries which satisfactorily transmit the pressure waves and which can be placed close to the dam do not seem possible in the time domain. However, a satisfactory discretization technique for infinite domains has been developed in the frequency domain for certain problems of solid mechanics involving layered media (8). This technique is more efficient and also more accurate than those employing infinite elements (6).

Foundation flexibility is another complicating factor, and both the dam and fluid interact with the foundation. Inclusion of foundation flexibility requires specification of free-field ground motions (those motions at the dam and fluid boundaries if the dam and fluid were absent) and incorporation of an appropriate mechanism to radiate energy into the foundation. The most extensive implementation of these features considers the two-dimensional gravity dam with the infinite fluid domain of constant depth and an elastic half-space foundation (9). Relatively little has been reported for three-dimensional arch dam-fluid systems because of the complicated geometry of the foundations. However, a boundary condition has been employed along the portion of the foundation adjacent to the fluid which absorbs a portion of the incident energy associated with a pressure wave striking this boundary (5). An equivalent form of this boundary condition has also been used to modify hydrodynamic pressures generated by the vertical component of ground motion (3,7,9,10).

1.3 Scope

An analysis procedure is developed for determining the earthquake response of a dam, assumed to be linearly elastic, including interactive and water compressibility effects. The procedure can handle the rigid foundation case, but also includes a more general form of the boundary condition (5) which approximately accounts for interaction between the fluid and the foundation. The analysis procedure is a generalization of the substructure approach (3,7) to arbitrary two and three-dimensional geometries. Finite element techniques are employed for both the dam and fluid domain substructures. The only geometric restriction is that an infinite fluid domain must maintain a uniform cross-section beyond some point in the upstream direction. For such a fluid domain, an adaptation of a procedure dealing with an infinite soil layer and the transmission of Love waves (8) provides a satisfactory and efficient solution technique.

Chapters 2 to 5 deal with two-dimensional dam-fluid systems and Chapters 6 to 8 with three-dimensional systems. In Chapter 2, the frequency domain equations of motion of the dam including frequency dependent hydrodynamic terms are written for two-dimensional gravity dam-fluid systems subjected to horizontal and vertical ground motions. Equations of motion of the fluid domain including appropriate boundary conditions are also presented. Finite element analysis procedures for these equations are described in Chapter 3 for finite and infinite fluid domains. Computation of the hydrodynamic terms from the resulting pressures along the dam-fluid interface is also discussed. In Chapters 4 and 5, the effects of presence of water, compressibility of water, fluid domain shape, fluid-foundation interaction, and direction of ground motion on the responses of concrete and earth gravity dams, respectively, are investigated. Frequency response functions for the dam crest acceleration and the hydrodynamic force on a rigid dam are presented. Chapters 6 and 7 generalize the analysis procedures of Chapters 2 and 3 to three-dimensional dam-fluid systems. An analysis of Morrow Point Dam, an arch dam, is presented in Chapter 8 where effects of presence of water, compressibility of water, fluid-foundation interaction, and direction of ground motion are investigated.

2. TWO-DIMENSIONAL ANALYSIS PROCEDURE FOR DAM RESPONSE

2.1 Systems and Ground Motion

Concrete gravity dams are treated as two-dimensional systems in which the planar vibration of individual monoliths of a dam are considered (Fig. 2.1a). This simplification appears to be reasonable because, at large amplitudes of motion, the monoliths tend to vibrate independently (11). Each monolith is assumed to be in plane stress. An earth or rockfill dam with a length several times its cross-sectional dimensions may be idealized to be in plane strain, thus reducing it to a two-dimensional system (Fig. 2.1b). The plane strain assumption is also applicable to the water if the valley cross-section is wide and if the variation in dam motion is small along its length. These two-dimensional idealizations are not capable of considering cross-stream components of ground motion. Behaviors within the elastic dam and compressible water are assumed linear.

The reservoir may extend only a short distance upstream (Fig. 2.1b) or to a large enough distance so that it can be assumed infinite for purposes of analysis (Fig. 2.1a). In the latter case, a convenient assumption is that the reservoir floor is horizontal beyond some point in the upstream direction.

The base of the dam and reservoir floor in Fig. 2.1 undergo a prescribed acceleration time history described by the horizontal and vertical (x and y) components of ground motion. By specifying these accelerations of the fluid boundaries, the foundation is assumed rigid, and no interaction can take place between the dam and foundation or between the fluid and foundation. Inclusion of foundation interaction

Preceding page blank

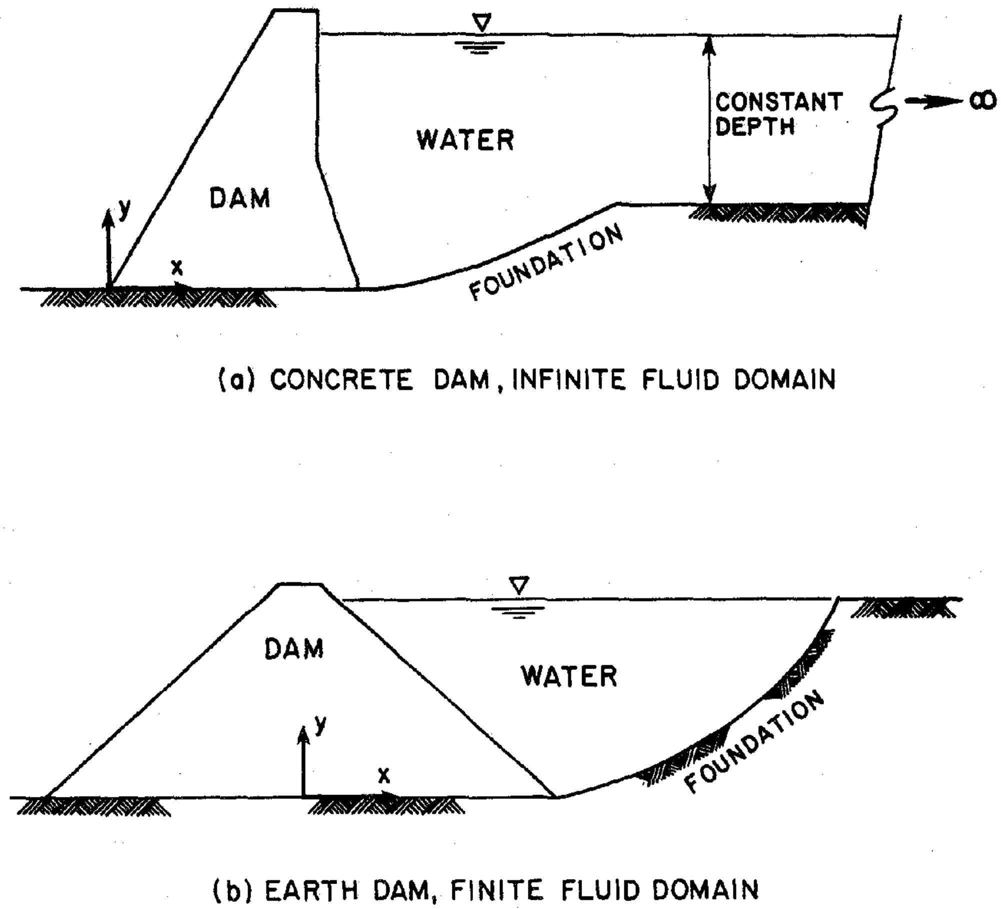

FIG. 2.1 TWO-DIMENSIONAL GRAVITY DAM-FLUID SYSTEMS

effects requires a flexible foundation model and specification of free-field accelerations along the dam base and reservoir floor (those accelerations resulting from the earthquake if the dam and fluid were absent). A procedure for determining the dynamic response of the dam on a rigid foundation is described in Secs. 2.2 to 2.4. Some modifications to this procedure which approximately account for interaction between the fluid and foundation are discussed in Sec. 2.5.

2.2 Equations of Motion for Rigid Foundation Case

2.2.1 Dam

Discretized equations of motion for the dam can be constructed by the finite element method. The dam is subdivided into elements (Fig. 2.2a) connected at nodal points where displacement degrees of freedom (DOF), the unknowns in the problem, are defined. The equations corresponding to DOF for nodes above the rigid base can be expressed as

$$\underline{m}\,\ddot{\underline{v}}(t) + \underline{c}\,\dot{\underline{v}}(t) + \underline{k}\,\underline{v}(t) = -\,\underline{E}^{\ell}\,a_g^{\ell}(t) - \underline{Q}(t), \qquad \ell = x,y \tag{2.1}$$

where $\underline{v}(t)$ = vector of nodal displacements relative to the ground; $\underline{m}$, $\underline{c}$, and $\underline{k}$ = symmetric mass, damping and stiffness matrices for the finite element system; $\underline{E}^{\ell}$ = vector of inertia forces on the dam due to a unit acceleration of the dam as a rigid body in the ℓ direction; $\underline{Q}(t)$ = vector of hydrodynamic forces on the dam arising from the hydrodynamic pressure response of the fluid (with non-zero terms only for nodes along the dam-fluid interface a-b in Fig. 2.2a); and

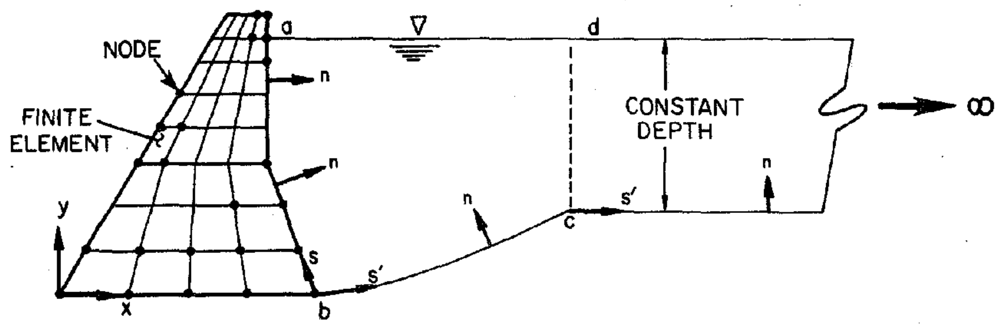

(a) FINITE ELEMENT DAM MODEL, INFINITE FLUID DOMAIN

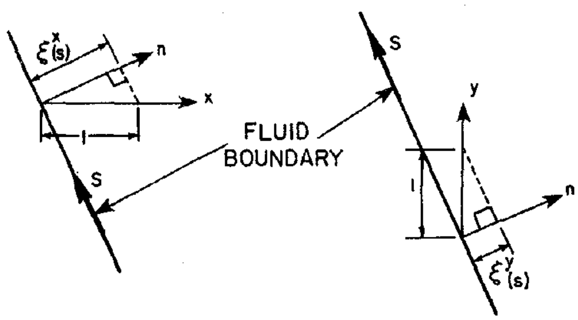

(b) DEFINITION OF $\xi^{\ell}(s)$, s = s, s'

FIG. 2.2 IDEALIZED DAM-FLUID SYSTEM, DEFINITIONS AND NOTATION

$a_g^\ell(t)$ is the component of ground acceleration in the ℓ direction. $\underline{E}^\ell$ is given by

$$\underline{E}^\ell = [\underline{m} \mid \underline{m}_g]\, \underline{e}^\ell \qquad (2.2)$$

where $\underline{m}_g$ = a mass matrix coupling DOF above the base with those along the base (non-zero for consistent mass matrices only); and where the ith term of $\underline{e}^\ell$ equals the length of the component of a unit vector along ℓ in the direction of the ith translational DOF. The vectors e^x and e^y, for ground motions in the x and y directions, contain ones in positions corresponding to x and y translational DOF, respectively, with zeros elsewhere.

The displacements of the dam, including hydrodynamic effects, are approximately expressed as a linear combination of the first J mode shapes of vibration of the dam:

$$\underline{v}(t) = \sum_{j=1}^{J} \underline{\phi}_j \, Y_j^\ell(t) \qquad (2.3)$$

where $\underline{\phi}_j$ = undamped mode of natural vibration of the dam without water, and $Y_j^\ell(t)$ = generalized displacement in that mode. The mode shapes $\underline{\phi}_j$ and natural frequencies ω_j are computed from the eigenproblem:

$$\underline{k}\, \underline{\phi}_j = \omega_j^2 \, \underline{m}\, \underline{\phi}_j \qquad (2.4)$$

The expansion in Eq. 2.3 is complete if J equals the number of DOF in the dam model above the base. Good accuracy is possible, however, for J less than the number of DOF.

Applying the transformation Eq. 2.3 to Eq. 2.1 results in a set of J equations, the jth of which appears as

$$M_j \ddot{Y}_j^{\ell}(t) + C_j \dot{Y}_j^{\ell}(t) + K_j Y_j^{\ell}(t) = P_j^{\ell}(t) \tag{2.5}$$

where M_j, C_j, K_j and $P_j^{\ell}(t)$ = generalized mass, damping, stiffness and load for the jth mode of vibration, which are expressed as

$$\begin{aligned} M_j &= \underline{\phi}_j^T \underline{m} \, \underline{\phi}_j \\ C_j &= 2 \, \xi_j \, \omega_j \, M_j \\ K_j &= \omega_j^2 \, M_j \\ P_j^{\ell}(t) &= - \underline{\phi}_j^T \underline{E}^{\ell} \, a_g^{\ell}(t) - \{\underline{\phi}_j^f\}^T \underline{Q}^f(t) \end{aligned} \tag{2.6}$$

and where ξ_j = critical damping ratio for the jth vibration mode; $\underline{\phi}_j^f$ lists the x and y components of the jth mode for all nodes along the dam-fluid interface; and $\underline{Q}^f(t)$ lists the x and y components of the hydrodynamic forces (ordered to correspond to $\underline{\phi}_j^f$) for the interface nodes. The nodal force vector $\underline{Q}^f(t)$ is the static equivalent of the hydrodynamic pressures on the upstream face of the dam. The forces are computed from the pressures by the method of virtual work.

2.2.2 Fluid

The hydrodynamic pressure distribution $p(x,y,t)$ in excess of the hydrostatic pressure, is governed by the two-dimensional wave equation which is valid for small displacements, irrotational motion, and negligible viscous effects:

$$\frac{\partial^2 p}{\partial x^2} + \frac{\partial^2 p}{\partial y^2} = \frac{1}{C^2}\frac{\partial^2 p}{\partial t^2} \tag{2.7}$$

where C = velocity of compression waves in water. Along accelerating fluid boundaries the pressures should satisfy:

$$\frac{\partial p}{\partial n}(s,t) = -\frac{w}{g}\, a_n(s,t), \qquad s = s,s' \tag{2.8}$$

where s,s' = coordinates along the dam-fluid interface and reservoir floor as shown in Fig. 2.2a; w = unit weight of water; g = acceleration of gravity; $a_n(s,t)$ = normal component of boundary acceleration, and n denotes the inward normal direction to a boundary. Neglecting waves at the free surface of the water $(y = H)$,

$$p(x,H,t) = 0 \tag{2.9}$$

In addition to the boundary conditions of Eqs. 2.8 and 2.9, the pressures should satisfy the radiation condition for fluid domains extending to infinity in the upstream direction.

The normal accelerations of the dam-fluid interface and reservoir floor, when the excitation is $a_g^\ell(t)$, are

$$a_n(s,t) = \varepsilon^\ell(s)\; a_g^\ell(t) + \sum_{j=1}^{J} \phi_j^f(s)\; \ddot{Y}_j^\ell(t) \qquad (2.10a)$$

$$a_n(s',t) = \varepsilon^\ell(s')\; a_g^\ell(t) \qquad (2.10b)$$

where $\varepsilon^\ell(s)$, $s = s,s'$ = a function defined along accelerating boundaries which gives the length of the component of a unit vector along ℓ in the direction of the inward normal n (Fig. 2.2b); and $\phi_j^f(s)$ = a continuous function representation of the component normal to the dam-fluid interface of $\underline{\phi}_j^f$. Within straight portions of a fluid boundary, $\varepsilon^\ell(s)$ does not vary because the direction of n is unchanged. For the infinite reservoir of Fig. 2.2a, $\varepsilon^\ell(s')$ is constant to the right of c because the reservoir floor is horizontal; it equals zero for x ground motion and one for y ground motion.

In Eq. 2.10 the terms $\varepsilon^\ell(s)\; a_g^\ell(t)$ and $\varepsilon^\ell(s')\; a_g^\ell(t)$ represent accelerations of the fluid boundaries due to an acceleration $a_g^\ell(t)$ of the ground with the dam rigid. The second term in Eq. 2.10a represents accelerations due to motions of the flexible dam relative to its base.

2.3 Response to Harmonic Ground Motion

The steady state responses to harmonic ground acceleration $a_g^\ell(t) = e^{i\omega t}$, $\ell = x,y$ can be expressed as follows:

$$
\begin{aligned}
Y_j^{\ell}(t) &= \bar{Y}_j^{\ell}(\omega)\, e^{i\omega t} \\
\dot{Y}_j^{\ell}(t) &= i\omega\, \bar{Y}_j^{\ell}(\omega)\, e^{i\omega t} \\
\ddot{Y}_j^{\ell}(t) &= -\omega^2\, \bar{Y}_j^{\ell}(\omega)\, e^{i\omega t} \\
p(x,y,t) &= \bar{p}(x,y,\omega)\, e^{i\omega t} \\
\underset{\sim}{Q}^f(t) &= \bar{\underset{\sim}{Q}}^f(\omega)\, e^{i\omega t}
\end{aligned}
\tag{2.11}
$$

where the complex frequency response function for a response quantity, say $r(t)$, is denoted by $\bar{r}(\omega)$. Substituting the appropriate terms of Eq. 2.11 into Eq. 2.5 results in

$$\left(-\omega^2 M_j + i\omega C_j + K_j\right) \bar{Y}_j^{\ell}(\omega) = P_j^{\ell}(\omega), \qquad \ell = x,y \tag{2.12}$$

where

$$P_j^{\ell}(\omega) = -\underset{\sim}{\phi}_j^T \underset{\sim}{E}^{\ell} - \{\underset{\sim}{\phi}_j^f\}^T \bar{\underset{\sim}{Q}}^f(\omega) \tag{2.13}$$

Substituting the above expressions for $a_g^{\ell}(t)$, $\ddot{Y}_j^{\ell}(t)$, and $p(x,y,t)$ into Eqs. 2.7 to 2.10 leads to the Helmholtz equation:

$$\frac{\partial^2 \bar{p}}{\partial x^2} + \frac{\partial^2 \bar{p}}{\partial y^2} + \frac{\omega^2}{C^2}\, \bar{p} = 0 \tag{2.14}$$

with the boundary condition along the dam-fluid interface and reservoir floor,

$$\frac{\partial \bar{p}}{\partial n}(s,\omega) = -\frac{w}{g}\, a_n(s,\omega), \qquad s = s,s' \tag{2.15}$$

where

$$a_n(s,\omega) = \varepsilon^{\ell}(s) - \omega^2 \sum_{j=1}^{J} \phi_j^f(s)\, \bar{Y}_j^{\ell}(\omega)$$
$$a_n(s',\omega) = \varepsilon^{\ell}(s') \tag{2.16}$$

and the boundary condition at the free surface,

$$\bar{p}(x,H,\omega) = 0 \tag{2.17}$$

$\bar{p}(x,y,\omega)$ is the solution of Eq. 2.14 subject to the boundary conditions of Eqs. 2.15 and 2.17 along with the radiation condition if the fluid domain is infinite.

Because the governing equation as well as boundary conditions are linear, using superposition $\bar{p}(x,y,\omega)$ can be expressed as

$$\bar{p}(x,y,\omega) = \bar{p}_o^{\ell}(x,y,\omega) - \omega^2 \sum_{j=1}^{J} \bar{p}_j(x,y,\omega)\, \bar{Y}_j^{\ell}(\omega) \tag{2.18}$$

where $\bar{p}_o^{\ell}(x,y,\omega)$ is the solution of Eq. 2.14 with boundary conditions Eqs. 2.15 and 2.17 where

$$a_n(s) = \varepsilon^{\ell}(s), \qquad s = s,s' \tag{2.19}$$

$\bar{p}_j(x,y,\omega)$ is the solution of Eq. 2.14 with boundary conditions

Eqs. 2.15 and 2.17, where

$$a_n(s) = \phi_j^f(s) \qquad a_n(s') = 0 \tag{2.20}$$

The accelerations of Eqs. 2.19 and 2.20 are no longer functions of frequency so the ω has been dropped from $a_n(s,\omega)$ and $a_n(s',\omega)$.

$\bar{p}_0^{\ell}(x,y,\omega)$, $\ell = x,y$ is the complex frequency response function for the hydrodynamic pressure when the excitation is the ground acceleration and the dam is rigid. $\bar{p}_j(x,y,\omega)$ is the corresponding function when the excitation is the acceleration of the dam in its jth vibration mode and there is no motion of the reservoir floor.

An expression similar to Eq. 2.18 can be written for the complex frequency response function for the hydrodynamic forces $\bar{\underline{Q}}^f(\omega)$ on the upstream face of the dam:

$$\bar{\underline{Q}}^f(\omega) = \bar{\underline{Q}}_0^{f\ell}(\omega) - \omega^2 \sum_{j=1}^{J} \bar{\underline{Q}}_j^f(\omega)\ \bar{Y}_j^{\ell}(\omega) \tag{2.21}$$

where $\bar{\underline{Q}}_0^{f\ell}(\omega)$ and $\bar{\underline{Q}}_j^f(\omega)$ are the static equivalents of the pressure functions $\bar{p}_0^{\ell}(x,y,\omega)$ and $\bar{p}_j(x,y,\omega)$, respectively, along the dam-fluid interface.

Substitution of Eq. 2.21 into Eq. 2.13 results in

$$P_j^{\ell}(\omega) = -\ \underline{\phi}_j^T\ \underline{E}^{\ell} - \left\{\underline{\phi}_j^f\right\}^T \left\{\bar{\underline{Q}}_0^{f\ell}(\omega) - \omega^2 \sum_{j=1}^{J} \bar{\underline{Q}}_j^f(\omega)\ \bar{Y}_j^{\ell}(\omega)\right\}, \qquad \ell = x,y \tag{2.22}$$

Equations 2.12 and 2.22 for $j = 1,2,\ldots,J$ can be rearranged and assembled into matrix form as

$$\underset{=}{S}(\omega)\ \bar{\underset{-}{Y}}^{\ell}(\omega) = \underset{-}{L}^{\ell}(\omega), \qquad \ell = x,y \tag{2.23}$$

where

$$S_{jk}(\omega) = -\omega^2 \ \{\underset{-}{\phi}_j^f\}^T \ \bar{\underset{-}{Q}}_k^f(\omega)$$

$$S_{jj}(\omega) = -\omega^2 M_j + i\omega C_j + K_j - \omega^2 \ \{\underset{-}{\phi}_j^f\}^T \ \bar{\underset{-}{Q}}_j^f(\omega) \tag{2.24}$$

$$L_j^{\ell}(\omega) = -\underset{-}{\phi}_j^T \ \underset{-}{E}^{\ell} - \{\underset{-}{\phi}_j^f\}^T \ \bar{\underset{-}{Q}}_o^{f\ell}(\omega)$$

$\underset{=}{S}(\omega)$ is a symmetric matrix and is the same for $\ell = x,y$ components of ground motion.

Hydrodynamic terms appear on both sides of Eq. 2.23, as added loads on the right and added masses on the left, the latter also coupling the modal equations. The added load terms are associated with hydrodynamic pressures on the dam face due to ground accelerations while the dam is rigid. Added mass terms arise from hydrodynamic pressures due to motions of the dam relative to its base. The hydrodynamic terms depend on the excitation frequency, a consequence of the fluid compressibility. For an incompressible fluid $C = \infty$, and Eq. 2.14 reduces to the Laplace equation; the hydrodynamic terms become independent of frequency.

2.4 Response to Arbitrary Ground Motions

The complex frequency response functions $\bar{Y}_j^{\ell}(\omega)$, $j = 1,2,\ldots,J$ are obtained by solving the set of equations (Eq. 2.23) for a range of values of the excitation frequency ω. Solutions corresponding to ℓ = x and y are $\bar{Y}_j^x(\omega)$ and $\bar{Y}_j^y(\omega)$, respectively. Responses to an arbitrary ground acceleration $a_g^\ell(t)$ can be obtained from the complex frequency responses by a Fourier synthesis of the responses to individual harmonic components:

$$Y_j^\ell(t) = \frac{1}{2\pi} \int_{-\infty}^{\infty} \bar{Y}_j^\ell(\omega)\, A_g^\ell(\omega)\, e^{i\omega t}\, d\omega, \qquad \ell = x,y \tag{2.25}$$

where $A_g^\ell(\omega)$ is the Fourier transform of $a_g^\ell(t)$:

$$A_g^\ell(\omega) = \int_0^{t_d} a_g^\ell(t)\, e^{-i\omega t}\, dt, \qquad \ell = x,y \tag{2.26}$$

and where t_d = duration of ground motion. The transforms of Eqs. 2.25 and 2.26 are performed on discrete functions using the Fast Fourier Transform (FFT) algorithm.

The total response $Y_j(t)$ to simultaneous horizontal and vertical components of ground motion is

$$Y_j(t) = Y_j^x(t) + Y_j^y(t) \tag{2.27}$$

The nodal displacements $\underline{v}(t)$ are then obtained using the transformation of Eq. 2.3. At any instant of time, stresses in each finite element can be determined from the nodal displacements by stress-displacement transformation matrices for the finite elements.

2.5 Modifications to Include Fluid-Foundation Interaction

At the boundary of a fluid and a flexible foundation, the acceleration boundary condition which states proportionality between the pressure gradient normal to the boundary and the normal component of acceleration is still valid. However, these accelerations can not be specified as in the rigid foundation case because they depend on the interaction between the fluid and the flexible foundation. The actual accelerations, then, are composed of a free-field part and a part caused by the interaction. Furthermore, a pressure wave travelling in the fluid which strikes a flexible but stationary foundation produces accelerations at the boundary, but by interaction only since the free-field accelerations are zero. Such an incident pressure wave is only partially reflected since a portion refracts into the foundation.

2.5.1 One-dimensional fluid-foundation system

Consider the one-dimensional problem of Fig. 2.3 which consists of adjoining fluid and foundation half-spaces. This problem is one-dimensional because no variations are present in the x direction. Harmonically varying pressures in the fluid and displacements in the foundation are $\bar{p}(y,\omega)$ and $\bar{u}(y,\omega)$, respectively. The excitation is provided by an incident displacement wave travelling upward through the foundation.

Pressures within the fluid obey the one-dimensional version of Eq. 2.14:

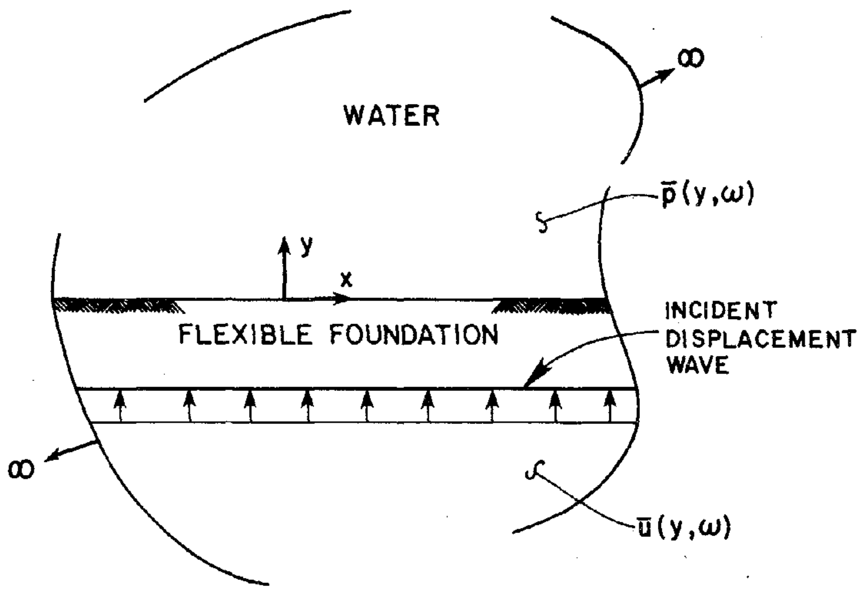

FIG. 2.3 ONE-DIMENSIONAL FLUID-FOUNDATION SYSTEM

$$\frac{d^2\bar{p}}{dy^2} + \frac{\omega^2}{C^2}\,\bar{p} = 0 \tag{2.28}$$

Taking the fluid-foundation boundary as the $y = 0$ line, the acceleration boundary condition for the fluid can be written from Eq. 2.15 as

$$\frac{d\bar{p}}{dy}\,(o,\omega) = \frac{w}{g}\,\omega^2\,\bar{u}(o,\omega) \tag{2.29}$$

Within the foundation displacements are also governed by the one-dimensional Helmholtz equation

$$\frac{d^2\bar{u}}{dy^2} + \frac{\omega^2}{C_r^{\,2}}\,\bar{u} = 0 \tag{2.30}$$

where C_r = compression wave velocity in the foundation. The general solution to Eq. 2.30 is

$$\bar{u}(y,\omega) = A(\omega)\,e^{i\frac{\omega}{C_r}y} + B(\omega)\,e^{-i\frac{\omega}{C_r}y} \tag{2.31}$$

where $A(\omega)$ is the unknown amplitude of the reflected displacement wave and $B(\omega)$ is the specified amplitude of the incident wave. A free-field acceleration of a_y is obtained if

$$B(\omega) = -\frac{1}{2\omega^2}\,a_y \tag{2.32}$$

Such an upward propagating wave has an acceleration amplitude of $\frac{1}{2} a_y$ which doubles to a_y upon reflection at a free boundary at $y = 0$.

$A(\omega)$ in Eq. 2.31 is evaluated from the condition that the pressure in the fluid at the foundation equals the normal foundation stress there. Taking compression positive,

$$\bar{p}(o,\omega) = - E_r \frac{d\bar{u}}{dy} (o,\omega) \tag{2.33}$$

where E_r = the elastic modulus of the foundation rock given by

$$E_r = \frac{w_r}{g} C_r^{\,2} \tag{2.34}$$

and where w_r = unit weight of the rock. Substitution of Eqs. 2.31 and 2.32 into Eq. 2.33 and solution for $A(\omega)$ yields

$$A(\omega) = - \frac{1}{2\omega^2} a_y + \frac{i}{\omega C_r} \frac{g}{w_r} \bar{p}(o,\omega) \tag{2.35}$$

And substitution of Eqs. 2.31, 2.32 and 2.35 into Eq. 2.29 yields a new form of the fluid boundary condition:

$$\frac{d\bar{p}}{dy} (o,\omega) = - \frac{w}{g} a_y + i\omega q \; \bar{p}(o,\omega) \tag{2.36}$$

where $q = \frac{w}{w_r C_r}$. Terms on the right side of Eq. 2.36 represent portions of the fluid boundary acceleration due to free-field motions and interaction, respectively. Since the interactive acceleration is proportional to $i\omega\, \bar{p}(o,\omega)$, the derivative of the pressure at $y = 0$ with respect to time, it can be interpreted as a damper and q as a damping coefficient. For a rigid foundation, $q = 0$ in Eq. 2.36, and a_y is an actual, specified acceleration of the fluid boundary.

Equation 2.36 also provides for the proper partial reflections of a downward travelling pressure wave which strikes the fluid-foundation boundary. The general solution of Eq. 2.28 is

$$\bar{p}(y,\omega) = A(\omega)\, e^{i \frac{\omega}{C} y} + B(\omega)\, e^{-i \frac{\omega}{C} y} \tag{2.37}$$

where $A(\omega)$ is the specified amplitude of the hydrodynamic pressure wave incident to the reservoir floor, and $B(\omega)$ is the amplitude of the reflected wave. The ratio $B(\omega)/A(\omega)$, termed the reflection coefficient α_r, can be found by substituting Eq. 2.37 into the boundary condition Eq. 2.36 with $a_y = 0$ (zero free-field accelerations). Thus,

$$\alpha_r = \frac{1 - qC}{1 + qC} = \frac{1 - \frac{wC}{w_r C_r}}{1 + \frac{wC}{w_r C_r}} \tag{2.38a}$$

which is independent of frequency ω. Also,

$$q = \frac{1}{C}\, \frac{1 - \alpha_r}{1 + \alpha_r} \tag{2.38b}$$

2.5.2 Two-dimensional fluid-foundation systems

Equation 2.36, although strictly applicable to one-dimensional systems, can be applied as the acceleration boundary condition along the reservoir floors of Fig. 2.1 to approximately account for fluid-foundation interaction. Equation 2.36 is generalized to

$$\frac{\partial \bar{p}}{\partial n}(s',\omega) = -\frac{w}{g}a_n(s') + i\omega q\,\bar{p}(s',\omega) \tag{2.39}$$

which replaces the portion of Eq. 2.15 along the reservoir floor. Equation 2.15 then is a special case of Eq. 2.39 for $q = 0$, the rigid foundation case. $a_n(s')$ of Eq. 2.39 is the free-field acceleration of the reservoir floor. It is zero for computation of the pressures $\bar{p}_j(x,y,\omega)$ as stated by Eq. 2.20 and usually non-zero for computation of the pressures $\bar{p}_0^{\ell}(x,y,\omega)$, $\ell = x,y$. In the latter case, the variation of $a_n(s')$ along the floor can approximately be defined by Eq. 2.19 with the same function $\varepsilon^{\ell}(s')$ as used for the rigid motion.

Equation 2.39 can be interpreted as the result of idealizing the foundation as shown in Fig. 2.4. Portions of the foundation beneath the fluid are sliced into columns of infinite length and infinitesimal width extending in a direction perpendicular to the fluid boundary. Resulting foundation motions are due entirely to axially travelling compression waves in the columns, each of which vibrates independently of its neighbor. Continuity is maintained between normal displacement and stress across the fluid-foundation boundary. The properties E_r, w_r, and C_r are now those of the columns.

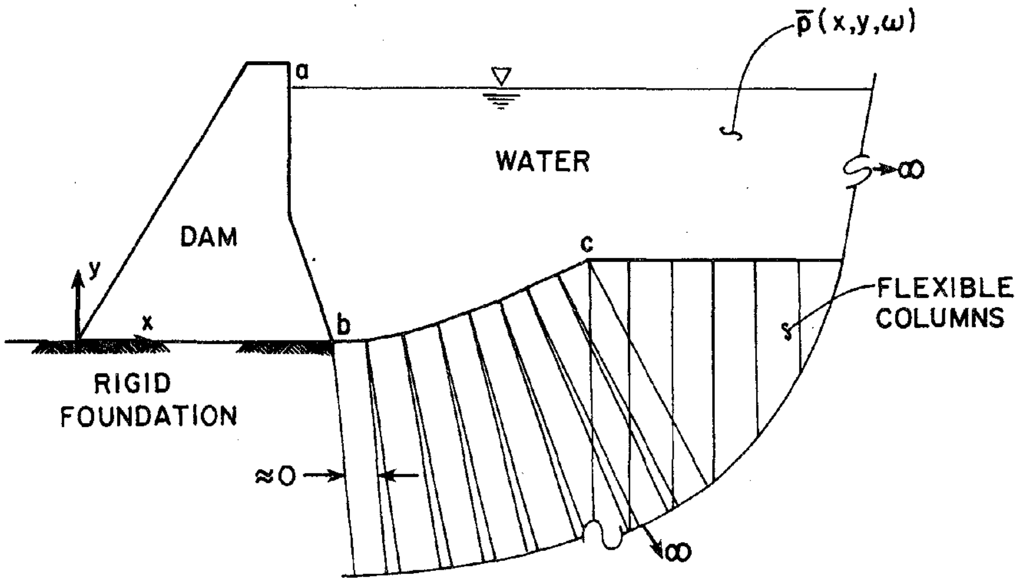

FIG. 2.4 IDEALIZATION OF THE FLEXIBLE FOUNDATION BENEATH THE FLUID

Consideration of a single column, an incident wave travelling toward the fluid domain, and the pressure response $\bar{p}(s',\omega)$ at the end of the column leads to Eq. 2.39 by a derivation similar to that of Eq. 2.36. $a_n(s')$ is the free field acceleration at the end of the column.

The foundation model of Fig. 2.4 and the equivalent formulation Eq. 2.39 are simplifications of real situations, but they do provide an additional mechanism for energy loss (radiation through the foundation) which does exist in real problems and which is not accounted for by a rigid foundation model. The amount of energy loss depends on the value chosen for the damping coefficient q. Magnitudes of C_r and w_r used in computing q can be taken as actual values of the foundation rock or adjusted to improve the performance of the sliced column foundation. For example, in Fig. 2.4, increasing C_r and w_r above foundation rock values would approximately cancel the loss in stiffness due to the slicing and the loss in mass due to the empty spaces between columns. Both adjustments result in a smaller q and a value of the reflection coefficient α_r closer to one. Should a silt layer overlie the foundation rock, a higher value of q may be appropriate.

As shown in later chapters, a reasonable value of q affects the fluid response only locally in the vicinities of frequencies where the fluid response is very high. The radiation of energy into the foundation reduces these high (and unrealistic) responses which occur for the rigid foundation model. Thus, the approximate flexible foundation model is a significant improvement.

3. TWO-DIMENSIONAL ANALYSIS OF HYDRODYNAMIC FORCE VECTORS

3.1 Boundary Value Problems and Solution Techniques

As seen in Chapter 2, hydrodynamic force vectors of Eq. 2.24 are of two types: added load $\bar{\underset{\sim}{Q}}{}_o^{f\ell}(\omega)$, $\ell = x,y$ and added mass $\bar{\underset{\sim}{Q}}{}_j^{f}(\omega)$. These vectors are obtained from hydrodynamic pressure distributions along the dam-fluid interface which are found by solving the Helmholtz equation:

$$\frac{\partial^2 \bar{p}}{\partial x^2} + \frac{\partial^2 \bar{p}}{\partial y^2} + \frac{\omega^2}{C^2}\,\bar{p} = 0 \qquad (3.1)$$

subject to the acceleration boundary condition along the dam-fluid interface

$$\frac{\partial \bar{p}}{\partial n}\,(s,\omega) = -\,\frac{w}{g}\,a_n(s) \qquad (3.2a)$$

and along the reservoir floor

$$\frac{\partial \bar{p}}{\partial n}\,(s',\omega) = -\,\frac{w}{g}\,a_n(s') + i\omega q\,\bar{p}(s',\omega) \qquad (3.2b)$$

the zero pressure condition at the free surface $(y = H)$

$$\bar{p}(x,H,\omega) = 0 \qquad (3.3)$$

and the radiation condition if the fluid domain extends to infinity in the upstream direction. In Eq. 3.2b, values of the damping coefficient

Preceding page blank

q greater than zero are used to approximately account for fluid-foundation interaction effects; in which case, $a_n(s')$ is the free-field acceleration of the reservoir floor. For a rigid foundation, $q = 0$.

For computation of $\bar{\underline{Q}}_0^{f\ell}(\omega)$, $\ell = x,y$, the acceleration in Eq. 3.2 is given by (see Eq. 2.19)

$$a_n(s) = \varepsilon^{\ell}(s), \qquad s = s,s' \tag{3.4}$$

and the solution to the resulting boundary value problem (B.V.P.) is the hydrodynamic pressure $\bar{p}_0^{\ell}(x,y,\omega)$. The force vector $\bar{\underline{Q}}_0^{f\ell}(\omega)$ can be obtained from the pressures along the dam-fluid interface by the method of virtual work. For computation of $\bar{\underline{Q}}_j^{f}(\omega)$ (see Eq. 2.20),

$$a_n(s) = \phi_j^{f}(s) \tag{3.5a}$$

$$a_n(s') = 0 \tag{3.5b}$$

for each of the J natural modes of vibration of the dam. $\bar{p}_j(x,y,\omega)$ is the solution to the resulting B.V.P. with corresponding force vector $\bar{\underline{Q}}_j^{f}(\omega)$.

If the fluid domain extends a short distance upstream (Fig. 3.1a), the above B.V.P.'s are solvable with the finite element method. This technique which can handle arbitrary, but finite, fluid domain geometries is described in Sec. 3.2. Should the fluid domain extend a great distance upstream, then an infinite model is more appropriate. The

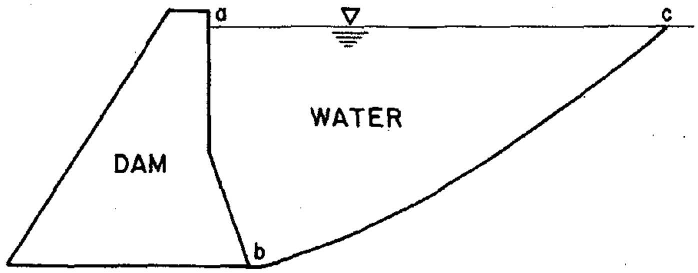

(a) FINITE, IRREGULAR GEOMETRY

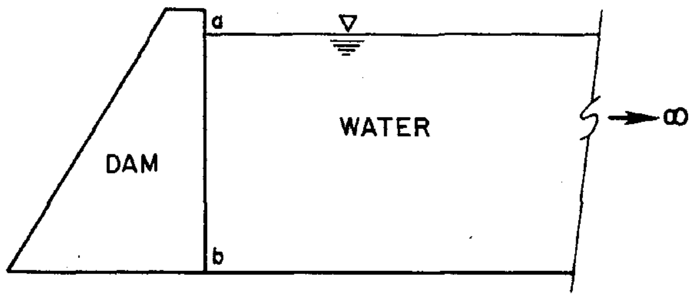

(b) INFINITE, CONSTANT DEPTH

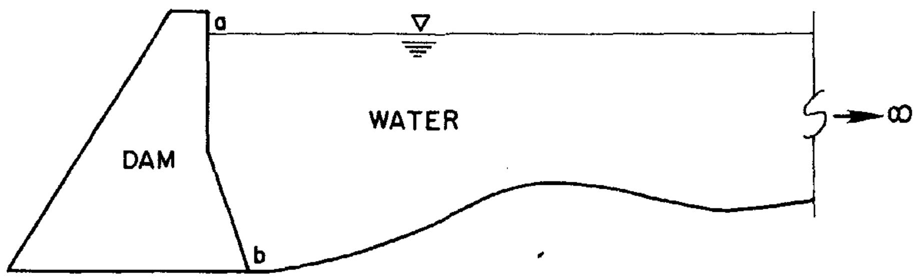

(c) INFINITE, IRREGULAR GEOMETRY

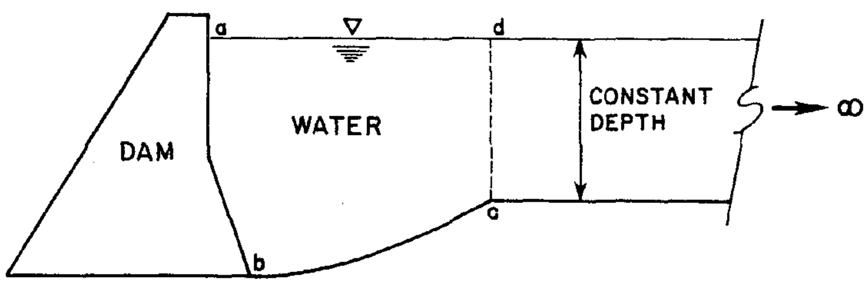

(d) INFINITE, IDEALIZED IRREGULAR GEOMETRY

FIG. 3.1 FLUID DOMAIN TYPES

simplest such case, shown in Fig. 3.1b, has a vertical dam-fluid interface a-b and horizontal reservoir floor. For this fluid domain, series solutions to the B.V.P.'s have been reported (7) and are outlined in Appendix E. A combined finite element-continuum solution of the same problem is presented in Sec. 3.3. Both treatments for the fluid domain of Fig. 3.1b require that the acceleration of the reservoir floor not vary along the infinite length of the floor. This requirement is consistent with the zero acceleration condition of Eq. 3.5b and also, since the floor is straight, with the $\varepsilon^{\ell}(s')$ condition of Eq. 3.4.

Figure 3.1c shows a more realistic fluid domain with geometric irregularities. If this fluid domain is idealized as shown in Fig. 3.1d with a finite region a-b-c-d-a of irregular geometry coupled to an infinite region of constant depth to the right of the vertical line c-d, then the B.V.P.'s can be solved by a method described in Sec. 3.4. This method utilizes the standard finite element formulation of Sec. 3.2 for the region a-b-c-d-a and the finite element-continuum treatment of Sec. 3.3 for the infinite region. Accelerations of the horizontal reservoir floor to the right of c can not vary along the infinite length, a requirement consistent with Eqs. 3.4 and 3.5b.

The analysis procedures of Secs. 3.2 to 3.4 are for hydrodynamic pressures and are written for general accelerations rather than the specific conditions of Eqs. 3.4 and 3.5. These specific conditions are considered in Sec. 3.5 as is the actual computation of $\bar{\underset{\sim}{Q}}_0^{f\ell}(\omega)$, $\ell = x,y$ and $\bar{\underset{\sim}{Q}}_j^{f}(\omega)$ from the resulting pressures along the dam-fluid interface.

3.2 Finite Fluid Domains of Irregular Geometry

Solution of the B.V.P. of Sec. 3.1 (Eq. 3.1 subject to boundary conditions of Eqs. 3.2 and 3.3) for finite fluid domains of irregular geometry (Fig. 3.2a) can be obtained numerically by the finite element method (12). In this approach, the fluid domain is divided into two-dimensional finite elements as shown in Fig. 3.2b. The interelement hydrodynamic pressure is defined in terms of discrete values $\bar{p}_i(\omega)$ at the element nodal points. These nodal pressures are the unknowns in the B.V.P., one DOF for each node below the fluid free surface (where the nodal pressures are zero) assembled into the vector $\bar{\underline{p}}(\omega)$. A finite element discretization of the B.V.P. of Eqs. 3.1 to 3.3 leads to the matrix equation (Appendix B.1):

$$\left[\underline{H} + i\omega q\, \underline{B} - \frac{\omega^2}{C^2}\underline{G}\right] \bar{\underline{p}}(\omega) = \frac{w}{g}\underline{D} \tag{3.6}$$

where $\underline{H}$, $\underline{B}$, and $\underline{G}$ are symmetric matrices analogous to stiffness, damping, and mass matrices arising in dynamics of solid continua; and $\underline{D}$ = vector of nodal accelerations computed from the normal accelerations $a_n(s)$ along the dam-fluid interface a-b and $a_n(s')$ along the reservoir floor b-c, and thus can have non-zero terms for only nodes along a-b-c. The non-zero portion of $\underline{B}$ is a submatrix corresponding to nodes along b-c where the boundary condition of Eq. 3.2b is applied. Only DOF for nodes below the free surface a-c are included in Eq. 3.6.

The unknown pressures $\bar{\underline{p}}(\omega)$ can be determined by solving the set of algebraic equations (Eq. 3.6) simultaneously. For the case

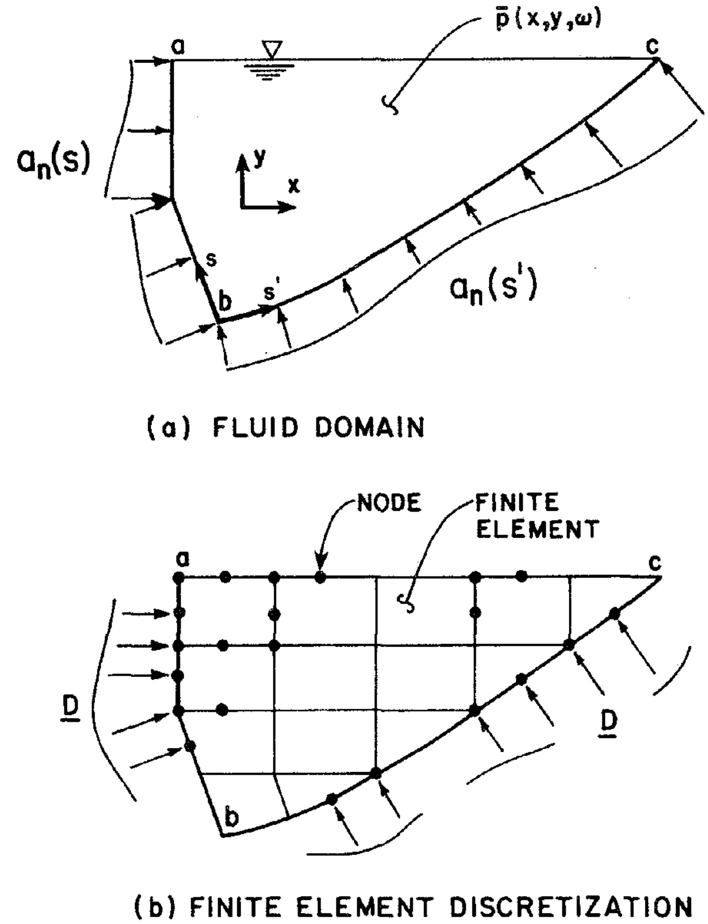

FIG. 3.2 FINITE FLUID DOMAIN OF IRREGULAR GEOMETRY

$q = 0$, $\bar{\underline{p}}(\omega)$ can also be determined using an eigenvector expansion. The eigenproblem associated with Eq. 3.6 for $q = 0$ is

$$\underline{H}\ \underline{\zeta} = \gamma^2\ \underline{G}\ \underline{\zeta} \tag{3.7}$$

which upon solution yields real valued eigenvalues γ_m and eigenvectors $\underline{\zeta}_m$. The eigenvectors are orthogonal to $\underline{H}$ and $\underline{G}$ and are normalized so that

$$\underline{\zeta}_m^T\ \underline{G}\ \underline{\zeta}_m = 1 \tag{3.8a}$$

and they then satisfy

$$\underline{\zeta}_m^T\ \underline{H}\ \underline{\zeta}_m = \gamma_m^2 \tag{3.8b}$$

$\bar{\underline{p}}(\omega)$ is expressed approximately as a linear combination of the first M eigenvectors:

$$\bar{\underline{p}}(\omega) = \sum_{m=1}^{M} \underline{\zeta}_m\ \bar{\alpha}_m(\omega) = \underline{Z}\ \bar{\underline{\alpha}}(\omega) \tag{3.9}$$

Substituting Eq. 3.9 into Eq. 3.6 with $q = 0$, premultiplying the result by $\underline{Z}^T$, and solving for $\bar{\underline{\alpha}}(\omega)$ using the orthogonality property of the eigenvectors results in

$$\bar{\underline{\alpha}}(\omega) = \frac{w}{g}\ \underline{\Gamma}^{-1}\ \underline{Z}^T\ \underline{D} \tag{3.10}$$

where $\underline{\Gamma}$ = an $M \times M$ diagonal matrix with mth diagonal term $= \gamma_m^2 - \omega^2/C^2$. From Eqs. 3.9 and 3.10

$$\underline{\bar{p}}(\omega) = \frac{w}{g} \underline{Z} \, \underline{\Gamma}^{-1} \, \underline{Z}^T \, \underline{D} \tag{3.11}$$

Thus $\underline{\bar{p}}(\omega)$ for $q = 0$ can be determined either by solving the algebraic equations (Eq. 3.6) simultaneously or directly from Eq. 3.11. For $q > 0$ the above eigenvectors do not diagonalize $\underline{B}$ of Eq. 3.6.

The variation of $\underline{\bar{p}}(\omega)$ with excitation frequency ω can be deduced for $q = 0$ by examining Eq. 3.11. The amplitude of the mth eigenvector is real valued and resonates to infinity at an eigenfrequency $\omega_m^b = \gamma_m C$ with opposite sign on each side. Thus $\underline{\bar{p}}(\omega)$ is a real valued function of frequency unbounded at the ω_m^b. This response behavior of a finite fluid domain is characteristic of any undamped finite solid. For $q > 0$ the behavior of $\underline{\bar{p}}(\omega)$ is similar to that of a finite solid with non-proportional damping; i.e., bounded at all frequencies and complex valued for $\omega > 0$. The lack of infinite resonances and the presence of an imaginary component of $\underline{\bar{p}}(\omega)$ are due to the outward radiation of energy through the flexible foundation (foundation radiation damping).

3.3 Infinite Fluid Domain of Constant Depth

3.3.1 Boundary value problems

The B.V.P. of Eqs. 3.1 to 3.3 is solved below for the fluid domain of Fig. 3.3 with an acceleration $a_x(y)$ of the vertical dam-fluid interface a-b and for an acceleration $a_y(x) = a_y^{\ell}$ unvarying along the horizontal reservoir floor. Solutions are carried out separately for these two acceleration conditions which are shown in Figs. 3.3a and c. Continuum solutions are presented in Appendix E.

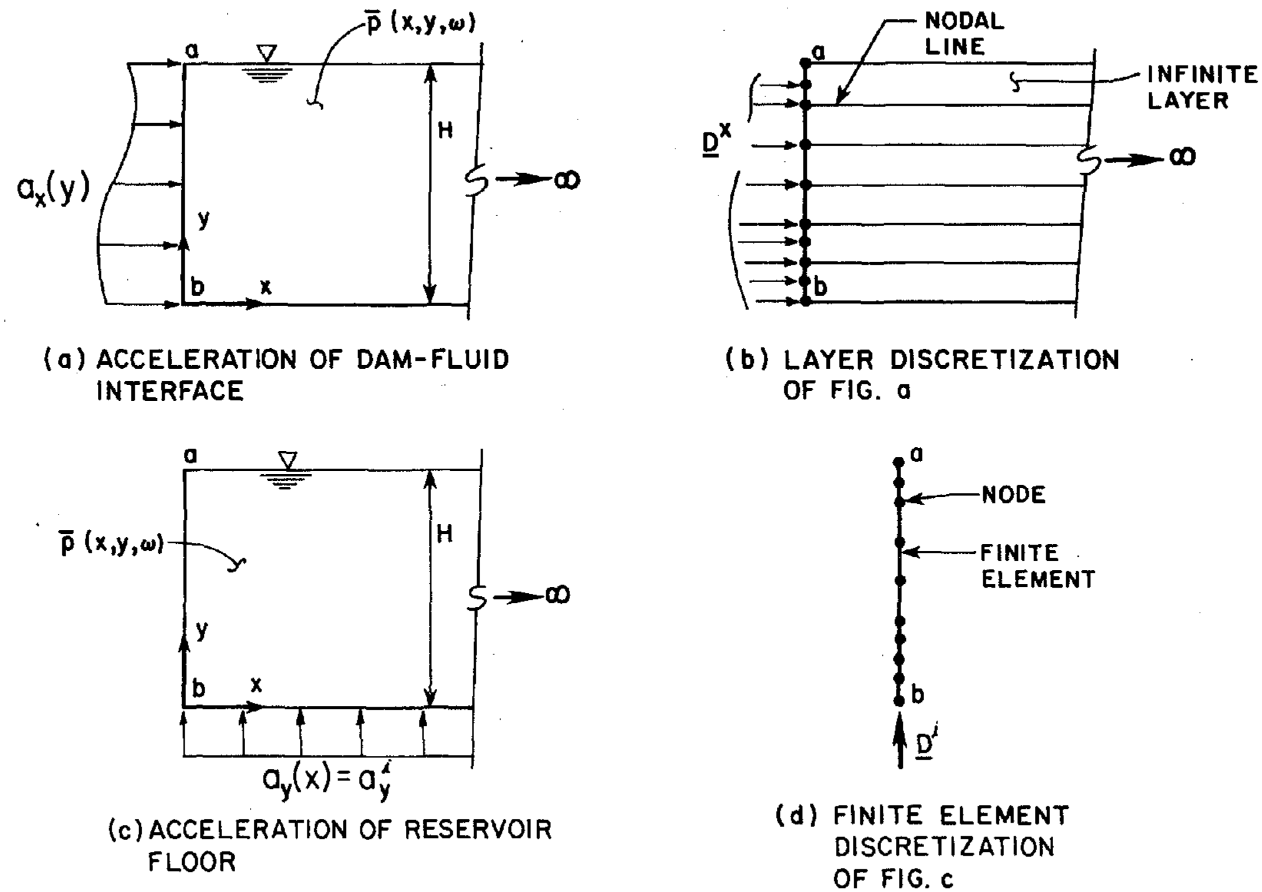

FIG. 3.3 INFINITE FLUID DOMAIN OF CONSTANT DEPTH

The governing Eq. 3.1 with the boundary conditions

$$\frac{\partial \bar{p}}{\partial x}(0,y,\omega) = -\frac{w}{g}\, a_x(y) \tag{3.12a}$$

$$\frac{\partial \bar{p}}{\partial y}(x,0,\omega) = i\omega q\; \bar{p}(x,0,\omega) \tag{3.12b}$$

$$\bar{p}(x,H,\omega) = 0 \tag{3.12c}$$

defines the first B.V.P. Equation 3.1 with the boundary conditions

$$\frac{\partial \bar{p}}{\partial x}(0,y,\omega) = 0 \tag{3.13a}$$

$$\frac{\partial \bar{p}}{\partial y}(x,0,\omega) = -\frac{w}{g}\, a_y^{\ell} + i\omega q\; \bar{p}(x,0,\omega) \tag{3.13b}$$

$$\bar{p}(x,H,\omega) = 0 \tag{3.13c}$$

defines the second B.V.P.

3.3.2 First B.V.P.

The simple geometry of the infinite fluid domain of constant depth permits a separation of variables in Eq. 3.1:

$$\bar{p}(x,y,\omega) = \bar{p}_x(x,\omega)\; \bar{p}_y(y,\omega) \tag{3.14}$$

where $\bar{p}_x(x,\omega)$ must satisfy

$$\frac{d^2\bar{p}_x}{dx^2} - \kappa^2\,\bar{p}_x = 0 \tag{3.15a}$$

and $\bar{p}_y(y,\omega)$ must satisfy

$$\frac{d^2\bar{p}_y}{dy^2} + \lambda^2\,\bar{p}_y = 0 \tag{3.15b}$$

where κ is a separation constant; and

$$\lambda^2 = \kappa^2 + \frac{\omega^2}{c^2} \tag{3.16}$$

Boundary conditions include Eq. 3.12a and the separated conditions

$$\frac{d\bar{p}_y}{dy}(0,\omega) = i\omega q\,\bar{p}_y(0,\omega) \tag{3.17a}$$

$$\bar{p}_y(H,\omega) = 0 \tag{3.17b}$$

The one-dimensional Eq. 3.15b with boundary conditions of Eq. 3.17 defines an eigenvalue problem. A finite element discretization of the eigenproblem using a one-dimensional mesh (Fig. 3.3d) leads to the matrix equation:

$$\left[\underline{H}^{\ell} + i\omega q\,\underline{B}^{\ell}\right]\underline{\psi} = \lambda^2\,\underline{G}^{\ell}\,\underline{\psi} \tag{3.18}$$

whose derivation follows from that in Appendix B.2, and where the matrices $\underline{H}^{i}$, $\underline{B}^{i}$ and $\underline{G}^{i}$ are symmetric. The non-zero portion of $\underline{B}^{i}$ is one diagonal term corresponding to the node at b. Only DOF for nodes below the zero pressure node at a are included in Eq. 3.18.

The eigenvalues λ_n and eigenvectors $\underline{\psi}_n$ determined from Eq. 3.18 are complex valued and dependent on the excitation frequency ω unless $q = 0$; in which case, they are real valued and frequency independent. The $\underline{\psi}_n$ are orthogonal and are normalized so that

$$\underline{\psi}_n^T \, \underline{G}^{i} \, \underline{\psi}_n = 1 \tag{3.19a}$$

and they then satisfy

$$\underline{\psi}_n^T \left[\underline{H}^{i} + i\omega q \, \underline{B}^{i} \right] \underline{\psi}_n = \lambda_n^2 \tag{3.19b}$$

The separated function for the y coordinate, $\bar{p}_y(y,\omega)$ from Eq. 3.15b, is expressed in discrete form as

$$\bar{\underline{p}}_y(\omega) = \underline{\psi}_n \, \bar{\eta}_n(\omega), \qquad n = 1,2,\ldots \tag{3.20}$$

Discretization in the x direction is inappropriate because the fluid domain extends to infinity in that direction. Therefore, continuum solutions to Eq. 3.15a are employed. The κ in Eq. 3.16 can take on only the values given by

$$\kappa_n = \sqrt{\lambda_n^2 - \omega^2/C^2} = \mu_n + i\nu_n \tag{3.21}$$

Since the infinite fluid domain is excited at $x = 0$, $\bar{p}_x(x,\omega)$ must decay with increasing x or travel from $x = 0$ to $x = \infty$. Thus, it is of the form

$$\bar{p}_x(x,\omega) = e^{-\kappa_n x}, \qquad n = 1,2,\ldots \tag{3.22}$$

where the root with both μ_n and ν_n positive is taken in computing κ_n from Eq. 3.21. Including the first N terms in $\bar{\underline{p}}_y$ and $\bar{p}_x$ leads to an approximate expression for $\bar{\underline{p}}(x,\omega)$:

$$\bar{\underline{p}}(x,\omega) = \sum_{n=1}^{N} \underline{\psi}_n \, e^{-\kappa_n x} \, \bar{\eta}_n(\omega) = \underline{\Psi} \, \underline{e}(x) \, \bar{\underline{\eta}}(\omega) \tag{3.23}$$

where $\underline{e}(x)$ = an $N \times N$ diagonal matrix with nth diagonal term $= e^{-\kappa_n x}$. If $q = 0$, then λ_n is real; and κ_n is real or imaginary depending on whether ω is less than or greater than $\lambda_n C$; i.e., $\kappa_n = \mu_n$, or $\kappa_n = i\nu_n$.

The above formulation can be interpreted as a discretization of the fluid domain into layers of infinite length (Fig. 3.3b) separated by nodal lines. The ith term of the vector $\bar{\underline{p}}(x,\omega)$ in Eq. 3.23 represents the variation of pressure with x along the ith nodal line. The $\bar{\eta}_n(\omega)$ are determined to satisfy the discrete form of the boundary condition Eq. 3.12a (Appendix C.1):

$$\underset{\sim}{G}^{i} \frac{d\bar{\underset{\sim}{p}}}{dx}(0,\omega) = -\frac{w}{g}\underset{\sim}{D}^{x} \tag{3.24}$$

where $\underset{\sim}{G}^{i}$ is the same matrix as in Eq. 3.18; and $\underset{\sim}{D}^{x}$ = a vector of nodal accelerations corresponding to the acceleration $a_x(y)$ of the dam-fluid interface.

Substituting Eq. 3.23 into Eq. 3.24 results in

$$\underset{\sim}{G}^{i}\,\underset{\sim}{\Psi}\,\underset{\sim}{K}\,\bar{\underset{\sim}{\eta}}(\omega) = \frac{w}{g}\underset{\sim}{D}^{x} \tag{3.25}$$

where $\underset{\sim}{K}$ = an $N \times N$ diagonal matrix with nth diagonal term = κ_n. Premultiplication of Eq. 3.25 by $\underset{\sim}{\Psi}^T$ and solution for $\bar{\underset{\sim}{\eta}}(\omega)$ using the orthogonality property of the eigenvectors leads to

$$\bar{\underset{\sim}{\eta}}(\omega) = \frac{w}{g}\underset{\sim}{K}^{-1}\,\underset{\sim}{\Psi}^{T}\,\underset{\sim}{D}^{x} \tag{3.26}$$

Substitution of Eq. 3.26 back into Eq. 3.23 results in

$$\bar{\underset{\sim}{p}}(x,\omega) = \frac{w}{g}\underset{\sim}{\Psi}\,\underset{\sim}{e}(x)\,\underset{\sim}{K}^{-1}\,\underset{\sim}{\Psi}^{T}\,\underset{\sim}{D}^{x} \tag{3.27}$$

At $x = 0$, Eq. 3.27 reduces to

$$\bar{\underset{\sim}{p}}(0,\omega) = \frac{w}{g}\underset{\sim}{\Psi}\,\underset{\sim}{K}^{-1}\,\underset{\sim}{\Psi}^{T}\,\underset{\sim}{D}^{x} \tag{3.28}$$

For $q = 0$, λ_n and $\underline{\psi}_n$ are real valued. Then from Eq. 3.27, the amplitude of $\underline{\psi}_n$ decays exponentially with increasing x at $e^{-\mu_n x}$ (when $\omega < \lambda_n C$) or is a nondecaying harmonic $e^{-i\nu_n x}$ (when $\omega > \lambda_n C$). At an eigenfrequency $\omega_n^{\ell} = \lambda_n C$, $\kappa_n = 0$ and the amplitude of $\underline{\psi}_n$ is infinite. The part of the amplitude that approaches infinity is real below ω_n^{ℓ} and imaginary above. Thus, $\underline{\bar{p}}(x,\omega)$ is real for $\omega < \omega_1^{\ell}$, complex for $\omega > \omega_1^{\ell}$, and unbounded at frequencies ω_n^{ℓ}. The harmonic, nondecaying distribution with x in the amplitude of an eigenvector $\underline{\psi}_n$ for $\omega > \omega_n^{\ell}$ represents a radiation of energy in the infinite, upstream direction of the fluid domain. This fluid radiation damping is non-zero for $\omega > \omega_1^{\ell}$ and is responsible for the imaginary component of $\underline{\bar{p}}(x,\omega)$. It does not, however, prevent the infinite resonances at frequencies ω_n^{ℓ} above ω_1^{ℓ} because of the orthogonality of the eigenvectors; i.e., a resonating eigenvector $\underline{\psi}_n$ is orthogonal to the fluid radiation damping which is associated with the lower eigenvectors. The ω_n^{ℓ} approximate the eigenfrequencies $\omega_n^r = (2n-1)\pi C/2H$ for the continuum fluid domain (Appendix E). For $q > 0$, the complex eigenvector $\underline{\psi}_n$ has an x distribution of $e^{-\mu_n x} e^{-i\nu_n x}$, an exponentially decaying harmonic. Thus, all energy is eventually radiated by the foundation. Since this foundation radiation damping occurs for all frequencies greater than zero, $\underline{\bar{p}}(x,\omega)$ is bounded at all frequencies and complex valued for $\omega > 0$.

3.3.3 Second B.V.P.

The B.V.P. of Eq. 3.1 with the boundary conditions of Eq. 3.13 contains no variation in the x direction, and is thus one-dimensional in the y coordinate. Omitting the x variations from these equations results in the one-dimensional Helmholtz equation for $\bar{p}(y,\omega)$

$$\frac{d^2\bar{p}}{dy^2} + \frac{\omega^2}{C^2}\,\bar{p} = 0 \tag{3.29}$$

and the boundary conditions

$$\frac{d\bar{p}}{dy}\,(0,\omega) = -\,\frac{w}{g}\,a_y^{\ell} + i\omega q\;\bar{p}(0,\omega) \tag{3.30a}$$

$$\bar{p}(H,\omega) = 0 \tag{3.30b}$$

Solution of Eq. 3.29 subject to the boundary conditions of Eq. 3.30 can be obtained by the finite element method using a one-dimensional mesh (Fig. 3.3d). The finite element discretization of the one-dimensional B.V.P. is the matrix equation (Appendix B.2):

$$\left[\underset{\sim}{H}^{\ell} + i\omega q\,\underset{\sim}{B}^{\ell} - \frac{\omega^2}{C^2}\,\underset{\sim}{G}^{\ell}\right]\bar{\underset{\sim}{p}}(\omega) = \frac{w}{g}\,\underset{\sim}{D}^{\ell} \tag{3.31}$$

where $\underset{\sim}{H}^{\ell}$, $\underset{\sim}{B}^{\ell}$ and $\underset{\sim}{G}^{\ell}$ are the same symmetric matrices as in Eq. 3.18; $\bar{\underset{\sim}{p}}(\omega)$ = vector of unknown nodal pressures; and $\underset{\sim}{D}^{\ell}$ = vector of nodal accelerations (a zero vector except the term corresponding to the node at b, whose value is a_y^{ℓ}). Only DOF for nodes below the zero pressure node at a are included in Eq. 3.31.

The pressures $\bar{\underset{\sim}{p}}(\omega)$ can be obtained by solving the algebraic equations (Eq. 3.31) simultaneously. Alternatively, $\bar{\underset{\sim}{p}}(\omega)$ can be determined using an eigenvector expansion, employing the complex valued and frequency dependent eigenvalues λ_n and eigenvectors $\underline{\psi}_n$ resulting from the associated eigenproblem, Eq. 3.18. Except for $q = 0$ when both λ_n and $\underline{\psi}_n$ are real valued and frequency independent, the eigencoordinate solution of Eq. 3.31 is inefficient compared to solving the equations simultaneously. However, if the first B.V.P. is being solved concurrently, then the frequency dependent λ_n and $\underline{\psi}_n$ are available. Following Eqs. 3.9 to 3.11, $\bar{\underline{p}}(\omega)$ is approximately expressed in terms of the first N eigenvectors as

$$\bar{\underline{p}}(\omega) = \frac{w}{g} \underline{\Psi} \, \underline{\Lambda}^{-1} \, \underline{\Psi}^T \, \underline{D}^{i} \tag{3.32}$$

where $\underline{\Psi} = [\underline{\psi}_1, \underline{\psi}_2, \ldots, \underline{\psi}_N]$ and $\underline{\Lambda}$ = an $N \times N$ diagonal matrix with nth diagonal term = $\lambda_n^2 - \omega^2/C^2$. Thus, $\bar{\underline{p}}(\omega)$ can be determined either by solving the set of equations 3.31 simultaneously or from Eq. 3.32. Note that $\underline{\Lambda}$ is related to $\underline{K}$ from Eq. 3.27 by

$$\underline{\Lambda} = \underline{K}^2 \tag{3.33}$$

The frequency variation of $\bar{\underline{p}}(\omega)$ is similar to that of the finite fluid domain of Sec. 3.2. For $q = 0$, $\bar{\underline{p}}(\omega)$ is a real valued function of frequency with infinite resonances at the eigenfrequencies $\omega_n^{i} = \lambda_n C$ (same as the first B.V.P.). For $q > 0$, $\bar{\underline{p}}(\omega)$ is bounded at all frequencies and complex valued for $\omega > 0$, which are consequences of foundation radiation damping.

3.4 Infinite Fluid Domains of Irregular Geometry

A solution scheme for the B.V.P. of Eqs. 3.1 to 3.3 is presented below for the fluid domain of Fig. 3.4a where a finite region a-b-c-d-a of irregular shape is connected to an infinite region of constant depth to the right of the vertical line c-d. Normal accelerations of the dam-fluid interface a-b and reservoir floor are $a_n(s)$ and $a_n(s')$, respectively. To the right of c, $a_n(s') = a_y^{\ell}$, unvarying along the infinite length of the horizontal floor. The fluid domain is discretized as shown in Fig. 3.4b. The finite region a-b-c-d-a is divided into two-dimensional finite elements as discussed in Sec. 3.2. Within the infinite region, the layer discretization of Sec. 3.3 is employed, matching the adjacent two-dimensional mesh along c-d.

Figures 3.4c and d show the discretized fluid domain separated at c-d. The separated fluid domains, analogous to free bodies of solid continua, require that the normal accelerations along the line of separation be preserved. The finite element matrix equation 3.6 is written for the region a-b-c-d-a including only DOF for nodes below the free surface and is partitioned as follows:

$$\left[\left[\begin{array}{c|c} \underset{\sim}{H}_{11} & \underset{\sim}{H}_{12} \\ \hline \underset{\sim}{H}_{21} & \underset{\sim}{H}_{22} \end{array}\right] + i\omega q \left[\begin{array}{c|c} \underset{\sim}{B}_{11} & \underset{\sim}{B}_{12} \\ \hline \underset{\sim}{B}_{21} & \underset{\sim}{B}_{22} \end{array}\right] - \frac{\omega^2}{C^2} \left[\begin{array}{c|c} \underset{\sim}{G}_{11} & \underset{\sim}{G}_{12} \\ \hline \underset{\sim}{G}_{21} & \underset{\sim}{G}_{22} \end{array}\right]\right] \left\{\begin{array}{c} \bar{\underset{\sim}{p}}_1(\omega) \\ \hline \bar{\underset{\sim}{p}}_2(\omega) \end{array}\right\} = \frac{w}{g} \left\{\begin{array}{c} \underset{\sim}{D}_1 \\ \hline \underset{\sim}{D}_2 - \underset{\sim}{D}_2^x(\omega) \end{array}\right\} \tag{3.34}$$

where nodes along c-d are identified by subscript 2 and remaining nodes by subscript 1. In Eq. 3.34 $\underset{\sim}{D}_1$ and $\underset{\sim}{D}_2$ are acceleration

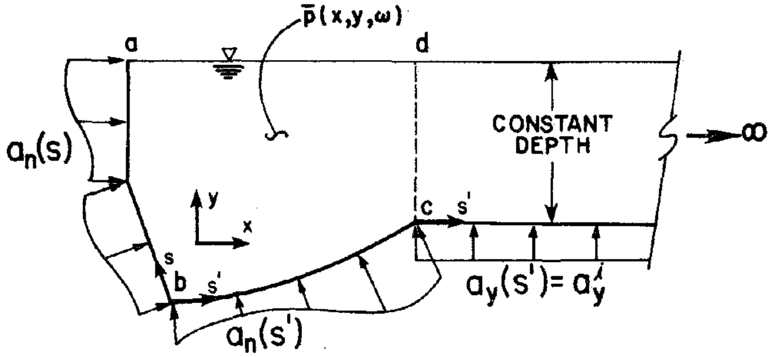

(a) IDEALIZED FLUID DOMAIN

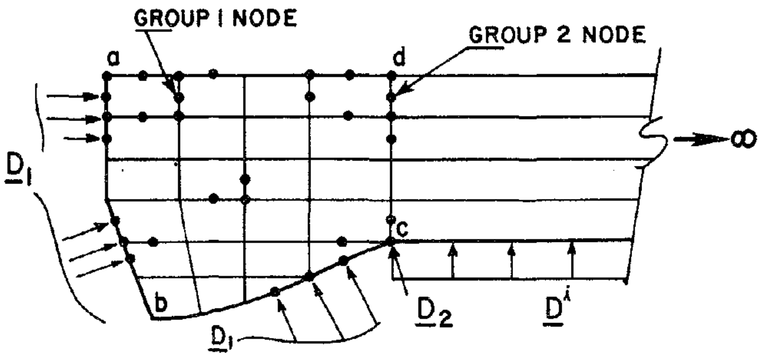

(b) FINITE ELEMENT DISCRETIZATION

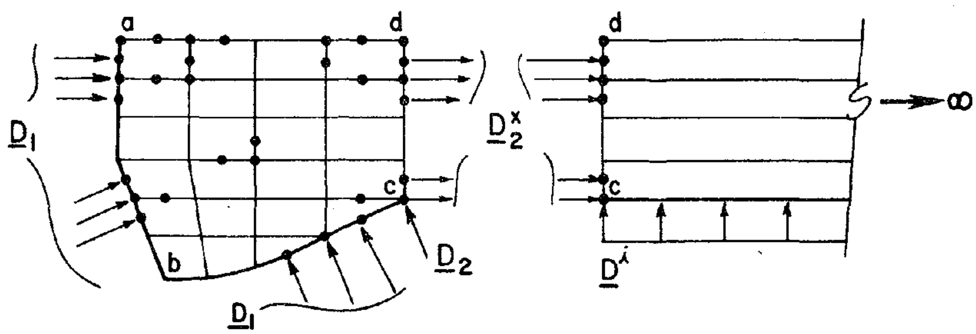

(c) FINITE ELEMENT DISCRETIZATION OF IRREGULAR REGION

(d) LAYER DISCRETIZATION OF INFINITE REGION

FIG. 3.4 INFINITE FLUID DOMAIN OF IRREGULAR GEOMETRY vectors of group 1 and group 2 nodes computed from $a_n(s)$, $s = s, s'$ along a-b-c; and $\underline{D}_2^x(\omega)$ = acceleration vector of group 2 nodes associated with the unknown x-direction acceleration of the line c-d. Equation 3.34 without $\underline{D}_2^x(\omega)$ is just a partitioned form of Eq. 3.6 written for a zero acceleration condition normal to c-d. However, as part of the infinite fluid domain of Fig. 3.4a, c-d is an interface between two subregions and undergoes, as yet, unknown accelerations which contribute the vector $\underline{D}_2^x(\omega)$ in Eq. 3.34.

Consideration of the infinite region of Fig. 3.4d leads to an expression for $\underline{D}_2^x(\omega)$. The vector $\bar{\underline{p}}_2(\omega)$ of nodal pressures along c-d arises from two sources: the unknown acceleration $\underline{D}_2^x(\omega)$ and the vertical acceleration a_y^i of the floor of the infinite section. Pressures at c-d due to $\underline{D}_2^x(\omega)$ and a_y^i are given by Eqs. 3.28 and 3.32, respectively. Using superposition, $\bar{\underline{p}}_2(\omega)$ can be expressed as

$$\bar{\underline{p}}_2(\omega) = \frac{w}{g} \underline{\Psi} \, \underline{K}^{-1} \left\{ \underline{K}^{-1} \, \underline{\Psi}^T \, \underline{D}^i + \underline{\Psi}^T \, \underline{D}_2^x(\omega) \right\} \tag{3.35}$$

where use has been made of Eq. 3.33.

If $\bar{\underline{p}}_2(\omega)$ is expressed by an eigenvector expansion using the first N eigenvectors $\underline{\psi}_n$

$$\bar{\underline{p}}_2(\omega) = \underline{\Psi} \, \bar{\underline{\eta}}_2(\omega) \tag{3.36}$$

then, from Eq. 3.35,

$$\bar{\underline{\eta}}_2(\omega) = \frac{w}{g} \underline{K}^{-1} \left\{ \underline{K}^{-1} \, \underline{\Psi}^T \, \underline{D}^i + \underline{\Psi}^T \, \underline{D}_2^x(\omega) \right\} \tag{3.37}$$

Multiplication of Eq. 3.37 by $\underset{\sim}{K}$ yields the expression for $\underset{\sim}{D}_2^x(\omega)$:

$$\frac{w}{g}\,\underset{\sim}{\Psi}^T\,\underset{\sim}{D}_2^x(\omega) = \underset{\sim}{K}\,\bar{\underset{\sim}{\eta}}_2(\omega) - \frac{w}{g}\,\underset{\sim}{K}^{-1}\,\underset{\sim}{\Psi}^T\,\underset{\sim}{D}^{\ell} \tag{3.38}$$

Substitution of Eqs. 3.36 and 3.38 into Eq. 3.34 with a premultiplication of the second submatrix equation by $\underset{\sim}{\Psi}^T$ yields

$$\left[\begin{array}{c|c} \left[\underset{\sim}{H}_{11} + i\omega q\,\underset{\sim}{B}_{11} - \frac{\omega^2}{C^2}\,\underset{\sim}{G}_{11}\right] & \left[\underset{\sim}{H}_{12} + i\omega q\,\underset{\sim}{B}_{12} - \frac{\omega^2}{C^2}\,\underset{\sim}{G}_{12}\right]\underset{\sim}{\Psi} \\ \hline \underset{\sim}{\Psi}^T\left[\underset{\sim}{H}_{21} + i\omega q\,\underset{\sim}{B}_{21} - \frac{\omega^2}{C^2}\,\underset{\sim}{G}_{21}\right] & \underset{\sim}{\Psi}^T\left[\underset{\sim}{H}_{22} + i\omega q\,\underset{\sim}{B}_{22} - \frac{\omega^2}{C^2}\,\underset{\sim}{G}_{22}\right]\underset{\sim}{\Psi} + \underset{\sim}{K} \end{array}\right]\left\{\begin{array}{c} \bar{\underset{\sim}{p}}_1(\omega) \\ \hline \bar{\underset{\sim}{\eta}}_2(\omega) \end{array}\right\} = \frac{w}{g}\left\{\begin{array}{c} \underset{\sim}{D}_1 \\ \hline \underset{\sim}{\Psi}^T\,\underset{\sim}{D}_2 + \underset{\sim}{K}^{-1}\,\underset{\sim}{\Psi}^T\,\underset{\sim}{D}^{\ell} \end{array}\right\} \tag{3.39}$$

The pressure vector $\bar{\underset{\sim}{p}}_1(\omega)$ can be obtained by solving the algebraic equations (Eq. 3.39).

For $q = 0$, several features of the frequency variation of $\bar{\underset{\sim}{p}}_1(\omega)$ are evident. When the frequency is below the first eigenfrequency ω_1^{ℓ} of the infinite region, no imaginary terms are present in Eq. 3.39, so $\bar{\underset{\sim}{p}}_1(\omega)$ is real valued. Above ω_1^{ℓ}, $\bar{\underset{\sim}{p}}_1(\omega)$ is complex valued due to fluid radiation damping. Also, when a_y^{ℓ} is non-zero, $\bar{\underset{\sim}{p}}_1(\omega)$ becomes unbounded at each ω_n^{ℓ} because of the infinite value attained by the nth diagonal term of the matrix $\underset{\sim}{K}^{-1}$ on the right side of Eq. 3.39. However, none of the frequencies ω_n^{ℓ} are eigenfrequencies of the complete fluid domain; the infinite responses are due to the infinite right side of Eq. 3.39 at these frequencies.

Eigenfrequencies of the complete fluid domain must satisfy the eigenvalue problem associated with Eq. 3.39, this equation with $q = 0$ and a zero right side, and be real valued. Such frequencies, if they occur, will be less than ω_1^i because above ω_1^i the eigenproblem is complex valued (complex matrix $\underline{K}$). At an excitation frequency equal to an eigenfrequency, $\bar{\underline{p}}_1(\omega)$ is unbounded if the right side of Eq. 3.39 is non-zero and if $q = 0$. For $q > 0$, $\bar{\underline{p}}_1(\omega)$ is bounded at all frequencies and complex valued for $\omega > 0$.

3.5 Computation of Hydrodynamic Force Vectors

For the fluid domains described in Secs. 3.2 to 3.4, computation of the hydrodynamic force vectors $\bar{\underline{Q}}_o^{f\ell}(\omega)$, $\ell = x,y$ and $\bar{\underline{Q}}_j^f(\omega)$ of Eq. 2.24 proceeds as follows:

1. The boundary accelerations of Eqs. 3.4 and 3.5 are converted into acceleration vectors for use in Eqs. 3.6 or 3.11 (finite fluid domain), Eqs. 3.28 and 3.32 (infinite fluid domain of constant depth), or Eq. 3.39 (infinite fluid domain of irregular geometry). For the finite fluid domain, these vectors are denoted by $\underline{D}_o^\ell$ and $\underline{D}_j$, and their computation is described in Appendix D.1. Use is made of the boundary portion of the finite element mesh along a-b-c in Fig. 3.2. Vectors $\{\underline{D}^x\}_o^\ell$, $\ell = x$ and $\{\underline{D}^x\}_j$ of Eq. 3.28 and $\{\underline{D}_1\}_o^\ell$, $\{\underline{D}_2\}_o^\ell$, $\ell = x,y$ and $\{\underline{D}_1\}_j$, $\{\underline{D}_2\}_j$ of Eq. 3.39 are computed using the boundary element meshes along a-b in Fig. 3.3 and a-b-c in Fig. 3.4, respectively, using the method of Appendix D.1. In the latter case, $\{\underline{D}_2\}_j = \underline{0}$. $\{\underline{D}^i\}_o^\ell$, $\ell = y$ in Eqs. 3.32 and 3.39 is computed with $a_y^i = 1$, and $\{\underline{D}^i\}_o^\ell$, $\ell = x$ and $\{\underline{D}^i\}_j$ of Eq. 3.39 are also zero vectors.

2. Using the acceleration vectors of step 1, hydrodynamic pressure vectors for a fluid domain are obtained by solving the appropriate equations of Sec. 3.2, 3.3, or 3.4. Pressures along the dam-fluid interface are assembled into $\bar{\underline{p}}_0^{f\ell}(\omega)$, $\ell = x,y$ and $\bar{\underline{p}}_j^{f}(\omega)$.

3. As also described in Appendix D.1, the hydrodynamic force vectors are computed from the pressures along the dam-fluid interface obtained in step 2.

3.6 Numerical Results

3.6.1 Infinite fluid domain of constant depth

The accelerations shown in Figs. 3.5a and 3.5b result from harmonic ground accelerations = $e^{i\omega t}$ in horizontal and vertical directions, respectively, with the dam and foundation assumed rigid. Continuum solutions to both these problems appear in Appendix E, and finite element-continuum formulations are discussed in Sec. 3.3. In order to demonstrate Eq. 3.39 $(q = 0)$, these problems are solved here using regular finite element meshes consisting of single columns of elements with maximum numbers of eigenvectors included in $\underline{\Psi}$. Three meshes are used employing 3, 6, and 12 linear elements (Fig. 3.5c) to demonstrate convergence as the mesh is refined. Two types of plots are presented: the hydrodynamic force $\bar{F}_0^{\ell}(\omega)$, $\ell = x,y$ on the rigid dam vs. frequency ω and the hydrodynamic pressure $\bar{p}_0^{f\ell}(y,\omega)$ along the dam-fluid interface a-b. $\bar{F}_0^{\ell}(\omega)$ is computed by integrating $\bar{p}_0^{f\ell}(y,\omega)$ over a-b. $\bar{F}_0^{\ell}(\omega)$ is normalized with the static force $F_{st} = \frac{1}{2} w H^2$, ω with $\omega_1^r = \pi C/2H$, and $\bar{p}_0^{f\ell}(y,\omega)$ with the static pressure at the reservoir floor wH, so that the results apply to

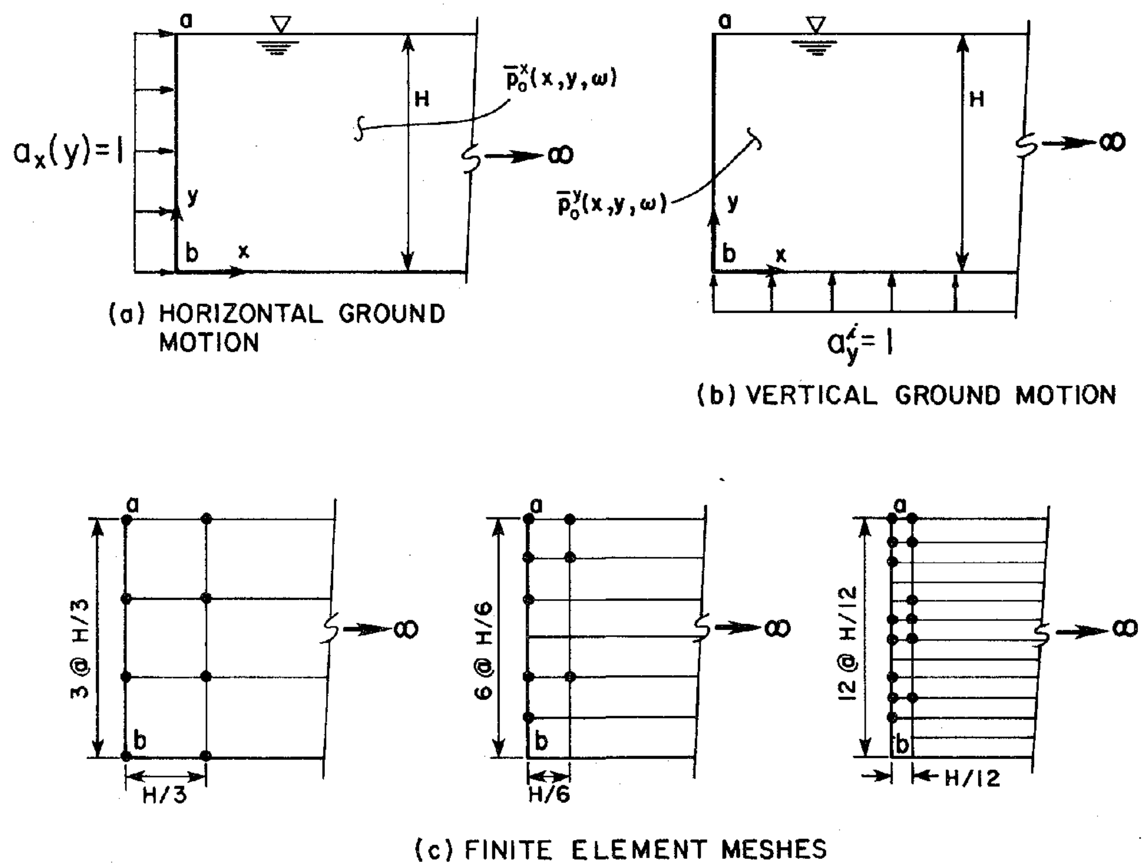

FIG. 3.5 INFINITE FLUID DOMAIN OF CONSTANT DEPTH SUBJECTED TO HARMONIC GROUND MOTIONS WITH RIGID DAM

fluid domains of any height. Continuum solutions obtained from the equations of Appendix E appear as solid lines in the figures.

Hydrodynamic forces and pressures due to horizontal ground motion (Fig. 3.5a) are plotted in Figs. 3.6 and 3.7, respectively. In the force plot of Fig. 3.6, the location of resonant peaks of the finite element curves, the eigenfrequencies ω_n^i, are shifted toward higher ω. This shift is due to the discretization and is noticeably less for the finer meshes. The method of resonance, real on the left and imaginary on the right of the eigenfrequencies, is truely reproduced by all three finite element solutions. Convergence of these solutions to the continuum solutions as the mesh is refined is evident in Fig. 3.6 and also in the pressure plots of Fig. 3.7. There, ω_n^i denotes either ω_n^r of the continuum results or ω_n^i of the finite element results.

For the vertical ground motion case of Fig. 3.5b, hydrodynamic forces and pressures are plotted in Figs. 3.8 and 3.9, and conclusions similar to those above can be made. Here, the method of resonance differs, always real but of opposite sign across the ω_n^i (typical of finite fluid domains), and is truely reproduced by all three meshes.

The effect on the frequency variation of $\bar{F}_0^{\ell}(\omega)$ of including less than the maximum number of eigenvectors in $\underline{\Psi}$ is illustrated in Figs. 3.10a and b for horizontal and vertical ground motions, respectively. The three curves plotted are for the six element mesh with six, two, or one eigenvectors included in $\underline{\Psi}$. The single eigenvector solution is satisfactory to just past the first resonant peak, and the two eigenvector solution is satisfactory to just past the second peak. Examination of the pressures (not shown) supports these

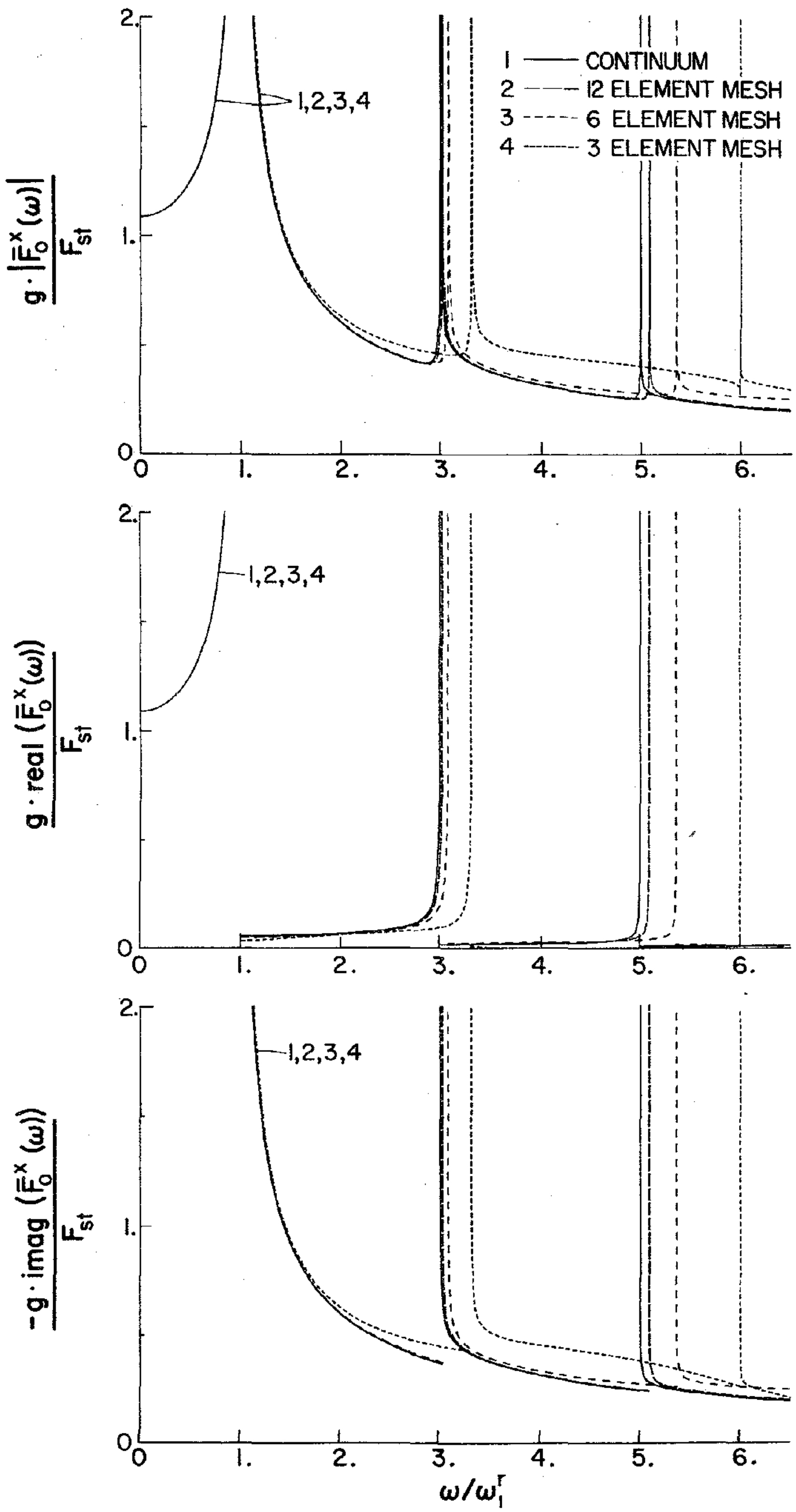

FIG. 3.6 HYDRODYNAMIC FORCE ON A RIGID DAM DUE TO HARMONIC, HORIZONTAL GROUND MOTION. FOUNDATION IS ASSUMED RIGID.

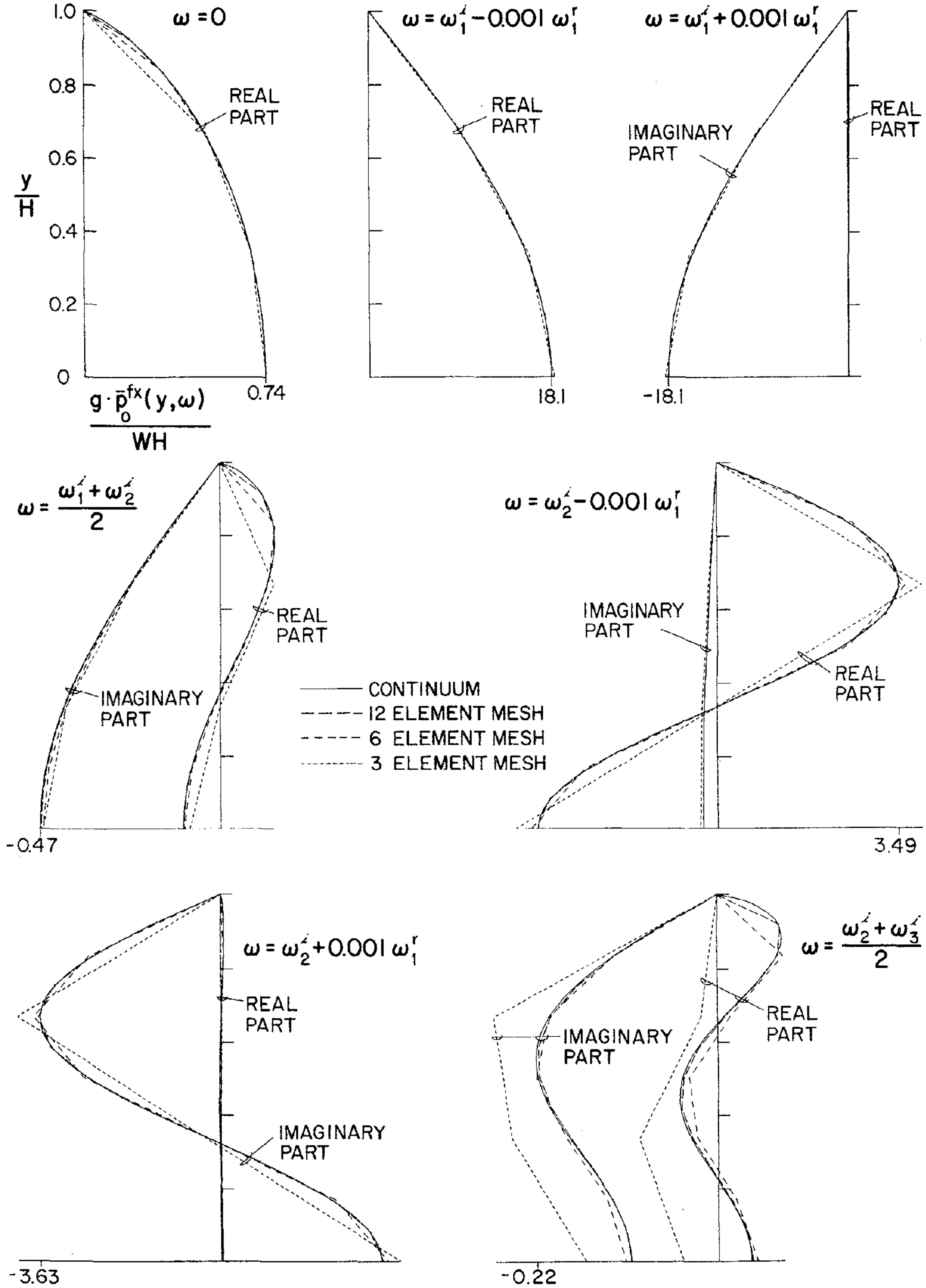

FIG. 3.7 HYDRODYNAMIC PRESSURES ON A RIGID DAM DUE TO HARMONIC, HORIZONTAL GROUND MOTION AT SELECTED EXCITATION FREQUENCIES. FOUNDATION IS ASSUMED RIGID.

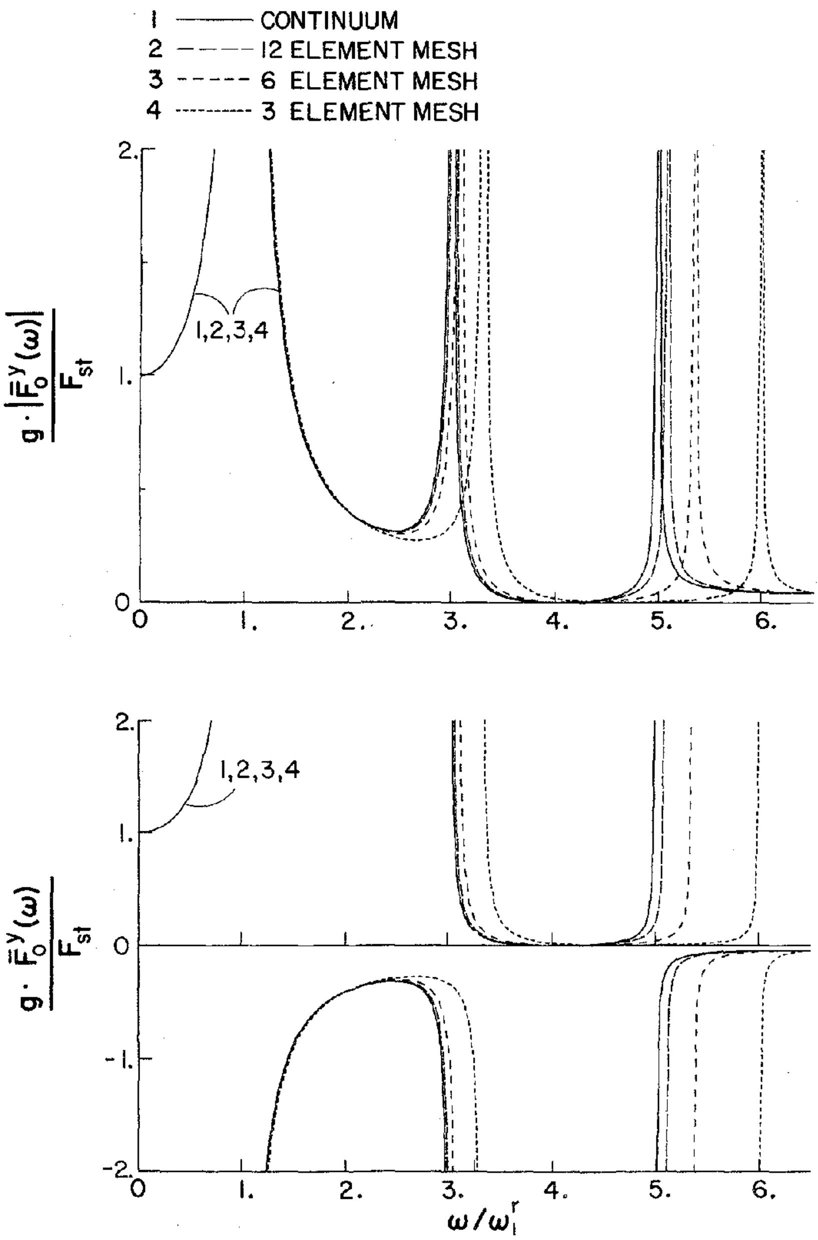

FIG. 3.8 HYDRODYNAMIC FORCE ON A RIGID DAM DUE TO HARMONIC, VERTICAL GROUND MOTION. FOUNDATION IS ASSUMED RIGID.

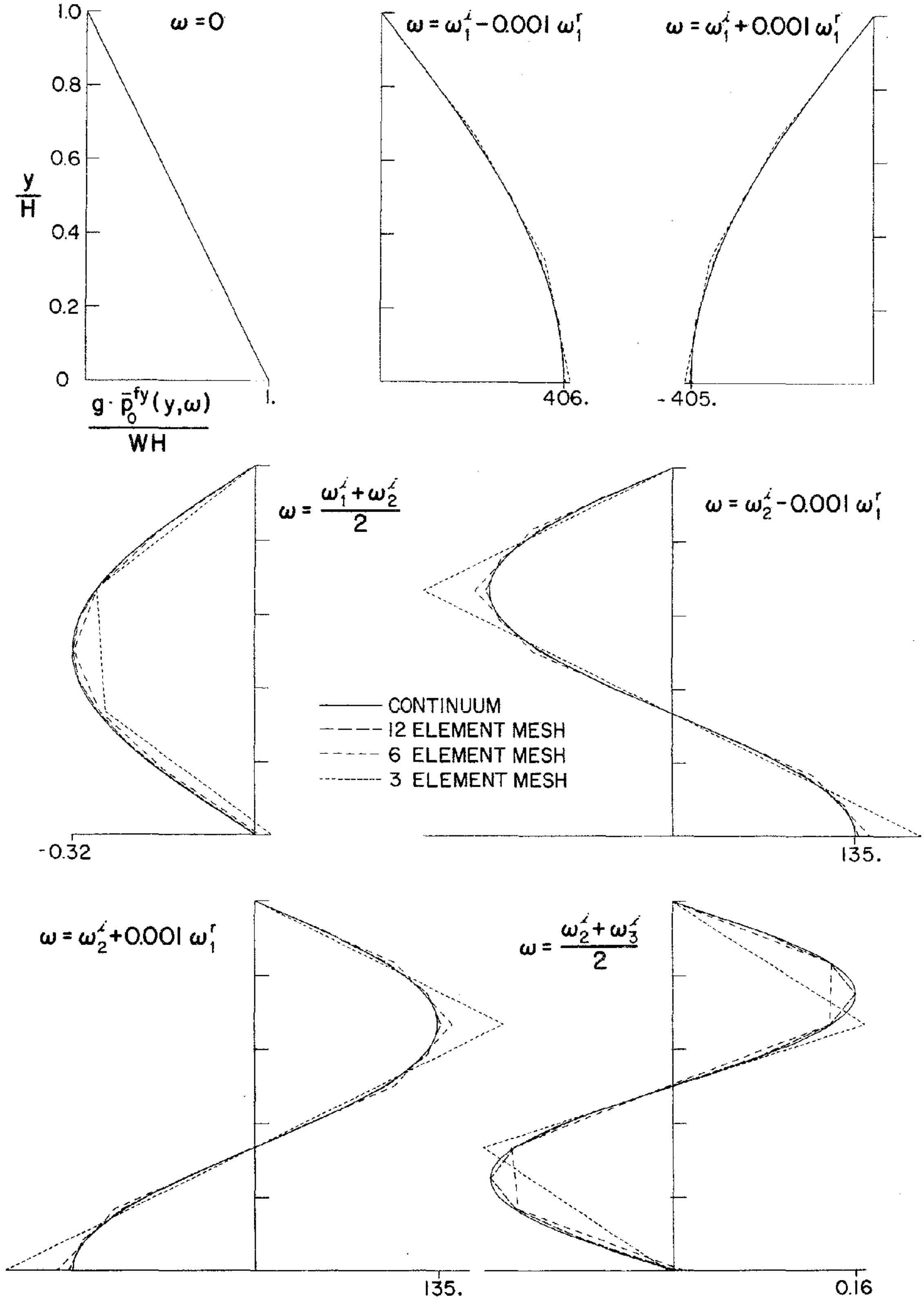

FIG. 3.9 HYDRODYNAMIC PRESSURES ON A RIGID DAM DUE TO HARMONIC, VERTICAL GROUND MOTION AT SELECTED EXCITATION FREQUENCIES. FOUNDATION IS ASSUMED RIGID.

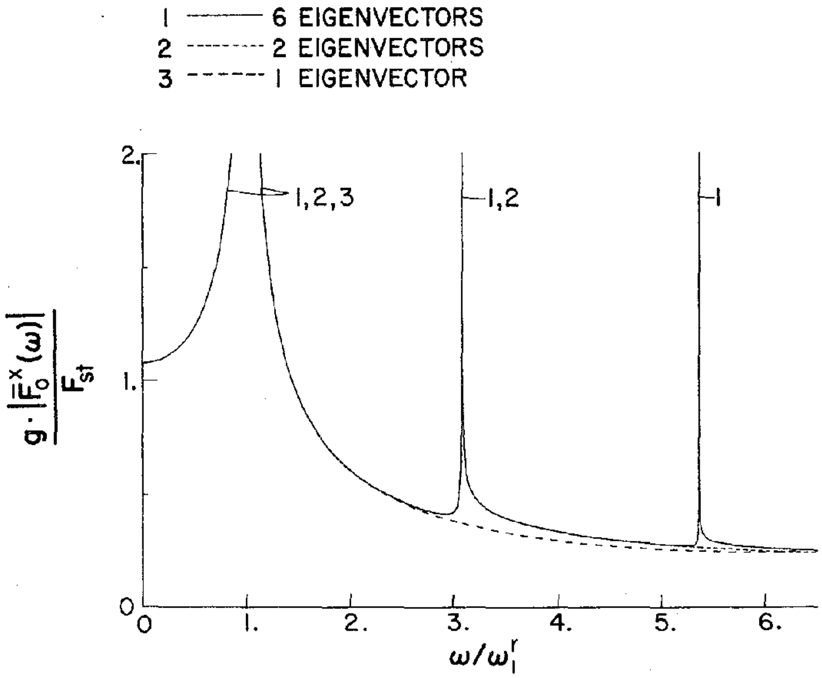

(a) HORIZONTAL GROUND MOTION

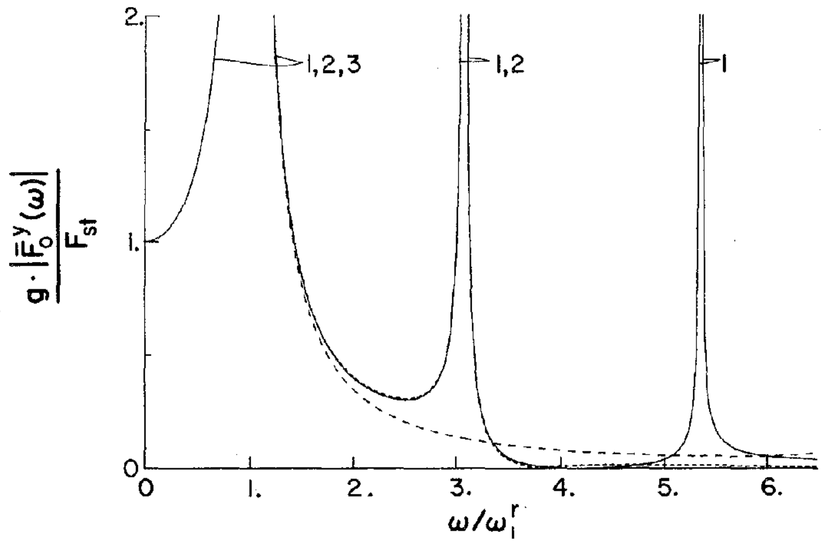

(b) VERTICAL GROUND MOTION

FIG. 3.10 HYDRODYNAMIC FORCE ON A RIGID DAM DUE TO HARMONIC GROUND MOTION COMPUTED WITH VARIABLE NUMBERS OF EIGENVECTORS. FOUNDATION IS ASSUMED RIGID.

observations. Thus, the number of eigenvectors included in an analysis can be less than the maximum and depends on the range of excitation frequency required. The shape of the acceleration distribution is another factor; non-uniform accelerations tend to excite higher eigenvectors so more need be included.

The problems of Figs. 3.5a and b are also solved with damping incorporated into the acceleration boundary condition along the reservoir floor to approximately account for fluid-foundation interaction as discussed in Sec. 2.5. a_y^i is now a free-field acceleration, and the reflection coefficient α_r is chosen as .85. $\bar{F}_o^\ell(\omega)$ vs. ω curves are presented in Figs. 3.11 and 3.12 for horizontal and vertical ground motions, respectively. Continuum solutions are from Appendix E, while the finite element results were obtained with Eq. 3.39 and the twelve element mesh of Fig. 3.5c with all twelve eigenvectors included in $\underline{\Psi}$. Agreement between the curves is comparable to that obtained for the corresponding curves of Figs. 3.6 and 3.8 for the rigid fluid foundation. Note that responses accounting for fluid-foundation interaction are bounded functions of excitation frequency ω and complex valued for $\omega > 0$. For the horizontal ground motion case (Fig. 3.11), finite real and imaginary peaks replace the infinite real and imaginary responses of Fig. 3.6. And for vertical ground motion (Fig. 3.12), finite real peaks replace the infinite real responses of Fig. 3.8, and new imaginary peaks appear centrally located over the ω_n^i. The behavior for vertical ground motion is typical of that for finite fluid domains.

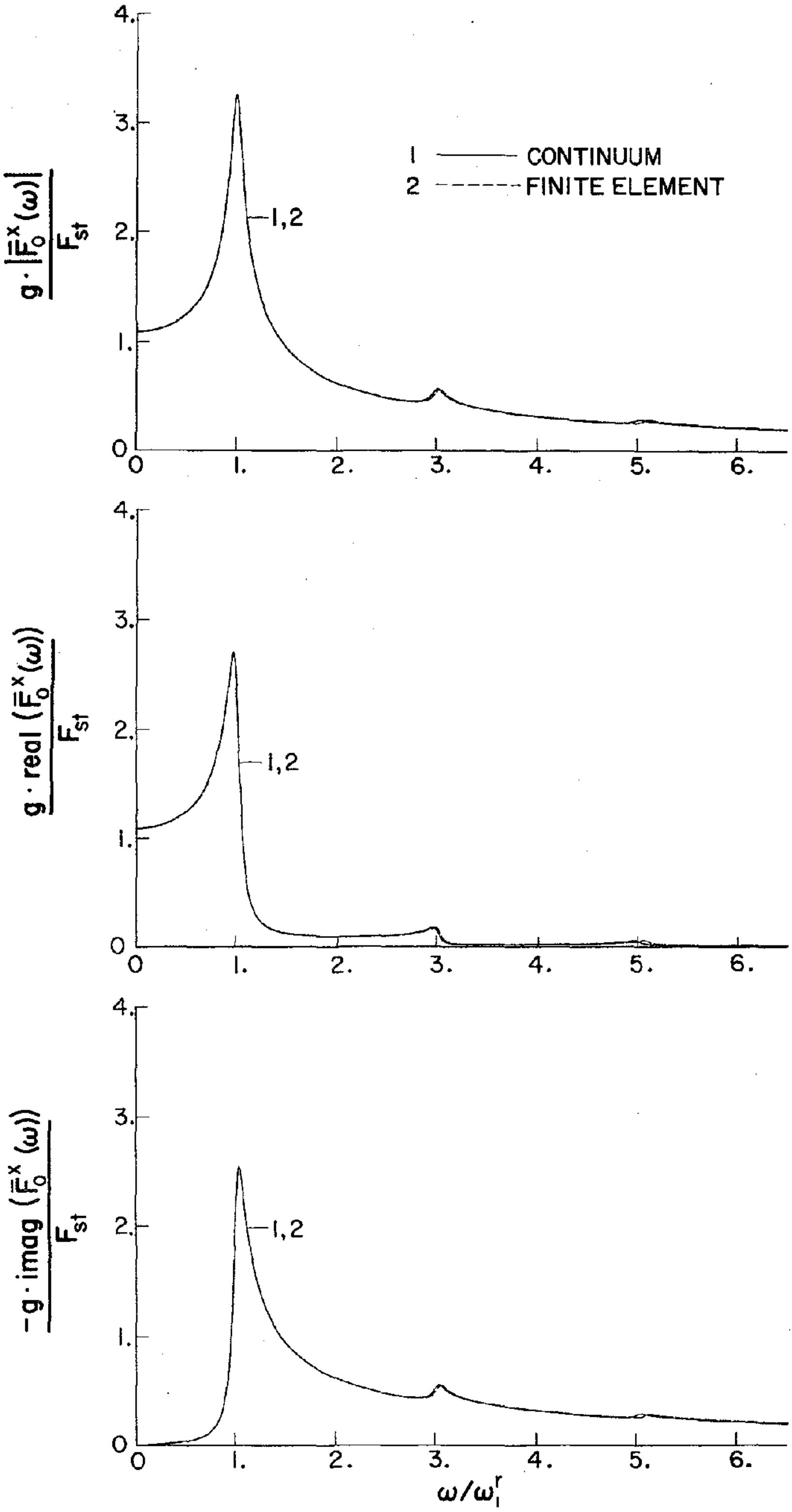

FIG. 3.11 HYDRODYNAMIC FORCE ON A RIGID DAM DUE TO HARMONIC, HORIZONTAL GROUND MOTION. FLUID-FOUNDATION INTERACTION IS INCLUDED.

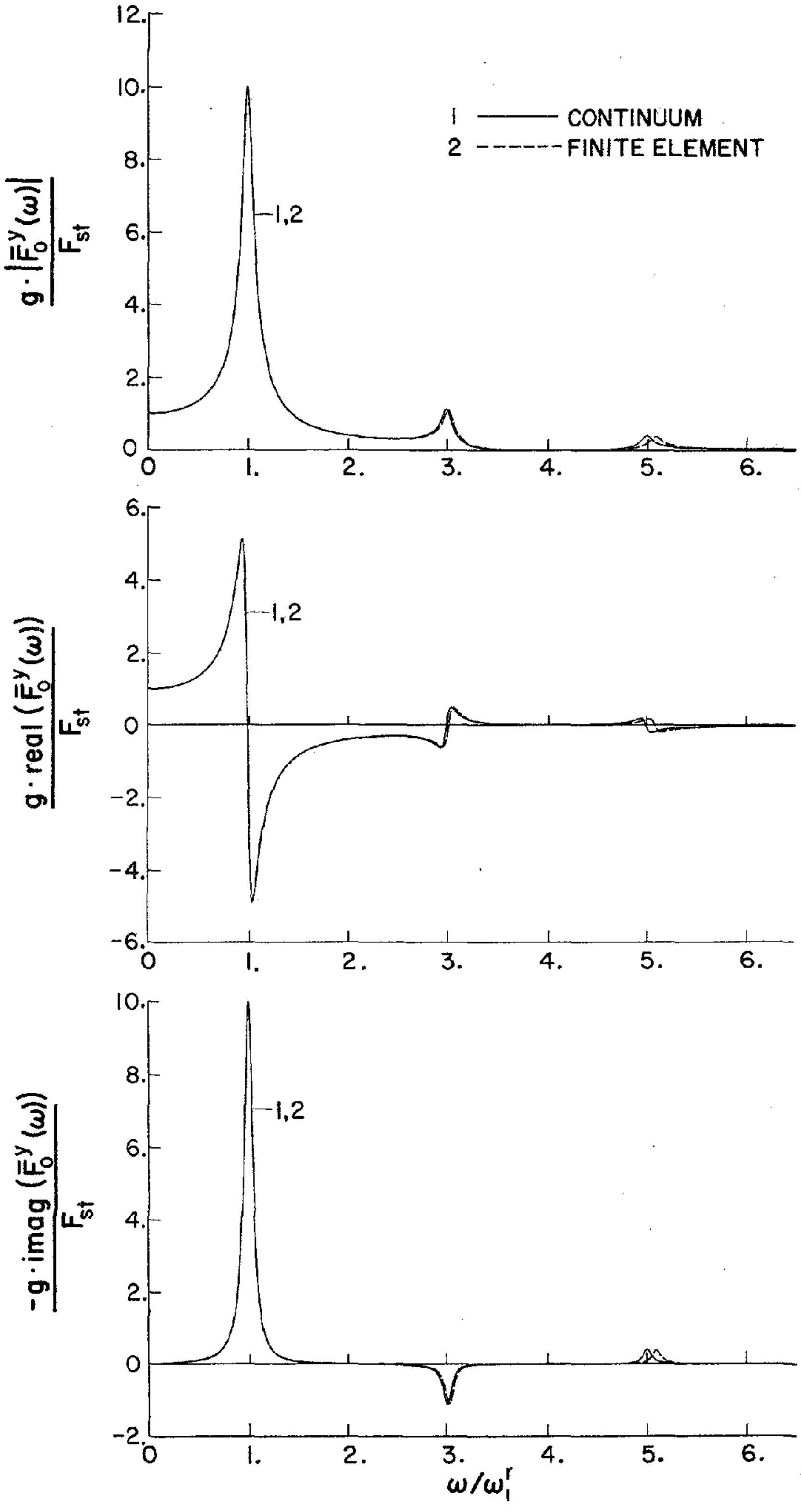

FIG. 3.12 HYDRODYNAMIC FORCE ON A RIGID DAM DUE TO HARMONIC, VERTICAL GROUND MOTION. FLUID-FOUNDATION INTERACTION IS INCLUDED.

3.6.2 Infinite fluid domain with sloped dam-fluid interface

As shown in Fig. 3.13 the dam-fluid interface slopes outward at slope β:1; the depth of the fluid domain is constant beyond the toe of the dam. The accelerations in Figs. 3.13a and b result from harmonic ground accelerations = $e^{i\omega t}$ in horizontal and vertical directions, respectively, with the dam and foundation assumed rigid. For an excitation frequency of zero, the incompressible water case, independent solutions to the problems of Figs. 3.13a and b exist and can be compared with finite element results from Eq. 3.39. For the horizontal motion case of Fig. 3.13a, Fig. 3.14 shows the pressure distribution $\bar{p}_0^{fx}(s,0)$ along the dam face, normalized with wH, for β = .5, 1, 2. Solid lines are an integral equation solution obtained by conformal mapping techniques (13). Results from Eq. 3.39 $(q = 0)$ using the mesh of Fig. 3.13c with all six eigenvectors are also shown. Agreement is close. Pressures due to vertical ground motion (Fig. 3.13b) vary linearly with depth and are independent of β. The finite element analysis leads to exact results (Fig. 3.14).

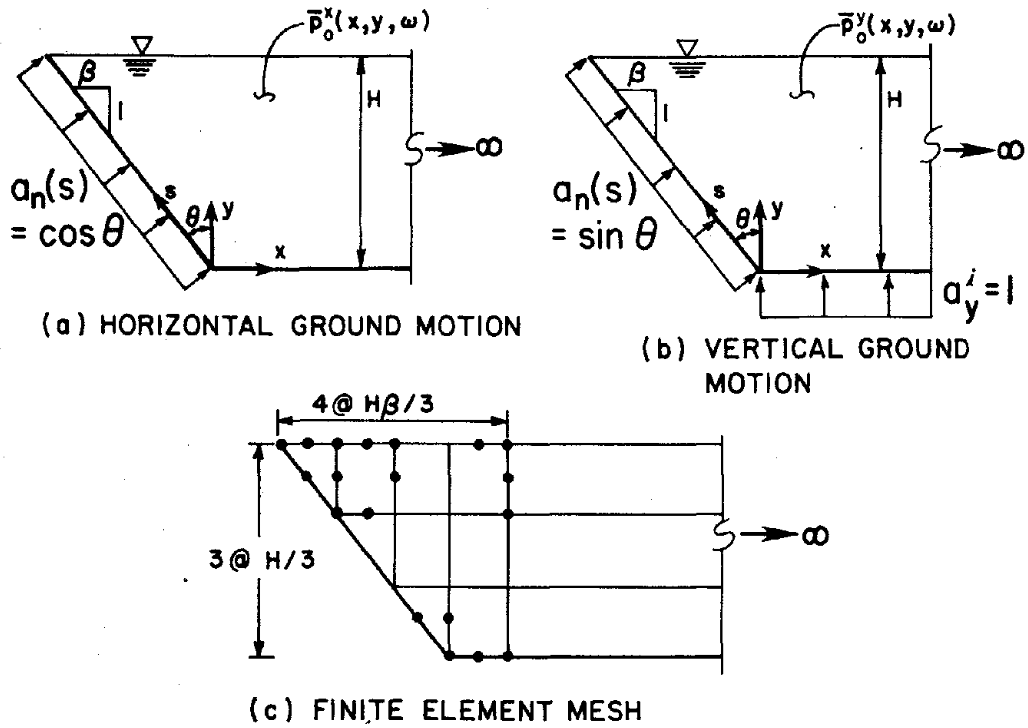

FIG. 3.13 INFINITE FLUID DOMAIN WITH SLOPED DAM-FLUID INTERFACE SUBJECTED TO HARMONIC GROUND MOTIONS WITH RIGID DAM

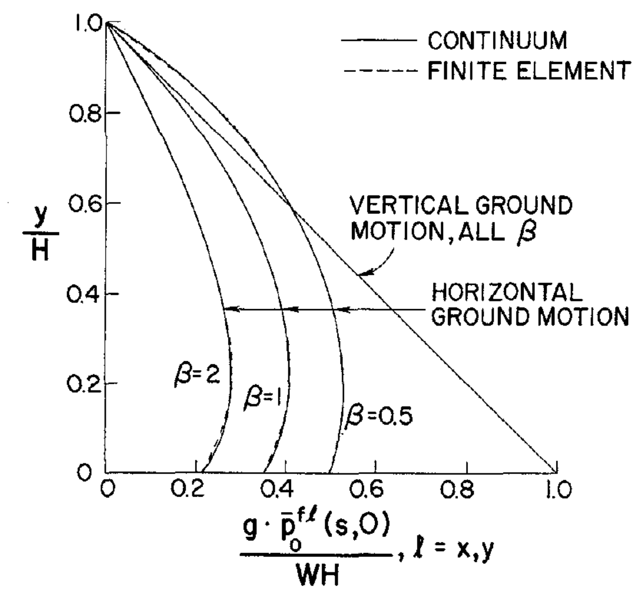

FIG. 3.14 HYDRODYNAMIC PRESSURE ON A SLOPED, RIGID DAM AT AN EXCITATION FREQUENCY OF ZERO. FOUNDATION IS ASSUMED RIGID.

4. HYDRODYNAMIC EFFECTS IN RESPONSE OF CONCRETE GRAVITY DAMS

4.1 Systems, Ground Motion and Outline of Analysis

The dam monolith is idealized as a triangle with vertical upstream face and downstream face with slope of 0.8:1. In order to study the effects of fluid domain geometry on the dam response, three different idealized shapes are considered for the reservoir. These three shapes are shown in Fig. 4.1, and they illustrate each of the types discussed in Chapter 3: infinite with constant depth, finite, and infinite with variable depth. The water depth H at the upstream face of the dam is the same for the three fluid domains and equals the dam height H_d.

Ground motions in the horizontal and vertical directions are considered. A modified vertical ground motion is also employed for the infinite fluid domain of constant depth; the vertical excitation is applied to the dam and only a finite length L_e of the reservoir floor adjacent to the dam.

The finite element discretization of the dam (Fig. 4.2a) employs plane stress elements with quadratic shape functions. Properties chosen for the mass concrete of the dam are elastic modulus $E_d = 5 \times 10^6$ psi, unit weight $w_d = 155$ pcf, and Poisson's ratio $\nu = .17$. The damping ratio for all modes of vibration of the dam $\xi_j = 5\%$. Finite element discretizations of the fluid domains are shown in Figs. 4.2b, c and d, also employing two-dimensional finite elements with quadratic shape functions. At the dam-fluid interface, the finite element mesh for the dam coincides with the fluid domain

Preceding page blank

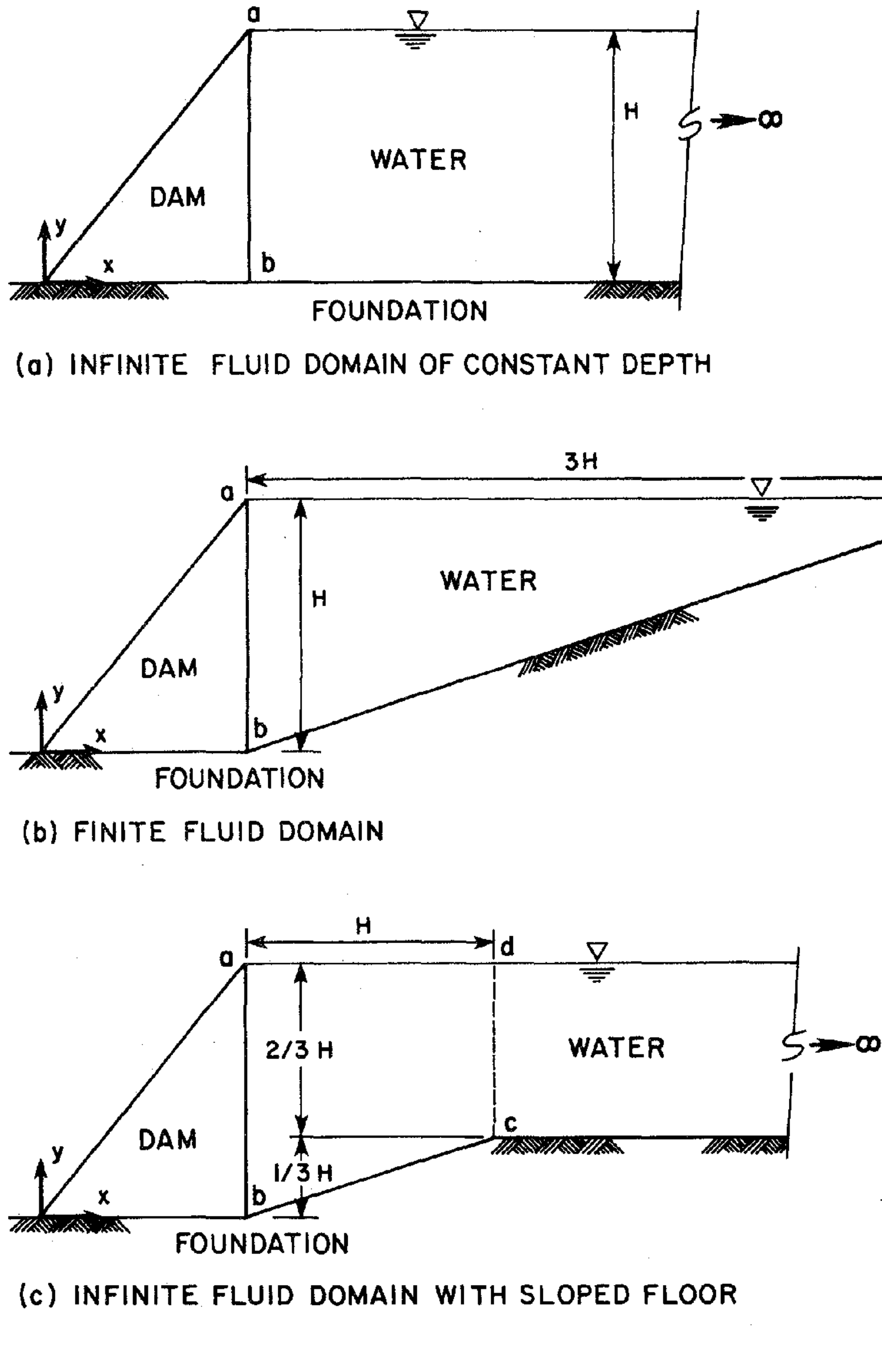

FIG. 4.1 CONCRETE GRAVITY DAM-FLUID SYSTEMS

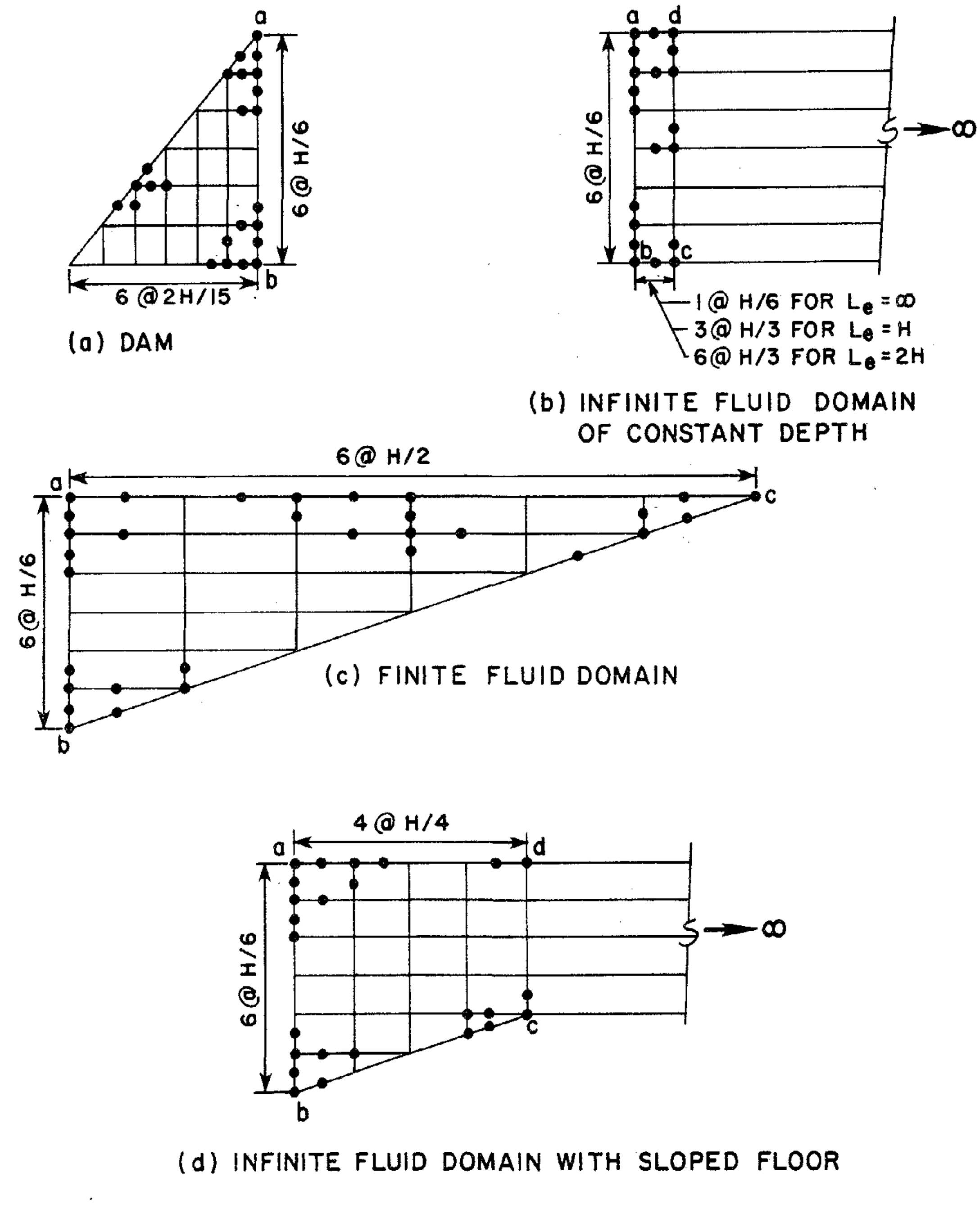

FIG. 4.2 FINITE ELEMENT MESHES

meshes. The water has unit weight $w = 62.4$ pcf and compression wave velocity $C = 4720$ ft/sec. The foundation unit weight w_r and compression wave velocity C_r are chosen so that the reflection coefficient α_r computed from Eq. 2.38a equals .85. The damping coefficient q along the reservoir floor is then given by Eq. 2.38b.

Responses of the dam-fluid system to harmonic ground motions were computed by the procedure of Chapters 2 and 3. The vectors $\underline{\bar{Q}}_j^f(\omega)$ and $\underline{\bar{Q}}_0^{f\ell}(\omega)$ of Eq. 2.24 were obtained as described in Sec. 3.5 from hydrodynamic pressure solutions $\underline{\bar{p}}_j^f(\omega)$ and $\underline{\bar{p}}_0^{f\ell}(\omega)$ of Eq. 3.6 (finite fluid domain) or Eq. 3.39 (infinite fluid domains). The full set of eigenvectors $\underline{\psi}_n$ were employed in Eq. 3.39, which for the infinite fluid domains of constant depth and sloped floor are 12 and 8. For partial vertical ground motion, $\underline{D}^{\ell}$ in Eq. 3.39 is a zero vector. The dam responses were obtained by combining responses of the first six modes of vibration of the dam computed from Eq. 2.23. The frequencies ω_j and shapes $\underline{\phi}_j$ of these modes appear in Fig. 4.3.

The analyses of this chapter were carried out with the computer program EADFS (14). Sample solution times for computing the frequency responses of the dam are presented in Appendix F.

4.2 Hydrodynamic Forces on Rigid Dams

The absolute value (or modulus) of $\bar{F}_0^{\ell}(\omega)$, the complex frequency response function for hydrodynamic force on a rigid dam due to harmonic ground acceleration = $e^{i\omega t}$ is presented. $\bar{F}_0^{\ell}(\omega)$ is the resultant of the pressures $\underline{\bar{p}}_0^{f\ell}(\omega)$ (Sec. 3.5) on the upstream dam face. For each of the three fluid domains of Fig. 4.1, the hydrodynamic forces presented are due to horizontal ground motion (Fig. 4.4)

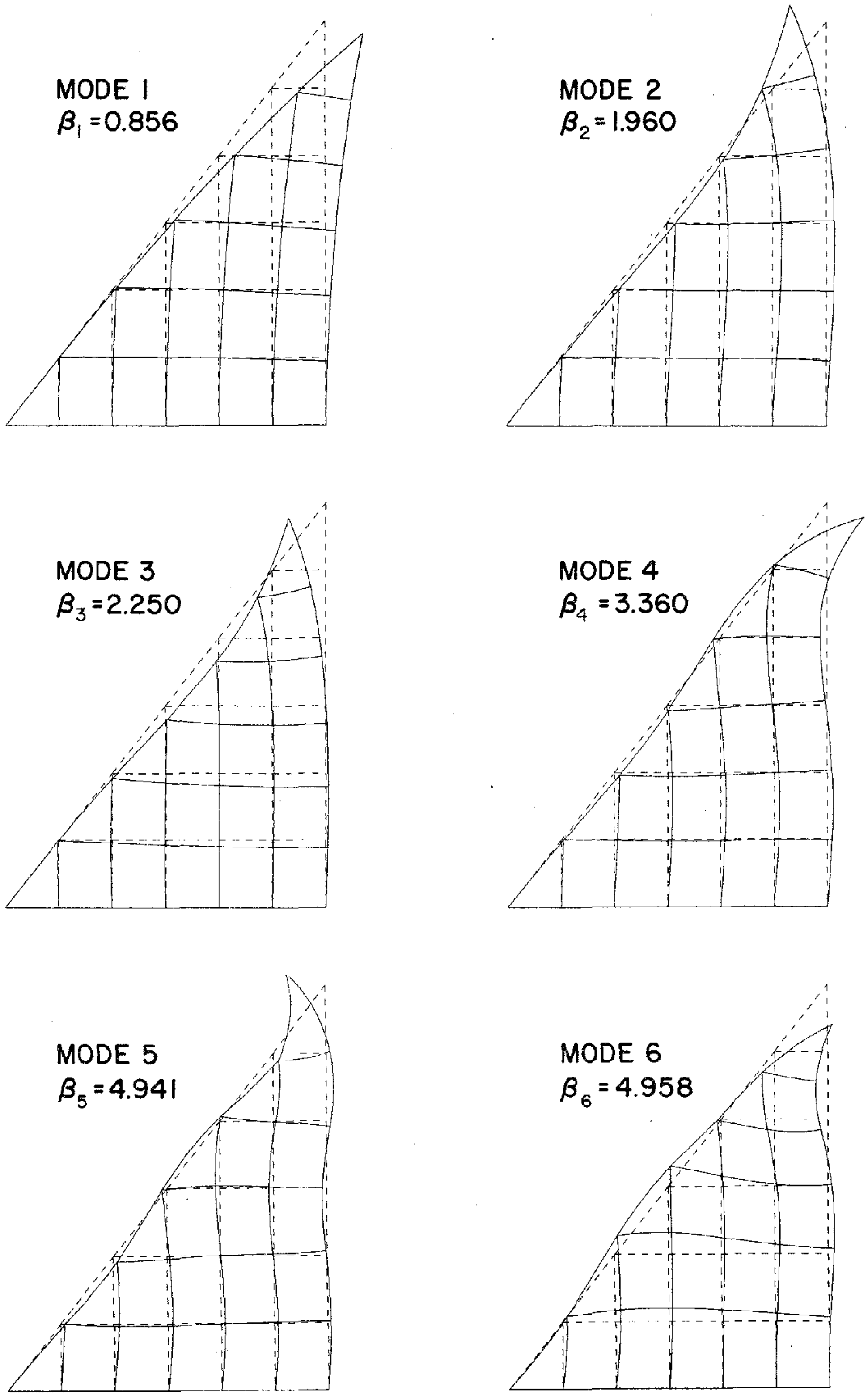

FIG. 4.3 MODE SHAPES OF THE DAM. NATURAL FREQUENCIES ARE

$$\omega_j = \beta_j \frac{1}{H_d} \sqrt{Eg/w_d} \, .$$

and vertical ground motion over the entire reservoir floor (Fig. 4.5), with fluid-foundation interaction both neglected and included. For the infinite fluid domain of constant depth, the hydrodynamic force due to a partial vertical excitation of the reservoir floor is presented in Fig. 4.6. Fluid-foundation interaction is neglected in this analysis. $\bar{F}_0^{\ell}(\omega)$ is normalized with the hydrostatic force $F_{st} = \frac{1}{2} wH^2$ and the excitation frequency ω with $\omega_1^r = \pi C/2H$. When presented in this form, the results apply to similarly shaped fluid domains of any depth.

4.2.1 Water compressibility effects

Excluding effects of water compressibility, the hydrodynamic force on a rigid dam is independent of excitation frequency and equal to the zero frequency ordinates of the response curves in Figs. 4.4 and 4.5. $\bar{F}_0^x(0)$ due to horizontal ground motion depends only slightly on the shape of the fluid domain, and $\bar{F}_0^y(0)$ due to vertical ground motion is independent of the shape because the hydrodynamic pressures along the dam face have the same linear distribution.

The frequency variation of hydrodynamic force on the dam is influenced greatly by the shape of the fluid domain when effects of water compressibility are considered. For the infinite fluid domain of constant depth, the hydrodynamic forces due to both directions of ground motion are unbounded at excitation frequencies equal to its eigenfrequencies ω_n^{i} (Sec. 3.3). The resonant amplitudes are greater over wider frequency intervals for vertical ground motion (Fig. 4.5a) than horizontal ground motion (Fig. 4.4a). Examination of Eqs. 3.28

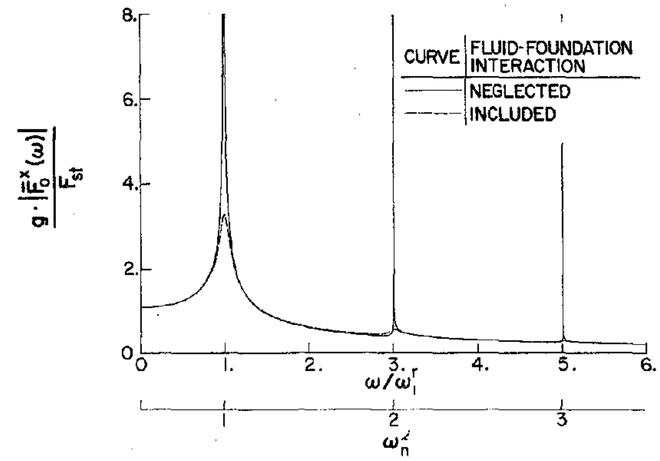

(a) INFINITE FLUID DOMAIN OF CONSTANT DEPTH

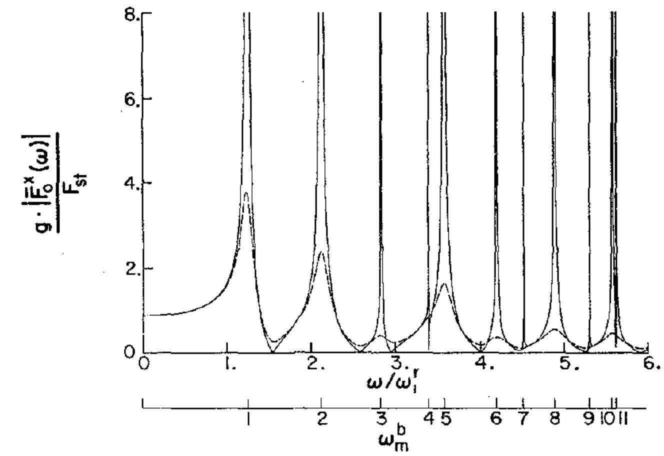

(b) FINITE FLUID DOMAIN

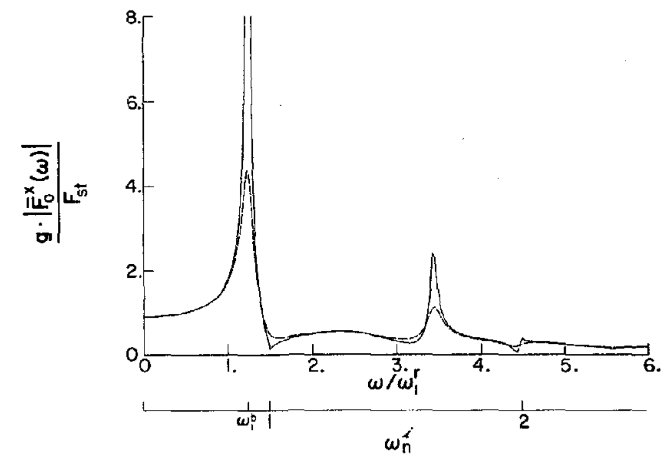

(c) INFINITE FLUID DOMAIN WITH SLOPED FLOOR

FIG. 4.4 HYDRODYNAMIC FORCE ON A RIGID DAM DUE TO HARMONIC, HORIZONTAL GROUND MOTION

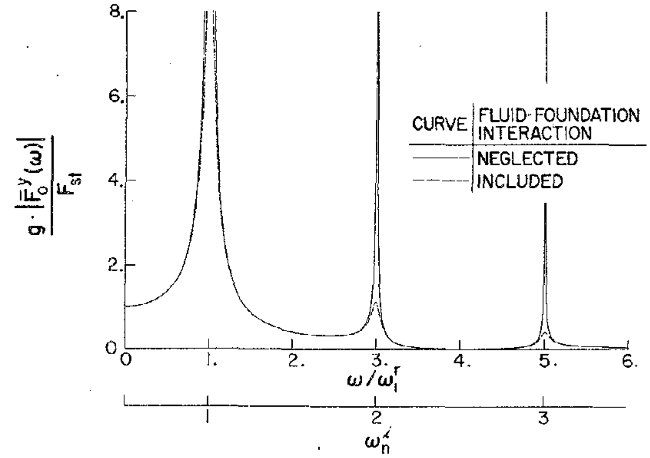

(a) INFINITE FLUID DOMAIN OF CONSTANT DEPTH

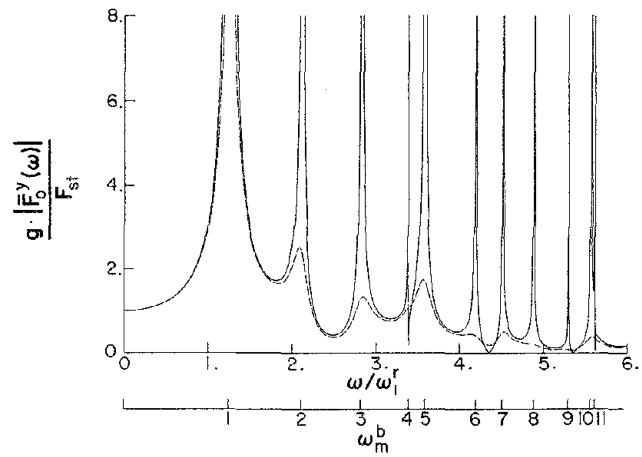

(b) FINITE FLUID DOMAIN

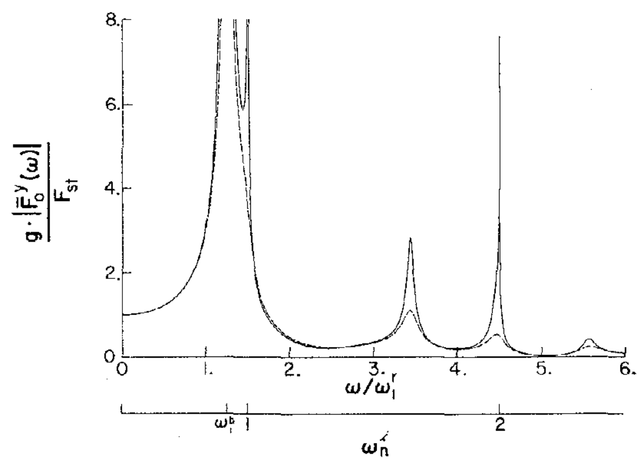

(c) INFINITE FLUID DOMAIN WITH SLOPED FLOOR

FIG. 4.5 HYDRODYNAMIC FORCE ON A RIGID DAM DUE TO HARMONIC, VERTICAL GROUND MOTION and 3.32 (with $q = 0$) reveals that in the neighborhood of ω_n^i, $\bar{F}_o^x(\omega)$ due to horizontal ground motion is controlled by the term $\left(\omega^2 - (\omega_n^i)^2\right)^{-1/2}$, and $\bar{F}_o^y(\omega)$ due to vertical ground motion by $\left(\omega^2 - (\omega_n^i)^2\right)^{-1}$. The second term approaches infinity as ω approaches ω_n^i faster than the first term; in fact, the ratio $\bar{F}_o^y(\omega)/\bar{F}_o^x(\omega)$ of hydrodynamic forces due to the two directions of ground motion approaches infinity. The hydrodynamic force due to horizontal ground motion is real valued at excitation frequencies below ω_1^i and complex valued at higher frequencies, whereas the force due to vertical ground motion is real valued at all excitation frequencies.

In the case of the finite fluid domain, the hydrodynamic force due to horizontal or vertical ground motion (Figs. 4.4b and 4.5b) is unbounded at excitation frequencies equal to its eigenfrequencies ω_m^b (Sec. 3.2), which are more numerous than the ω_n^i of the infinite fluid domain of constant depth. The resonant frequencies ω_m^b become more densely populated in the low frequency range as the fluid domain length is increased, but they always exceed ω_1^i because the triangularly shaped domain always has an average depth smaller than the domain of constant depth H. Examination of Eq. 3.11 reveals that for the finite fluid domain, the hydrodynamic force due to either direction of ground motion is controlled in the vicinity of ω_m^b by $\left(\omega^2 - (\omega_m^b)^2\right)^{-1}$, similar to the term above for the infinite fluid domain of constant depth subjected to vertical ground motion. The hydrodynamic force due to either direction of ground motion is a real valued function of frequency.

The hydrodynamic force on a rigid dam with the infinite fluid domain with sloped floor is presented in Figs. 4.4c and 4.5c. According to the discussion in Sec. 3.4, the hydrodynamic force is real valued at excitation frequencies below ω_1^{ℓ} and complex valued at higher frequencies. The force due to horizontal ground motion is bounded at excitation frequencies equal to ω_n^{ℓ} (the eigenfrequencies of the infinite region of depth $\frac{2}{3}$ H), but unbounded at a frequency ω_1^b (Fig. 4.4c) which is less than ω_1^{ℓ}. The response in the vicinity of ω_1^b is real valued and has the resonant characteristics of a finite fluid domain, hence the similar notation. This eigenfrequency of the complete fluid domain (Sec. 3.4) is due to the sloped portion of the reservoir floor which increases the average fluid depth to a value greater than $\frac{2}{3}$ H. The resonant peaks at higher frequencies in Fig. 4.4c are bounded because of fluid-radiation damping. The hydrodynamic force due to vertical ground motion displays response characteristics similar to those above, but with additional unbounded responses at excitaton frequencies equal to ω_n^{ℓ}. These unbounded responses are due to the acceleration of the entire infinite length of the reservoir floor; i.e., the acceleration vector $\underline{D}^{\ell}$ on the right side of Eq. 3.39 is non-zero for vertical ground motion. Because the geometries of the finite fluid domain and the infinite fluid domain with sloped floor (Figs. 4.1b and c) are similar to a distance H from the dam, the hydrodynamic forces associated with the two fluid domains display similar resonse characteristics for excitation frequencies up to the frequencies ω_1^b, which are nearly the same as well for the two fluid domains.

4.2.2 Partial vertical excitation of the reservoir floor

The hydrodynamic force on a rigid dam due to a vertical acceleration over a length L_e of the floor of the infinite fluid domain of constant depth is presented in Fig. 4.6. The frequency response functions shown are for $L_e = H$, 2H, and ∞. Fluid-foundation interaction is not included in this analysis. The force at excitation frequencies equal to the eigenfrequencies ω_n^{ℓ} is unbounded even when L_e is finite, but the resonant peaks are narrower indicating a reduced response. In the vicinity of ω_n^{ℓ}, the hydrodynamic force is controlled by the term $\left(\omega^2 - (\omega_n^{\ell})^2\right)^{-1/2}$ when L_e is finite, in contrast to the controlling term $\left(\omega^2 - (\omega_n^{\ell})^2\right)^{-1}$ when the ground motion is over the entire reservoir floor. Thus, near ω_n^{ℓ} the frequency variation of hydrodynamic force due to vertical ground motion over a partial length of the reservoir floor is similar to that due to horizontal ground motion discussed in Sec. 4.2.1.

4.2.3 Fluid-foundation interaction effects

As shown in Figs. 4.4 and 4.5, the radiation damping associated with fluid-foundation interaction reduces the hydrodynamic force amplitudes. The reductions are primarily in the vicinities of the resonant frequencies, resulting in bounded responses at these frequencies for the three fluid domains considered and for both directions of ground motion. Due to fluid-foundation interaction, the hydrodynamic forces are complex valued for all excitation frequencies above zero.

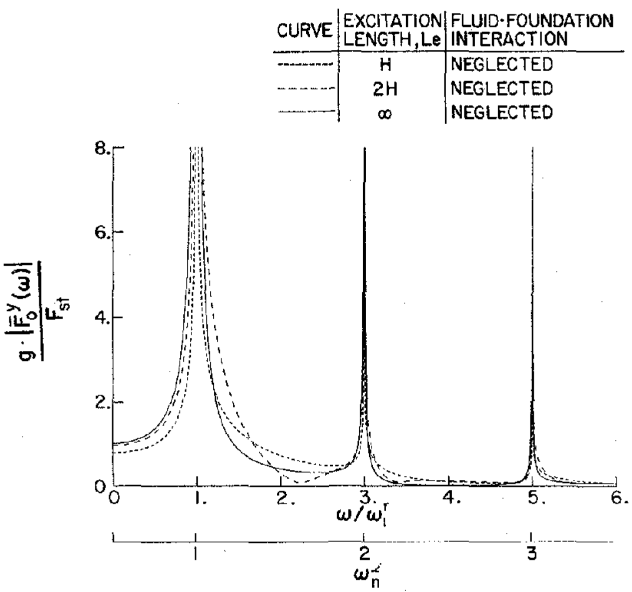

FIG. 4.6 HYDRODYNAMIC FORCE ON A RIGID DAM DUE TO HARMONIC, PARTIAL VERTICAL GROUND MOTION. FLUID DOMAIN IS INFINITE OF CONSTANT DEPTH.

4.3 Dam Responses to Horizontal Ground Motion

The responses of the dam to harmonic ground acceleration = $e^{i\omega t}$ in the horizontal direction are presented for four conditions: dam without water, dam with full reservoir considering water compressibility in one case but not the other (fluid-foundation interaction neglected), and dam with full reservoir including both water compressibility and fluid-foundation interaction. These analyses were performed for each of the three fluid domains of Fig. 4.1. Results are presented in the form of complex frequency response functions for accelerations of the dam relative to the ground acceleration (Fig. 4.7). The absolute value (or modulus) of $\ddot{\bar{r}}^{x}(\omega)$, the horizontal component of acceleration at the dam crest, is plotted against the normalized excitation frequency parameter ω/ω_1, where ω_1 = the fundamental frequency of the dam. When presented in this form, the results apply to similarly shaped dam-fluid systems of any height. Furthermore, if the reservoir is empty or if the water is assumed incompressible, the results are also independent of the concrete elastic modulus E_d.

4.3.1 Dam-fluid interaction effects

The response of the dam without water is representative of a multi-degree-of-freedom system with constant mass, stiffness, and damping parameters. The presence of water, assumed to be incompressible, provides added masses $\underset{-}{\bar{Q}}{}_j^f(0)$ and added load $\underset{-}{\bar{Q}}{}_0^{fx}(0)$. Similar to the hydrodynamic force $\bar{F}_0^x(0)$ on a rigid dam (Fig. 4.4a), the added masses and added load are essentially unaffected by the

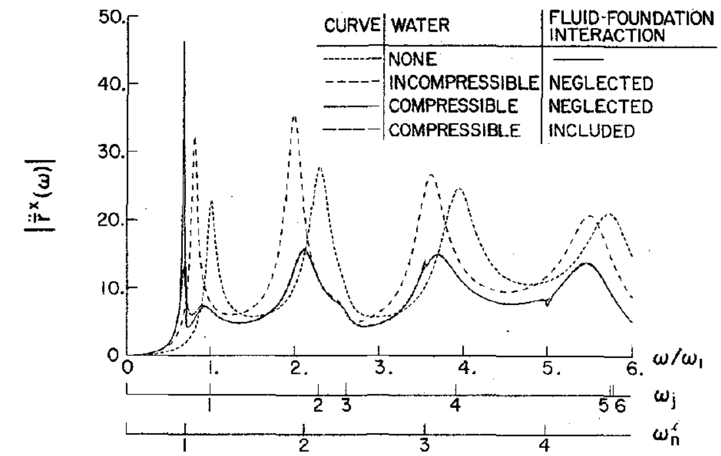

(a) INFINITE FLUID DOMAIN OF CONSTANT DEPTH

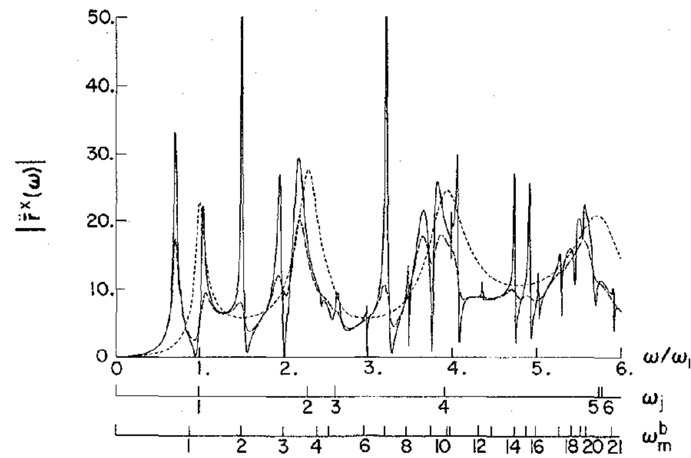

(b) FINITE FLUID DOMAIN

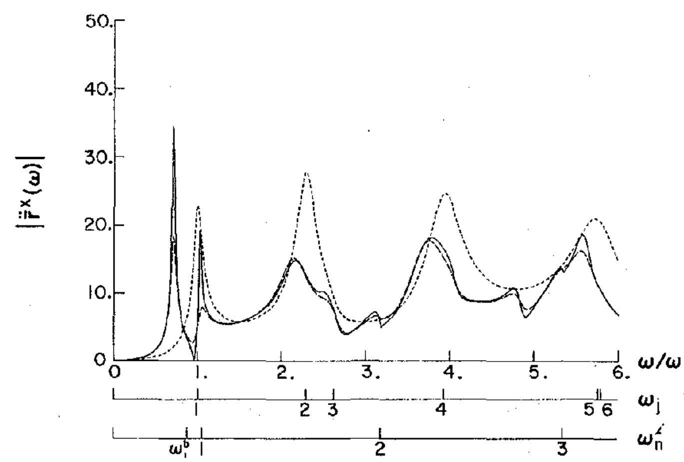

(c) INFINITE FLUID DOMAIN WITH SLOPED FLOOR

FIG. 4.7 HORIZONTAL COMPONENT OF DAM CREST ACCELERATION DUE TO HARMONIC, HORIZONTAL GROUND MOTION shape of the fluid domain. Consequently, if water compressibility effects are neglected, the dam response is also essentially independent of fluid domain shape, and only responses of the dam with the infinite fluid domain of constant depth are presented (Fig. 4.7a). The resonant frequencies of the system are lowered and the resonant amplitudes are increased.

When water compressibility is considered, the added masses $\bar{\underline{Q}}_j^f(\omega)$ and added load $\bar{\underline{Q}}_o^{fx}(\omega)$ vary with excitation frequency in a manner similar to the frequency variation of $\bar{F}_0^x(\omega)$ as discussed in Sec. 4.2.1. At excitation frequencies where the $\bar{\underline{Q}}^f(\omega)$ vectors are unbounded, the dam responses can only be computed from Eq. 2.23 as limit solutions. For horizontal ground motion, these limits are finite because the ratios of the terms of $\bar{\underline{Q}}_o^{fx}(\omega)$ to the terms of $\bar{\underline{Q}}_j^f(\omega)$ approach finite values. Thus, dam responses to horizontal ground motion, with any of the fluid domains considered, are bounded functions of excitation frequency.

For the infinite fluid domain of constant depth, inclusion of water compressibility shifts the first resonant peak to a frequency below ω_1^ℓ, a greater shift with a greater increase in amplitude than caused by incompressible water (Fig. 4.7a). These increases are due to the greater hydrodynamic added mass and added load. At excitation frequencies above ω_1^ℓ, the $\bar{\underline{Q}}^f(\omega)$ vectors are complex valued. The imaginary part of the added mass vectors $\bar{\underline{Q}}_j^f(\omega)$ represents fluid radiation damping which adds to the damping of the dam and reduces the acceleration responses below those without water or with incompressible water.

When water compressibility is considered for the finite fluid domain, the acceleration response of the dam displays many sharp spikes throughout the entire frequency range (Fig. 4.7b). For finite fluid domains, the hydrodynamic added mass and added load are real valued functions of excitation frequency which are unbounded at frequencies equal to ω_m^b. Because the added mass in this case has no imaginary component, the fluid domain adds none of the radiation damping which occurs in an infinite fluid domain. The resulting dam responses are affected greatly by the rapid variations with excitation frequency of the hydrodynamic added mass and added load.

The acceleration response of the dam with the infinite fluid domain with sloped floor is similar to its response with the finite fluid domain in the lower part of the frequency range (Figs. 4.7b and c), because the $\underline{\bar{Q}}^f(\omega)$ vectors vary with frequency in a similar manner for the two fluid domains. This similarity was noted in Sec. 4.2.1 with $\bar{F}_0^x(\omega)$. At excitation frequencies above ω_1^{ℓ}, fluid radiation damping reduces the acceleration responses below those without water or with incompressible water, similar to the reductions occurring with the infinite fluid domain of constant depth.

4.3.2 Fluid-foundation interaction effects

The effects of fluid-foundation interaction on the acceleration response of the dam to horizontal ground motion are evident from the two results of Fig. 4.7 which include water compressibility, and include fluid-foundation interaction in one case but not the other. Fluid-foundation interaction considerably reduces the dam accelerations at excitation frequencies below ω_1^{ℓ} if the fluid domain is infinite (Figs. 4.7a and c) and throughout the entire frequency range when the fluid domain is finite (Fig. 4.7b). These reductions are due to the foundation radiation damping associated with the imaginary component of the added mass vectors $\bar{Q}_j^f(\omega)$ and the smaller resonant amplitudes of the added load vector $\bar{Q}_0^{fx}(\omega)$. Fluid-foundation interaction has significant influence on the dam accelerations only in the frequency ranges where fluid radiation damping arising from an infinite extent of the reservoir does not exist.

Figure 4.7 also shows that the shape of the fluid domain has little influence on the dam accelerations when fluid-foundation interaction effects are considered. For all three fluid domains, the resonant responses of the dam including water compressibility and fluid-foundation interaction are reduced in amplitude below those without water and with incompressible water and have lower resonant frequencies.

4.4 Dam Responses to Vertical Ground Motion

The responses of the dam to harmonic ground acceleration = $e^{i\omega t}$ in the vertical direction over the entire reservoir floor are presented in Fig. 4.8 for four conditions: dam without water, dam with full reservoir considering water compressibility in one case but not the other (fluid-foundation interaction neglected), and the dam with full reservoir including both water compressibility and fluid-foundation interaction. These analyses were performed for each of

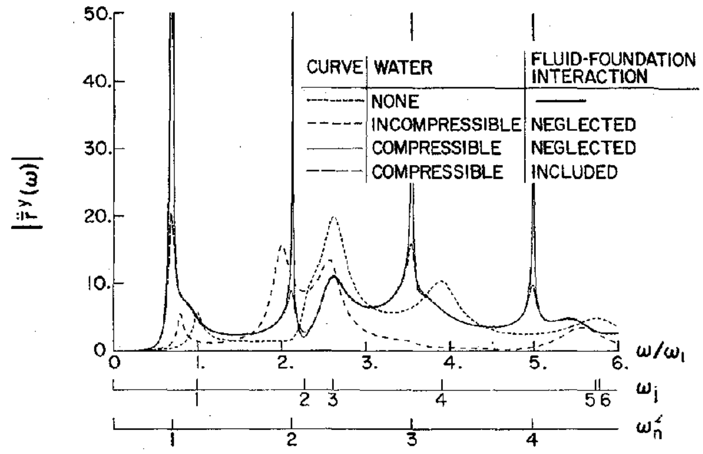

(a) INFINITE FLUID DOMAIN OF CONSTANT DEPTH

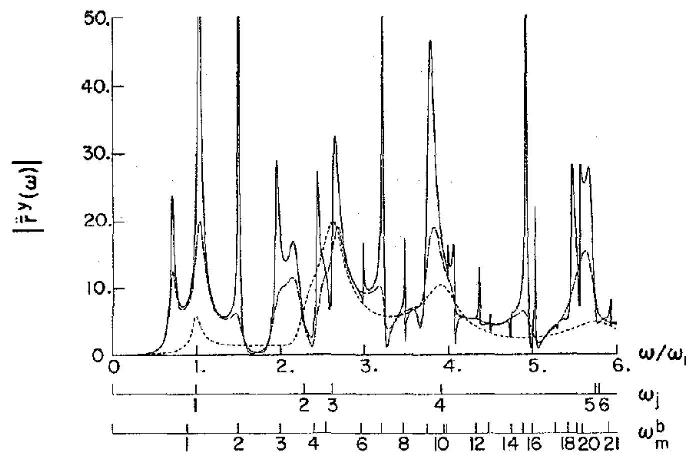

(b) FINITE FLUID DOMAIN

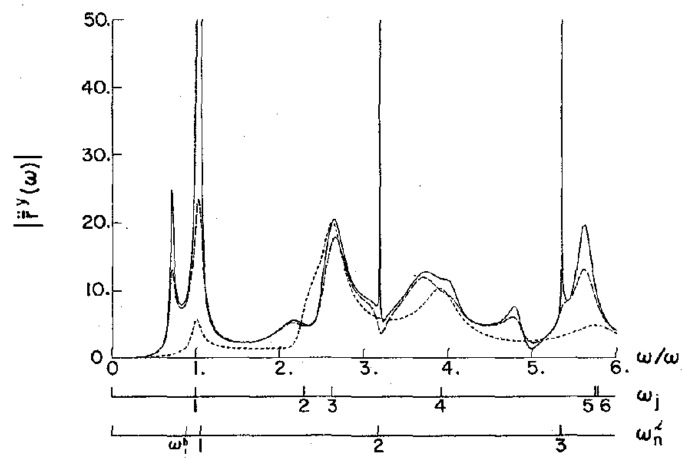

(c) INFINITE FLUID DOMAIN WITH SLOPED FLOOR

FIG. 4.8 HORIZONTAL COMPONENT OF DAM CREST ACCELERATION DUE TO HARMONIC, VERTICAL GROUND MOTION the three fluid domains of Fig. 4.1. Additionally, the response of the dam with the infinite fluid domain of constant depth to vertical ground motion, applied over a length L_e = H or 2H of the reservoir floor adjacent to the dam, is presented in Fig. 4.9. Fluid-foundation interaction is neglected in this analysis. The dam responses are presented as complex frequency response functions for accelerations relative to the ground acceleration. The absolute value (or modulus) of $\ddot{\tilde{r}}^y(\omega)$, the horizontal component of acceleration at the dam crest, is plotted against the normalized excitation frequency parameter ω/ω_1, where ω_1 = the fundamental frequency of the dam.

4.4.1 Dam-fluid interaction effects

The resonant amplitudes in the acceleration response of the dam without water to vertical ground motion are less than those due to horizontal ground motion except for the third mode of vibration (Fig. 4.3) which is dominant in vertical motion. If water is present and assumed incompressible, the hydrodynamic effects in the dam response to vertical ground motion are essentially independent of fluid domain shape, and only responses of the dam with the infinite fluid domain of constant depth are presented (Fig. 4.8a). The resonant amplitudes are increased in some cases and decreased in others, unlike the uniform increases that occur for horizontal ground motion (Fig. 4.7a) indicating some cancellation between the dam's inertia load and the hydrodynamic added load when the ground motion is vertical.

When water compressibility is considered and the fluid domain is infinite, the dam response is unbounded at excitation frequencies equal to ω_n^{ℓ} (Figs. 4.8a and c). At these frequencies the added mass and added load vectors $\bar{\underline{Q}}_j^{f}(\omega)$ and $\bar{\underline{Q}}_0^{fy}(\omega)$ are unbounded (similar to $\bar{F}_0^x(\omega)$ and $\bar{F}_0^y(\omega)$ of Secs. 4.2.1), and the limiting values of the dam response from Eq. 2.23 are also unbounded. At excitation frequencies below ω_1^{ℓ}, the resonant response of the dam to vertical ground motion exceeds that due to horizontal ground motion because of the greater hydrodynamic added load. At excitation frequencies above ω_1^{ℓ} and between the infinite spikes in Figs. 4.8a and c, fluid radiation damping limits the dam accelerations to about those without water. Even though responses at excitation frequencies equal to ω_n^{ℓ} approach infinity, they do so at a slow enough rate so that the areas under the unbounded peaks are finite. Thus, the Fourier Transform procedure of Sec. 2.4 for computing responses to arbitrary ground motions is applicable.

When water compressibility is considered and the fluid domain is finite, the acceleration responses to vertical ground motion display many sharp spikes throughout the entire frequency range (Fig. 4.8b), as does the response to horizontal ground motion. This similarity is due to the similar frequency variations of the hydrodynamic added loads for both directions of ground motion, as seen in Sec. 4.2.1 for $\bar{F}_0^x(\omega)$ and $\bar{F}_0^y(\omega)$. In the lower portion of the frequency range, the accelerations of the dam with the finite fluid domain are similar to those with the infinite fluid domain with sloped floor (Figs. 4.8b and c), which was also true of the acceleration respones to horizontal ground motion.

4.4.2 Partial vertical excitation of the reservoir floor

As noted in Sec. 4.4.1, the responses of dams with infinite fluid domains to vertical ground motion are unbounded at excitation frequencies equal to ω_n^{ℓ}. Figure 4.9 shows that for the infinite fluid domain of constant depth, these unbounded responses are reduced to bounded values if the vertical acceleration is limited to a finite length L_e of the reservoir floor adjacent to the dam. At the frequencies ω_n^{ℓ}, the added loads $\underline{\bar{Q}}_o^{fy}(\omega)$ resonate within narrower frequency bands when L_e is finite (similar to $\bar{F}_o^y(\omega)$ of Sec. 4.2.2) causing the limit solutions of Eq. 2.23 to be bounded. From Fig. 4.9, the acceleration responses decrease as L_e decreases, and large reductions occur in the vicinity of ω_1^{ℓ}.

4.4.3 Fluid-foundation interaction effects

The responses of the dam at excitation frequencies equal to ω_n^{ℓ}, which are unbounded if the fluid domain is infinite and subjected to full vertical ground motion, are reduced to bounded values. This is a consequence of the added load $\underline{\bar{Q}}_o^{fy}(\omega)$ being a bounded function of excitation frequency when fluid foundation interaction is included. And as in the case of horizontal ground motion, fluid-foundation interaction considerably reduces the acceleration responses of the dam at excitation frequencies below ω_1^{ℓ} if the fluid domain is infinite (Figs. 4.8a and c) and at all frequencies if the fluid domain is finite (Fig. 4.8b). The dam accelerations including fluid-foundation

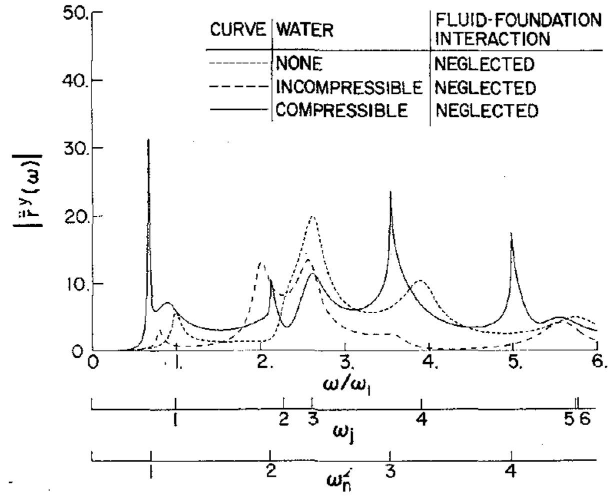

(a) $L_e = H$

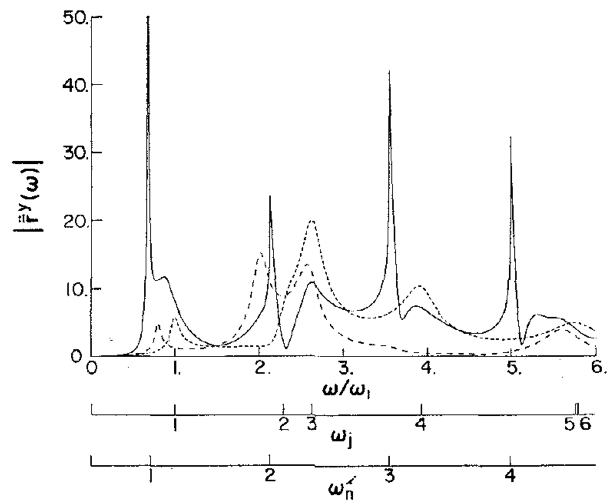

(b) $L_e = 2H$

FIG. 4.9 HORIZONTAL COMPONENT OF DAM CREST ACCELERATION DUE TO HARMONIC, PARTIAL VERTICAL GROUND MOTION. FLUID DOMAIN IS INFINITE OF CONSTANT DEPTH. L_e IS THE EXCITATION LENGTH.

interaction appear to depend somewhat more on fluid domain shape than do the acceleration responses to horizontal ground motion. When the ground motion is vertical, the hydrodynamic added load is a more significant fraction of the dam's inertia load; consequently, differences in the hydrodynamic added load due to fluid domain shape have a greater effect on the acceleration responses to vertical ground motion.

Acceleration responses of the dam to vertical ground motion considering water compressibility and fluid-foundation interaction (Fig. 4.8) generally exceed those responses without water and with incompressible water especially in the vicinity of ω_1^{ℓ} or ω_1^b where the hydrodynamic added load is large. These increases contrast to the reductions in the acceleration response of the dam to horizontal ground motion when water compressibility and fluid-foundation interaction are considered. The result is an increased importance of the vertical component of ground motion on the dam accelerations to a level comparable to the horizontal component.

5. HYDRODYNAMIC EFFECTS IN RESPONSE OF EARTH DAMS

5.1 System Considered and Outline of Analysis

The earth dam-fluid system investigated is shown in Fig. 5.1. The dam is symmetrical about a vertical center line with equal upstream and downstream slopes of β:1 . To emphasize hydrodynamic effects, β is chosen as 1.5 resulting in a slope that is steeper than those commonly used for earth dams, but typical of rock-fill dams. The fluid domain is of infinite length and constant depth H (equal to the dam height H_s) beyond the toe of the dam. It is of the infinite, irregular type discussed in Sec. 3.4.

The dam is modeled in a continuum state as a linearly elastic shear beam. Such a representation is adequate for the present purpose of investigating hydrodynamic effects on the dam response. A shear wave velocity C_s within the dam of 2000 ft/sec, an upper bound value, is chosen to emphasize hydrodynamic effects. Also, for the dam, w_s = 130 pcf and ξ_j = 10% for each mode of vibration. The fluid domain is discretized by the mesh of Fig. 5.2 which employs two-dimensional elements with quadratic shape functions. For the fluid domain, w = 62.4 pcf, C = 4720 ft/sec, and the reflection coefficient α_r = .85.

Results presented in this chapter are complex frequency response functions due to harmonic ground acceleration = $e^{i\omega t}$: the horizontal component of hydrodynamic force $\bar{F}_0^{\ell}(\omega)$ on a rigid dam and the acceleration $\ddot{\bar{r}}^{\ell}(\omega)$ of the dam crest relative to the ground acceleration. The vectors $\underline{\bar{Q}}_j^f(\omega)$ and $\underline{\bar{Q}}_0^{f\ell}(\omega)$ of Eq. 2.24 are obtained as described

Preceding page blank

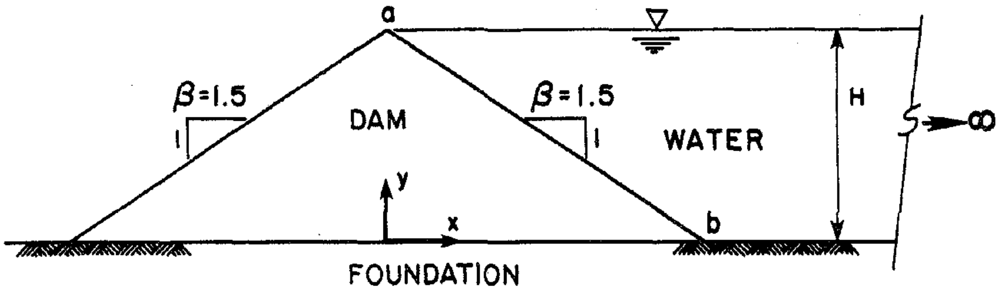

FIG. 5.1 EARTH DAM, INFINITE FLUID DOMAIN

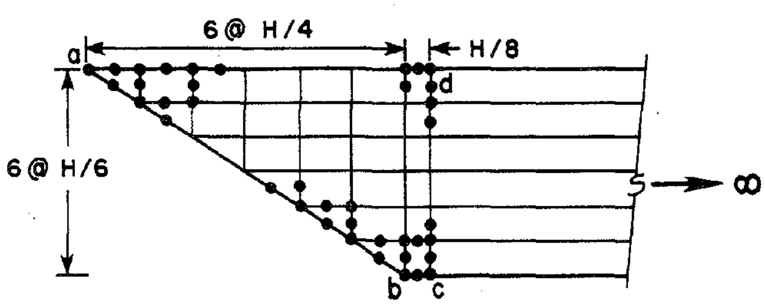

FIG. 5.2 FLUID DOMAIN FINITE ELEMENT MESH

in Sec. 3.5 from hydrodynamic pressure solutions $\bar{\underline{p}}_j^f(\omega)$ and $\bar{\underline{p}}_o^{f\ell}(\omega)$ of Eq. 3.39. $\bar{F}_o^{\ell}(\omega)$ is also computed from $\bar{\underline{p}}_o^{f\ell}(\omega)$. All twelve eigenvectors $\underline{\psi}_n$ are employed in Eq. 3.39.

The dam accelerations $\ddot{\bar{r}}^{\ell}(\omega)$ are obtained from the modal responses $\bar{Y}_j(\omega)$ computed from Eq. 2.23. For a triangular shear beam model of the dam with the width varying linearly with height, the terms of Eq. 2.24 related to the dam are available as continuum expressions (15). The jth undamped mode shape is given by the Bessel function of the first kind of order zero:

$$\phi_j(y) = J_o\left(\tau_j(1 - y/H_s)\right) \tag{5.1}$$

where the displacements defined by $\phi_j(y)$ are horizontal and result from the shearing actions of the dam; and where τ_j = the jth zero of J_o. (τ_j = 2.40, 5.52, 8.65,...) The vector $\underline{\phi}_j^f$ of Eq. 2.24 contains only horizontal DOF and lists the values of $\phi_j(y)$ which occur at the heights of the nodal points along a - b in Fig. 5.2. The jth natural frequency of the dam is given by

$$\omega_j = \frac{\tau_j \, C_s}{H_s} \tag{5.2}$$

Neither $\phi_j(y)$ nor ω_j depend on the slope β. The jth modal mass is found as

$$M_j = \beta\, H_s^2\, \frac{w_s}{g}\, J_1^2\,(\tau_1) \tag{5.3}$$

where J_1 is the Bessel function of order one. C_j and K_j are determined from Eq. 2.6. The inertia loading terms for the jth dam mode for ground motions in horizontal and vertical directions are

$$E_j^x = 2\beta\, H_s^2\, \frac{w_s}{g}\, \frac{J_1(\tau_1)}{\tau_1}$$

$$E_j^y = 0 \tag{5.4}$$

E_j^y is zero because the shear beam assumption permits only horizontal dam motions relative to the base.

The first three dam modes are employed here in the computation of $\ddot{\bar{r}}^{\ell}(\omega)$. These modes $\phi_j(y)$ together with their natural frequencies ω_j appear in Fig. 5.3. The analysis of this chapter was carried out with the computer program EADFS (14).

5.2 Hydrodynamic Forces on a Rigid Dam

The absolute value of $\bar{F}_0^{\ell}(\omega)$, the horizontal component of hydrodynamic force on a rigid dam, is presented in Figs. 5.4a and b for ground motions in the horizontal and vertical directions, respectively. Included are results for the fluid domain of Fig. 5.1 which has a sloped dam-fluid interface and for the infinite fluid domain of constant depth (Fig. 4.1a) which has a vertical interface.

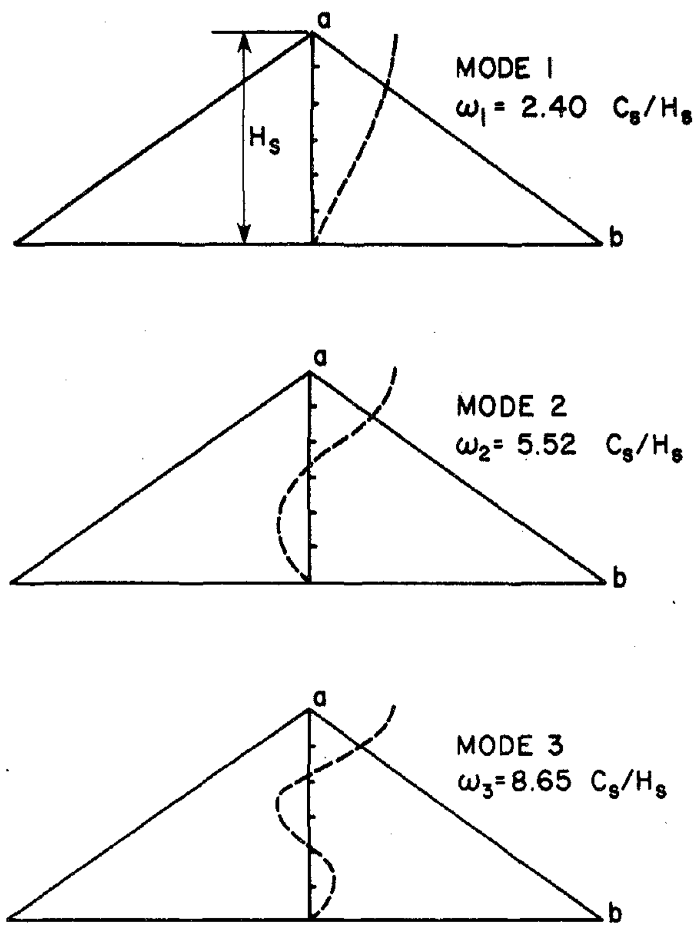

FIG. 5.3 MODE SHAPES AND NATURAL FREQUENCIES OF THE DAM

$\bar{F}_0^{\ell}(\omega)$ is normalized with the horizontal component of hydrostatic force $F_{st} = \frac{1}{2}\,wH^2$ and ω with $\omega_1^r = \pi C/2H$. The plotted results are independent of water depth H. Effects of water compressibility and fluid-foundation interaction are described below.

5.2.1 Water compressibility effects

The hydrodynamic force varies with excitation frequency if water compressibility is considered. Whereas the hydrodynamic force on the vertical face is unbounded at frequencies equal to ω_n^{ℓ} (the eigenfrequencies of the infinite region of depth H), the force on the sloped face is a bounded function of frequency when the ground motion is horizontal (Fig. 5.4a). Thus, this fluid domain with outward sloping dam face has no eigenfrequencies. The sloped interface irregularity reduces the average water depth to a value less than H. Thus, any eigenfrequencies and their associated infinite responses for such a fluid domain have to occur above the frequency ω_1^{ℓ}. Such occurrence, however, is impossible because the eigenproblem associated with Eq. 3.39 is complex valued over this frequency range. Fluid radiation damping, then keeps the responses to horizontal ground motion bounded above ω_1^{ℓ}. Figure 5.4a indicates that the sloped dam face is a less efficient generator of hydrodynamic pressure than is the vertical face (see also Fig. 3.14).

The hydrodynamic force due to vertical ground motion (Fig. 5.4b) is unbounded at excitation frequencies equal to ω_n^{ℓ} whether the dam face slopes or not, a consequence of the acceleration of the infinite reservoir floor; i.e., the acceleration vector $\underline{D}^{\ell}$ on the right side of Eq. 3.39 is non-zero. The resonant peaks in Fig. 5.4b for the

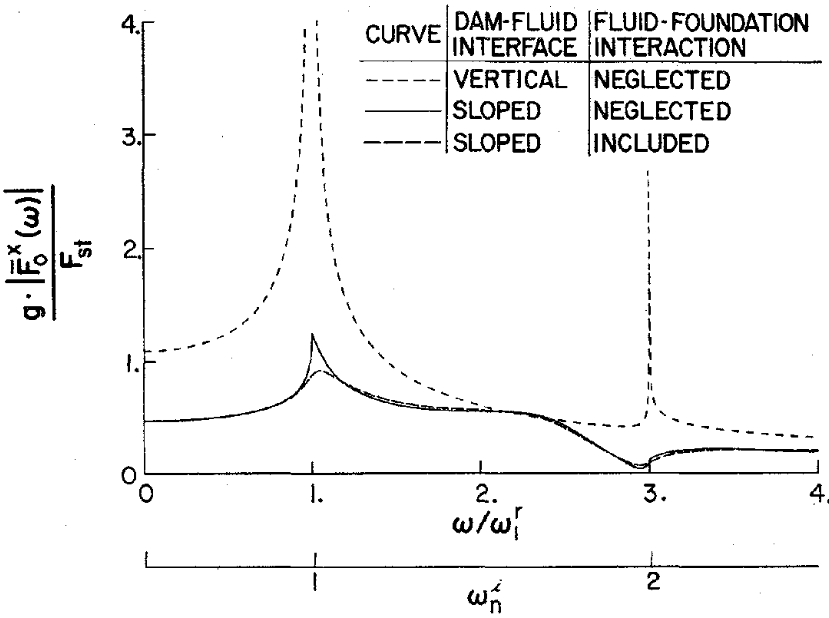

(a) HORIZONTAL GROUND MOTION

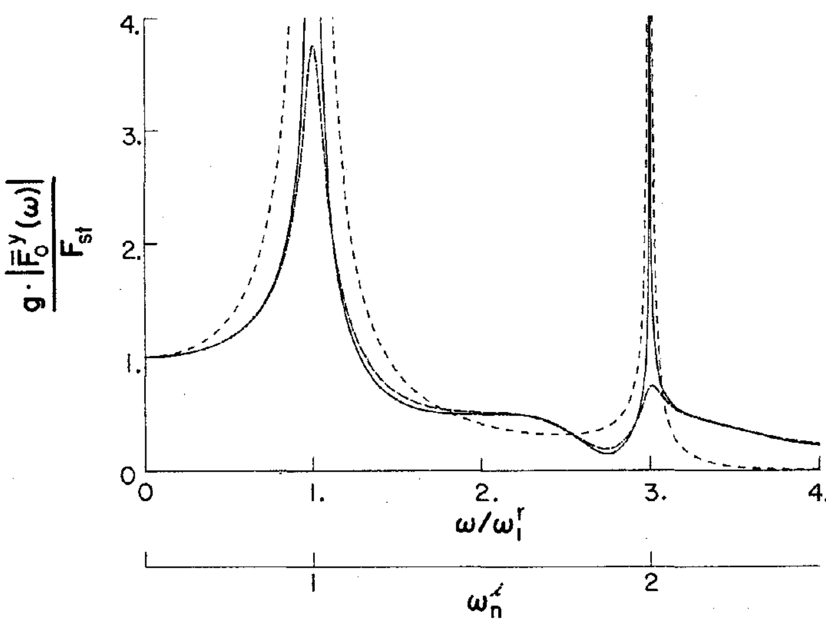

(b) VERTICAL GROUND MOTION

FIG. 5.4 HORIZONTAL COMPONENT OF HYDRODYNAMIC FORCE ON A RIGID DAM DUE TO HARMONIC GROUND MOTION fluid domain with sloped dam face are narrower than those with the vertical face, indicating a reduced response. With a rigid foundation, responses of the fluid domain with sloped dam face are real valued below ω_1^{ℓ} and complex valued above for both directions of ground motion.

5.2.2 Fluid-foundation interaction effects

When fluid-foundation interaction is considered, the hydrodynamic forces are bounded at all frequencies and complex valued for $\omega > 0$. The force amplitudes due to vertical ground motion (Fig. 5.4b) are affected significantly by fluid-foundation interaction; the infinite responses at excitation frequencies equal to ω_n^{ℓ} are replaced by bounded peaks. The hydrodynamic force due to horizontal ground motion (Fig. 5.4a) is affected only slightly.

5.3 Responses of the Dam

The absolute value of crest acceleration $\ddot{r}^{\ell}(\omega)$ is presented in Figs. 5.5a and b for horizontal and vertical ground motions, respectively. The excitation frequency ω is normalized with the fundamental frequency of the dam ω_1, and the plotted results are independent of dam height H_s. If the water is absent or incompressible, the results are also independent of shear wave velocity C_s. Because of the shear beam assumption, the dam response without water is zero when the ground motion is vertical. Dam-fluid interaction effects and fluid-foundation interaction effects on the acceleration response of the dam are described below.

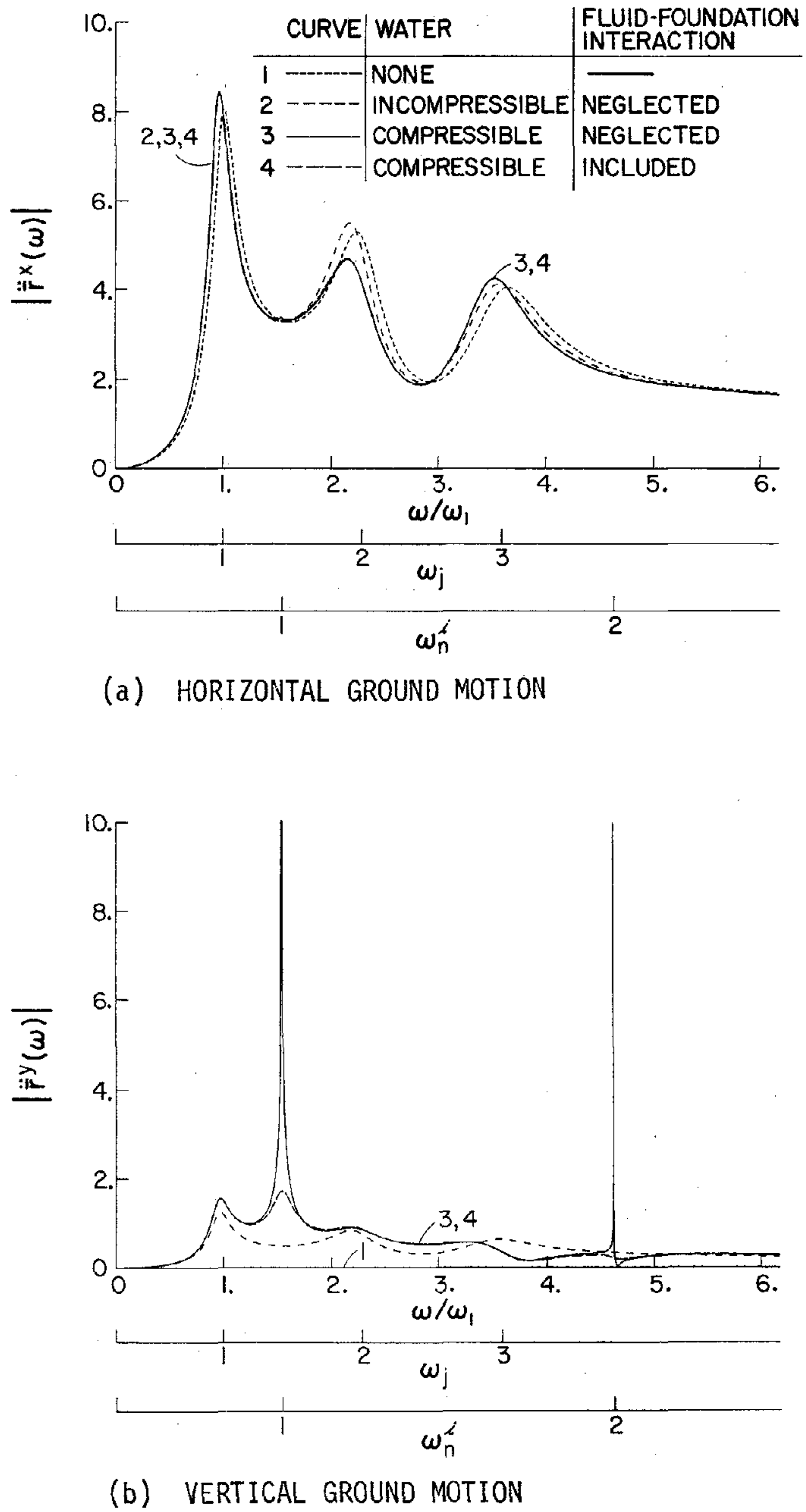

FIG. 5.5 ACCELERATION OF THE DAM CREST DUE TO HARMONIC GROUND MOTION

5.3.1 Dam-fluid interaction effects

If the water is assumed to be incompressible, the hydrodynamic effects are equivalent to frequency independent added masses $\bar{\underline{Q}}_j^f(0)$ and added loads $\bar{\underline{Q}}_o^{f\ell}(0)$. The resulting resonances in the acceleration response to horizontal ground motion (Fig. 5.5a) occur at lower frequencies with greater amplitudes than the resonances without water, but the changes are smaller than those occurring in the response of the concrete gravity dam (Fig. 4.7a). These hydrodynamic effects are smaller for the earth dam because of its greater mass and its sloped upstream face which, as discussed earlier, is a less efficient generator of hydrodynamic pressures. For vertical ground motion (Fig. 5.5b), non-zero response occurs although its amplitude is small.

If water compressibility is considered, then the hydrodynamic force vectors $\bar{\underline{Q}}_j^f(\omega)$ and $\bar{\underline{Q}}_o^{fx}(\omega)$ vary with excitation frequency similarly to the hydrodynamic force $\bar{F}_0^x(\omega)$ on the rigid dam due to horizontal ground motion (Fig. 5.4a), while $\bar{\underline{Q}}_o^{fy}(\omega)$ varies similarly to $\bar{F}_0^y(\omega)$ due to vertical ground motion (Fig. 5.4b). Figure 5.4a indicates that $\bar{\underline{Q}}_j^f(\omega)$ and $\bar{\underline{Q}}_o^{fx}(\omega)$ would be nearly independent of frequency until just below ω_1^{ℓ}. Thus, for this frequency range, water compressibility has little influence on the acceleration response to horizontal ground motion. Above ω_1^{ℓ} water compressibility slightly decreases the dam accelerations because of fluid radiation damping associated with the imaginary component of the added masses $\bar{\underline{Q}}_j^f(\omega)$. The response to vertical ground motion is unbounded at excitation frequencies equal to ω_n^{ℓ} due to infinite values attained by the added load $\bar{\underline{Q}}_o^{fy}(\omega)$. Thus, at these frequencies water compressibility has the effect of significantly increasing the dam accelerations.

Areas under the infinite spikes in Fig. 5.5 are finite, and the Fourier Transform procedure of Sec. 2.5 for computing responses to arbitrary ground motions is applicable.

5.3.2 Fluid-foundation interaction effects

Fluid-foundation interaction has a negligible effect on the acceleration response to horizontal ground motion (Fig. 5.5a) because of the similar $\underline{\bar{Q}}^f(\omega)$ vectors for rigid and flexible foundations (as seen in Fig. 5.4a with the similar $\bar{F}_0^x(\omega)$ responses). Overall, hydrodynamic effects are small in the response of the earth dam to horizontal ground motion. For vertical ground motion (Fig. 5.5b), fluid-foundation interaction replaces the unbounded responses at the ω_n^ℓ with small bounded peaks. No infinite responses can occur because the added load $\underline{\bar{Q}}_0^{fy}(\omega)$ is now bounded. The acceleration response to vertical ground motion including water compressibility and fluid-foundation interaction is small compared to that to horizontal ground motion. Thus, hydrodynamic effects are unimportant in responses of the earth dam to both horizontal and vertical ground motions. And since the chosen values for dam slope and shear wave velocity are extreme values for earth dams to emphasize hydrodynamic effects, this conclusion is valid for earth dams in general.

 Preceding page blank

6. THREE-DIMENSIONAL ANALYSIS PROCEDURE FOR DAM RESPONSE

6.1 Systems and Ground Motion

The three-dimensional structural behavior of an arch dam must be considered in analyzing its response to earthquake ground motion. The reservoir may extend only a short distance upstream (Fig. 6.1a) or to a large enough distance so that it can be considered infinite for purposes of analysis (Fig. 6.1b). In the latter case, the reservoir cross-section is assumed to be uniform beyond some point in the upstream direction. Behaviors within the elastic dam and compressible water are assumed to be linear.

The earthquake ground motion is defined by the upstream-downstream (x), cross-stream (z), and vertical (y) components of acceleration. With a rigid foundation (Sec. 6.2), no interaction takes place between the dam and foundation or between the fluid and foundation. Ground motions at all points along the foundation boundaries of the dam and fluid are the same. To approximately consider fluid-foundation interaction effects (Sec. 6.3), the ground motion along the reservoir floor and sides is described by free-field accelerations which are assumed uniform. The actual acceleration of these boundaries depends on the interaction.

6.2 Response to Harmonic Ground Motion Neglecting Fluid-Foundation Interaction

The procedures of Chapter 2 for a ground motion $a_g^\ell(t) = e^{i\omega t}$ lead to the following equations which are of the same form as Eqs. 2.23 and 2.24:

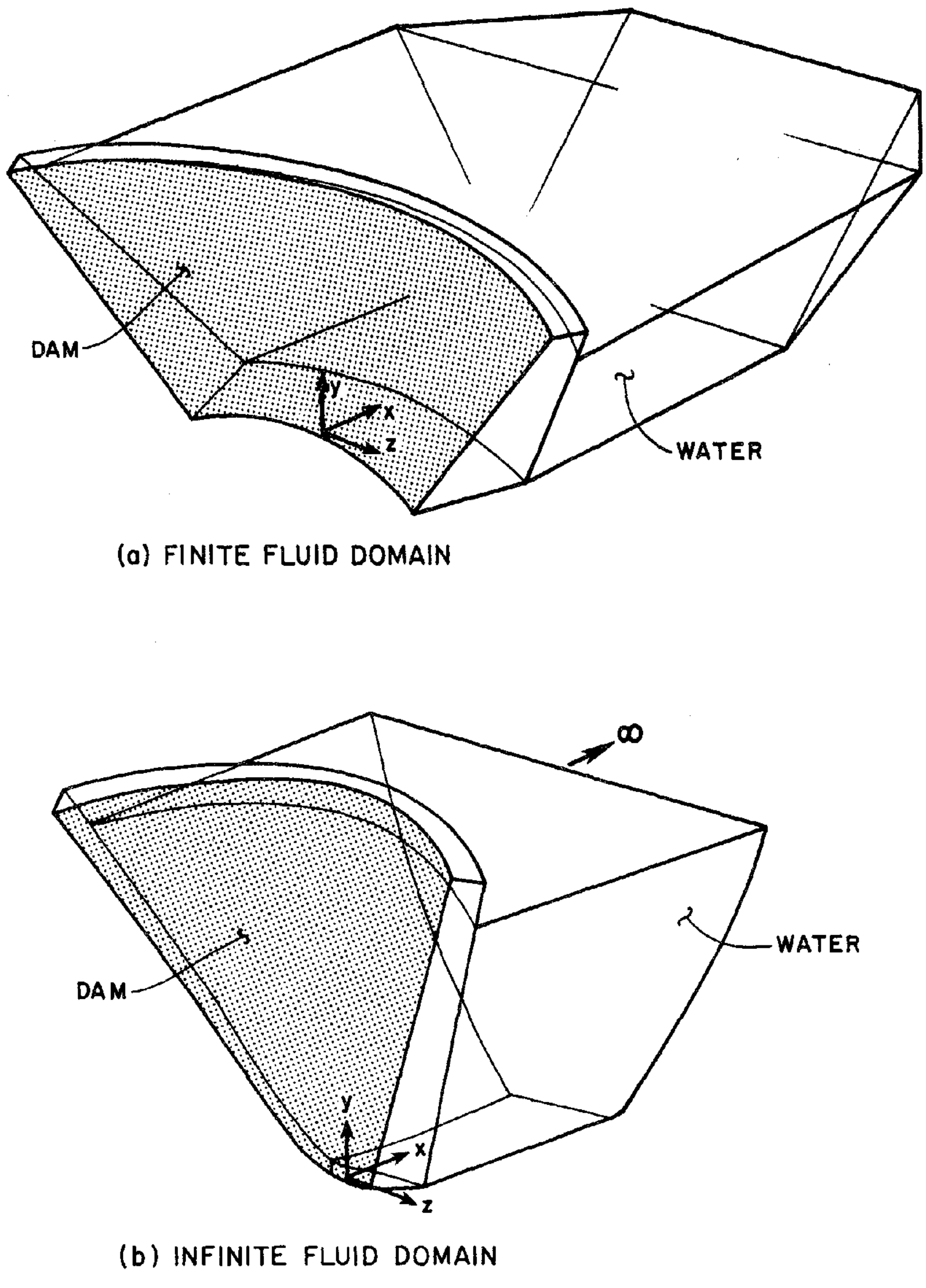

FIG. 6.1 THREE-DIMENSIONAL ARCH DAM-FLUID SYSTEMS

$$\underset{\sim}{S}(\omega)\,\bar{\underset{\sim}{Y}}^{\ell}(\omega) = \underset{\sim}{L}^{\ell}(\omega), \qquad \ell = x,y,z \tag{6.1}$$

where

$$S_{jk}(\omega) = -\omega^2 \left\{\underset{\sim}{\phi}_j^f\right\}^T \bar{\underset{\sim}{Q}}_k^f(\omega)$$

$$S_{jj}(\omega) = -\omega^2 M_j + i\omega C_j + K_j - \omega^2 \left\{\underset{\sim}{\phi}_j^f\right\}^T \bar{\underset{\sim}{Q}}_j^f(\omega) \tag{6.2}$$

$$L_j^{\ell}(\omega) = -\underset{\sim}{\phi}_j^T \underset{\sim}{E}^{\ell} - \left\{\underset{\sim}{\phi}_j^f\right\}^T \bar{\underset{\sim}{Q}}_o^{f\ell}(\omega)$$

$$\underset{\sim}{E}^{\ell} = [\underset{\sim}{m} \mid \underset{\sim}{m}_g]\, \underset{\sim}{e}^{\ell}$$

and where $\bar{\underset{\sim}{Y}}^{\ell}(\omega)$ = a vector of complex frequency response functions for generalized displacements of the first J undamped natural modes of vibration of the dam. The remaining terms of Eq. 6.1 are discussed below in a three-dimensional context referring to the arch dam-infinite fluid domain system of Fig. 6.2.

The arch dam of Fig. 6.2 is discretized with finite elements. The first J natural frequencies ω_j and mode shapes $\underset{\sim}{\phi}_j$ are computed from the eigenproblem

$$\underset{\sim}{k}\,\underset{\sim}{\phi}_j = \omega_j^2\,\underset{\sim}{m}\,\underset{\sim}{\phi}_j \tag{6.3}$$

where $\underset{\sim}{m}$ and $\underset{\sim}{k}$ = symmetric mass and stiffness matrices for the finite element system. Only DOF for interior nodes not along the dam-foundation boundary are included in Eq. 6.3. $\underset{\sim}{\phi}_j^f$ in Eq. 6.2 lists the x, y, and z components of the dam's jth mode shape for all nodes along the dam-fluid interface a-b-c-d-a. M_j, C_j, and K_j are the

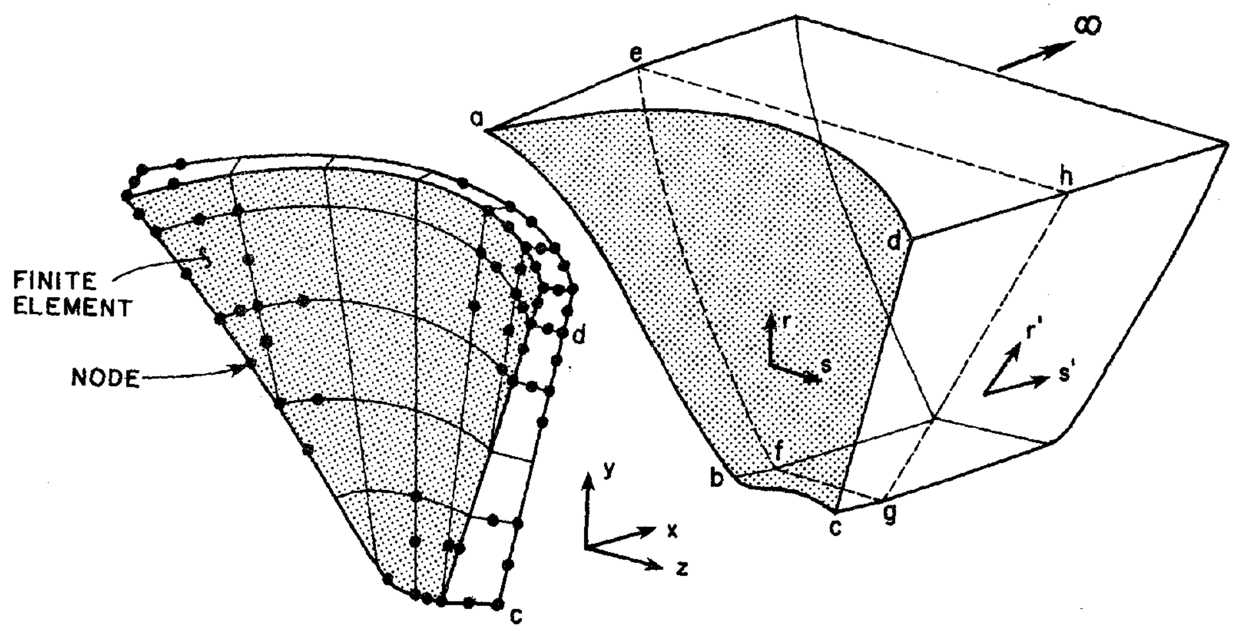

FIG. 6.2 FINITE ELEMENT DAM MODEL, INFINITE FLUID DOMAIN

jth modal mass, damping, and stiffness defined by the following equations:

$$M_j = \underset{\sim}{\phi}_j^T \, \underset{\sim}{m} \, \underset{\sim}{\phi}_j \tag{6.4a}$$

$$C_j = 2 \, \xi_j \, \omega_j \, M_j \tag{6.4b}$$

$$K_j = \omega_j^2 \, M_j \tag{6.4c}$$

where ξ_j = the jth modal damping ratio. $\underset{\sim}{E}^{\ell}$ is a vector of inertia forces on the dam arising from a unit acceleration of the dam as a rigid body in the ℓ direction. $\underset{\sim}{m}_g$ is a mass matrix coupling DOF on the dam-foundation boundary with the interior DOF (non-zero for consistent mass matrices only). The ith term of $\underset{\sim}{e}^{\ell}$ equals the length of the component of a unit vector along ℓ in the direction of the ith translational DOF. The vectors $\underset{\sim}{e}^x$, $\underset{\sim}{e}^y$ and $\underset{\sim}{e}^z$, for ground motions in the x, y and z directions, contain ones in positions corresponding to x, y and z translational DOF, respectively, with zeros elsewhere.

$\bar{\underset{\sim}{Q}}_o^{f\ell}(\omega)$, $\ell = x,y,z$ and $\bar{\underset{\sim}{Q}}_j^f(\omega)$ in Eq. 6.2 account for effects of the fluid and are associated with various boundary conditions presented below. All are vectors listing the x, y, and z components of hydrodynamic forces on the dam at the dam-fluid interface with terms ordered to correspond to those of $\underset{\sim}{\phi}_j^f$. The force vectors are computed from hydrodynamic pressures on the dam-fluid interface by the method of virtual work. Hydrodynamic pressures $\bar{p}(x,y,z,\omega)$ within the fluid domain obey the three-dimensional Helmholtz equation:

$$\frac{\partial^2 \bar{p}}{\partial x^2} + \frac{\partial^2 \bar{p}}{\partial y^2} + \frac{\partial^2 \bar{p}}{\partial z^2} + \frac{\omega^2}{C^2} \bar{p} = 0 \tag{6.5}$$

Along accelerating fluid boundaries, the pressures should satisfy

$$\frac{\partial \bar{p}}{\partial n}(s,r,\omega) = -\frac{w}{g} a_n(s,r), \qquad s,r = s,r \text{ or } s',r' \tag{6.6}$$

where s,r = coordinates over the dam-fluid interface, and s',r' = coordinates over the reservoir floor and sides as shown in Fig. 6.2; $a_n(s,r)$ = normal component of boundary acceleration; and n denotes the inward normal direction to a boundary. Other boundary conditions to Eq. 6.5 include the zero pressure condition at the free surface ($y = H$)

$$\bar{p}(x,H,z,\omega) = 0 \tag{6.7}$$

and the radiation condition for infinite fluid domains.

$\bar{\underset{\sim}{Q}}{}_0^{f\ell}(\omega)$ is obtained from the pressures $\bar{p}_0^{f\ell}(s,r,\omega)$ along the dam-fluid interface arising from accelerations of the foundation in the direction ℓ while the dam is rigid. For this case, $a_n(s,r)$ from Eq. 6.6 is defined as

$$a_n(s,r) = \varepsilon^{\ell}(s,r), \qquad s,r = s,r \text{ or } s',r' \tag{6.8}$$

where $\epsilon^{\ell}(s,r)$ = a function defined over accelerating boundaries which gives the length of the component of a unit vector along ℓ in the direction of the inward normal n (a three-dimensional generalization of the function $\epsilon^{\ell}(s)$ of Eq. 2.10). $\bar{Q}_j^f(\omega)$ is obtained from $\bar{p}_j^f(s,r,\omega)$ on the dam-fluid interface which arises from accelerations of the dam in its jth vibration mode. Thus,

$$a_n(s,r) = \phi_j^f(s,r) \tag{6.9a}$$

$$a_n(s',r') = 0 \tag{6.9b}$$

where $\phi_j^f(s,r)$ = a continuous function representation of the component of the jth mode normal to the dam-fluid interface.

6.3 Modifications to Include Fluid-Foundation Interaction

The acceleration boundary condition along the reservoir floor and sides can be modified to approximately account for interaction between the fluid and foundation in accordance with Sec. 2.5. The portion of Eq. 6.6 along the reservoir floor and sides is replaced by

$$\frac{\partial \bar{p}}{\partial n}(s',r',\omega) = -\frac{w}{g}\, a_n(s',r') + i\omega q\, \bar{p}(s',r',\omega) \tag{6.10}$$

where the damping coefficient $q = w/w_r C_r$; w_r and C_r = unit weight and compression wave velocity of the foundation rock; and $a_n(s',r')$ is the free-field acceleration of the reservoir floor and sides defined by Eq. 6.8 or 6.9b. The hydrodynamic force vectors $\bar{Q}_0^{f\ell}(\omega)$, $\ell = x,y,z$

and $\bar{Q}_j^f(\omega)$ are obtained from the pressures $\bar{p}_o^{f\ell}(s,r,\omega)$ and $\bar{p}_j^f(s,r,\omega)$ found as solutions to Eq. 6.5 subject to the boundary conditions of Eq. 6.6 (dam-fluid interface), Eq. 6.10 (reservoir floor and sides), and Eq. 6.7 with accelerations defined by Eqs. 6.8 and 6.9. Terms of Eq. 6.2 related to the dam are unaffected.

The boundary condition Eq. 6.10 can be interpreted as the result of idealizing the foundation as an assemblage of elastic, independently acting columns of infinitesimal cross-section and infinite length extending outward in a normal direction from the reservoir floor and sides. This idealization and its implications were discussed in Sec. 2.5.2.

7. THREE-DIMENSIONAL ANALYSIS OF HYDRODYNAMIC FORCE VECTORS

7.1 Boundary Value Problems and Solution Techniques

The hydrodynamic force vectors $\bar{Q}_0^{f\ell}(\omega)$, $\ell = x,y,z$ and $\bar{Q}_j^f(\omega)$ of Eq. 6.2 are obtained from hydrodynamic pressure distributions along the dam-fluid interface which are found by solving the three-dimensional Helmholtz equation:

$$\frac{\partial^2 \bar{p}}{\partial x^2} + \frac{\partial^2 \bar{p}}{\partial y^2} + \frac{\partial^2 \bar{p}}{\partial z^2} + \frac{\omega^2}{C^2}\,\bar{p} = 0 \tag{7.1}$$

subject to the acceleration boundary condition along the dam-fluid interface

$$\frac{\partial \bar{p}}{\partial n}\,(s,r,\omega) = -\frac{w}{g}\,a_n(s,r) \tag{7.2a}$$

and along the reservoir floor and sides

$$\frac{\partial \bar{p}}{\partial n}\,(s',r',\omega) = -\frac{w}{g}\,a_n(s',r') + i\omega q\,\bar{p}(s',r',\omega) \tag{7.2b}$$

the zero pressure condition at the free surface $(y = H)$

$$\bar{p}(x,H,z,\omega) = 0 \tag{7.3}$$

and the raditation condition for infinite fluid domains. Values of the damping coefficient q in Eq. 7.2b greater than zero are used to approximately account for fluid-foundation interaction effects; in which case, $a_n(s',r')$ is the free-field acceleration of the reservoir floor and sides.

The accelerations in Eq. 7.2 are given by

$$a_n(s,r) = \varepsilon^{\ell}(s,r), \qquad s,r = s,r \text{ or } s',r' \tag{7.4}$$

for computation of the hydrodynamic added load vectors $\bar{\underline{Q}}_0^{f\ell}(\omega)$, $\ell = x,y,z$ and by

$$a_n(s,r) = \phi_j^f(s,r) \tag{7.5a}$$

$$a_n(s',r') = 0 \tag{7.5b}$$

for the hydrodynamic added mass vectors $\bar{\underline{Q}}_j^f(\omega)$. Corresponding solutions to the B.V.P.'s are $\bar{p}_0^{\ell}(x,y,z,\omega)$ and $\bar{p}_j(x,y,z,\omega)$, respectively. The $\bar{\underline{Q}}^f(\omega)$ vectors are computed from pressures on the dam-fluid interface by the method of virtual work.

Solutions to the above B.V.P.'s within finite fluid domains of irregular geometry (Fig. 7.1) can be obtained by the finite element method of Sec. 7.2. If the fluid domain is infinite but of uniform cross-section, then the B.V.P. solutions can be obtained with the finite element-continuum treatment of Sec. 7.3. Such a fluid domain is shown in Fig. 7.2 and extends to infinity along the x axis with uniform $y-z$ cross-section. In this treatment accelerations of the reservoir floor and sides can not vary in the x direction, but can vary arbitrarily along the boundary of a y-z cross-section. This requirement is consistent with the zero acceleration condition of

Eq. 7.5b and also, since the fluid boundaries are straight in the x direction, with the $\varepsilon^{\ell}(s',r')$ condition of Eq. 7.4.

The fluid domain of Fig. 7.3 has a finite region of irregular geometry connected to a region that extends to infinity along the x axis with uniform y - z cross-section. As described in Sec. 7.4, solutions to the above B.V.P.'s can be obtained by a method utilizing the standard finite element treatment of Sec. 7.2 for the finite region and the finite element-continuum treatment of Sec. 7.3 for the infinite region. Accelerations of the infinite region of uniform cross-section can not vary in the x direction, a requirement consistent with Eqs. 7.4 and 7.5b.

The analysis procedures of Secs. 7.2 to 7.4 are for hydrodynamic pressures and are written for general accelerations rather than the specific conditions of Eqs. 7.4 and 7.5. These conditions are considered in Sec. 7.5 as is the actual computation of $\underline{\bar{Q}}_0^{f\ell}(\omega)$, $\ell = x,y,z$ and $\underline{\bar{Q}}_j^{f}(\omega)$ from the resulting pressures along the dam-fluid interface.

7.2 Finite Fluid Domains of Irregular Geometry

Solution of the B.V.P. of Eqs. 7.1 to 7.3 within finite fluid domains (Fig. 7.1a) can be obtained numerically by the finite element method (12). The fluid domain is divided into three-dimensional elements as shown in Fig. 7.1b. The resulting matrix equation (Appendix B.3) takes the same form as Eq. 3.6:

$$\left[\underline{H} + i\omega q\,\underline{B} - \frac{\omega^2}{C^2}\,\underline{G}\right]\underline{\bar{p}}(\omega) = \frac{w}{g}\,\underline{D} \qquad (7.6)$$

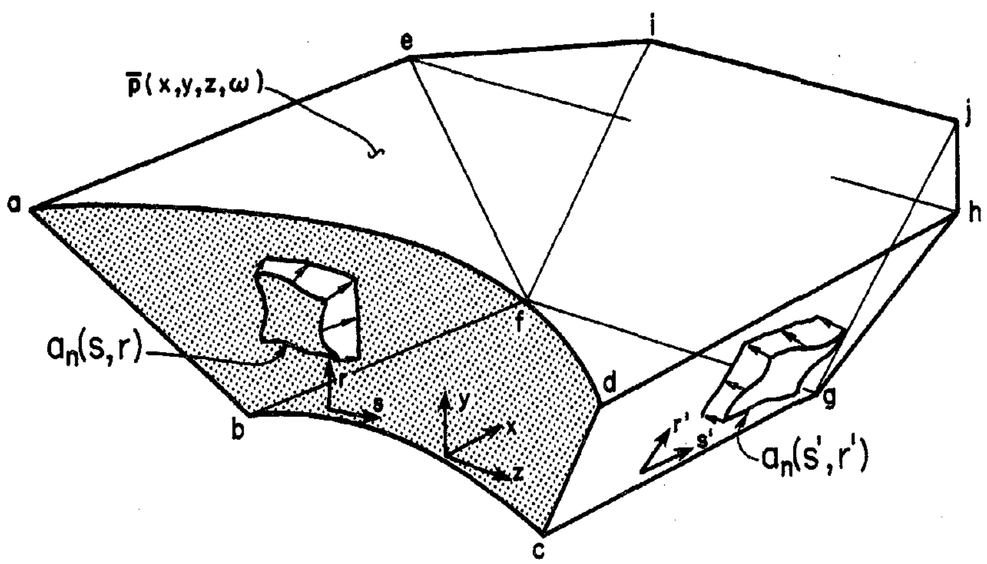

(a) FLUID DOMAIM

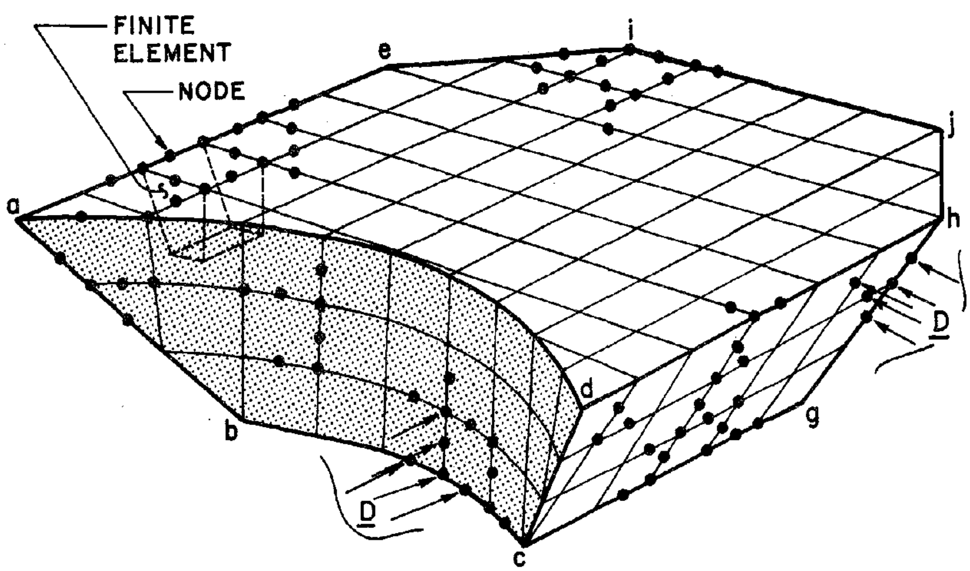

(b) FINITE ELEMENT DISCRETIZATION

FIG. 7.1 FINITE FLUID DOMAIN OF IRREGULAR GEOMETRY where $\underline{H}$, $\underline{B}$, and $\underline{G}$ are symmetric matrices analogous to stiffness, damping, and mass matrices arising in dynamics of solid continua; $\bar{\underline{p}}(\omega)$ = vector of unknown nodal pressures; and $\underline{D}$ = vector of nodal accelerations computed from $a_n(s,r)$ along the dam-fluid interface a-b-c-d-a and $a_n(s',r')$ along the reservoir floor and sides b-f-i-j-g-c-b, a-e-i-f-b-a, and d-h-j-g-c-d. The non-zero portion of $\underline{B}$ is a submatrix corresponding to nodes along the reservoir floor and sides where the boundary condition of Eq. 7.2b is applied. Only DOF for nodes below the free surface are included in Eq. 7.6.

The pressures $\bar{\underline{p}}(\omega)$ can be determined by solving the algebraic equations (Eq. 7.6). For the case $q = 0$, $\bar{\underline{p}}(\omega)$ can also be determined using an eigenvector expansion with the real valued eigenvectors $\underline{\zeta}_m$ resulting from the associated eigenproblem of Eq. 7.6:

$$\underline{H}\ \underline{\zeta} = \gamma^2\ \underline{G}\ \underline{\zeta} \tag{7.7}$$

The eigenvectors are orthogonal to $\underline{H}$ and $\underline{G}$ and are normalized with respect to $\underline{G}$. The result, following the procedure of Sec. 3.2, takes the form of Eq. 3.11:

$$\bar{\underline{p}}(\omega) = \frac{w}{g}\ \underline{Z}\ \underline{\Gamma}^{-1}\ \underline{Z}^T\ \underline{D} \tag{7.8}$$

where the first M eigenvectors are included; and where $\underline{Z} = [\underline{\zeta}_1, \underline{\zeta}_2, \ldots, \underline{\zeta}_M]$; $\underline{\Gamma}$ = an $M \times M$ diagonal matrix with mth diagonal term = $\gamma_m^2 - \omega^2/C^2$; and γ_m is the mth real valued eigenvalue from Eq. 7.7. For $q > 0$, the above eigenvectors do not diagonalize $\underline{B}$ of Eq. 7.6.

$\bar{p}(\omega)$ varies with excitation frequency as described in Sec. 3.2 for two-dimensional finite fluid domains. For $q = 0$, the amplitude of the mth eigenvector resonates to infinity at an eigenfrequency $\omega_m^b = \gamma_m C$ with opposite sign on each side. Thus, $\bar{p}(\omega)$ is a real valued function of frequency unbounded at the ω_m^b. For $q > 0$, $\bar{p}(\omega)$ is bounded at all frequencies and complex valued for $\omega > 0$, which are consequences of foundation radiation damping.

7.3 Infinite Fluid Domains of Uniform Cross-Section

7.3.1 Boundary value problems

The fluid domain of Fig. 7.2 extends to infinity along the x axis with uniform $y-z$ cross-section. The B.V.P. of Eqs. 7.1 to 7.3 is solved below for an acceleration $a_x(y,z)$ of the dam-fluid interface a-b-c-d-a and for an acceleration $a_n(s',r') = a_n^{\ell}(r')$ of the reservoir floor and sides, unvarying in the upstream direction. The coordinate s' is parallel to the x axis and r' follows the boundary around a $y-z$ cross-section. Solutions are carried out separately for these two acceleration conditions which are shown in Figs. 7.2a and c.

The governing Eq. 7.1 with the boundary conditions

$$\frac{\partial \bar{p}}{\partial x}(0,y,z,\omega) = -\frac{w}{g}\,a_x(y,z) \tag{7.9a}$$

$$\frac{\partial \bar{p}}{\partial n}(x,r',\omega) = i\omega q\,\bar{p}(x,r',\omega) \tag{7.9b}$$

$$\bar{p}(x,H,z,\omega) = 0 \tag{7.9c}$$

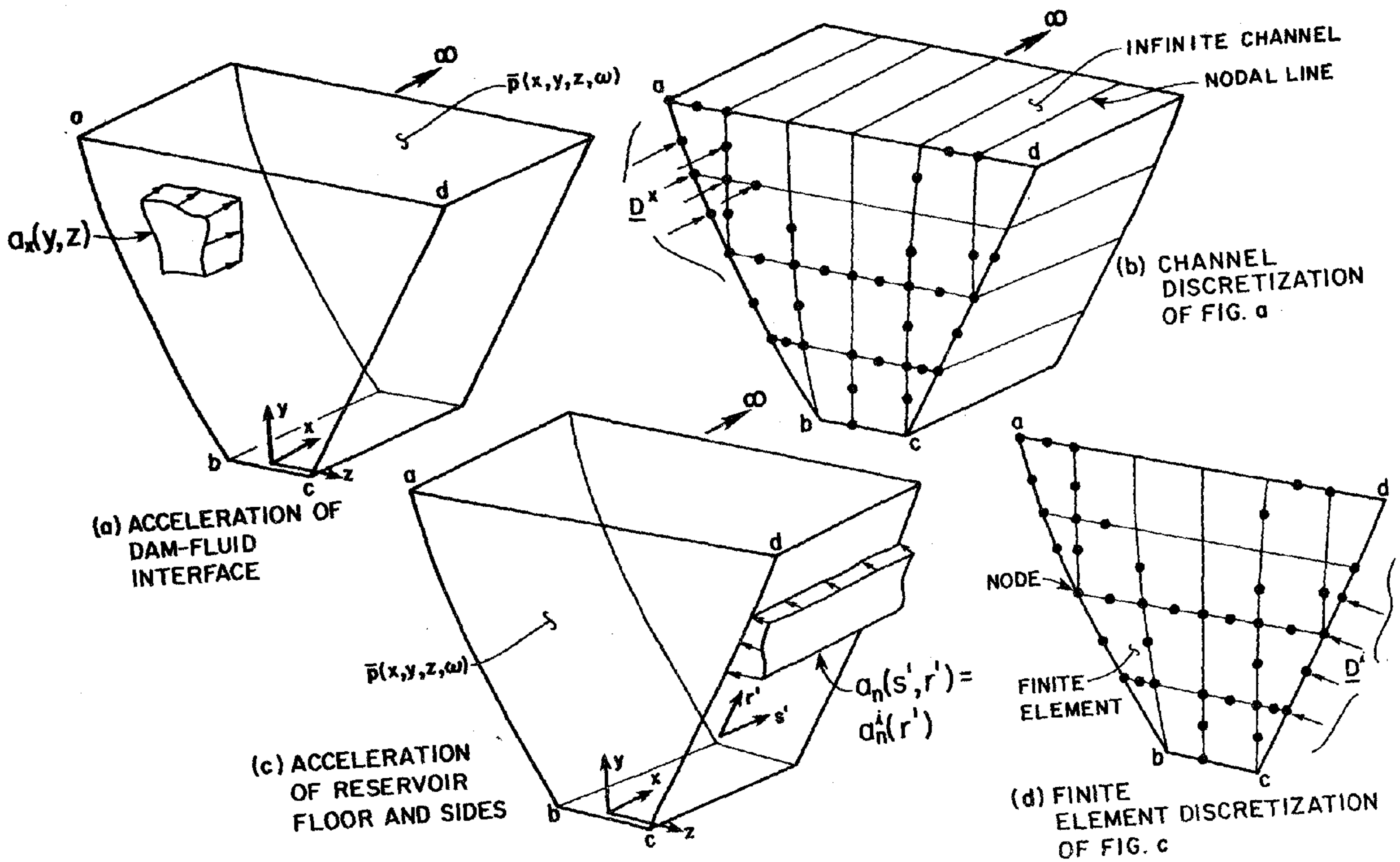

FIG. 7.2 INFINITE FLUID DOMAIN OF UNIFORM CROSS-SECTION

defines the first B.V.P. Equation 7.1 with boundary conditions

$$\frac{\partial \bar{p}}{\partial x}(0,y,z,\omega) = 0 \tag{7.10a}$$

$$\frac{\partial \bar{p}}{\partial n}(x,r',\omega) = -\frac{w}{g}\, a_n^{i}(r') + i\omega q\, \bar{p}(x,r',\omega) \tag{7.10b}$$

$$\bar{p}(x,H,z,\omega) = 0 \tag{7.10c}$$

defines the second B.V.P.

7.3.2 First B.V.P.

The uniform cross-section of this fluid domain allows the x distribution of pressure to be separated from the y-z distribution. Thus,

$$\bar{p}(x,y,z,\omega) = \bar{p}_x(x,\omega)\, \bar{p}_{yz}(y,z,\omega) \tag{7.11}$$

where $\bar{p}_x(x,\omega)$ must satisfy

$$\frac{d^2\bar{p}_x}{dx^2} - \kappa^2\, \bar{p}_x = 0 \tag{7.12a}$$

and $\bar{p}_{yz}(y,z,\omega)$ must satisfy

$$\frac{\partial^2\bar{p}_{yz}}{\partial y^2} + \frac{\partial^2\bar{p}_{yz}}{\partial z^2} + \lambda^2\, \bar{p}_{yz} = 0 \tag{7.12b}$$

where κ is a separation constant; and

$$\lambda^2 = \kappa^2 + \frac{\omega^2}{C^2} \tag{7.13}$$

Boundary conditions include Eq. 7.9a and the separated conditions

$$\frac{\partial \bar{p}_{yz}}{\partial n}(r',\omega) = i\omega q \; \bar{p}_{yz}(r',\omega) \tag{7.14a}$$

$$\bar{p}_{yz}(H,z,\omega) = 0 \tag{7.14b}$$

A finite element-continuum treatment is applied combining a finite element eigensolution in the $y-z$ plane with a continuum formulation in the x direction. This process can be interpreted as a discretization of the fluid domain into channels of infinite length (Fig. 7.2b). A finite element discretization of the eigenvalue problem defined by Eqs. 7.12b and 7.14 using a two-dimensional mesh (Fig. 7.2d) takes the form of Eq. 3.18:

$$\left[\underline{H}^{i} + i\omega q \; \underline{B}^{i}\right] \underline{\psi} = \lambda^2 \; \underline{G}^{i} \; \underline{\psi} \tag{7.15}$$

whose derivation follows from that in Appendix B.1, and where the matrices $\underline{H}^{i}$, $\underline{B}^{i}$, and $\underline{G}^{i}$ are symmetric. The non-zero portion of $\underline{B}^{i}$ is a submatrix corresponding to nodes along the boundary a-b-c-d in Fig. 7.2d. Only DOF for nodes below the free surface are included in Eq. 7.15. The eigenvalues λ_n and eigenvectors $\underline{\psi}_n$ are complex valued and dependent on the excitation frequency. The eigenvectors are orthogonal and are normalized with respect to $\underline{G}^{i}$.

Following the procedure of Sec. 3.3.2, the vector of pressures $\bar{\underline{p}}(x,\omega)$ along the nodal lines below the free surface lines in Fig. 7.2b can be expressed in terms of the first N eigenvectors as

$$\bar{\underline{p}}(x,\omega) = \underline{\Psi}\ \underline{e}(x)\ \bar{\underline{\eta}}(\omega) \tag{7.16}$$

where $\underline{\Psi} = [\underline{\psi}_1, \underline{\psi}_2, \ldots, \underline{\psi}_N]$; $\underline{e}(x)$ = an $N \times N$ diagonal matrix with nth diagonal term = $e^{-\kappa_n x}$; and

$$\kappa_n = \sqrt{\lambda_n^2 - \frac{\omega^2}{C^2}} = \mu_n + i\nu_n \tag{7.17}$$

κ_n is computed from Eq. 7.17 by taking the root with both μ_n and ν_n positive.

The vector of eigenvector amplitudes $\bar{\underline{\eta}}(\omega)$ from Eq. 7.16 is determined using the discrete form of the boundary condition Eq. 7.9a (Appendix C.2):

$$\underline{G}^{i} \frac{d\bar{\underline{p}}}{dx}(0,\omega) = -\frac{w}{g}\,\underline{D}^{x} \tag{7.18}$$

where $\underline{G}^{i}$ is the same matrix as in Eq. 7.15, and $\underline{D}^{x}$ = a vector of nodal accelerations corresponding to the acceleration $a_x(y,z)$ of the dam-fluid interface. Solution for $\bar{\underline{\eta}}(\omega)$ as in Sec. 3.3.2 and substitution back onto Eq. 7.16 results in

$$\bar{\underline{p}}(x,\omega) = \frac{w}{g}\,\underline{\Psi}\;\underline{e}(x)\;\underline{K}^{-1}\;\underline{\Psi}^{T}\;\underline{D}^{x} \tag{7.19}$$

which is of the same form as Eq. 3.27, and where $\underline{K}$ = an $N \times N$ diagonal matrix with nth diagonal term = κ_n. At $x = 0$, Eq. 7.19 reduces to

$$\bar{\underline{p}}(0,\omega) = \frac{w}{g}\,\underline{\Psi}\;\underline{K}^{-1}\;\underline{\Psi}^{T}\;\underline{D}^{x} \tag{7.20}$$

Since Eqs. 3.27 and 7.19 are of the same form, the frequency variation of $\bar{\underline{p}}(x,\omega)$ from these equations will be similar. For $q = 0$, λ_n and $\underline{\psi}_n$ are real valued and frequency independent, and κ_n is real or imaginary depending on whether ω is less than or greater than $\lambda_n C$. Thus, $\bar{\underline{p}}(x,\omega)$ is real for $\omega < \lambda_1 C$, complex for $\omega > \lambda_1 C$, and unbounded at eigenfrequencies $\omega_n^{\ell} = \lambda_n C$. The part that approaches infinity is real below each ω_n^{ℓ} and imaginary above. The imaginary part of $\bar{\underline{p}}(x,\omega)$ for frequencies greater than ω_1^{ℓ} is due to fluid radiation damping. For $q > 0$, $\bar{\underline{p}}(x,\omega)$ is bounded at all frequencies and complex valued for $\omega > 0$, which are consequences of foundation radiation damping.

7.3.3 Second B.V.P.

The B.V.P. of Eq. 7.1 with the boundary conditions of Eq. 7.10 is two-dimensional in the y,z coordinates. Omitting the x variations from these equations results in the two-dimensional Helmholtz equation for $\bar{p}(y,z,\omega)$

$$\frac{\partial^2 \bar{p}}{\partial y^2} + \frac{\partial^2 \bar{p}}{\partial z^2} + \frac{\omega^2}{C^2}\,\bar{p} = 0 \tag{7.21}$$

and the boundary conditions

$$\frac{\partial \bar{p}}{\partial n}(r',\omega) = -\frac{w}{g}\, a_n^{i}(r') + i\omega q\, \bar{p}(r',\omega) \qquad (7.22a)$$

$$\bar{p}(H,z,\omega) = 0 \qquad (7.22b)$$

Solution of Eq. 7.21 subject to the boundary conditions of Eq. 7.22 can be obtained by the finite element method using a two-dimensional mesh (Fig. 7.2d). The finite element discretization of this two-dimensional B.V.P. takes the same form as Eq. 3.31:

$$\left[\underline{H}^{i} + i\omega q\, \underline{B}^{i} - \frac{\omega^2}{C^2}\, \underline{G}^{i}\right] \bar{\underline{p}}(\omega) = \frac{w}{g}\, \underline{D}^{i} \qquad (7.23)$$

whose derivation follows from that in Appendix B.1; and where $\underline{H}^{i}$, $\underline{B}^{i}$, and $\underline{G}^{i}$ are the same symmetric matrices as in Eq. 7.15; $\bar{\underline{p}}(\omega)$ = vector of unknown nodal pressures; and $\underline{D}^{i}$ = vector of nodal accelerations computed from $a_n^{i}(r')$ along the boundary a-b-c-d. Only DOF for nodes below the free surface are included in Eq. 7.23.

If the N complex valued and frequency dependent eigenvalues λ_n and eigenvectors $\underline{\psi}_n$ of the associated eigenproblem Eq. 7.15 are available from a solution of the first B.V.P., then $\bar{\underline{p}}(\omega)$ of Eq. 7.23 can be expressed in terms of these quantities as

$$\bar{\underline{p}}(\omega) = \frac{w}{g}\, \underline{\Psi}\, \underline{\Lambda}^{-1}\, \underline{\Psi}^{T}\, \underline{D}^{i} \qquad (7.24)$$

which is of the same form as Eq. 3.32; and where $\underline{\Lambda}$ = an $N \times N$ diagonal matrix with nth diagonal term = $\lambda_n^2 - \omega^2/C^2$. Note that $\underline{\Lambda}$ is related to $\underline{K}$ from Eq. 7.19 by

$$\underline{\Lambda} = \underline{K}^2 \qquad (7.25)$$

The frequency variation of $\bar{\underline{p}}(\omega)$ is typical of finite fluid domains. For $q = 0$, $\bar{\underline{p}}(\omega)$ is a real valued function of ω, unbounded at the eigenfrequencies $\omega_n^{\ell} = \lambda_n C$ with opposite sign on each side. For $q > 0$, $\bar{\underline{p}}(\omega)$ is bounded at all frequencies and complex valued for $\omega > 0$.

7.4 Infinite Fluid Domains of Irregular Geometry

The fluid domain of Fig. 7.3a has a finite region of irregular shape connected to a region extending to infinity in the x direction with uniform y - z cross-section. The plane of connection is the y - z cross-section e-f-g-h-e. Normal accelerations of the dam-fluid interface a-b-c-d-a and reservoir floor and sides are $a_n(s,r)$ and $a_n(s',r')$, respectively. Beyond e-f-g-h-e, $a_n(s',r') = a_n^{\ell}(r')$, unvarying in the x direction. In this region s' is parallel to the x axis, and r' follows the boundary around a y - z cross-section.

Development of the finite element solution scheme follows the procedure of Sec. 3.4. The finite region is discretized into three-dimensional finite elements (Fig. 7.3b) and the infinite region into channels (Fig. 7.3c) matching the adjacent mesh along e-f-g-h-e. Equation 7.6 is written for the finite region with the unknown accelerations normal to e-f-g-h-e represented by $\underline{D}_2^x(\omega)$ (as in Eq. 3.34).

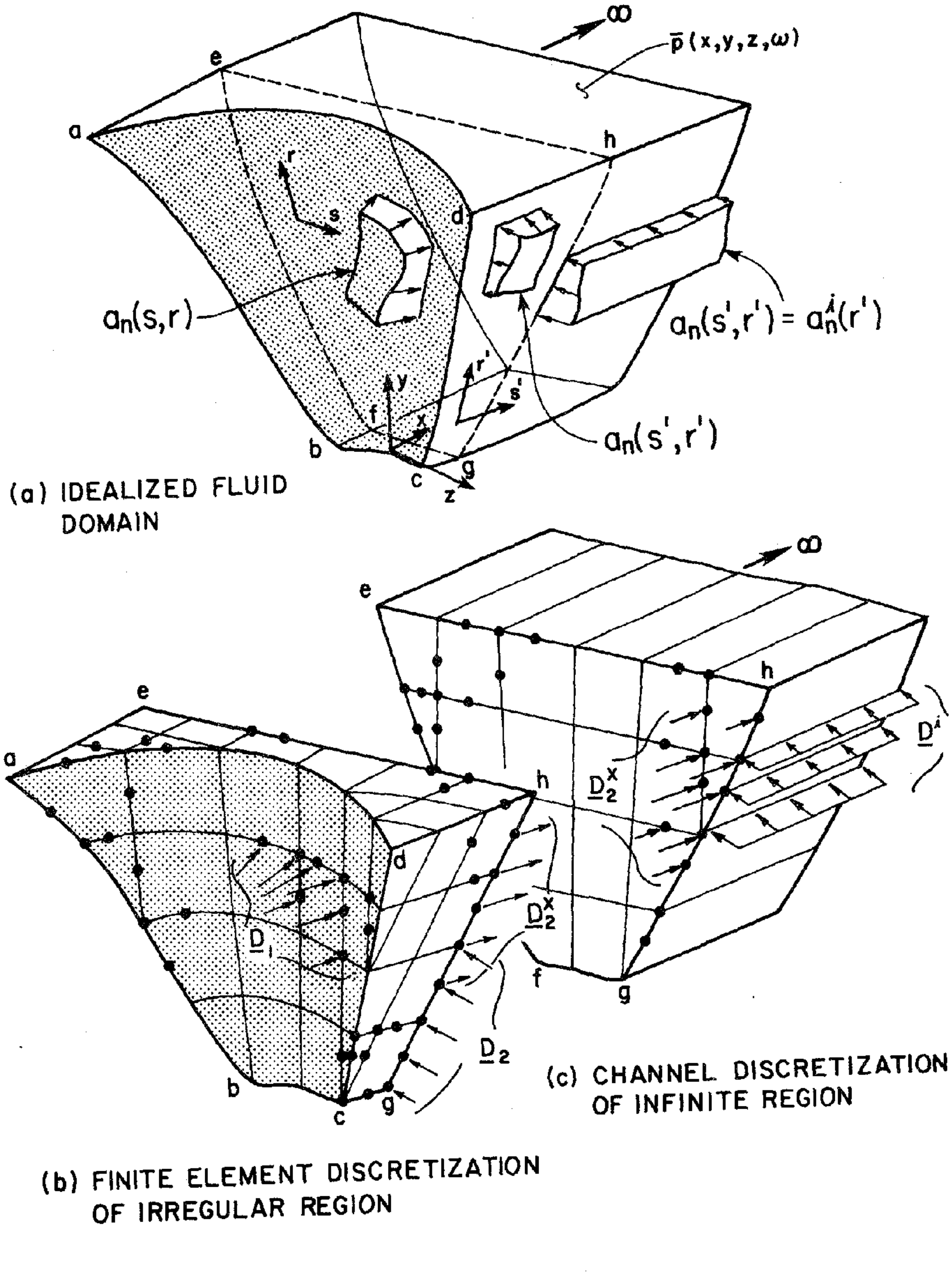

FIG. 7.3 INFINITE FLUID DOMAIN OF IRREGULAR GEOMETRY

Application of the results of Sec. 7.3 to the infinite region leads to a relation between $\underline{D}_2^x(\omega)$ and the pressures along e-f-g-h-e (as in Eq. 3.38). Combining these two results leads to Eq. 7.26 which is of the same form as Eq. 3.39:

$$\left[\begin{array}{c|c} \left[\underline{H}_{11} + i\omega q\ \underline{B}_{11} - \frac{\omega^2}{C^2}\underline{G}_{11}\right] & \left[\underline{H}_{12} + i\omega q\ \underline{B}_{12} - \frac{\omega^2}{C^2}\underline{G}_{12}\right]\underline{\Psi} \\ \hline \underline{\Psi}^T\left[\underline{H}_{21} + i\omega q\ \underline{B}_{21} - \frac{\omega^2}{C^2}\underline{G}_{21}\right] & \underline{\Psi}^T\left[\underline{H}_{22} + i\omega q\ \underline{B}_{22} - \frac{\omega^2}{C^2}\underline{G}_{22}\right]\underline{\Psi} + \underline{K} \end{array}\right]\left\{\begin{array}{c} \bar{\underline{p}}_1(\omega) \\ \hline \bar{\underline{\eta}}_2(\omega) \end{array}\right\} =$$

$$\frac{w}{g}\left\{\begin{array}{c} \underline{D}_1 \\ \hline \underline{\Psi}^T\ \underline{D}_2 + \underline{K}^{-1}\ \underline{\Psi}^T\ \underline{D}^{\ell} \end{array}\right\} \qquad (7.26)$$

where only DOF for nodes below the free surface are included; and where nodes along e-f-g-h-e are identified by subscript 2 and remaining nodes by subscript 1. The finite element matrices $\underline{H}_{11}, \underline{B}_{11}, \ldots, \underline{G}_{22}$ are written for the three-dimensional discretization of the finite region. $\underline{D}_1$ and $\underline{D}_2$ are acceleration vectors of groups 1 and 2 nodes computed from the accelerations of the exterior boundaries of the finite region; i.e., the dam-fluid interface a-b-c-d-a and the floor and sides b-f-g-c-b, a-e-f-b-a, and d-h-g-c-d. The matrices $\underline{K}$, $\underline{\Psi}$, and $\underline{D}^{\ell}$ result from consideration of the infinite region as described in Sec. 7.3.

Since Eqs. 3.39 and 7.26 are of the same form, the frequency variation of $\bar{\underline{p}}_1(\omega)$ from these equations will be similar. For $q = 0$, $\bar{\underline{p}}_1(\omega)$ is real valued for frequencies below the first eigenfrequency

ω_1^i of the infinite region, and complex valued above due to fluid radiation damping. Also, when $a_n^i(r')$ is non-zero, $\bar{\underline{p}}_1(\omega)$ becomes unbounded at each frequency ω_n^i due to the infinite value attained by the nth diagonal term of the matrix $\underline{K}^{-1}$ on the right side of Eq. 7.26. Eigenfrequencies of the complete fluid domain and their associated infinite responses can only occur below ω_1^i where fluid radiation damping is not present. For $q > 0$, $\bar{\underline{p}}_1(\omega)$ is bounded at all frequencies and complex valued for $\omega > 0$.

7.5 Computation of Hydrodynamic Force Vectors

For the fluid domains of Secs. 7.2 to 7.4, computation of the hydrodynamic force vectors $\bar{\underline{Q}}_0^{f\ell}(\omega)$, $\ell = x,y,z$ and $\bar{\underline{Q}}_j^f(\omega)$ of Eq. 6.2 proceeds as follows:

1. The boundary accelerations of Eqs. 7.4 and 7.5 are converted into acceleration vectors for use in Eqs. 7.6 or 7.8 (finite fluid domain), Eqs. 7.20 and 7.24 (infinite fluid domain of uniform cross-section), or Eq. 7.26 (infinite fluid domain of irregular geometry). For the finite fluid domain, these vectors are denoted by $\underline{D}_0^\ell$ and $\underline{D}_j$, and their computation is described in Appendix D.2. Vectors $\{\underline{D}^x\}_0^\ell$, $\ell = x$ and $\{\underline{D}^x\}_j$ of Eq. 7.20 and $\{\underline{D}_1\}_0^\ell$, $\{\underline{D}_2\}_0^\ell$, $\ell = x,y,z$ and $\{\underline{D}_1\}_j$, $\{\underline{D}_2\}_j$ of Eq. 7.26 are computed similarly. In the latter case, $\{\underline{D}_2\}_j = \underline{0}$. $\{\underline{D}^i\}_0^\ell$, $\ell = y,z$ in Eqs. 7.24 and 7.26 is computed with $a_n^i(r') = \varepsilon^\ell(r')$ similar to the procedure of Appendix D.1, and $\{\underline{D}^i\}_0^\ell$, $\ell = x$ and $\{\underline{D}^i\}_j$ of Eq. 7.26 are also zero vectors.

2. Using the acceleration vectors of step 1, hydrodynamic pressure vectors for a fluid domain are obtained by solving the appropriate

equations of Sec. 7.2, 7.3, or 7.4. Pressures along the dam-fluid interface are assembled into $\bar{\underline{p}}_o^{f\ell}(\omega)$, $\ell = x,y,z$ and $\bar{\underline{p}}_j^{f}(\omega)$.

3. As described in Appendix D.2, the hydrodynamic force vectors are computed from the pressures along the dam-fluid interface obtained in step 2.

Preceding page blank

8. HYDRODYNAMIC EFFECTS IN RESPONSE OF MORROW POINT DAM

8.1 System Considered and Outline of Analysis

Morrow Point Dam is a 465 ft, approximately symmetric, single-centered arch dam on the Gunnison River in Colorado. In the analysis, it is assumed symmetric with dimensions averaged from the two halves. The fluid domain is assumed symmetric also, to extend to infinity in the upstream direction, and to have a water depth H equal to the dam height. The dam-fluid system is shown in Fig. 8.1 where the plane of symmetry is the $z = 0$ plane, and the averaged dimensions of the dam are listed in Table 8.1. The fluid domain is of the infinite, irregular type described in Sec. 7.4; the reservoir cross-section is assumed to be uniform upstream of the $y-z$ plane e-f-g-h-e. System properties are chosen as $E_d = 3 \times 10^6$ psi, $\nu = .2$, $w_d = 150$ pcf, $w = 62.4$ pcf, $C = 4720$ ft/sec, $\alpha_r = .90$, and $\xi_j = 5\%$ for each mode of vibration of the dam. E_d, ν and w_d are measured values of Morrow Point Dam (1).

Because the dam-fluid system is symmetric, dam and hydrodynamic pressure responses to upstream-downstream (x) and vertical (y) ground motions are symmetric about the plane of symmetry, and those due to cross-stream (z) ground motion are antisymmetric. Only half the dam and fluid domain need be considered in the analysis if appropriate boundary conditions along the plane of symmetry are employed. In the analysis for x and y ground motions, the components of dam displacement and fluid acceleration normal to the plane of symmetry are zero. The x and y components of dam displacement

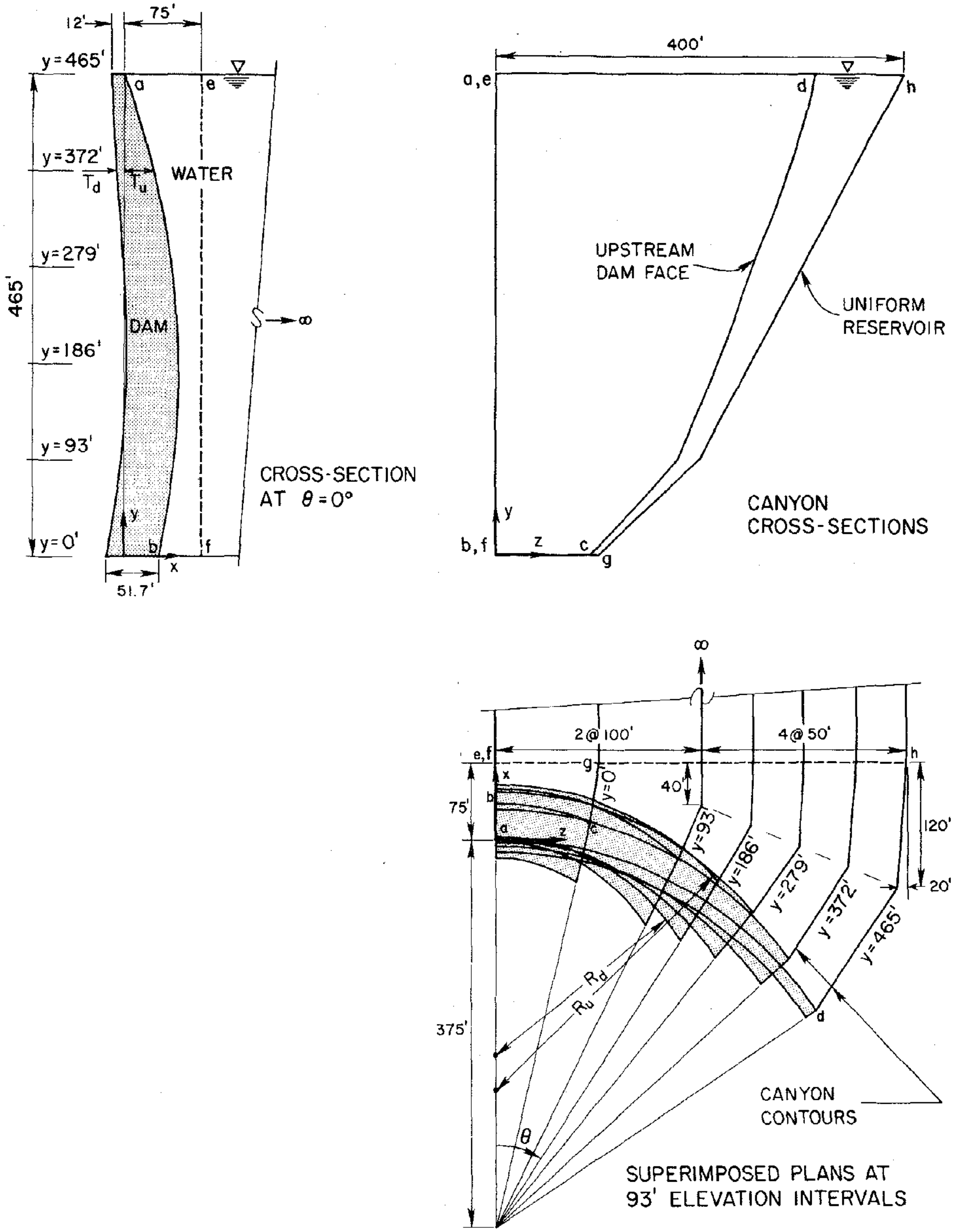

FIG. 8.1 MORROW POINT DAM, INFINITE FLUID DOMAIN

y (ft.)	T_u (ft.)	T_d (ft.)	R_u (ft.)	R_d (ft.)	θ (°)
465.	0.0	12.	375.0	363.0	56.20
372.	28.9	6.4	352.8	316.1	47.85
279.	46.3	0.8	324.9	258.0	39.50
186.	52.9	-2.6	296.5	210.8	33.00
93.	49.0	2.7	266.7	171.3	26.50
0.	34.4	17.2	234.8	136.6	13.25

TABLE 8.1 DIMENSIONS OF MORROW POINT DAM

and the hydrodynamic pressures at the plane of symmetry are zero for the z ground motion analysis.

The finite element mesh for the dam appears in Fig. 8.2a. The element employed is a shell element with quadratic shape functions and eight nodes located at mid-thickness (16). The element has been modified by removing an interior ninth node and by incorporating a consistent mass matrix (1). Five degrees of freedom are associated with each node: three translations and two rotations of the through-thickness nodal line about axes perpendicular to its own axis. Normal stresses perpendicular to the plane of the dam are assumed zero. The finite element mesh for the fluid domain (Fig. 8.2b) employs three-dimensional elements with quadratic shape functions, and the plane e-f-g-h-e is placed as close to the dam as possible to minimize the number of DOF in the mesh. The dam and fluid domain meshes coincide along the dam-fluid interface a-b-c-d-a.

Results presented in this chapter are complex frequency response functions due to harmonic ground acceleration = $e^{i\omega t}$: the x component of hydrodynamic force $\bar{F}_0^{\ell}(\omega)$ on half a rigid dam and the radial acceleration $\ddot{\bar{r}}^{\ell}(\omega)$ of the dam crest relative to the ground acceleration. The vectors $\bar{\underline{Q}}_j^{f}(\omega)$ and $\bar{\underline{Q}}_0^{f\ell}(\omega)$ of Eq. 6.2 are obtained as described in Sec. 7.5 from hydrodynamic pressure solutions $\bar{\underline{p}}_j^{f}(\omega)$ and $\bar{\underline{p}}_0^{f\ell}(\omega)$ of Eq. 7.26. $\bar{F}_0^{\ell}(\omega)$ is also computed from $\bar{\underline{p}}_0^{f\ell}(\omega)$. The first 31 symmetric eigenvectors $\underline{\psi}_n^{s}$ of the infinite, uniform region are included in Eq. 7.26 for the x and y ground motion analyses and the first 27 antisymmetric eigenvectors $\underline{\psi}_n^{a}$ for the z ground motion analysis. These totals are the numbers

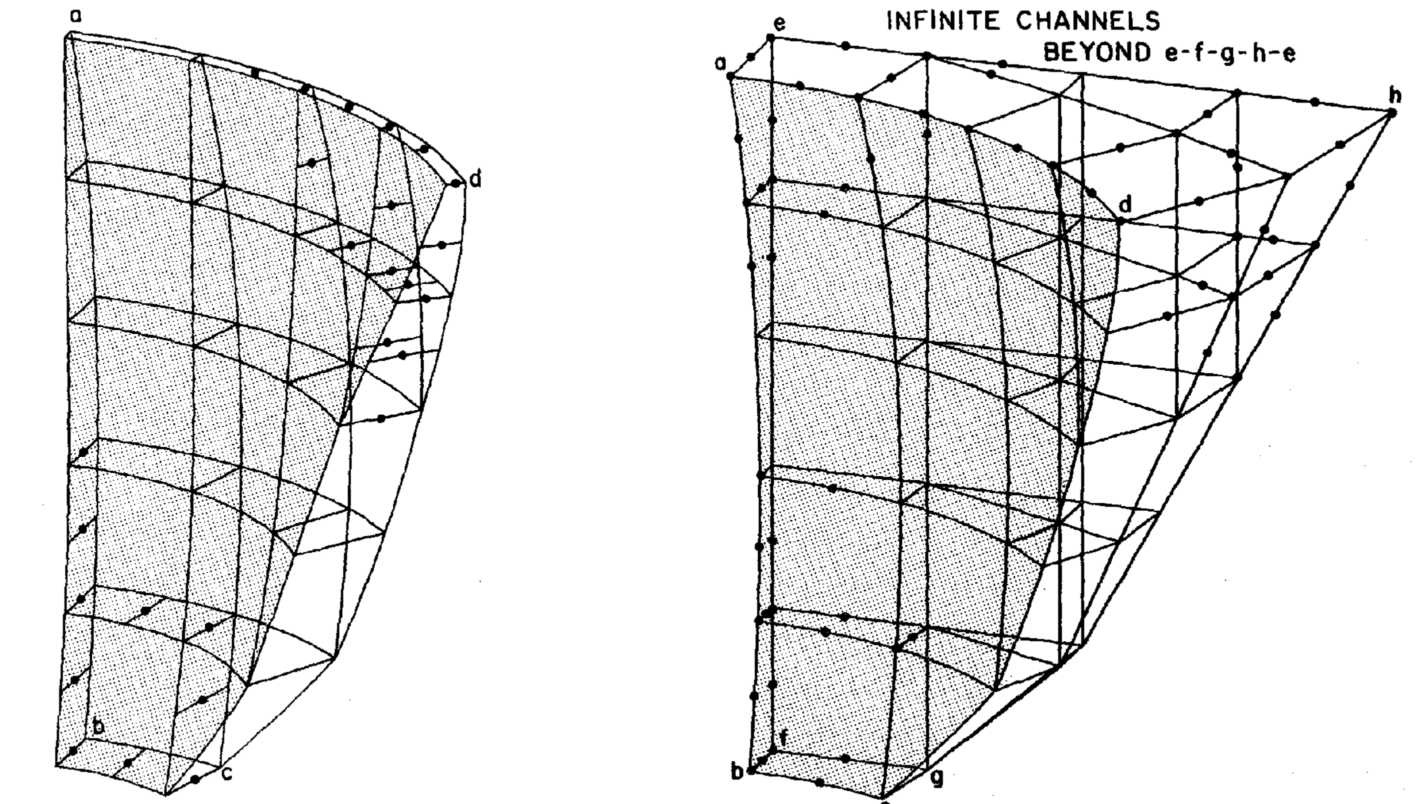

(a) MORROW POINT DAM

(b) FLUID DOMAIN

FIG. 8.2 FINITE ELEMENT MESHES

whose eigenfrequencies ω_n^{is} and ω_n^{ia} (Sec. 7.3) are less than $19.4\ \omega_1^r$, where $\omega_1^r = \pi C/2H$. The dam responses $\ddot{\bar{r}}^{\ell}(\omega)$ are obtained from the modal responses $\bar{Y}_j(\omega)$ computed from Eq. 6.1. The first 12 symmetric dam modes $\underline{\phi}_j^s$ are employed for x and y ground motion analyses, and the first 12 antisymmetric modes $\underline{\phi}_j^a$ are employed for the z ground motion analysis. Figures 8.3 and 8.4 show the first 8 symmetric and antisymmetric dam modes together with their natural frequencies ω_j^s and ω_j^a.

The analysis of this chapter was carried out with the computer program EADFS (14). Solution times for computing the frequency responses of the dam are presented in Appendix F.

8.2 Hydrodynamic Forces on a Rigid Dam

The absolute value of $\bar{F}_0^{\ell}(\omega)$, the x component of hydrodynamic force on half a rigid dam, is presented in Figs. 8.5a, b and c for ground motions in the x, y and z directions, respectively. $\bar{F}_0^{\ell}(\omega)$ is normalized with the hydrostatic force on the half dam $F_{st} = .208\ wH^2$ and ω with ω_1^r. When presented in this form, the plotted results apply to similarly shaped fluid domains of any depth. Effects of water compressibility and fluid-foundation interaction on $\bar{F}_0^{\ell}(\omega)$ are described below.

8.2.1 Water compressibility effects

When fluid-foundation interaction is neglected, the hydrodynamic forces are real valued at excitation frequencies below ω_1^{is} (x and y ground motions) or below ω_1^{ia} (z ground motion), and complex

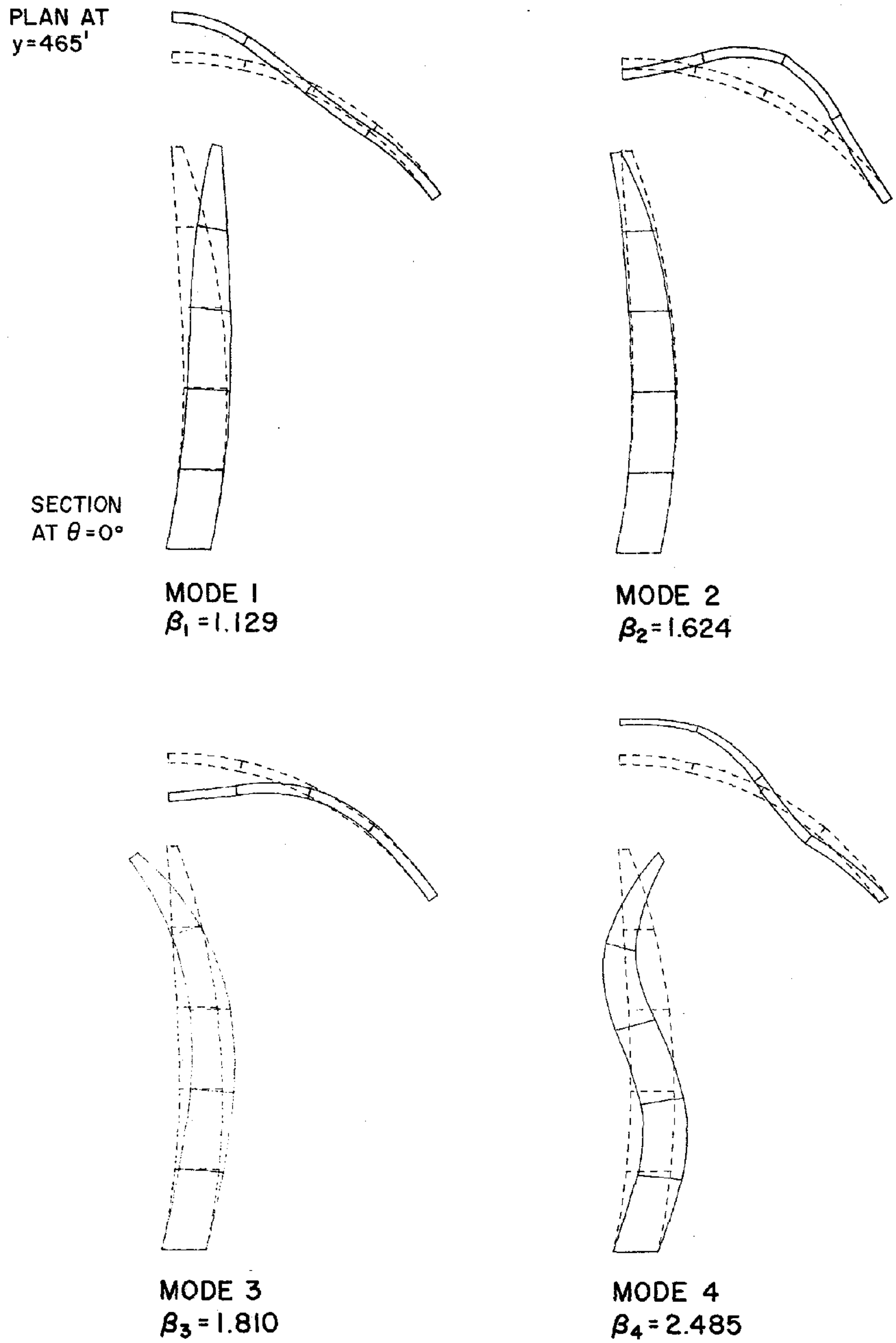

FIG. 8.3 SYMMETRIC MODE SHAPES OF MORROW POINT DAM. NATURAL FREQUENCIES ARE $\omega_j^s = \beta_j \frac{1}{H_d} \sqrt{Eg/w_d}$.

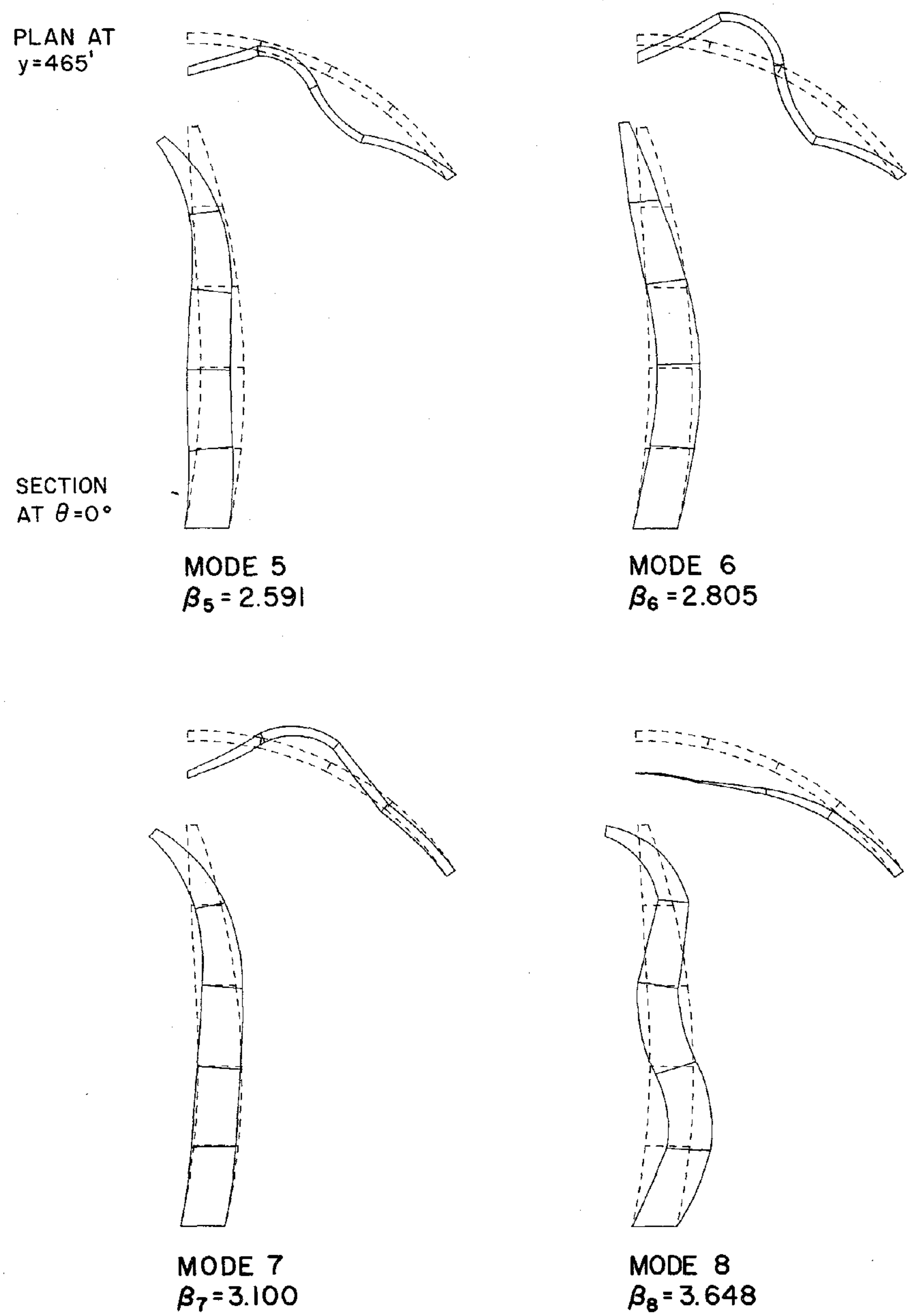

FIG. 8.3 (CONTINUED)

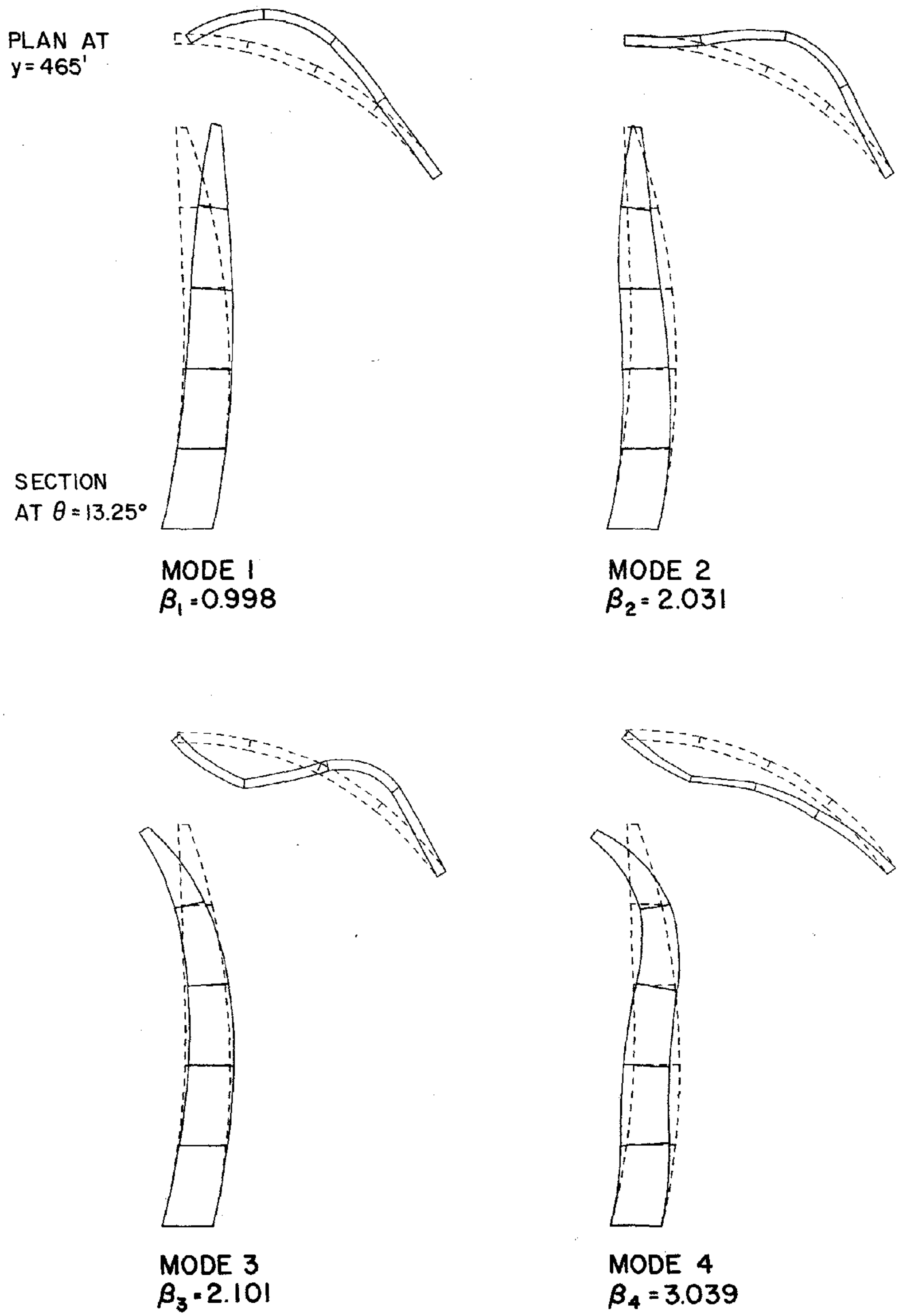

FIG. 8.4 ANTISYMMETRIC MODE SHAPES OF MORROW POINT DAM. NATURAL FREQUENCIES ARE $\omega_j^a = \beta_j \frac{1}{H_d} \sqrt{Eg/w_d}$.

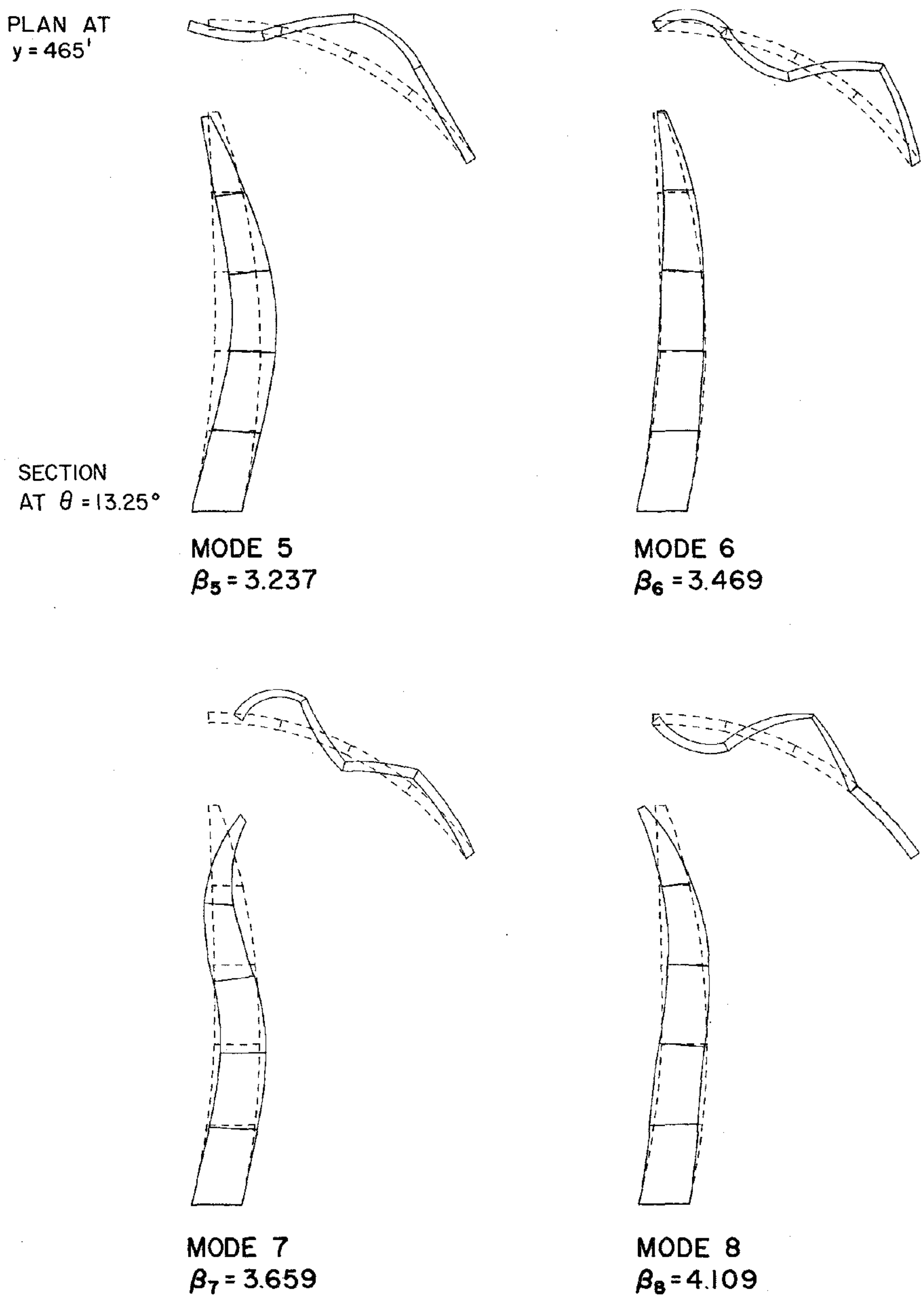

FIG. 8.4 (CONTINUED)

valued at higher frequencies. The hydrodynamic forces due to x ground motion (Fig. 8.5a) exhibit bounded peaks at frequencies equal to $\omega_n^{\ell s}$. Thus, no eigenfrequencies of the complete fluid domain associated with symmetric responses exist. This beahvior, which is dependent on the shape of the irregular portion of the fluid domain, resembles that of the two-dimensional, infinite fluid domain with sloped dam face described in Chapter 5.

Hydrodynamic forces due to y ground motion (Fig. 8.5b) are unbounded at excitation frequencies equal to $\omega_n^{\ell s}$, a consequence of the accelerations of the floor and sides of the infinite, uniform region; i.e., the acceleration vector $\underline{D}^{\ell}$ on the right side of Eq. 7.26 is non-zero. Similarly, z ground motion (Fig. 8.5c) produces unbounded hydrodynamic forces at frequencies equal to $\omega_n^{\ell a}$, as well as at a frequency ω_1^{ba} which is slightly less than $\omega_1^{\ell a}$. The frequency ω_1^{ba} is an eigenfrequency of the complete fluid domain associated with antisymmetric responses. This behavior, again dependent on the shape of the irregular portion of the fluid domain, resembles that of the two-dimensional, infinite fluid domain with sloped floor described in Chapter 4. The resonances at $\omega_1^{\ell s}$ due to y ground motion and at ω_1^{ba} and $\omega_1^{\ell a}$ due to z ground motion involve large amounts of response and have greater amplitude over a wider frequency interval than the x ground motion resonance at $\omega_1^{\ell s}$. The resonance due to z ground motion occurs at a much higher frequency.

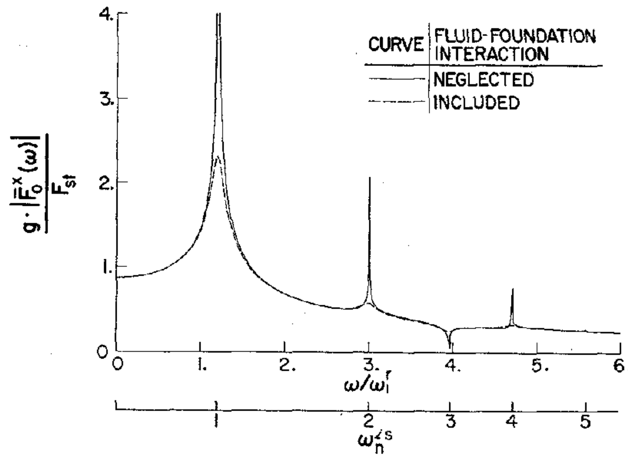

(a) UPSTREAM-DOWNSTREAM GROUND MOTION

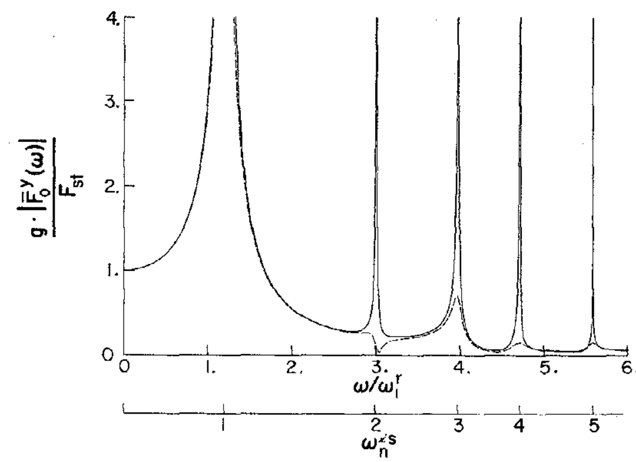

(b) VERTICAL GROUND MOTION

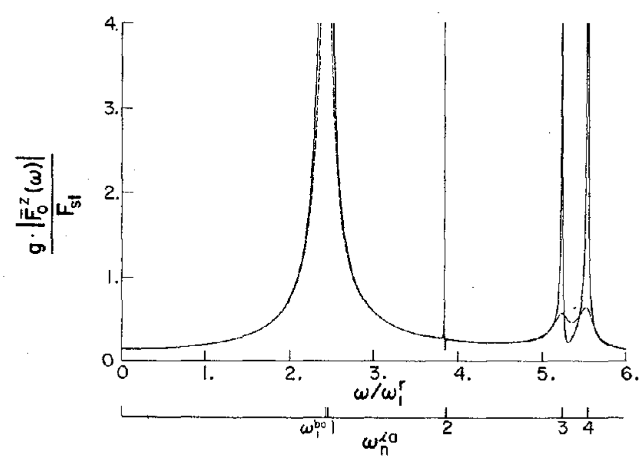

(c) CROSS-STREAM GROUND MOTION

FIG. 8.5 THE UPSTREAM-DOWNSTREAM COMPONENT OF HYDRODYNAMIC FORCE ON A RIGID DAM DUE TO HARMONIC GROUND MOTION

8.2.2 Fluid-foundation interaction effects

The hydrodynamic forces due to each of the three directions of ground motion are bounded functions of frequency and complex valued for $\omega > 0$ when fluid-foundation interaction is included. Figure 8.5 shows that the amplitude reductions in the hydrodynamic force $\bar{F}_0^{\ell}(\omega)$ due to fluid-foundation interaction are limited to vicinities of the resonant frequencies of the fluid domain. The resonances at ω_1^{is} due to y ground motion and at ω_1^{ba} and ω_1^{ia} due to z ground motion are still significant and have greater amplitude over a wider frequency interval than the x ground motion resonance at ω_1^{is}.

8.3 Responses of the Dam

The absolute value of $\ddot{r}^{\ell}(\omega)$, the radial component of dam crest acceleration, is presented in Figs. 8.6, 8.7 and 8.8 for ground motions in the x, y and z directions, respectively. Accelerations at four locations along the dam crest are presented. As shown in Fig. 8.8, the radial acceleration due to z ground motion is zero at the plane of symmetry. The excitation frequency ω is normalized with the dam natural frequency ω_1^s (x and y ground motion) or ω_1^a (z ground motion), and the plotted results apply to similarly shaped dam-fluid systems of any height. If the water is absent or incompressible, the results are also independent of the concrete elastic modulus E_d. Dam-fluid interaction effects and fluid-foundation interaction effects are described below.

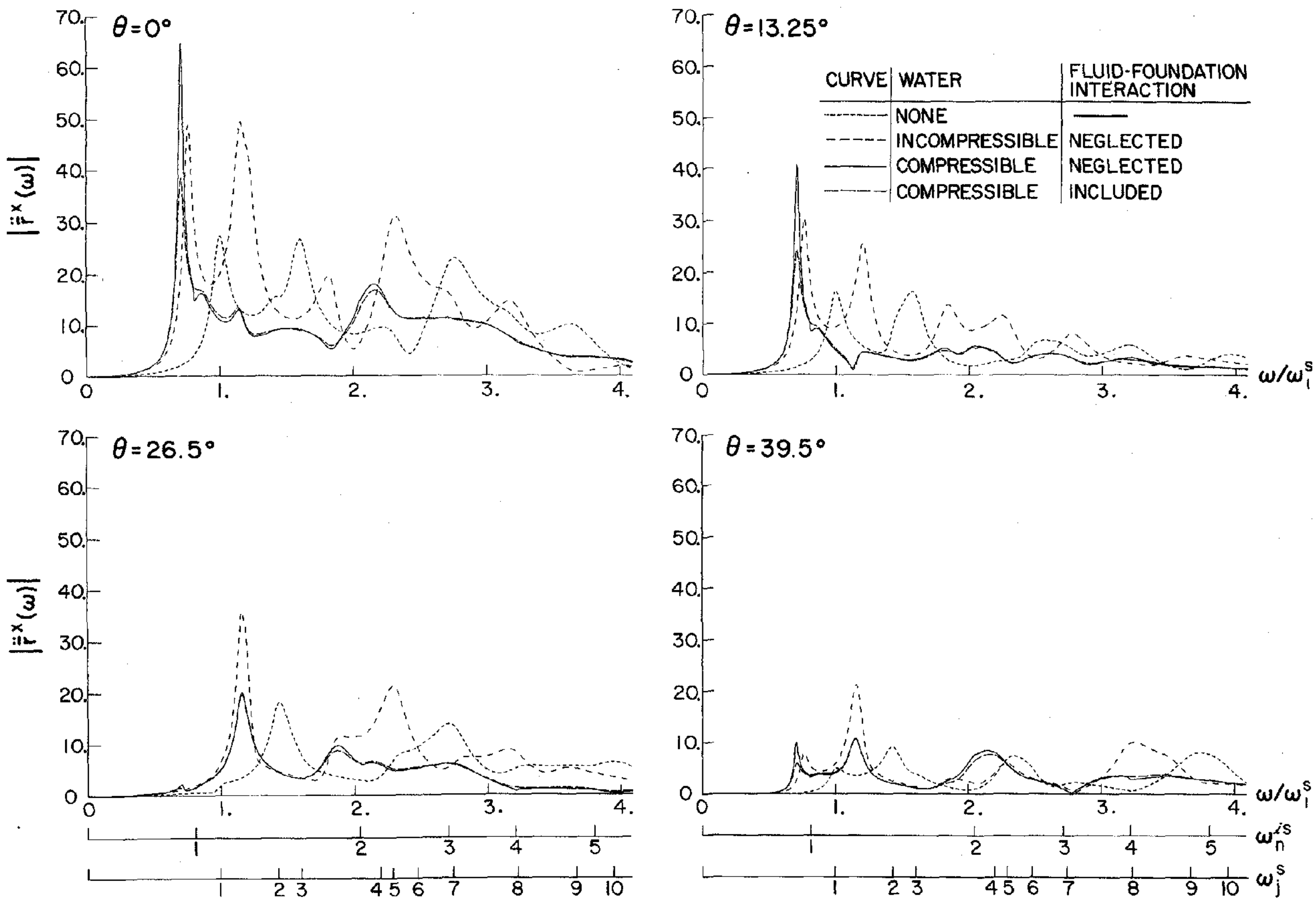

FIG. 8.6 RADIAL COMPONENTS OF DAM CREST ACCELERATION DUE TO HARMONIC, UPSTREAM-DOWNSTREAM GROUND MOTION

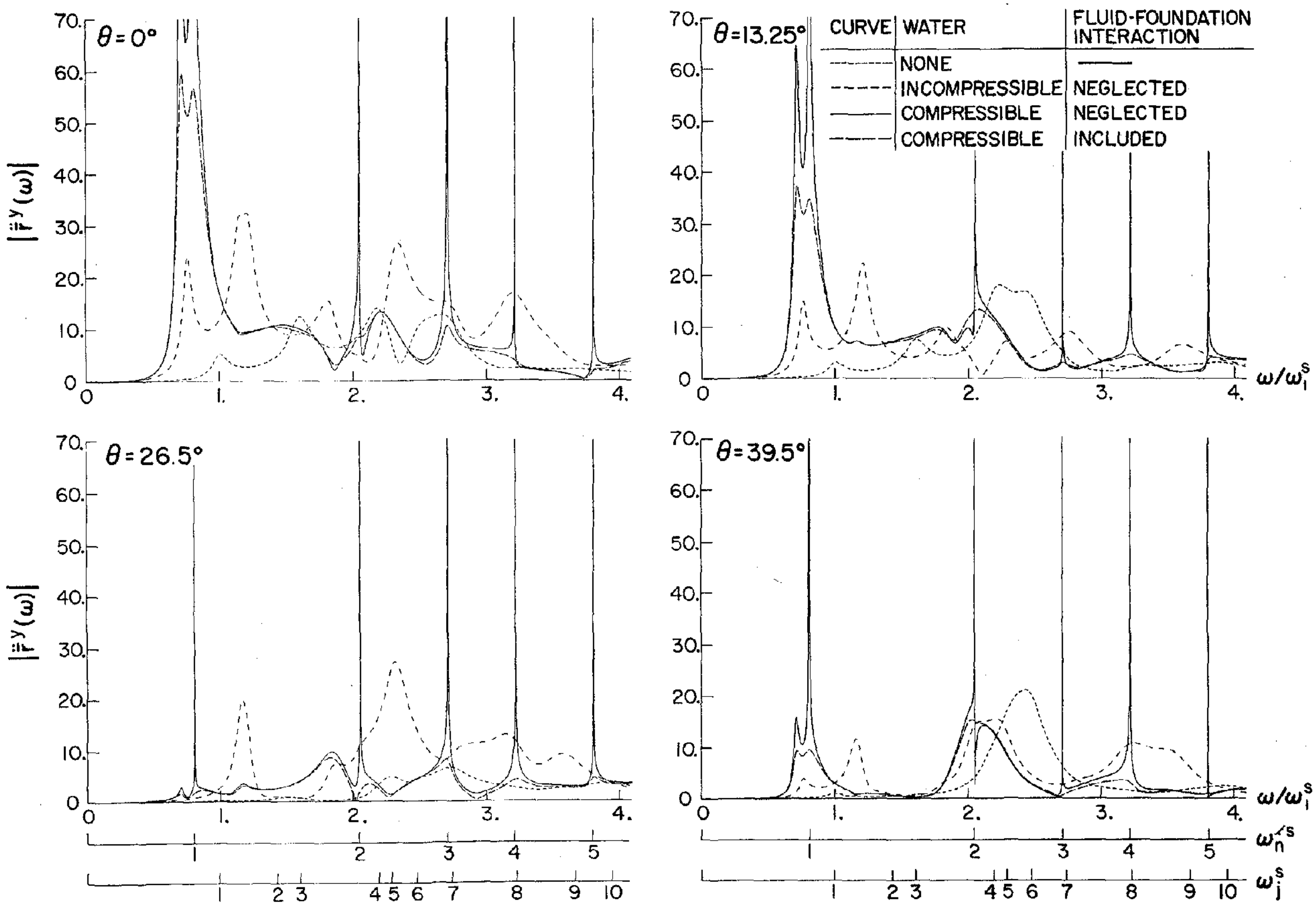

FIG. 8.7 RADIAL COMPONENTS OF DAM CREST ACCELERATION
DUE TO HARMONIC, VERTICAL GROUND MOTION

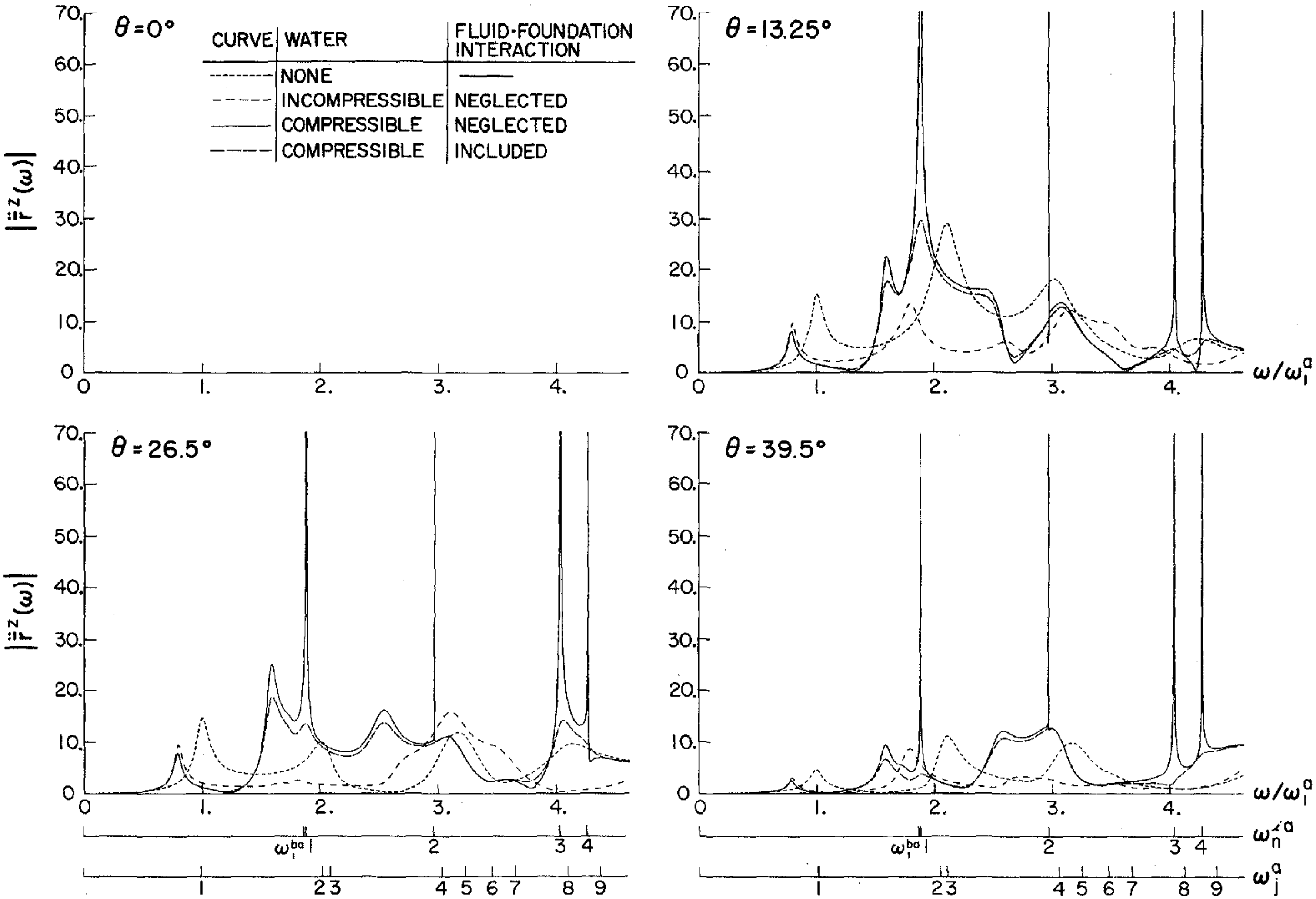

FIG. 8.8 RADIAL COMPONENTS OF DAM CREST ACCELERATION
DUE TO HARMONIC, CROSS-STREAM GROUND MOTION

8.3.1 Dam-fluid interaction effects

The dam accelerations without water due to x ground motion exceed those due to y or z ground motion. If water is present and assumed to be incompressible, the frequency independent added mass and added load reduce the resonant frequencies and alter the resonant amplitudes. These amplitudes are generally increased for x and y ground motions (Figs. 8.6 and 8.7) but are decreased for z ground motion (Fig. 8.8). The changes in resonant frequencies and amplitudes are more pronounced for the arch dam than the concrete gravity dam (Figs. 4.7 and 4.8) because the arch dam is lighter, and hence, the hydrodynamic added mass and added load are relatively more signficant fractions of the arch dam's mass and inertia load.

Water compressibility influences the dam responses through the frequency variations of the $\underline{\bar{Q}}^f(\omega)$ vectors. The added load vectors $\underline{\bar{Q}}_0^{fx}(\omega)$, $\underline{\bar{Q}}_0^{fy}(\omega)$ and $\underline{\bar{Q}}_0^{fz}(\omega)$ vary with excitation frequency similarly to $\bar{F}_0^x(\omega)$, $\bar{F}_0^y(\omega)$ and $\bar{F}_0^z(\omega)$, respectively, of Fig. 8.5 (fluid-foundation interaction neglected). The added mass vectors $\underline{\bar{Q}}_j^f(\omega)$ associated with symmetric dam modes vary similarly to $\bar{F}_0^x(\omega)$; the vectors $\underline{\bar{Q}}_j^f(\omega)$ associated with antisymmetric dam modes vary similarly to $\bar{F}_0^y(\omega)$, but with finite responses at the frequencies $\omega_n^{\ell a}$. The imaginary part of $\underline{\bar{Q}}_j^f(\omega)$ above $\omega_1^{\ell s}$ (x and y ground motions) or above $\omega_1^{\ell a}$ (z ground motion) provides fluid radiation damping.

In the acceleration response to x and y ground motions (Figs. 8.6 and 8.7), water compressibility further shifts the first resonant peak to a frequency below $\omega_1^{\ell s}$ with a larger increase in amplitude, a result of the greater hydrodynamic added mass and added load. Dam accelerations due to y ground motion are unbounded at excitation frequencies equal to $\omega_n^{\ell s}$ because of the infinite values attained by $\bar{Q}_0^{fy}(\omega)$. The resonant amplitude of $\bar{Q}_0^{fy}(\omega)$ at $\omega_1^{\ell s}$ is large over a wide frequency interval (as for $\bar{F}_0^y(\omega)$ in Fig. 8.5b) and results in very large dam accelerations in the vicinity of $\omega_1^{\ell s}$ as shown in Fig. 8.7. The increases in acceleration response near $\omega_1^{\ell s}$ in Figs. 8.6 and 8.7 due to water compressibility exceed the corresponding increases in the concrete gravity dam response (Figs. 4.7 and 4.8). Thus, in this lower part of the frequency range, water compressibility appears to be more important for the arch dam than the concrete gravity dam due to the greater relative importance of the hydrodynamic forces. At excitation frequencies above $\omega_1^{\ell s}$, however, this trend is offset due to a greater relative importance of fluid radiation damping for the arch dam. Above $\omega_1^{\ell s}$, the acceleration response including water compressibility is smaller than the response without water or with incompressible water in Fig. 8.6 and is reduced to small values between the infinite spikes in Fig. 8.7.

The acceleration response of the dam to z ground motion (Fig. 8.8) is unbounded at the frequencies $\omega_n^{\ell a}$ when water compressibility is considered due to the infinite values attained by $\bar{Q}_0^{fz}(\omega)$. The resonant amplitude of $\bar{Q}_0^{fz}(\omega)$ near $\omega_1^{\ell a}$ is large over a wide frequency range (as for $\bar{F}_0^z(\omega)$ in Fig. 8.5c) and results in large dam accelerations in the vicinity of $\omega_1^{\ell a}$. Whereas the large dam responses to x and y ground motions near $\omega_1^{\ell s}$ are due primarily to vibration of the dam in its first symmetric mode, the large response to z ground motion near $\omega_1^{\ell a}$ (a significantly greater frequency than

ω_1^{is}) is due to dam vibration in a combination of its second and third antisymmetric modes. The response to z ground motion which is primarily of the first antisymmetric mode occurs at lower frequencies and is not affected by water compressibility. Between the frequencies ω_n^{ia} in Fig. 8.8, fluid radiation damping limits the dam accelerations to small values. The infinite responses at the ω_n^{ia} in Fig. 8.8 and those at ω_n^{is} in Fig. 8.7 approach infinity at slow enough rates so that the Fourier Transform procedure of Sec. 2.4 for computing responses to arbitrary ground motions is applicable.

8.3.2 Fluid-foundation interaction effects

The $\underline{\bar{Q}}^f(\omega)$ vectors are bounded functions of frequency and complex valued for $\omega > 0$ when fluid-foundation interaction is included. Dam responses are affected by reduced resonances of the added load vectors $\underline{\bar{Q}}_o^{f\ell}(\omega)$ and by the imaginary component of the added mass vectors $\underline{\bar{Q}}_j^f(\omega)$ which provides foundation radiation damping and which is now present below ω_1^{is} (x and y ground motion) or ω_1^{ia} (z ground motion).

Effects of fluid-foundation interaction on the acceleration response to x ground motion (Fig. 8.6) are limited to a reduction in amplitude of the first resonant peak located below ω_1^{is}. Thus, inclusion of water compressibility and fluid-foundation interaction provides a general reduction in the dam accelerations below those with incompressible water. However, the resonance below ω_1^{is} represents an important increase in acceleration response in the low frequency region compared to the response without water.

Fluid-foundation interaction effects on the acceleration response to y ground motion (Fig. 8.7) include a bounded instead of unbounded response at ω_1^{is}, reduction of the preceding bounded peak, and the elimination of the infinite spikes at the higher ω_n^{is}. Because $\bar{\underline{Q}}_0^{fy}(\omega)$ still undergoes a large resonance at ω_1^{is} (as does $\bar{F}_0^y(\omega)$ in Fig. 8.5b), the dam accelerations in the vicinity of ω_1^{is} are large and exceed greatly those accelerations without water or with incompressible water. Above ω_1^{i}, however, the acceleration response including water compressibility and fluid-foundation interaction is comparable in amplitude to the response without water and is generally less than that with incompressible water.

In the acceleration response of the dam to z ground motion (Fig. 8.8), the unbounded response at ω_1^{ia} is replaced by a bounded peak, the preceding bounded peak is reduced, and the infinite spikes at the higher ω_n^{ia} are eliminated because of fluid-foundation interaction. The resulting dam accelerations are still greater than those with incompressible water, and at some frequencies they are greater than and at other frequencies less than those accelerations without water.

Thus, the acceleration responses of the dam, including water compressibility and fluid foundation interaction, to x and y ground motions attain maximum amplitudes in the vicinity of ω_1^{is} and have much lower response levels at higher frequencies. In the vicinity of ω_1^{is}, the acceleration response to y ground motion has greater amplitude over a wider frequency interval compared to the response to x ground motion. For this reason, regarding dam accelerations, the

y component of ground motion is likely to be of more importance than the x component, a contrast to the dam accelerations without water and with incompressible water where the x component of ground motion is of greater importance. The relative importance of the z component of ground motion is uncertain and depends on the frequency content of the ground time history because the region of maximum response occurs in the vicinity of ω_1^{ia}, a significantly greater frequency than ω_1^{is}. The large responses at ω_1^{is} due to x and y ground motions are associated with hydrodynamic effects which appear to be greater for the arch dam than the concrete gravity dam.

9. CONCLUSIONS

Incorporation of finite element models of irregular fluid domains into the substructure method for determining dynamic responses of dams including hydrodynamic effects has proven successful. The finite element procedure applies to either two or three-dimensional fluid domains and to either finite domains or infinite domains consisting of an irregular region of finite size connected to a region of uniform cross-section extending to infinity in the upstream direction. For such an infinite uniform region, a finite element discretization within the cross-section combined with a continuum representation in the infinite direction provides for the proper transmission of pressure waves. The fluid domain model can account for water compressibility and can approximately account for fluid-foundation interaction with a damping boundary condition applied along the reservoir floor and sides. The dam foundation is assumed rigid.

The substructure method is an effective way to compute dam responses and include hydrodynamic effects. When water compressibility is considered, the computational effort is greatly increased, and practically all is spent to calculate the hydrodynamic terms which represent effects of the fluid in the dam equation of motion. Thus, the computational effort depends directly on the finite element mesh of the fluid domain. The infinite, uniform reservoir assumption beyond some point upstream of the dam will limit the finite element mesh to the region between this point and the dam. Inclusion of fluid-foundation interaction significantly increases the computational effort because most of the arithmetic becomes complex valued. Further, for infinite fluid domains the eigensolution associated with the infinite, uniform region depends on the excitation frequency and for a three-dimensional fluid domain will require a relatively large computational effort. Based on the Morrow Point Dam example, the Central Processor times on a CDC 7600 computer for analyzing a three-dimensional dam-infinite fluid domain system can be expected to be several hundred seconds if water compressibility is considered and from five to ten times this amount if fluid-foundation interaction is considered (depending on symmetry considerations and the extent of the finite element mesh).

Hydrodynamic effects due to water assumed to be incompressible are equivalent to an added mass and added load which reduce the resonant frequencies of the system and alter the resonant amplitudes. The added mass and added load vary with excitation frequency if water compressibility is considered, and factors influencing the dam response include resonances of the added load and the radiation damping associated with the imaginary component of the added mass. If fluid-foundation interaction is neglected, this damping occurs only for infinite fluid domains (fluid radiation damping) at frequencies above the first eigenfrequency ω_1^{i} of the infinite, uniform region (ω_1^{is} or ω_1^{ia} for the three-dimensional symmetric or antisymmetric case), but occurs at all frequencies for both infinite and finite domains if fluid-foundation interaction is included (foundation radiation damping). Fluid-foundation interaction also reduces the resonances of the added load which can be very large if the fluid foundation is assumed rigid.

Hydrodynamic effects significantly influence the response of concrete gravity dams to harmonic ground motions, as seen with the complex frequency response functions for the horizontal component of acceleration at the dam crest.

1. The dam accelerations with full reservoir are essentially independent of reservoir shape if the water is assumed to be incompressible. The resonant responses of the dam generally exceed those of the dam without water, but this does not hold for vertical ground motion.

2. When water compressibility is considered, the dam accelerations are very dependent on reservoir shape if fluid-foundation interaction is neglected. For infinite fluid domains, the acceleration response of the dam to horizontal ground motion at excitation frequencies above ω_1^{ℓ} is reduced by fluid radiation damping below those responses without water and with incompressible water. However, unbounded responses to vertical ground motion cccur at excitation frequencies equal to ω_n^{ℓ} if the vertical excitation is applied over the entire length of the infinite reservoir floor. Frequency ranges where fluid radiation damping is not present, below ω_1^{ℓ} for infinite fluid domains and at all excitation frequencies for finite fluid domains, are regions of high response which can vary rapidly with frequency.

3. Inclusion of fluid-foundation interaction reduces these large responses and reduces the unbounded responses that occur for infinite fluid domains under complete vertical ground motion to bounded values. The resulting dam accelerations depend much less on fluid domain shape, especially for horizontal ground motion. Compared to the accelerations without water and with incompressible water, the acceleration response to horizontal ground motion including water compressibility and fluid-foundation interaction is reduced, and that to vertical ground motion is increased especially in the vicinity of the first resonant frequency of each fluid domain. The result, regarding dam accelerations, is a comparable level of importance for both horizontal and vertical components of ground motion.

Hydrodynamic effects in the acceleration response of earth dams to harmonic ground motions were investigated by employing a shear beam model for the dam. In the response to horizontal ground motion, hydrodynamic effects are unimportant due to the large mass of the dam and the small hydrodynamic pressures produced by the accelerations of the sloped dam face. If the ground motion is vertical, the dam response without water is zero because of the shear beam assumption, and that with incompressible water is small. For the infinite fluid domain considered, the dam response to vertical ground motion considering water compressibility is unbounded at excitation frequencies equal to ω_n^{ℓ} if fluid-foundation interaction is neglected. However, inclusion of fluid-foundation interaction reduces these unbounded responses to bounded values, and the dam accelerations are again small compared to those due to horizontal ground motion. Thus, hydrodynamic effects are unimportant in the acceleration response of earth dams to both horizontal and vertical ground motions.

For Morrow Point Dam, an arch dam, hydrodynamic effects appear to be more important than for the concrete gravity dam because the added mass and added load are more significant fractions of the arch dam's smaller mass and inertia load. These effects were investigated for the frequency response functions of radial acceleration at the dam crest due to harmonic ground motion.

1. When the water is assumed incompressible, the resonant amplitudes of acceleration responses to upstream-downstream (x) and vertical (y) ground motions generally exceed those of the dam without water, while the resonant amplitudes due to cross-stream (z) ground motion are decreased.

2. For the infinite fluid domain considered, water compressibility produces large dam accelerations in the vicinities of $\omega_1^{\ell s}$ (x and y ground motions) and $\omega_1^{\ell a}$ (z ground motion), especially for y and z ground motions where unbounded responses occur at these frequencies. Dam accelerations above $\omega_1^{\ell s}$ or $\omega_1^{\ell a}$ are much lower due to fluid radiation damping except for infinite spikes which occur at the higher $\omega_n^{\ell s}$

(y ground motion) or ω_n^{ia} (z ground motion) due to the non-zero accelerations of the floor and sides of the infinite reservoir.

3. Inclusion of fluid-foundation interaction eliminates these infinite spikes, but large acceleration responses still occur in the vicinities of ω_1^{is} (x and y ground motions) or ω_1^{ia} (z ground motion). These dam accelerations near ω_1^{is} due to y ground motion greatly exceed those due to x ground motion; thus, the y component of ground motion is likely to be of more importance, a contrast to the cases without water and with incompressible water where the x component is of more importance. The relative importance of the z component of ground motion depends on the frequency content of the earthquake time history since the maximum responses occur near ω_1^{ia}, a significantly greater frequency than ω_1^{is}.

The method of analysis needs to be improved to account for foundation interaction with the dam. Such a provision should include realistic free-field motions along the canyon walls in arch dam analyses. Regarding computational efficiency, large savings would result from a more efficient treatment of the frequency dependent eigenproblem associated with the infinite, uniform region of a three-dimensional fluid domain when fluid-foundation interaction is considered. Several such schemes are currently under study. Further work is needed to extend the investigation of hydrodynamic effects on dam responses to earthquake ground motions, including stress responses.

REFERENCES

1. R. W. Clough, J. M. Raphael, and S. Mojtahedi, "ADAP - A Computer Program for Static and Dynamic Analysis of Arch Dams," Earthquake Engineering Research Center Report No. EERC 73-14, University of California, Berkeley, June 1973.

2. P. Chakrabarti and A. K. Chopra, "Hydrodynamic Effects in Earthquake Response of Gravity Dams," Journal of the Structural Division, ASCE, Vol. 100, No. ST6, June 1974, pp. 1211-1224.

3. C. S. Porter and A. K. Chopra, "Dynamic Response of Simple Arch Dams Including Hydrodynamic Interaction," Earthquake Engineering Research Center Report No. UCB/EERC-80/17, University of California, Berkeley, July 1980.

4. R. Priscu, A. Popovici, L. Ilie and D. Stematiu, "New Aspects in the Earthquake Analysis of Arch Dams," Criteria and Assumptions for Numerical Analysis of Dams, Ed. by D. N. Naylor, et al., Proceedings of an International Symposium, Swansea, United Kingdom, Sept. 1975, pp. 710-722.

5. T. Hatano and T. Nakagawa, "Seismic Analysis of Arch Dams - Coupled Vibrations of Dam Body and Reservoir Water," Technical Report, Technical Laboratory No. 1, Central Research Institute of Electric Power Industry, Tokyo, Japan, Nov. 1972.

6. S. S. Saini, P. Bettess, and O. C. Zienkiewicz, "Coupled Hydrodynamic Response of Concrete Gravity Dams Using Finite and Infinite Elements," International Journal of Earthquake Engineering and Structural Dynamics, Vol. 6, No. 4, July-August 1978, pp. 363-374.

7. P. Chakrabarti and A. K. Chopra, "Earthquake Analysis of Gravity Dams Including Hydrodynamic Interaction," International Journal of Earthquake Engineering and Structural Dynamics, Vol. 2, No. 2, Oct.-Dec. 1973, pp. 143-160.

8. J. Lysmer and G. Waas, "Shear Waves in Plane Infinite Structures," Journal of the Engineering Mechanics Division, ASCE, Vol. 98, No. EM1, Feb. 1972, pp. 85-105.

9. A. K. Chopra, P. Chakrabarti, and S. Gupta, "Earthquake Response of Concrete Gravity Dams Including Hydrodynamic and Foundation Interaction Effects," Earthquake Engineering Research Center Report No. UCB/EERC-80/01, University of California, Berkeley, Jan. 1980.

10. E. Rosenblueth, "Presión hidrodinámica en presas debida a la aceleración vertical con refracción en el fondo," II Congreso Nacional de Ingeniería Sísmica, Veracruz, Mexico, May 1968.

11. D. Rea, C-Y. Liaw, and A. K. Chopra, "Mathematical Models for the Dynamic Analysis of Concrete Gravity Dams," International Journal of Earthquake Engineering and Structural Dynamics, Vol. 3, No. 3, Jan.-March 1975, pp. 249-258.

12. O. C. Zienkiewicz, The Finite Element Method, McGraw-Hill Book Company (UK) Limited, 1977.

13. A. T. Chwang, "Pressures on Sloping Dams During Earthquakes. Part 2. Exact Theory," Journal of Fluid Mechanics, Vol. 87, Part 2, July 1978, pp. 343-348.

14. J. F. Hall and A. K. Chopra, "A Computer Program for Earthquake Analysis of Dam-Fluid Systems," Earthquake Engineering Research Center Report, University of California, Berkeley (to be published).

15. G. R. Martin and H. B. Seed, "Dynamic Response Analyses for Earth Dams," Report No. TE 65-1, Institute of Transportation and Traffic Engineering, University of California, Berkeley, Aug. 1965.

16. S. F. Pawsey, "The Analysis of Moderately Thick to Thin Shells by the Finite Element Method," Report No. UC SESM 70-12, Structural Engineering Laboratory, University of California, Berkeley, Aug. 1970.

17. K. J. Bathe, "Solution Methods for Large Generalized Eigenvalue Problems in Structural Engineering," Report No. UC SESM 71-20, Structural Engineering Laboratory, University of California, Berkeley, Nov. 1971.

18. D. P. Mondkar and G. H. Powell, "Towards Optimal In-Core Equation Solving," Computers and Structures, Vol. 4, No. 3, May 1974, pp. 531-548.

19. R. W. Clough and J. Penzien, Dynamics of Structures, McGraw-Hill, Inc., 1975.

APPENDIX A. NOTATION

a_g^ℓ = component of ground acceleration in the ℓ direction

a_n = component of acceleration normal to a fluid boundary

a_n^i = component of acceleration normal to the boundary of the uniform cross-section of an infinite fluid domain

$A, \mathcal{A}, B, \mathcal{B}$ = incident and reflected wave amplitudes employed in Sec. 2.5

A_g^ℓ = Fourier transform of a_g^ℓ

$\underline{B}$ = finite element "damping" matrix for a finite fluid domain

$\underline{B}^i$ = finite element "damping" matrix for the uniform cross-section of an infinite fluid domain

$\underline{c}$ = finite element damping matrix for the dam

C = velocity of compression waves in water

C_j = generalized damping of the jth natural mode of vibration of the dam

C_r = velocity of compression waves in the foundation rock

C_s = velocity of shear waves in an earth dam

$\underline{D}$ = vector of nodal accelerations for a fluid domain

$\underline{D}^x$ = vector of nodal accelerations at the dam-fluid interface of an infinite fluid domain of uniform cross-section

$\underline{D}^i$ = vector of nodal accelerations for the uniform cross-section of an infinite fluid domain

$\underline{D}_o^\ell$ = vector of nodal accelerations due to a harmonic ground acceleration = $e^{i\omega t}$ in the ℓ direction with rigid dam

$\underset{\sim}{D}_j$ = vector of nodal accelerations due to a harmonic acceleration of the dam in its jth natural mode of vibration

$\underset{\sim}{e}(x)$ = an $N \times N$ diagonal matrix with nth diagonal term = $e^{-\kappa_n x}$

$\underset{\sim}{e}^{\ell}$ = a vector defined for Eqs. 2.2 and 6.2

E_d = modulus of elasticity of concrete

E_r = modulus of elasticity of foundation rock

$\underset{\sim}{E}^{\ell}$ = vector of inertia loads on the dam due to a unit acceleration of the dam as a rigid body in the ℓ direction

F_{st} = x component of force on the dam (or half of a symmetric dam) due to hydrostatic pressure

F_0^{ℓ} = x component of hydrodynamic force on a rigid dam (or half of a symmetric, rigid dam) due to ground acceleration in the ℓ direction

$\bar{F}_0^{\ell}$ = complex frequency response of F_0^{ℓ}

g = acceleration of gravity

$\underset{\sim}{G}$ = finite element "mass" matrix for a finite fluid domain

$\underset{\sim}{G}^{i}$ = finite element "mass" matrix for the uniform cross-section of an infinite fluid domain

H = water depth adjacent to the dam

H_d = height of a concrete dam

H_s = height of an earth dam

$\underset{\sim}{H}$ = finite element "stiffness" matrix for a finite fluid domain

$\underset{\sim}{H}^{i}$ = finite element "stiffness" matrix for the uniform cross-section of an infinite fluid domain

$i = \sqrt{-1}$

J = number of $\underset{\sim}{\phi}_j$ included for the dam

J_0, J_1 = Bessel functions of the first kind of orders zero and one, respectively

$\underset{\sim}{k}$ = finite element stiffness matrix for the dam

K_j = generalized stiffness for the jth natural mode of vibration of the dam

ℓ = direction of ground motion, either x, y, or z

L_e = excitation length for the floor of an infinite fluid domain of constant depth

L_j^ℓ = generalized load for the jth natural mode of vibration of the dam including hydrodynamic added load and due to ground acceleration in the ℓ direction

$\underset{\sim}{L}^\ell$ = vector of dimension J with jth term = L_j^ℓ

$\underset{\sim}{m}$ = finite element mass matrix for the dam

$\underset{\sim}{m}_g$ = mass matrix for the dam coupling DOF along the foundation with interior DOF

M = number of $\underset{\sim}{\zeta}_m$ included for a finite fluid domain

M_j = generalized mass for the jth natural mode of vibration of the dam

n denotes the inward normal direction to a fluid boundary

N = number of $\underset{\sim}{\psi}_n$ included for an infinite fluid domain

p = hydrodynamic pressures in excess of static pressure

p^f = pressures at the dam-fluid interface

p_o^ℓ = pressures due to ground acceleration in the ℓ direction with rigid dam

p_j = pressures due to an acceleration of the dam in its jth natural mode of vibration

p_x, p_y, p_{yz} = separated pressure functions in the x direction, y direction, and y - z plane, respectively

$\bar{p}$ = complex frequency response of p

$\underline{\bar{p}}$ = vector of nodal pressures in the fluid domain

P_j^ℓ = generalized load for the jth natural mode of vibration of the dam including hydrodynamic effects and due to ground acceleration in the ℓ direction

q = $w/C_r w_r$, the damping coefficient along the fluid-foundation boundary

$\underline{Q}$ = vector of hydrodynamic forces corresponding to DOF of the dam

$\underline{Q}^f$ = vector of hydrodynamic forces for nodes along the dam-fluid interface

$\underline{Q}_o^{f\ell}$ = static equivalent of $p_o^{f\ell}$

$\underline{Q}_j^f$ = static equivalent of p_j^f

$\underline{\bar{Q}}$ = complex frequency response of $\underline{Q}$

$\ddot{r}^\ell$ = acceleration of the dam crest due to ground acceleration in the ℓ direction

$\bar{\ddot{r}}^\ell$ = complex frequency response of $\ddot{r}$

r,s = fluid boundary coordinates along the dam-fluid interface

r',s' = fluid boundary coordinates along the reservoir floor and sides

R_u, R_d = radii to upstream and downstream faces of an arch dam

$\underset{\sim}{S}$ = the $J \times J$ dynamic stiffness matrix for the dam including hydrodynamic added mass

t = time variable

t_d = duration of ground motion

T_u, T_d = thickness parameters to upstream and downstream faces of an arch dam

u = vertical foundation displacement

$\bar{u}$ = complex frequency response of u

$\underset{\sim}{v}$ = vector of nodal displacements of the dam relative to the ground

w = unit weight of water

w_d = unit weight of concrete in a dam

w_r = unit weight of foundation rock

w_s = unit weight of earth in a dam

x,y,z = orthogonal coordinates in upstream-downstream, vertical, and cross-stream directions, respectively

Y_j^{ℓ} = generalized displacement of the jth natural mode of vibration of the dam due to ground acceleration in the ℓ direction

$\bar{Y}_j^{\ell}$ = complex frequency response of Y_j^{ℓ}

$\underset{\sim}{\bar{Y}}^{\ell}$ = vector of dimension J with jth term = $\bar{Y}_j^{\ell}$

α_r = the reflection coefficient for an incident pressure wave striking the foundation rock

α_m = amplitude of $\underset{\sim}{\zeta}_m$

$\bar{\alpha}_m$ = complex frequency response of α_m

$\bar{\underset{\sim}{\alpha}}$ = vector of dimension M with mth term = $\bar{\alpha}_m$

β = parameter defining the slope of an earth dam

β_j = parameter used to define the jth natural frequency of the dam

γ_m = mth eigenvalue of a finite fluid domain (q = 0)

Γ = an $M \times M$ diagonal matrix with mth diagonal term = $\gamma_m^2 - \dfrac{\omega^2}{C^2}$

ε^{ℓ} = function defined for Eqs. 2.10 and 6.8

$\underset{\sim}{\zeta}_m$ = mth eigenvector of a finite fluid domain (q = 0)

$\underset{\sim}{Z}$ = matrix with the M eigenvectors $\underset{\sim}{\zeta}_m$ as columns

η_n = amplitude of $\underset{\sim}{\psi}_n$

$\bar{\eta}_n$ = complex frequency response of η_n

$\bar{\underset{\sim}{\eta}}$ = vector of dimension N with nth term = $\bar{\eta}_n$

θ = abutment angle for an arch dam

$\kappa_n = \sqrt{\lambda_n^2 - \dfrac{\omega^2}{C^2}}$, with positive real and imaginary parts

$\underset{\sim}{K}$ = an $N \times N$ diagonal matrix with nth diagonal term = κ_n

λ_n = nth eigenvalue of the uniform cross-section of an infinite fluid domain ($q \geqslant 0$)

$\underset{\sim}{\Lambda}$ = an $N \times N$ diagonal matrix with nth diagonal term = $\lambda_n^2 - \dfrac{\omega^2}{C^2}$

μ_n = real part (positive) of κ_n

ν = Poisson's ratio

ν_n = imaginary part (positive) of κ_n

ξ_j = damping ratio for the jth natural mode of vibration of the dam

τ_j = jth zero of J_o

$\underline{\phi}_j$ = vector of the jth natural mode of vibration of the dam

$\underline{\phi}_j^f$ = vector of the jth dam mode for nodes along the dam-fluid interface

ϕ_j^f = continuum function representation of $\underline{\phi}_j^f$

$\underline{\psi}_n$ = nth eigenvector of the uniform cross-section of an infinite fluid domain $(q \geqslant 0)$

$\underline{\Psi}$ = a matrix with the N eigenvectors $\underline{\psi}_n$ as columns

ω = frequency of excitation

ω_j = jth natural frequency of vibration of a dam

ω_m^b = $\gamma_m C$, the mth eigenfrequency of a finite fluid domain $(q = 0)$. Also, if it exists, the mth eigenfrequency of an infinite fluid domain of irregular geometry $(q = 0)$.

ω_n^r = $(2n-1)\pi C/2H$, the nth eigenfrequency of the cross-section of the two-dimensional, infinite fluid domain of constant depth obtained in a continuum analysis $(q = 0)$

ω_n^{ℓ} = $\lambda_n C$, the nth eigenfrequency of the uniform cross-section of an infinite fluid domain $(q = 0)$

1,2 = partitioning subscripts for the DOF of an infinite fluid domain of irregular geometry (Secs. 3.4 and 7.4)

s,a = superscripts to denote a symmetric or antisymmetric response quantity of a three-dimensional, symmetric dam or fluid domain

APPENDIX B. FINITE ELEMENT DERIVATIONS FOR FINITE FLUID DOMAINS

For the fluid domains of Figs. B.1 to B.3, finite element formulations which relate the harmonic, hydrodynamic pressure response to harmonic, normal components of boundary accelerations are derived below. The fluid domains of the figures are two, one, and three-dimensional, respectively. Terms of the final matrix equations are integral expressions which can be efficiently evaluated by the method of Gauss quadrature. More complete treatments which include discussion of convergence requirements can be found elsewhere (12).

B.1 Two-Dimensional Fluid Domains

B.1.1 Governing equations

The hydrodynamic pressure $\bar{p}(x,y,\omega)$ within the fluid domain of Fig. B.1a is governed by the two-dimensional Helmholtz equation

$$\frac{\partial^2 \bar{p}}{\partial x^2} + \frac{\partial^2 \bar{p}}{\partial y^2} + \frac{\omega^2}{C^2}\,\bar{p} = 0 \tag{B.1}$$

subject to boundary conditions along accelerating boundaries

$$\frac{\partial \bar{p}}{\partial n}(s,\omega) = -\frac{w}{g}\,a_n(s) \tag{B.2a}$$

$$\frac{\partial \bar{p}}{\partial n}(s',\omega) = -\frac{w}{g}\,a_n(s') + i\omega q\,\bar{p}(s',\omega) \tag{B.2b}$$

Preceding page blank

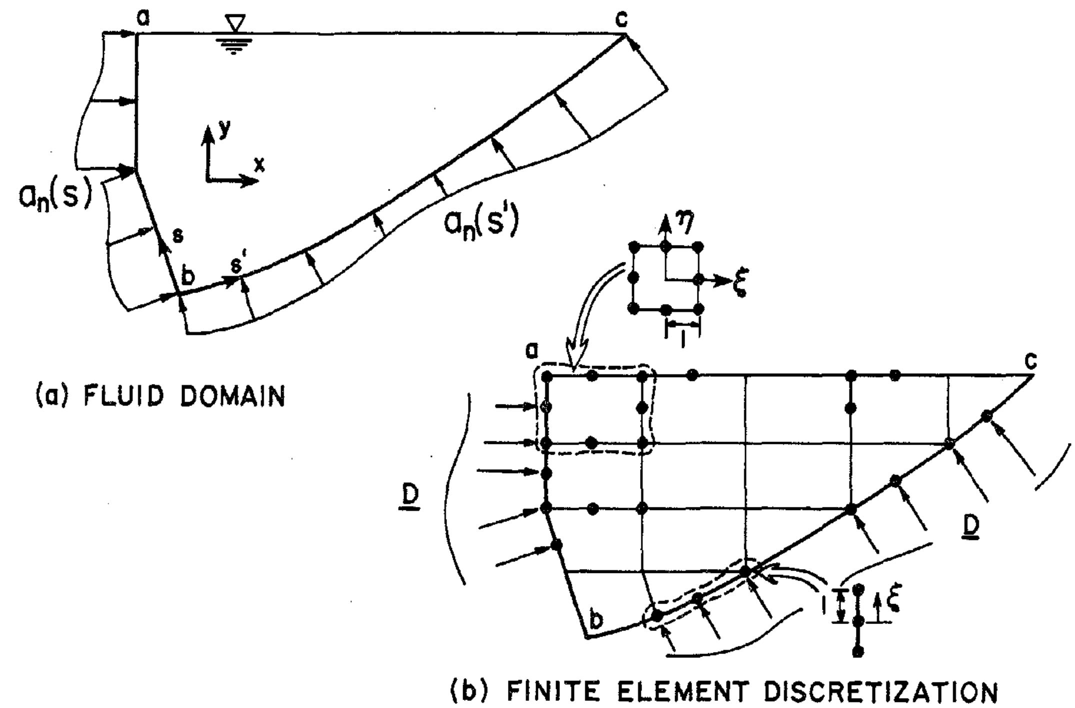

FIG. B.1 TWO-DIMENSIONAL FINITE FLUID DOMAIN and at the free surface $(y = H)$

$$\bar{p}(x,H,\omega) = 0 \tag{B.3}$$

In Eq. B.2, s and s' are coordinates along the dam fluid interface a-b (denoted by $\mathcal{D}$) and the reservoir floor b-c (denoted by $\mathcal{D}'$), respectively.

The equations above are satisfied by that $\bar{p}(x,y,\omega)$ which minimizes a functional $\chi(\bar{p})$ defined by

$$\chi(\bar{p}) = \int_{\mathcal{V}} \frac{1}{2}\left(\left(\frac{\partial\bar{p}}{\partial x}\right)^2 + \left(\frac{\partial\bar{p}}{\partial y}\right)^2 - \frac{\omega^2}{C^2}\,\bar{p}^2\right) d\mathcal{V} - \int_{\mathcal{D},\mathcal{D}'} \frac{w}{g}\, a_n(s)\; \bar{p}(s,\omega)\; d\mathcal{D}$$

$$+ \int_{\mathcal{D}'} \frac{1}{2}\, i\omega q \left(\bar{p}(s',\omega)\right)^2 d\mathcal{D}, \qquad s = s,s' \tag{B.4}$$

where $\mathcal{V}$ is the two-dimensional domain of the fluid a-b-c-a. In the finite element method, minimization of Eq. B.4 is carried out within subregions $\mathcal{V}^e$ of $\mathcal{V}$ (finite elements) and within subboundaries $\mathcal{D}^e$ of $\mathcal{D},\mathcal{D}'$ (boundary elements). In Fig. B.1b the region $\mathcal{V}$ is discretized into finite elements. This process automatically divides the accelerating boundaries $\mathcal{D},\mathcal{D}'$ into boundary elements. The functional $\chi(\bar{p})$ can be expressed as a summation over the elements:

$$\chi(\bar{p}) = \sum_{V} \int_{V^e} \frac{1}{2}\left(\left(\frac{\partial \bar{p}^e}{\partial x}\right)^2 + \left(\frac{\partial \bar{p}^e}{\partial y}\right)^2 - \frac{\omega^2}{c^2}\left(\bar{p}^e\right)^2\right) dV$$

$$- \sum_{D,D'} \int_{D^e} \frac{w}{g}\, a_n^e(s)\, \bar{p}^e(s,\omega)\, dD + \sum_{D'} \int_{D^e} \frac{1}{2}\, i\omega q \left(\bar{p}^e(s',\omega)\right)^2 dD, \quad s = s,s' \tag{B.5}$$

where the superscript e denotes an element quantity, either interior or boundary.

B.1.2 Element mapping

Each finite element V^e is mapped onto the x,y plane from a simple shape in an image coordinate system. The mapping is controlled by specifying locations in the x,y plane into which certain points (nodal points) in the image plane are mapped. For example, the circled element of Fig. B.1b is mapped from the rectangle $-1 \leqslant \xi \leqslant 1$, $-1 \leqslant \eta \leqslant 1$ according to

$$\begin{aligned} x &= \sum_i N_i(\xi,\eta)\, x_i^e = \underset{\sim}{N}^T \underset{\sim}{x}^e \\ y &= \sum_i N_i(\xi,\eta)\, y_i^e = \underset{\sim}{N}^T \underset{\sim}{y}^e \end{aligned} \tag{B.6}$$

where $N_i(\xi,\eta)$ = a shape function whose value is one at the ith node and zero at all other element nodes; (x_i^e, y_i^e) is the x,y location of the ith node; and $\sum_i$ is over all element nodes. The magnitude of an incremental area dV in the x,y plane mapped from an area

$d\xi d\eta$ is given by

$$dV = \det[\underline{J}]\, d\xi d\eta \tag{B.7}$$

where $\det[\underline{J}]$ is the determinant of $\underline{J}$, the transformation matrix for shape function partial derivatives. Thus,

$$\begin{Bmatrix} \dfrac{\partial N_i}{\partial \xi} \\ \\ \dfrac{\partial N_i}{\partial \eta} \end{Bmatrix} = \underline{J} \begin{Bmatrix} \dfrac{\partial N_i}{\partial x} \\ \\ \dfrac{\partial N_i}{\partial y} \end{Bmatrix} \tag{B.8}$$

where

$$\underline{J} = \begin{bmatrix} \dfrac{\partial x}{\partial \xi} & \dfrac{\partial y}{\partial \xi} \\ \\ \dfrac{\partial x}{\partial \eta} & \dfrac{\partial y}{\partial \eta} \end{bmatrix} \tag{B.9}$$

The terms of $\underline{J}$ are computed by taking the appropriate partial derivatives of Eq. B.6. Versions of the above equations are available for triangular image shapes using area coordinates (12).

The boundary $\mathcal{D},\mathcal{D}'$ is entirely defined by the above procedure. However, for convenience a separate, but equivalent, mapping is introduced in which each boundary element $\mathcal{D}^e$ is mapped from the region $1 \leqslant \xi \leqslant 1$ on the ξ axis (see the circled boundary element in Fig. B.1b). Thus,

$$\begin{aligned} x^b &= \sum_j M_j(\xi)\, x_j^{be} = \underline{M}^T\, \underline{x}^{be} \\ y^b &= \sum_j M_j(\xi)\, y_j^{be} = \underline{M}^T\, \underline{y}^{be} \end{aligned} \tag{B.10}$$

where $M_j(\xi)$ = a shape function for a boundary element whose value is one at the jth node and zero at all other boundary element nodes; (x_j^{be}, y_j^{be}) is the x,y location of the jth node; and $\sum_j$ is over all boundary element nodes. $M_j(\xi)$ is computed from $N_i(\xi,\eta)$ of the adjacent interior element where j and i refer to the same nodal point. Thus, if the $\eta = -1$ side of the interior element maps onto $\mathcal{D}^e$, then

$$M_j(\xi) = N_i(\xi,-1) \tag{B.11}$$

with similar expressions if other sides of the interior element map onto $\mathcal{D}^e$. The magnitude of an incremental length $d\mathcal{D}$ in the x,y plane mapped from a length $d\xi$ is given by

$$d\mathcal{D} = |n| \; d\xi \tag{B.12}$$

where $|n|$ is the absolute value of the normal vector along $\mathcal{D}^e$ whose x and y components are defined by

$$\begin{aligned} n_x &= \frac{dy^b}{d\xi} \\ n_y &= -\frac{dx^b}{d\xi} \end{aligned} \tag{B.13}$$

The derivatives of Eq. B.13 are computed from Eq. B.10. With a proper choice of sign, n is the inward normal to the fluid domain.

B.1.3 Element pressure definition

A similar procedure to Eq. B.6 expresses the element pressure $\bar{p}^e(x,y,\omega)$ within each V^e in terms of values at the nodes. Thus, $\bar{p}^e(x,y,\omega)$ is defined as $\bar{p}^e(\xi,\eta,\omega)$ where

$$\bar{p}^e(\xi,\eta,\omega) = \sum_i N_i(\xi,\eta)\, \bar{p}_i^e(\omega) = \underline{N}^T\, \underline{\bar{p}}^e(\omega) \tag{B.14}$$

and where $\bar{p}_i^e(\omega)$ = ith nodal pressure of the element. The shape function $N_i(\xi,\eta)$, then, describes the pressure distribution throughout the element when $\bar{p}_i^e(\omega)$ increases a unit amount.

For convenience, the boundary element pressure along $\mathcal{D},\mathcal{D}'$ is expressed in a manner similar to Eq. B.10. Thus, within each $\mathcal{D}^e$, $\bar{p}^e(s,\omega)$ or $\bar{p}^e(s',\omega)$ is defined as $\bar{p}^e(\xi,\omega)$ where

$$\bar{p}^e(\xi,\omega) = \sum_j M_j(\xi)\, \bar{p}_j^{be}(\omega) = \underline{M}^T\, \underline{\bar{p}}^{be}(\omega) \tag{B.15}$$

and where $\bar{p}_j^{be}(\omega)$ = the jth nodal pressure of the boundary element. The normal acceleration $a_n^e(s)$ or $a_n^e(s')$ can also be defined on the ξ axis as $a_n^e(\xi)$. This process is described in Appendix D.1.

B.1.4 Functional integration and minimization

Using the above equations, integration of Eq. B.5 can be carried out in the image coordinate systems. Substitutions into Eq. B.5 result in

$$\tilde{X}(\bar{p}) = \sum_{V} \left\{\bar{\underline{p}}^{e}(\omega)\right\}^{T} \left[\int_{-1}^{1}\int_{-1}^{1} \left(\frac{\partial \underline{N}}{\partial x}\frac{\partial \underline{N}^{T}}{\partial x} + \frac{\partial \underline{N}}{\partial y}\frac{\partial \underline{N}^{T}}{\partial y} - \frac{\omega^{2}}{C^{2}}\,\underline{N}\,\underline{N}^{T}\right) \det[\underline{J}]\; d\xi d\eta\right] \bar{\underline{p}}^{e}(\omega)$$

$$- \sum_{\mathcal{D},\mathcal{D}'} \left\{\bar{\underline{p}}^{be}(\omega)\right\}^{T} \left\{\frac{w}{g}\int_{-1}^{1} \underline{M}\; a_{n}^{e}(\xi)\; |n|\; d\xi\right\}$$

$$+ \sum_{\mathcal{D}'} \left\{\bar{\underline{p}}^{be}(\omega)\right\}^{T} \left[i\omega q \int_{-1}^{1} \underline{M}\;\underline{M}^{T}\; |n|\; d\xi\right] \bar{\underline{p}}^{be}(\omega) \qquad \text{(B.16)}$$

where the shape function partial derivatives are computed by solving Eq. B.8 for each node i of an element. The functional is now approximate (denoted by ~) because of the assumed interelement pressure distributions. Equation B.16 is written as

$$\tilde{X}(\bar{p}) = \sum_{V} \left\{\bar{\underline{p}}^{e}(\omega)\right\}^{T} \left[\underline{H}^{e} - \frac{\omega^{2}}{C^{2}}\,\underline{G}^{e}\right] \bar{\underline{p}}^{e}(\omega) - \sum_{\mathcal{D},\mathcal{D}'} \left\{\bar{\underline{p}}^{be}(\omega)\right\}^{T} \frac{w}{g}\,\underline{D}^{e}$$

$$+ \sum_{\mathcal{D}'} \left\{\bar{\underline{p}}^{be}(\omega)\right\}^{T} i\omega q\; \underline{B}^{e}\; \bar{\underline{p}}^{be}(\omega) \qquad \text{(B.17)}$$

where

$$H_{ij}^{e} = \int_{-1}^{1}\int_{-1}^{1} \left(\frac{\partial N_{i}}{\partial x}\frac{\partial N_{j}}{\partial x} + \frac{\partial N_{i}}{\partial y}\frac{\partial N_{j}}{\partial y}\right) \det[\underline{J}]\; d\xi d\eta$$

$$\text{(B.18)}$$

$$G_{ij}^{e} = \int_{-1}^{1}\int_{-1}^{1} N_{i}\, N_{j}\, \det[\underline{J}]\; d\xi d\eta$$

$$D_i^e = \int_{-1}^{1} M_i \; a_n^e(\xi) \; |n| \; d\xi$$

(B.18) cont'd

$$B_{ij}^e = \int_{-1}^{1} M_i \; M_j \; |n| \; d\xi$$

Symmetry of the element matrices is evident.

The matrices and vectors of Eq. B.17 can be assembled into a single, larger set. In this process portions corresponding to the nodes at the free surface a-c are not assembled because according to Eq. B.3 the nodal pressures there are zero. Thus,

$$\tilde{X}(\bar{p}) = \underline{\bar{p}}(\omega)^T \left[\underline{H} + i\omega q \; \underline{B} - \frac{\omega^2}{C^2} \underline{G} \right] \underline{\bar{p}}(\omega) - \underline{\bar{p}}(\omega)^T \frac{w}{g} \underline{D} \qquad \text{(B.19)}$$

where the dimension of the vectors and symmetric matrices equals the number of nodes below the free surface in Fig. B.1b. Minimization of Eq. B.19 is carried out by setting the derivative with respect to each $\bar{p}_i(\omega)$ to zero, resulting in

$$\left[\underline{H} + i\omega q \; \underline{B} - \frac{\omega^2}{C^2} \underline{G} \right] \underline{\bar{p}}(\omega) = \frac{w}{g} \underline{D} \qquad \text{(B.20)}$$

The non-zero portion of $\underline{B}$ is a submatrix corresponding to nodes along $\mathcal{D}'$ where the boundary condition of Eq. B.2b is applied. $\underline{D}$ has non-zero terms for only nodes along $\mathcal{D},\mathcal{D}'$ where accelerations are applied.

B.2 One-Dimensional Fluid Domain

The fluid domain of Fig. B.2a arises as a cross-section of a two-dimensional fluid domain when no variations in geometry or accelerations are present in the x direction. The hydrodynamic pressure $\bar{p}(y,\omega)$ is governed by the one-dimensional Helmholtz equation

$$\frac{d^2\bar{p}}{dy^2} + \frac{\omega^2}{C^2}\,\bar{p} = 0 \tag{B.21}$$

subject to boundary conditions

$$\frac{d\bar{p}}{dy}\,(0,\omega) = -\frac{w}{g}\,a_y^{\ell} + i\omega q\;\bar{p}(0,\omega) \tag{B.22}$$

$$\bar{p}(H,\omega) = 0 \tag{B.23}$$

The functional to be minimized is

$$\chi(\bar{p}) = \int_0^H \frac{1}{2}\left(\left(\frac{d\bar{p}}{dy}\right)^2 - \frac{\omega^2}{C^2}\,\bar{p}^2\right) dy - \frac{w}{g}\,a_y^{\ell}\;\bar{p}(0,\omega) + \frac{1}{2}\,i\omega q\,\left(\bar{p}(0,\omega)\right)^2 \tag{B.24}$$

For a one-dimensional finite element discretization (Fig. B.2b), the functional becomes a summation over the elements. Thus,

$$\chi(\bar{p}) = \sum_{V}\int_{V^e} \frac{1}{2}\left(\left(\frac{d\bar{p}^e}{dy}\right)^2 - \frac{\omega^2}{C^2}\,(\bar{p}^e)^2\right) dy - \frac{w}{g}\,a_y^{\ell}\;\bar{p}(0,\omega) + \frac{1}{2}\,i\omega q\,\left(\bar{p}(0,\omega)\right)^2 \tag{B.25}$$

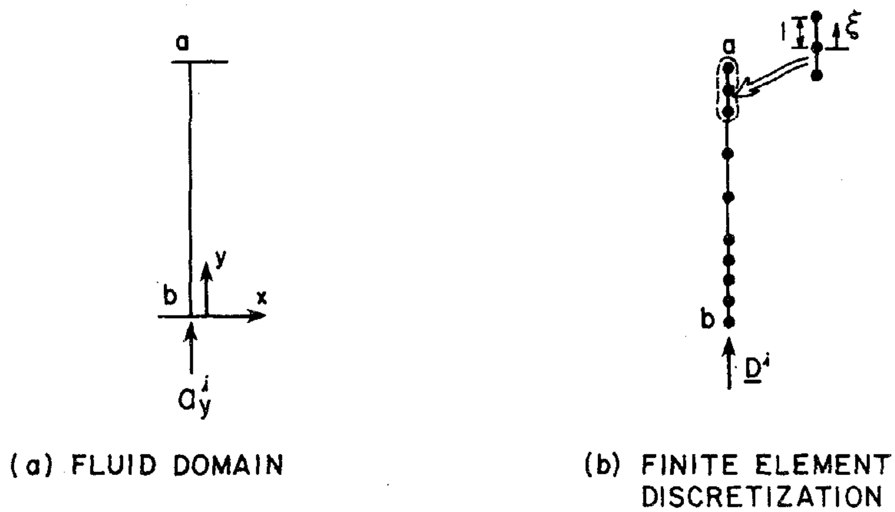

FIG. B.2 ONE-DIMENSIONAL FINITE FLUID DOMAIN where V is the domain a-b of the fluid.

Each element V^e is mapped onto the y axis from the region $-1 \leqslant \xi \leqslant 1$ on the ξ axis (see the circled element in Fig. B.2b). Thus,

$$y = \sum_i N_i(\xi)\ y_i^e = \underline{N}^T\ \underline{y}^e \tag{B.26}$$

where $N_i(\xi)$ = shape function for the ith node; y_i^e is the y location of the ith node; and $\sum_i$ is over all element nodes. The magnitude of an incremental length dy mapped from the length $d\xi$ is given by

$$dy = \frac{dy}{d\xi}\, d\xi \tag{B.27}$$

where the derivative is computed from Eq. B.26. Also,

$$\frac{dN_i}{d\xi} = \frac{dy}{d\xi}\,\frac{dN_i}{dy} \tag{B.28}$$

The element pressure distribution $\bar{p}^e(y,\omega)$ is defined with $\bar{p}^e(\xi,\omega)$ where

$$\bar{p}^e(\xi,\omega) = \sum_i N_i(\xi)\ \bar{p}_i^e(\omega) = \underline{N}^T\ \underline{\bar{p}}^e(\omega) \tag{B.29}$$

and where $\bar{p}_i^e(\omega)$ is the ith nodal pressure of the element.

Using the above equations, integration of Eq. B.25 can be carried out in the ξ coordinate system. Substitutions into Eq. B.25 result in

$$\tilde{X}(\bar{p}) = \sum_{\mathcal{V}} \left\{\bar{\underline{p}}^e(\omega)\right\}^T \left[\underline{H}^e - \frac{\omega^2}{C^2}\,\underline{G}^e\right] \bar{\underline{p}}^e(\omega) - \frac{w}{g}\, a_y^{\ell}\, \bar{p}(0,\omega) + \frac{1}{2}\, i\omega q \left(\bar{p}(0,\omega)\right)^2 \tag{B.30}$$

where

$$H_{ij}^e = \int_{-1}^{1} \frac{dN_i}{dy}\,\frac{dN_j}{dy}\,\frac{dy}{d\xi}\, d\xi$$

$$G_{ij}^e = \int_{-1}^{1} N_i\, N_j\, \frac{dy}{d\xi}\, d\xi \tag{B.31}$$

and where the shape function derivatives are found from Eq. B.28.

The matrices and vectors of Eq. B.30 can be assembled into a single, larger set. The result, omitting portions corresponding to the node at a to satisfy Eq. B.23, is

$$\tilde{X}(\bar{p}) = \bar{\underline{p}}(\omega)^T \left[\underline{H}^{\ell} - \frac{\omega^2}{C^2}\,\underline{G}^{\ell}\right] \bar{\underline{p}}(\omega) - \frac{w}{g}\, a_y^{\ell}\, \bar{p}_k(\omega) + \frac{1}{2}\, i\omega q \left(\bar{p}_k(\omega)\right)^2 \tag{B.32}$$

where $\bar{p}_k(\omega) = \bar{p}(0,\omega)$, and k corresponds to the node at b. Minimization of Eq. B.32 is carried out by setting the derivative with respect to each $\bar{p}_i(\omega)$ to zero, resulting in

$$\left[\underline{H}^{\ell} + i\omega q\,\underline{B}^{\ell} - \frac{\omega^2}{C^2}\,\underline{G}^{\ell}\right] \bar{\underline{p}}(\omega) = \frac{w}{g}\,\underline{D}^{\ell} \tag{B.33}$$

where $\underline{B}^{\ell}$ is a zero matrix except $B_{kk}^{\ell} = 1$; and $\underline{D}^{\ell}$ is a zero vector except $D_k^{\ell} = a_y^{\ell}$. The matrices of Eq. B.33 are symmetric.

B.3 Three-Dimensional Fluid Domains

B.3.1 Governing equations

The hydrodynamic pressure $\bar{p}(x,y,z,\omega)$ within the fluid domain of Fig. B.3a is governed by the three-dimensional Helmholtz equation:

$$\frac{\partial^2\bar{p}}{\partial x^2} + \frac{\partial^2\bar{p}}{\partial y^2} + \frac{\partial^2\bar{p}}{\partial z^2} + \frac{\omega^2}{C^2}\,\bar{p} = 0 \qquad \text{(B.34)}$$

subject to boundary conditions along accelerating boundaries

$$\frac{\partial\bar{p}}{\partial n}(s,r,\omega) = -\frac{w}{g}\,a_n(s,r) \qquad \text{(B.35a)}$$

$$\frac{\partial\bar{p}}{\partial n}(s',r',\omega) = -\frac{w}{g}\,a_n(s',r') + i\omega q\,\bar{p}(s',r',\omega) \qquad \text{(B.35b)}$$

and at the fluid free surface

$$\bar{p}(x,H,z,\omega) = 0 \qquad \text{(B.36)}$$

In Eq. B.35, s,r are coordinates along the dam-fluid interface a-b-c-d-a (denoted by $\mathcal{D}$), and s',r' are coordinates along the reservoir floor and sides b-f-i-j-g-c-b, a-e-i-f-b-a, and d-h-j-g-c-d (denoted by $\mathcal{D}'$).

The functional to be minimized is

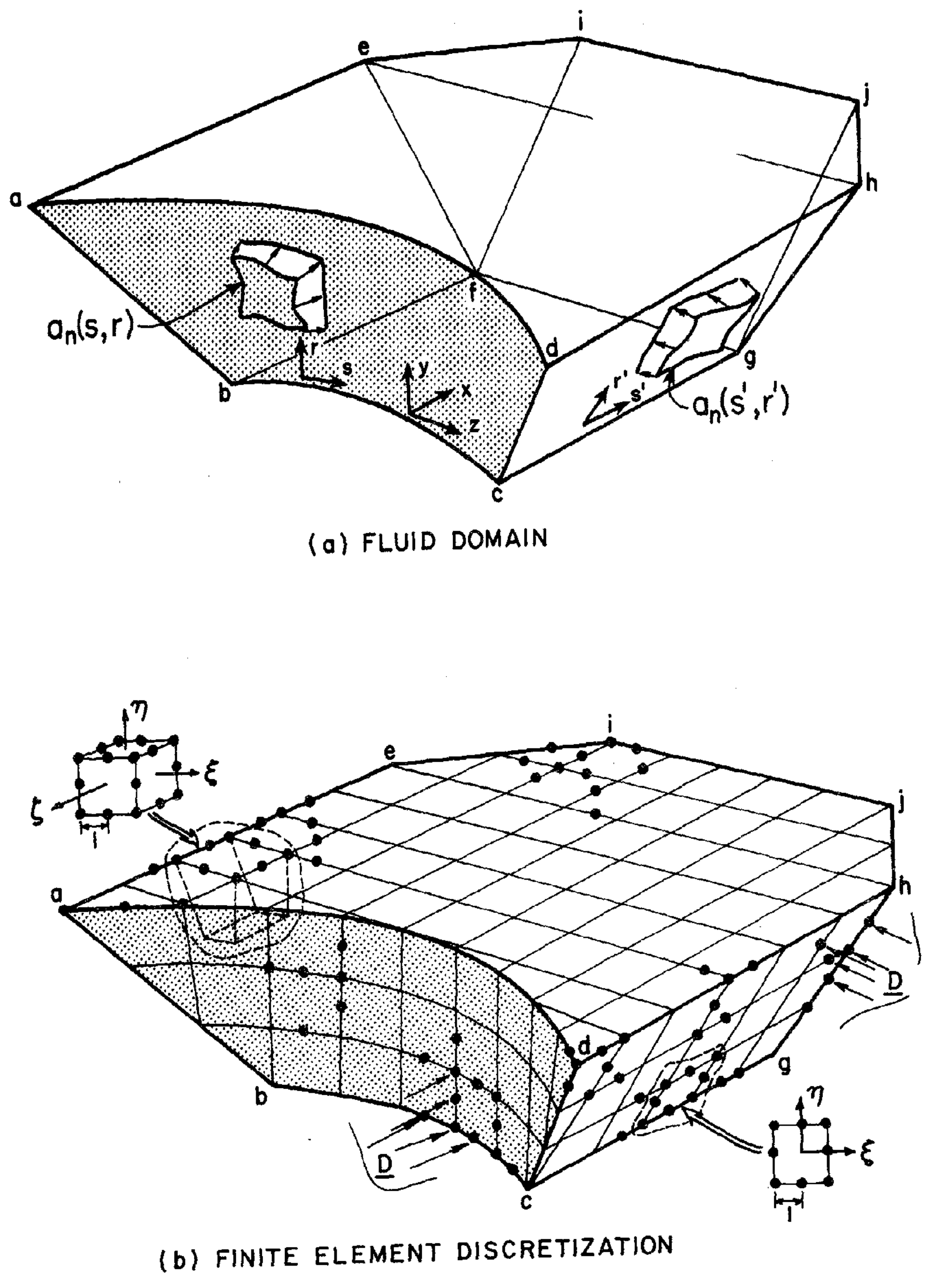

FIG. B.3 THREE-DIMENSIONAL FINITE FLUID DOMAIN

$$X(\bar{p}) = \int_{V} \frac{1}{2}\left(\left(\frac{\partial\bar{p}}{\partial x}\right)^2 + \left(\frac{\partial\bar{p}}{\partial y}\right)^2 + \left(\frac{\partial\bar{p}}{\partial z}\right)^2 - \frac{\omega^2}{C^2}\bar{p}^2\right) dV$$

$$- \int_{\mathcal{D},\mathcal{D}'} \frac{w}{g} a_n(s,r)\ \bar{p}(s,r,\omega)\ d\mathcal{D} + \int_{\mathcal{D}'} \frac{1}{2}\, i\omega q\ \left(\bar{p}(s',r',\omega)\right)^2 d\mathcal{D},$$

$$s,r = s,r \quad \text{or} \quad s',r' \qquad \text{(B.37)}$$

where V is the three-dimensional domain of the fluid. For the finite element discretization of Fig. B.3b, the functional becomes a summation over the elements. Thus

$$X(\bar{p}) = \sum_{V} \int_{V^e} \frac{1}{2}\left(\left(\frac{\partial\bar{p}^e}{\partial x}\right)^2 + \left(\frac{\partial\bar{p}^e}{\partial y}\right)^2 + \left(\frac{\partial\bar{p}^e}{\partial z}\right)^2 - \frac{\omega^2}{C^2}\ (\bar{p}^e)^2\right) dV$$

$$- \sum_{\mathcal{D},\mathcal{D}'} \int_{\mathcal{D}^e} \frac{w}{g} a_n^e(s,r)\ \bar{p}^e(s,r,\omega)\ d\mathcal{D} + \sum_{\mathcal{D}'} \int_{\mathcal{D}^e} \frac{1}{2}\, i\omega q\ \left(\bar{p}^e(s',r',\omega)\right)^2 d\mathcal{D},$$

$$s,r = s,r \quad \text{or} \quad s',r' \qquad \text{(B.38)}$$

B.3.2 Element mapping

Each finite element V^e is mapped into the x,y,z coordinate system from a simple shape in an image coordinate system. For example, the circled element of Fig. B.3b is mapped from the rectangular prism $1 \leqslant \xi \leqslant 1$, $1 \leqslant \eta \leqslant 1$, $1 \leqslant \zeta \leqslant 1$ according to

$$x = \sum_i N_i(\xi,\eta,\zeta)\, x_i^e = \underline{N}^T\, \underline{x}^e$$

$$y = \sum_i N_i(\xi,\eta,\zeta)\, y_i^e = \underline{N}^T\, \underline{y}^e \tag{B.39}$$

$$z = \sum_i N_i(\xi,\eta,\zeta)\, z_i^e = \underline{N}^T\, \underline{z}^e$$

where $N_i(\xi,\eta,\zeta)$ = shape function for the ith node; (x_i^e, y_i^e, z_i^e) is the x,y,z location of the ith node; and $\sum_i$ is over all element nodes. The magnitude of an incremental volume dV mapped from the volume $d\xi d\eta d\zeta$ is given by

$$dV = \det[\underline{J}]\, d\xi d\eta d\zeta \tag{B.40}$$

where

$$\begin{Bmatrix} \dfrac{\partial N_i}{\partial \xi} \\ \dfrac{\partial N_i}{\partial \eta} \\ \dfrac{\partial N_i}{\partial \zeta} \end{Bmatrix} = \underline{J} \begin{Bmatrix} \dfrac{\partial N_i}{\partial x} \\ \dfrac{\partial N_i}{\partial y} \\ \dfrac{\partial N_i}{\partial z} \end{Bmatrix} \tag{B.41}$$

and

$$\underline{J} = \begin{bmatrix} \dfrac{\partial x}{\partial \xi} & \dfrac{\partial y}{\partial \xi} & \dfrac{\partial z}{\partial \xi} \\ \dfrac{\partial x}{\partial \eta}, & \dfrac{\partial y}{\partial \eta} & \dfrac{\partial z}{\partial \eta} \\ \dfrac{\partial x}{\partial \zeta} & \dfrac{\partial y}{\partial \zeta} & \dfrac{\partial z}{\partial \zeta} \end{bmatrix} \tag{B.42}$$

The terms of $\underline{J}$ can be computed from Eq. B.39. Versions of the above equations are available for triangular prism and tetrahedral image shapes using area and volume coordinates (12).

The boundary $\mathcal{D},\mathcal{D}'$ is entirely defined by the above procedure. For convenience, a separate but equivalent mapping is introduced in which each boundary element $\mathcal{D}^e$ is mapped from a simple shape in an image coordinate system. For example, the circled boundary element of Fig. B.3b is mapped from the rectangle $-1 \leqslant \xi \leqslant 1$, $-1 \leqslant \eta \leqslant 1$ according to

$$x^b = \sum_j M_j(\xi,\eta)\ x_j^{be} = \underline{M}^T\ \underline{x}^{be}$$

$$y^b = \sum_j M_j(\xi,\eta)\ y_j^{be} = \underline{M}^T\ \underline{y}^{be} \qquad \text{(B.43)}$$

$$z^b = \sum_j M_j(\xi,\eta)\ z_j^{be} = \underline{M}^T\ \underline{z}^{be}$$

where $M_j(\xi,\eta)$ = shape function for the jth node of a boundary element; $(x_j^{be}, y_j^{be}, z_j^{be})$ is the x,y,z location of the jth node; and $\sum_j$ is over all boundary element nodes. $M_j(\xi,\eta)$ is computed from $N_i(\xi,\eta,\zeta)$ of the adjacent interior element where j and i refer to the same nodal point. The magnitude of an incremental area $d\mathcal{D}$ in the x,y,z system mapped from an area $d\xi d\eta$ is given by

$$d\mathcal{D} = |n|\ d\xi d\eta \qquad \text{(B.44)}$$

where $|n|$ is the absolute value of the normal vector along $\mathcal{D}^e$ whose x, y, and z components are defined by

$$n_x = \frac{\partial y^b}{\partial \eta}\frac{\partial z^b}{\partial \xi} - \frac{\partial y^b}{\partial \xi}\frac{\partial z^b}{\partial \eta}$$

$$n_y = \frac{-\partial x^b}{\partial \eta}\frac{\partial z^b}{\partial \xi} + \frac{\partial x^b}{\partial \xi}\frac{\partial z^b}{\partial \eta} \qquad \text{(B.45)}$$

$$n_z = \frac{\partial x^b}{\partial \eta}\frac{\partial y^b}{\partial \xi} - \frac{\partial x^b}{\partial \xi}\frac{\partial y^b}{\partial \eta}$$

and where the partial derivatives are computed from Eq. B.43. With a proper choice of sign, n is the inward normal to the fluid domain.

B.3.3 Element pressure definition

Within each V^e the element pressure is defined as $\bar{p}^e(\xi,\eta,\zeta,\omega)$ where

$$\bar{p}^e(\xi,\eta,\zeta,\omega) = \sum_i N_i(\xi,\eta,\zeta)\ \bar{p}_i^e(\omega) = \underline{N}^T\ \underline{\bar{p}}^e(\omega) \qquad \text{(B.46)}$$

and where $\bar{p}_i^e(\omega)$ = ith nodal pressure of the element. The pressure distribution $\bar{p}^e(s,r,\omega)$ or $\bar{p}^e(s',r',\omega)$ along $\mathcal{D},\mathcal{D}'$ within each $\mathcal{D}^e$ is defined as $\bar{p}^e(\xi,\eta,\omega)$ where

$$\bar{p}^e(\xi,\eta,\omega) = \sum_j M_j(\xi,\eta)\ \bar{p}_j^{be}(\omega) = \underline{M}^T\ \underline{\bar{p}}^{be}(\omega) \qquad \text{(B.47)}$$

and where $\bar{p}_j^{be}(\omega)$ = the jth nodal pressure of the boundary element. The normal acceleration $a_n^e(s,r)$ or $a_n^e(s',r')$ can be defined as $a_n^e(\xi,\eta)$ by the process described in Appendix D.2.

B.3.4 Functional integration and minimization

Using the above equations, integration of Eq. B.38 can be carried out in the image coordinate systems. Thus,

$$\tilde{X}(\bar{p}) = \sum_{V} \left\{\bar{\underline{p}}^{e}(\omega)\right\}^{T} \left[\underline{H}^{e} - \frac{\omega^{2}}{C^{2}}\underline{G}^{e}\right] \bar{\underline{p}}^{e}(\omega) - \sum_{D,D'} \left\{\bar{\underline{p}}^{be}(\omega)\right\}^{T} \frac{w}{g}\underline{D}^{e}$$

$$+ \sum_{D'} \left\{\bar{\underline{p}}^{be}(\omega)\right\}^{T} i\omega q\, \underline{B}^{e}\, \bar{\underline{p}}^{be}(\omega) \tag{B.48}$$

where

$$H^{e}_{ij} = \int_{-1}^{1}\int_{-1}^{1}\int_{-1}^{1} \left(\frac{\partial N_i}{\partial x}\frac{\partial N_j}{\partial x} + \frac{\partial N_i}{\partial y}\frac{\partial N_j}{\partial y} + \frac{\partial N_i}{\partial z}\frac{\partial N_j}{\partial z}\right) \det[\underline{J}]\, d\xi d\eta d\zeta$$

$$G^{e}_{ij} = \int_{-1}^{1}\int_{-1}^{1}\int_{-1}^{1} N_i\, N_j\, \det[\underline{J}]\, d\xi d\eta d\zeta$$

$$D^{e}_{i} = \int_{-1}^{1}\int_{-1}^{1} M_i\, a^{e}_{n}(\xi,\eta)\, |n|\, d\xi d\eta \tag{B.49}$$

$$B^{e}_{ij} = \int_{-1}^{1}\int_{-1}^{1} M_i\, M_j\, |n|\, d\xi d\eta$$

and where the shape function partial derivatives are computed by solving Eq. B.41.

The matrices and vectors of Eq. B.48 can be assembled into a single, larger set. The result, omitting portions corresponding to the nodes at the free surface a-e-i-j-h-d-a, is

$$\tilde{X}(\bar{p}) = \bar{\underline{p}}(\omega)^T \left[\underline{H} + i\omega q\ \underline{B} - \frac{\omega^2}{c^2}\ \underline{G}\right] \bar{\underline{p}}(\omega) - \bar{\underline{p}}(\omega)^T\ \frac{w}{g}\ \underline{D} \tag{B.50}$$

Minimization of the functional $\tilde{X}(\bar{p})$ leads to

$$\left[\underline{H} + i\omega q\ \underline{B} - \frac{\omega^2}{c^2}\ \underline{G}\right] \bar{\underline{p}}(\omega) = \frac{w}{g}\ \underline{D} \tag{B.51}$$

The matrices of Eq. B.51 are symmetric. The non-zero portion of $\underline{B}$ is a submatrix corresponding to nodes along $\mathcal{D}'$, and $\underline{D}$ has non-zero terms for only nodes along $\mathcal{D},\mathcal{D}'$.

APPENDIX C. BOUNDARY CONDITIONS FOR INFINITE FLUID DOMAINS

Figures C.1 and C.2 show infinite fluid domains of constant depth and uniform cross-section, respectively. The two-dimensional fluid domain of Fig. C.1a is discretized into layers (Fig. C.1b), and the three-dimensional fluid domain of Fig. C.2a is discretized into channels (Fig. C.2b). Discrete forms of the acceleration boundary conditions at $x = 0$ are derived below. Integrals of the final matrix equations can be evaluated by Gauss quadrature.

C.1 Infinite Fluid Domain of Constant Depth

The layer discretization in Fig. C.1b is defined by the one-dimensional discretization along a-b, and thus the mapping process of Sec. B.2 can be applied. Each one-dimensional element is mapped onto the y axis from the region $-1 \leqslant \xi \leqslant 1$ on the ξ axis (see the circled element in Fig. C.1b). Thus, from Eq. B.26,

$$y = \underline{N}^T \, \underline{y}^e \tag{C.1}$$

where $\underline{N}^T$ = vector of shape functions for an element; and $\underline{y}^e$ = coordinate vector for the element nodes. The pressure distribution $\bar{p}^e(x,y,\omega)$ within each layer is defined as $\bar{p}^e(x,\xi,\omega)$ where

$$\bar{p}^e(x,\xi,\omega) = \underline{N}^T \, \bar{\underline{p}}^e(x,\omega) \tag{C.2}$$

and where $\bar{\underline{p}}^e(x,\omega)$ = vector of pressures along nodal lines of a layer. The normal acceleration on the $x = 0$ face of a layer $a_x^e(y)$ can also

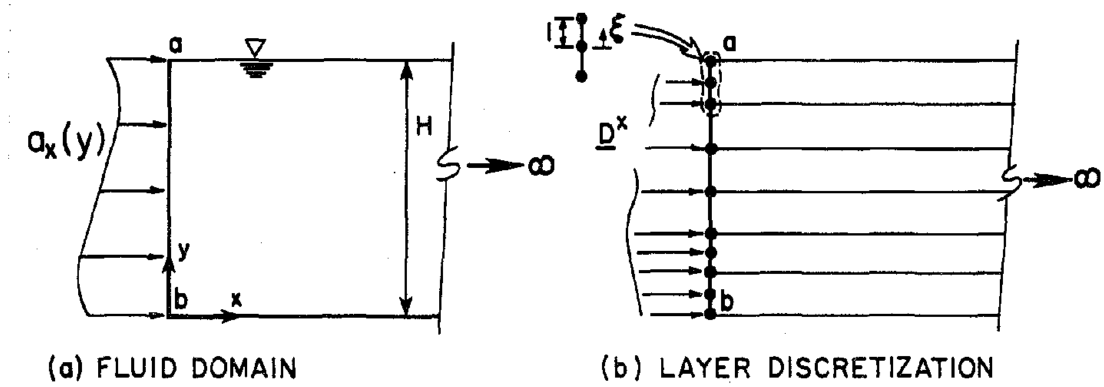

FIG. C.1 INFINITE FLUID DOMAIN OF CONSTANT DEPTH be defined on the ξ axis as $a_x^e(\xi)$.

The continuum boundary condition along the face a-b at $x = 0$ is given by

$$\frac{\partial \bar{p}}{\partial x}(0,y,\omega) = -\frac{w}{g}\, a_x(y) \tag{C.3}$$

and within a layer by

$$\frac{\partial \bar{p}^e}{\partial x}(0,\xi,\omega) = -\frac{w}{g}\, a_x^e(\xi) \tag{C.4}$$

According to Eq. B.18, the element vector of nodal accelerations is found as

$$\underset{\sim}{D}^e = \int_{-1}^{1} \underset{\sim}{N}\, a_x^e(\xi)\, \frac{dy}{d\xi}\, d\xi \tag{C.5}$$

where $\frac{dy}{d\xi}$ is computed from Eq. C.1. Substitution of Eq. C.2 into Eq. C.4 and the result into Eq. C.5 yields

$$\frac{w}{g}\underset{\sim}{D}^e = -\left[\int_{-1}^{1} \underset{\sim}{N}\,\underset{\sim}{N}^T \frac{dy}{d\xi}\, d\xi\right] \frac{d\underset{\sim}{\bar{p}}^e}{dx}(0,\omega) \tag{C.6}$$

Or, switching sides,

$$\underset{\sim}{G}^e \frac{d\underset{\sim}{\bar{p}}^e}{dx}(0,\omega) = -\frac{w}{g}\underset{\sim}{D}^e \tag{C.7}$$

where

$$G_{ij}^{e} = \int_{-1}^{1} N_i \; N_j \; \frac{dy}{d\xi} \, d\xi \tag{C.8}$$

Assembly for all elements along a-b results in

$$\underline{G}^{\ell} \, \frac{d\bar{\underline{p}}}{dx} \, (0,\omega) = - \frac{w}{g} \, \underline{D}^{x} \tag{C.9}$$

where the matrix $\underline{G}^{\ell}$ is the same one of Eq. B.33. Only equations for nodes below the free surface node at a are included in Eq. C.9.

C.2 Infinite Fluid Domain of Uniform Cross-Section

The channel discretization in Fig. C.2b is defined by the two-dimensional discretization along a-b-c-d-a, and thus the mapping procedure of Sec. B.1 is applicable. Each two-dimensional element is mapped onto the y,z plane from a simple shape in an image coordinate system. For example, the circled element of Fig. C.2b is mapped from the rectangle $-1 \leqslant \xi \leqslant 1$, $-1 \leqslant \eta \leqslant 1$. Thus, from Eq. B.6,

$$\begin{aligned} y &= \underline{N}^{T} \, \underline{y}^{e} \\ z &= \underline{N}^{T} \, \underline{z}^{e} \end{aligned} \tag{C.10}$$

where $\underline{N}^{T}$ = vector of shape functions for an element; and $\underline{y}^{e}, \underline{z}^{e}$ = coordinate vectors for the element nodes. The pressure distribution $\bar{p}^{e}(x,y,z,\omega)$ within each channel is defined as $\bar{p}^{e}(x,\xi,\eta,\omega)$ where

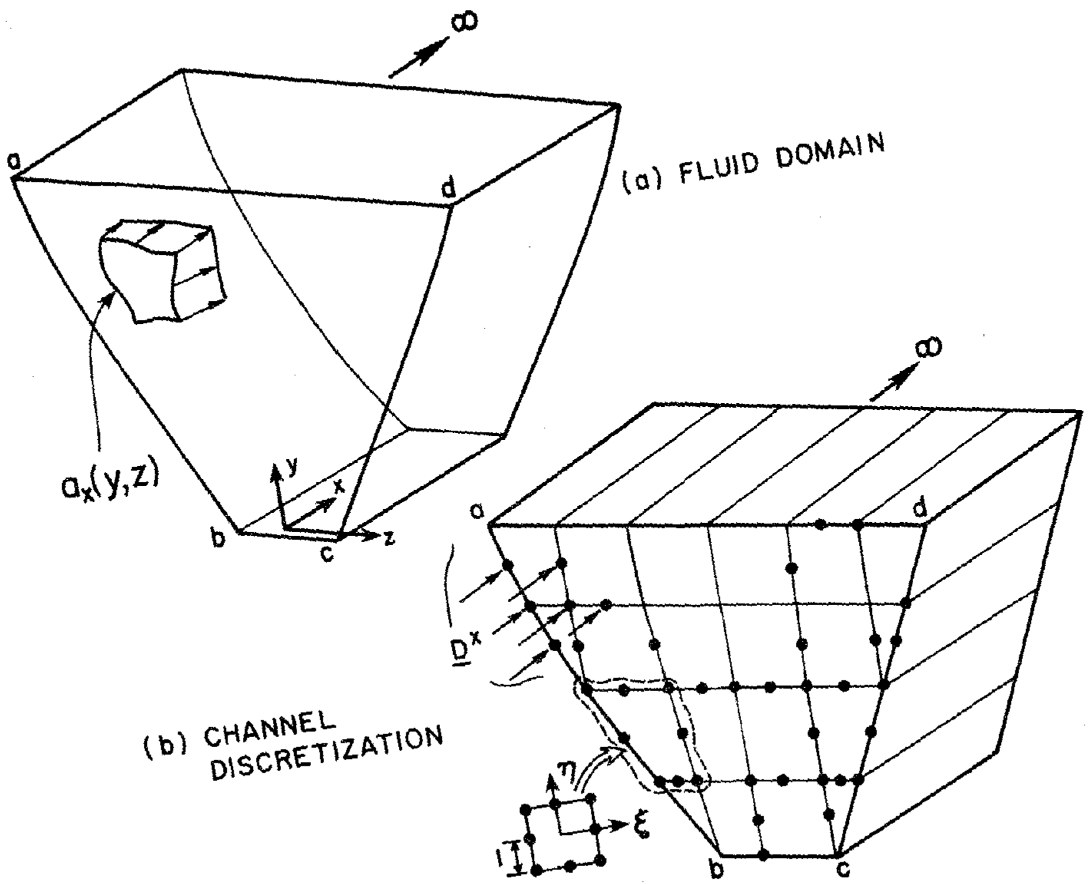

FIG. C.2 INFINITE FLUID DOMAIN OF UNIFORM CROSS-SECTION

$$\bar{p}^e(x,\xi,\eta,\omega) = \underset{\sim}{N}^T \; \bar{\underset{\sim}{p}}^e(x,\omega) \tag{C.11}$$

and where $\bar{\underset{\sim}{p}}^e(x,\omega)$ = vector of pressures along nodal lines of a channel. The normal acceleration on the $x = 0$ face of a channel $a_x^e(y,z)$ is defined as $a_x^e(\xi,\eta)$.

The continuum boundary condition along the face a-b-c-d-a at $x = 0$ is given by

$$\frac{\partial \bar{p}}{\partial x}(0,y,z,\omega) = -\frac{w}{g}\, a_x(y,z) \tag{C.12}$$

and within a channel by

$$\frac{\partial \bar{p}^e}{\partial x}(0,\xi,\eta,\omega) = -\frac{w}{g}\, a_x^e(\xi,\eta) \tag{C.13}$$

According to Eq. B.49, the element vector of nodal accelerations is found as

$$\underset{\sim}{D}^e = \int_{-1}^{1}\int_{-1}^{1} \underset{\sim}{N}\, a_x^e(\xi,\eta)\; |n_x| \; d\xi d\eta \tag{C.14}$$

where

$$n_x = \frac{\partial y}{\partial \eta}\frac{\partial z}{\partial \xi} - \frac{\partial y}{\partial \xi}\frac{\partial z}{\partial \eta} \tag{C.15}$$

and where the partial derivatives are computed from Eq. C.10. Substitution of Eq. C.11 into Eq. C.13 and the result into Eq. C.14 yields

$$\underset{\sim}{G}^e \frac{d\bar{p}^e}{dx} (0,\omega) = - \frac{w}{g} \underset{\sim}{D}^e \tag{C.16}$$

where

$$G^e_{ij} = \int_{-1}^{1} \int_{-1}^{1} N_i \, N_j \, |n_x| \, d\xi d\eta \tag{C.17}$$

Assembly for all elements within a-b-c-d-a results in

$$\underset{\sim}{G}^{i} \frac{d\bar{p}}{dx} (0,\omega) = - \frac{w}{g} \underset{\sim}{D}^x \tag{C.18}$$

where only equations for nodes below the fluid free surface are included.

APPENDIX D. BOUNDARY COMPUTATIONS FOR FINITE FLUID DOMAINS

The fluid domains considered here are the two and three-dimensional finite fluid domains of Figs. B.1 and B.3. Computation of the nodal acceleration vectors $\underline{D}_o^\ell$ and $\underline{D}_j$ resulting from accelerations of the ground in the direction ℓ with rigid dam and accelerations of the dam in its jth mode, respectively, is discussed. From pressure vectors $\underline{\bar{p}}_o^{f\ell}(\omega)$ and $\underline{\bar{p}}_j^{f}(\omega)$ along the dam-fluid interface, computation of the hydrodynamic force vectors $\underline{\bar{Q}}_o^{f\ell}(\omega)$ and $\underline{\bar{Q}}_j^{f}(\omega)$ is also discussed. Vectors and matrices with superscript f contain terms corresponding to all nodes along the dam-fluid interface. Integrals of the final matrix equations can be evaluated by Gauss quadrature.

D.1 Two-Dimensional Fluid Domains

D.1.1 Computation of $\underline{D}_o^\ell$, $\ell = x,y$ and $\underline{D}_j$

Accelerating fluid boundaries in Fig. B.1 include the dam-fluid interface a-b and reservoir floor b-c, denoted by $\mathcal{D}$ and $\mathcal{D}'$ with boundary coordinates s and s'. These boundaries are located by a mapping procedure described in Sec. B.1 in which each boundary element $\mathcal{D}^e$ is mapped from the region $-1 \leqslant \xi \leqslant 1$ on the ξ axis. Thus, from Eq. B.10,

$$\begin{aligned} x^b &= \underline{M}^T \underline{x}^{be} \\ y^b &= \underline{M}^T \underline{y}^{be} \end{aligned} \qquad \text{(D.1)}$$

where $\underline{M}$ = vector of shape functions for a boundary element; and $\underline{x}^{be}$, $\underline{y}^{be}$ = coordinate vectors for the boundary element nodes. If a boundary element $\mathcal{D}^e$ accelerates in the normal direction at $a_n^e(s)$ or $a_n^e(s')$, then from Eq. B.18 the element vector of nodal accelerations is found as

$$\underline{D}^e = \int_{-1}^{1} \underline{M}\, a_n^e(\xi)\, |n|\, d\xi \tag{D.2}$$

where $a_n^e(s)$ or $a_n^e(s')$ is defined on the ξ axis as $a_n^e(\xi)$; and $|n|$ is the absolute value of the normal vector along $\mathcal{D}^e$ whose x and y components are given by Eq. B.13 as

$$\begin{aligned} n_x &= \frac{dy^b}{d\xi} \\ n_y &= -\frac{dx^b}{d\xi} \end{aligned} \tag{D.3}$$

and where the derivatives are computed from Eq. D.1. With a proper choice of sign, n is the inward normal.

The acceleration vector $\underline{D}_o^\ell$, $\ell = x,y$ results from an acceleration $a_n(s) = \varepsilon^\ell(s)$, $s = s,s'$ of the boundary $\mathcal{D},\mathcal{D}'$. $\varepsilon^\ell(s)$ or $\varepsilon^\ell(s')$ defines the length of the component of a unit vector along ℓ in the direction of the inward normal n. Within each $\mathcal{D}^e$,

$$a_n^e(\xi) = \frac{n_\ell}{|n|} \tag{D.4}$$

and substitution into Eq. D.2 yields

$$\underset{\sim}{D}^e = \int_{-1}^{1} \underset{\sim}{M}\, n_\ell \, d\xi \tag{D.5}$$

Assembly of each $\underset{\sim}{D}^e$ over $\mathcal{D},\mathcal{D}'$ forms $\underset{\sim}{D}_o^\ell$. No terms are assembled from the free surface nodes.

$\underset{\sim}{D}_j$ results from an acceleration of $\mathcal{D}$ from the dam-fluid interface portion of the dam's jth mode $\underset{\sim}{\phi}_j^f$, whose x and y subvectors are denoted by $\{\underset{\sim}{\phi}_j^f\}_x$ and $\{\underset{\sim}{\phi}_j^f\}_y$. $a_n^e(\xi)$ is derived from the element subvectors $\{\underset{\sim}{\phi}_j^e\}_x$ and $\{\underset{\sim}{\phi}_j^e\}_y$ by

$$a_n^e(\xi) = \frac{n_x}{|n|} \underset{\sim}{M}^T \left\{\underset{\sim}{\phi}_j^e\right\}_x + \frac{n_y}{|n|} \underset{\sim}{M}^T \left\{\underset{\sim}{\phi}_j^e\right\}_y \tag{D.6}$$

Substitution of Eq. D.6 into Eq. D.2 yields

$$\underset{\sim}{D}^e = \left[\int_{-1}^{1} \underset{\sim}{M}\underset{\sim}{M}^T n_x \, d\xi\right] \left\{\underset{\sim}{\phi}_j^e\right\}_x + \left[\int_{-1}^{1} \underset{\sim}{M}\underset{\sim}{M}^T n_y \, d\xi\right] \left\{\underset{\sim}{\phi}_j^e\right\}_y \tag{D.7}$$

or

$$\underset{\sim}{D}^e = \underset{\sim}{B}_x^e \left\{\underset{\sim}{\phi}_j^e\right\}_x + \underset{\sim}{B}_y^e \left\{\underset{\sim}{\phi}_j^e\right\}_y \tag{D.8}$$

where

$$\left[\underline{B}_x^e\right]_{ij} = \int_{-1}^{1} M_i \; M_j \; n_x \; d\xi$$

$$\left[\underline{B}_y^e\right]_{ij} = \int_{-1}^{1} M_i \; M_j \; n_y \; d\xi \tag{D.9}$$

Assembly of Eq. D.8 over $\mathcal{D}$ for each $\mathcal{D}^e$ yields

$$\underline{D}_j^f = \underline{B}_x^f \left\{\underline{\phi}_j^f\right\}_x + \underline{B}_y^f \left\{\underline{\phi}_j^f\right\}_y \tag{D.10}$$

where $\underline{B}_x^f$ and $\underline{B}_y^f$ are symmetric matrices. $\underline{D}_j$ is assembled from terms of $\underline{D}_j^f$ corresponding to nodes below the free surface.

D.1.2 Computation of $\bar{\underline{Q}}_o^{f\ell}(\omega)$, $\ell = x,y$ and $\bar{\underline{Q}}_j^f(\omega)$

Solution of Eq. B.20 with acceleration vector $\underline{D}_o^\ell$ results in the pressure vector $\bar{\underline{p}}_o^\ell(\omega)$. Along $\mathcal{D}$, the pressure distribution within $\mathcal{D}^e$ is $\bar{p}^e(s,\omega)$, defined as $\bar{p}^e(\xi,\omega)$ where, from Eq. B.15,

$$\bar{p}^e(\xi,\omega) = \underline{M}^T \; \bar{\underline{p}}^{be}(\omega) \tag{D.11}$$

and where $\bar{\underline{p}}^{be}(\omega)$ = vector of boundary element nodal pressures. The x and y subvectors of $\bar{\underline{Q}}_o^{f\ell}(\omega)$ are denoted by $\{\bar{\underline{Q}}_o^{f\ell}(\omega)\}_x$ and $\{\bar{\underline{Q}}_o^{f\ell}(\omega)\}_y$, and within $\mathcal{D}^e$ by $\{\bar{\underline{Q}}^e(\omega)\}_x$ and $\{\bar{\underline{Q}}^e(\omega)\}_y$. By the method of virtual work

$$\left\{\underset{-}{\bar{Q}}^{e}(\omega)\right\}_x = \int_{-1}^{1} \underset{-}{M}\, \frac{n_x}{|n|}\, \bar{p}^{e}(\xi,\omega)\ |n|\ d\xi \tag{D.12}$$

Substitution of Eq. D.11 into Eq. D.12 yields

$$\left\{\underset{-}{\bar{Q}}^{e}(\omega)\right\}_x = \left[\int_{-1}^{1} \underset{-}{M}\, \underset{-}{M}^{T}\, n_x\ d\xi\right] \underset{-}{\bar{p}}^{be}(\omega) \tag{D.13}$$

or

$$\left\{\underset{-}{\bar{Q}}^{e}(\omega)\right\}_x = \underset{-}{B}_x^{e}\ \underset{-}{\bar{p}}^{be}(\omega) \tag{D.14}$$

Assembly of Eq. D.14 over $\mathcal{D}$ for each $\mathcal{D}^e$ yields

$$\left\{\underset{-}{\bar{Q}}_o^{f\ell}(\omega)\right\}_x = \underset{-}{B}_x^{f}\ \underset{-}{\bar{p}}_o^{f\ell}(\omega) \tag{D.15a}$$

and in like manner,

$$\left\{\underset{-}{\bar{Q}}_o^{f\ell}(\omega)\right\}_y = \underset{-}{B}_y^{f}\ \underset{-}{\bar{p}}_o^{f\ell}(\omega) \tag{D.15b}$$

$\underset{-}{B}_x^f$ and $\underset{-}{B}_y^f$ of Eqs. D.10 and D.15 are the same, and $\underset{-}{\bar{p}}_o^{f\ell}(\omega)$ lists the terms of $\underset{-}{\bar{p}}_o^{\ell}(\omega)$ along the dam-fluid interface $\mathcal{D}$ and includes a zero term for the surface node at a. $\underset{-}{\bar{Q}}_o^{f\ell}(\omega)$, $\ell = x,y$ is assembled from $\{\underset{-}{\bar{Q}}_o^{f\ell}(\omega)\}_x$ and $\{\underset{-}{\bar{Q}}_o^{f\ell}(\omega)\}_y$ of Eq. D.15 and ordered to correspond to $\underset{-}{\phi}_j^f$.

Solution of Eq. B.20 with $\underset{\sim}{D}_j$ results in $\bar{\underset{\sim}{p}}_j(\omega)$, and the vector $\bar{\underset{\sim}{p}}_j^f(\omega)$ for pressures along $\mathcal{D}$. $\bar{\underset{\sim}{Q}}_j^f(\omega)$ is assembled from the subvectors

$$\left\{\bar{\underset{\sim}{Q}}_j^f(\omega)\right\}_x = \underset{\sim}{B}_x^f\, \bar{\underset{\sim}{p}}_j^f(\omega)$$
$$\left\{\bar{\underset{\sim}{Q}}_j^f(\omega)\right\}_y = \underset{\sim}{B}_y^f\, \bar{\underset{\sim}{p}}_j^f(\omega) \tag{D.16}$$

and ordered to correspond to $\underset{\sim}{\phi}_j^f$.

The hydrodynamic terms of Eq. 2.24 are of the form $\{\underset{\sim}{\phi}_j^f\}^T\, \bar{\underset{\sim}{Q}}^f(\omega)$ and can be calculated in a direct manner. Premultiplication of Eq. D.15a by $\{\underset{\sim}{\phi}_j^f\}_x^T$, Eq. D.15b by $\{\underset{\sim}{\phi}_j^f\}_y^T$, and addition of the resulting equations yields

$$\left\{\underset{\sim}{\phi}_j^f\right\}_x^T \left\{\bar{\underset{\sim}{Q}}_o^{f\ell}(\omega)\right\}_x + \left\{\underset{\sim}{\phi}_j^f\right\}_y^T \left\{\bar{\underset{\sim}{Q}}_o^{f\ell}(\omega)\right\}_y = \left\{\underset{\sim}{\phi}_j^f\right\}_x^T \underset{\sim}{B}_x^f\, \bar{\underset{\sim}{p}}_o^{f\ell}(\omega) + \left\{\underset{\sim}{\phi}_j^f\right\}_y^T \underset{\sim}{B}_y^f\, \bar{\underset{\sim}{p}}_o^{f\ell}(\omega) \tag{D.17}$$

With use of Eq. D.10,

$$\left\{\underset{\sim}{\phi}_j^f\right\}^T \bar{\underset{\sim}{Q}}_o^{f\ell}(\omega) = \left\{\underset{\sim}{D}_j^f\right\}^T \bar{\underset{\sim}{p}}_o^{f\ell}(\omega), \qquad \ell = x,y \tag{D.18a}$$

for the hydrodynamic added load terms. Similarly,

$$\left\{\underset{\sim}{\phi}_j^f\right\}^T \bar{\underset{\sim}{Q}}_k^f(\omega) = \left\{\underset{\sim}{D}_j^f\right\}^T \bar{\underset{\sim}{p}}_k^f(\omega) \tag{D.18b}$$

for the hydrodynamic added mass terms.

D.2 Three-Dimensional Fluid Domains

D.2.1 Computation of $\underline{D}_o^{\ell}$, $\ell = x,y,z$ and $\underline{D}_j$

Accelerating fluid boundaries in Fig. B.3 include the dam-fluid interface a-b-c-d-a (denoted by $\mathcal{D}$ with boundary coordinates s,r) and the reservoir floor and sides b-f-i-j-g-c-b, a-e-i-f-b-a, and d-h-j-g-c-d (denoted by $\mathcal{D}'$ with boundary coordinates s',r'). These boundaries are located by a mapping procedure described in Sec. B.3 in which each boundary element is mapped from a simple shape in an image coordinate system. For example, the circled boundary element of Fig. B.3b is mapped from the rectangle $-1 \leqslant \xi \leqslant 1$, $-1 \leqslant \eta \leqslant 1$. Thus, from Eq. B.43

$$\begin{aligned} x^b &= \underline{M}^T \underline{x}^{be} \\ y^b &= \underline{M}^T \underline{y}^{be} \\ z^b &= \underline{M}^T \underline{z}^{be} \end{aligned} \tag{D.19}$$

where $\underline{M}$ = vector of boundary element shape functions; and $\underline{x}^{be}$, $\underline{y}^{be}$, $\underline{z}^{be}$ = coordinate vectors for the boundary element nodes. If a boundary element $\mathcal{D}^e$ accelerates at $a_n^e(s,r)$ or $a_n^e(s',r')$, then from Eq. B.49 the element vector of nodal accelerations is

$$\underline{D}^e = \int_{-1}^{1} \int_{-1}^{1} \underline{M}\, a_n^e(\xi,\eta)\ |n|\ d\xi d\eta \tag{D.20}$$

where $a_n^e(s,r)$ or $a_n^e(s',r')$ is defined as $a_n^e(\xi,\eta)$; and $|n|$ is the absolute value of the normal vector along $\mathcal{D}^e$ where, from Eq. B.45,

$$
\begin{aligned}
n_x &= \frac{\partial y^b}{\partial \eta}\frac{\partial z^b}{\partial \xi} - \frac{\partial y^b}{\partial \xi}\frac{\partial z^b}{\partial \eta} \\
n_y &= -\frac{\partial x^b}{\partial \eta}\frac{\partial z^b}{\partial \xi} + \frac{\partial x^b}{\partial \xi}\frac{\partial z^b}{\partial \eta} \\
n_z &= \frac{\partial x^b}{\partial \eta}\frac{\partial y^b}{\partial \xi} - \frac{\partial x^b}{\partial \xi}\frac{\partial y^b}{\partial \eta}
\end{aligned}
\tag{D.21}
$$

With a proper choice of sign, n is the inward normal.

$\underline{D}_o^\ell$, $\ell = x,y,z$ results from an acceleration $a_n(s,r) = \varepsilon^\ell(s,r)$, $s,r = s,r$ or s',r' of the boundary $\mathcal{D},\mathcal{D}'$. Within each $\mathcal{D}^e$,

$$
a_n^e(\xi,\eta) = \frac{n_\ell}{|n|}
\tag{D.22}
$$

and substitution into Eq. D.20 yields

$$
\underline{D}^e = \int_{-1}^{1}\int_{-1}^{1} \underline{M}\; n_\ell \; d\xi d\eta
\tag{D.23}
$$

Assembly of each $\underline{D}^e$ over $\mathcal{D},\mathcal{D}'$ forms $\underline{D}_o^\ell$. No terms are assembled from the free surface nodes.

$\underline{D}_j$ results from an acceleration of $\mathcal{D}$ from $\underline{\phi}_j^f$ whose x, y, and z subvectors are denoted by $\{\underline{\phi}_j^f\}_x$, $\{\underline{\phi}_j^f\}_y$, and $\{\underline{\phi}_j^f\}_z$. $a_n^e(\xi,\eta)$ is derived from the element subvectors by

$$a_n^e(\xi,\eta) = \frac{n_x}{|n|} \underline{M}^T \left\{\underline{\phi}_j^e\right\}_x + \frac{n_y}{|n|} \underline{M}^T \left\{\underline{\phi}_j^e\right\}_y + \frac{n_z}{|n|} \underline{M}^T \left\{\underline{\phi}_j^e\right\}_z \qquad \text{(D.24)}$$

Substitution into Eq. D.20 yields

$$\underline{D}^e = \underline{B}_x^e \left\{\underline{\phi}_j^e\right\}_x + \underline{B}_y^e \left\{\underline{\phi}_j^e\right\}_y + \underline{B}_z^e \left\{\underline{\phi}_j^e\right\}_z \qquad \text{(D.25)}$$

where

$$\left[\underline{B}_x^e\right]_{ij} = \int_{-1}^{1}\int_{-1}^{1} M_i\, M_j\, n_x\, d\xi d\eta$$

$$\left[\underline{B}_y^e\right]_{ij} = \int_{-1}^{1}\int_{-1}^{1} M_i\, M_j\, n_y\, d\xi d\eta \qquad \text{(D.26)}$$

$$\left[\underline{B}_z^e\right]_{ij} = \int_{-1}^{1}\int_{-1}^{1} M_i\, M_j\, n_z\, d\xi d\eta$$

Assembly of Eq. D.25 over $\mathcal{D}$ for each $\mathcal{D}^e$ yields

$$\underline{D}_j^f = \underline{B}_x^f \left\{\underline{\phi}_j^f\right\}_x + \underline{B}_y^f \left\{\underline{\phi}_j^f\right\}_y + \underline{B}_z^f \left\{\underline{\phi}_j^f\right\}_z \qquad \text{(D.27)}$$

where $\underline{B}_x^f$, $\underline{B}_y^f$, and $\underline{B}_z^f$ are symmetric matrices. $\underline{D}_j$ is assembled from terms of $\underline{D}_j^f$ corresponding to nodes below the free surface.

D.2.2 Computation of $\bar{\underline{Q}}_o^{f\ell}(\omega)$, $\ell = x,y,z$ and $\bar{\underline{Q}}_j^f(\omega)$

Solution of Eq. B.51 with acceleration vector $\underline{D}_o^\ell$ results in the pressure vector $\bar{\underline{p}}_o^\ell(\omega)$. Along $\mathcal{D}$, the pressure distribution within

$\mathcal{D}^e$ is $\bar{p}^e(s,r,\omega)$ defined as $\bar{p}^e(\xi,\eta,\omega)$ where, from Eq. B.47

$$\bar{p}^e(\xi,\eta,\omega) = \underset{\sim}{M}^T \, \bar{\underset{\sim}{p}}^{be}(\omega) \tag{D.28}$$

and where $\bar{\underset{\sim}{p}}^{be}(\omega)$ = vector of boundary element nodal pressures. The x, y, and z subvectors of $\bar{\underset{\sim}{Q}}_o^{f\ell}(\omega)$ are denoted by $\{\bar{\underset{\sim}{Q}}_o^{f\ell}(\omega)\}_x$, $\{\bar{\underset{\sim}{Q}}_o^{f\ell}(\omega)\}_y$ and $\{\bar{\underset{\sim}{Q}}_o^{f\ell}(\omega)\}_z$ and within $\mathcal{D}^e$ by $\{\bar{\underset{\sim}{Q}}^e(\omega)\}_x$, $\{\bar{\underset{\sim}{Q}}^e(\omega)\}_y$, and $\{\bar{\underset{\sim}{Q}}^e(\omega)\}_z$. By the method of virtual work

$$\left\{\bar{\underset{\sim}{Q}}^e(\omega)\right\}_x = \int_{-1}^{1}\int_{-1}^{1} \underset{\sim}{M} \, \frac{n_x}{|n|} \, \bar{p}^e(\xi,\eta,\omega) \; |n| \; d\xi d\eta \tag{D.29}$$

Substitution of Eq. D.28 into Eq. D.29 yields

$$\left\{\bar{\underset{\sim}{Q}}^e(\omega)\right\}_x = \underset{\sim}{B}_x^e \, \bar{\underset{\sim}{p}}^{be}(\omega) \tag{D.30}$$

Assembly of Eq. D.30 over $\mathcal{D}$ for each $\mathcal{D}^e$ yields

$$\left\{\bar{\underset{\sim}{Q}}_o^{f\ell}(\omega)\right\}_x = \underset{\sim}{B}_x^f \, \bar{\underset{\sim}{p}}_o^{f\ell}(\omega) \tag{D.31a}$$

and in like manner

$$\left\{\bar{\underset{\sim}{Q}}_o^{f\ell}(\omega)\right\}_y = \underset{\sim}{B}_y^f \, \bar{\underset{\sim}{p}}_o^{f\ell}(\omega) \tag{D.31b}$$

$$\left\{\bar{\underset{\sim}{Q}}_o^{f\ell}(\omega)\right\}_z = \underset{\sim}{B}_z^f \, \bar{\underset{\sim}{p}}_o^{f\ell}(\omega) \tag{D.31c}$$

$\underline{B}_x^f$, $\underline{B}_y^f$ and $\underline{B}_z^f$ of Eqs. D.27 and D.31 are the same, and $\bar{\underline{p}}_o^{f\ell}(\omega)$ lists the terms of $\bar{\underline{p}}_o^{\ell}(\omega)$ along $\mathcal{D}$ and includes zero terms for nodes at the free surface. $\bar{\underline{Q}}_o^{f\ell}(\omega)$, $\ell = x,y,z$ is assembled from the component vectors of Eq. D.31 and ordered to correspond to $\underline{\phi}_j^f$. The hydrodynamic added load terms of Eq. 2.24 can be found directly as

$$\left\{\underline{\phi}_j^f\right\}^T \bar{\underline{Q}}_o^{f\ell}(\omega) = \left\{\underline{D}_j^f\right\}^T \bar{\underline{p}}_o^{f\ell}(\omega), \qquad \ell = x,y,z \tag{D.32a}$$

Solution of Eq. B.51 with $\underline{D}_j$ results in $\bar{\underline{p}}_j(\omega)$, and the vector $\bar{\underline{p}}_j^f(\omega)$ for pressures along $\mathcal{D}$. The hydrodynamic added mass terms of Eq. 2.24 can be found as

$$\left\{\underline{\phi}_j^f\right\}^T \bar{\underline{Q}}_k^f(\omega) = \left\{\underline{D}_j^f\right\}^T \bar{\underline{p}}_k^f(\omega) \tag{D.32b}$$

APPENDIX E. CONTINUUM SOLUTION FOR THE INFINITE FLUID DOMAIN OF CONSTANT DEPTH

E.1 First B.V.P.

The hydrodynamic pressure $\bar{p}(x,y,\omega)$ within the fluid domain of Fig. E.1a arises from an acceleration $a_x(y)$ of the dam-fluid interface a-b. The acceleration boundary condition at a-b is

$$\frac{\partial \bar{p}}{\partial x}(0,y,\omega) = -\frac{w}{g}\, a_x(y) \tag{E.1}$$

By a separation of variables, $\bar{p}(x,y,\omega)$ is expressed as

$$\bar{p}(x,y,\omega) = \bar{p}_x(x,\omega)\ \bar{p}_y(y,\omega) \tag{E.2}$$

where $\bar{p}_x(x,\omega)$ must satisfy

$$\frac{d^2\bar{p}_x}{dx^2} - \kappa^2\, \bar{p}_x = 0 \tag{E.3a}$$

and $\bar{p}_y(y,\omega)$ must satisfy

$$\frac{d^2\bar{p}_y}{dy^2} + \lambda^2\, \bar{p}_y = 0 \tag{E.3b}$$

where κ = separation constant; and

Preceding page blank

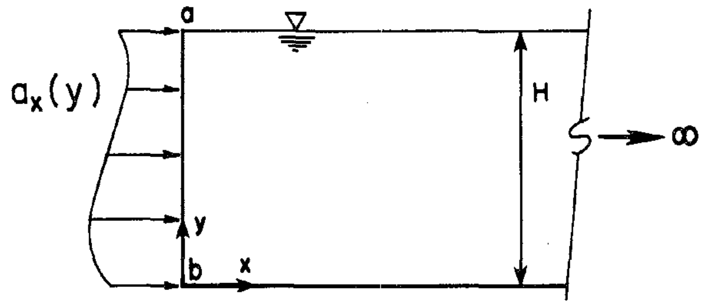

(a) ACCELERATION OF DAM-FLUID INTERFACE

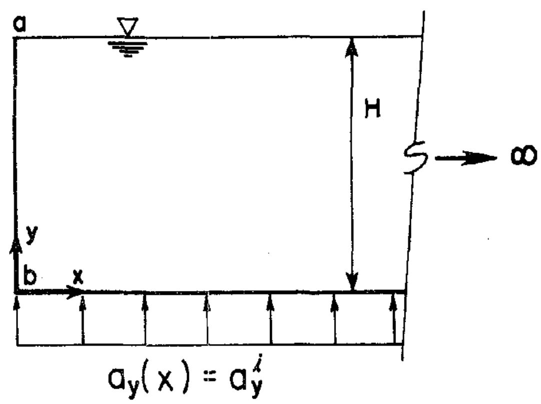

(b) ACCELERATION OF RESERVOIR FLOOR

FIG. E.1 INFINITE FLUID DOMAIN OF CONSTANT DEPTH

$$\lambda^2 = \kappa^2 + \frac{\omega^2}{c^2} \tag{E.4}$$

Boundary conditions for Eq. E.3b are

$$\frac{d\bar{p}_y}{dy}(0,\omega) = i\omega q \; \bar{p}_y(0,\omega) \tag{E.5a}$$

$$\bar{p}_y(H,\omega) = 0 \tag{E.5b}$$

Equation E.3b together with the boundary conditions of Eq. E.5 defines an eigenvalue problem. The nth eigenfunction is denoted by $\psi_n(y)$ and to satisfy Eq. E.3b must be of the form

$$\psi_n(y) = A_n(\omega)\, e^{-i\lambda_n y} + B_n(\omega)\, e^{i\lambda_n y} \tag{E.6}$$

where λ_n is the nth eigenvalue. Equation E.5a imposes the condition that

$$B_n(\omega) = A_n(\omega)\, \frac{\lambda_n + \omega q}{\lambda_n - \omega q} \tag{E.7}$$

and substitution into Eq. E.6 with $A_n(\omega)$ chosen as $(\lambda_n - \omega q)/2\lambda_n$ results in

$$\psi_n(y) = \frac{(\lambda_n - \omega q)\, e^{-i\lambda_n y} + (\lambda_n + \omega q)\, e^{i\lambda_n y}}{2\lambda_n} \tag{E.8}$$

Application of the boundary condition of Eq. E.5b leads to the transcendental equation

$$e^{2i\lambda_n H} = -\frac{\lambda_n - \omega q}{\lambda_n + \omega q} \tag{E.9}$$

from which the eigenvalues are computed.

The eigenfunctions $\psi_n(y)$ and eigenvalues λ_n from Eqs. E.8 and E.9 are complex valued and frequency dependent. The orthogonality property of the eigenfunctions is summarized as

$$\int_0^H \psi_n(y)\ \psi_m(y)\ dy = \begin{cases} \dfrac{H(\lambda_n^2 - \omega^2 q^2) + i\omega q}{2\lambda_n^2} & \text{if} \quad n = m \\ \\ 0 \quad \text{if} \quad n \neq m \end{cases} \tag{E.10}$$

The separated pressure function for the y coordinate is expressed as

$$\bar{p}_y(y,\omega) = \bar{\eta}_n(\omega)\ \psi_n(y), \quad n = 1,2,\ldots \tag{E.11}$$

The κ in Eq. E.4 can now take on only the values given by

$$\kappa_n = \sqrt{\lambda_n^2 - \frac{\omega^2}{C^2}} = \mu_n + i\nu_n \tag{E.12}$$

Since the infinite fluid domain is excited at $x = 0$, $\bar{p}_x(x,\omega)$ must decay with increasing x or travel from $x = 0$ to $x = \infty$. Thus, it is of the form

$$\bar{p}_x(x,\omega) = e^{-\kappa_n x}, \quad n = 1,2,... \tag{E.13}$$

where the root with both μ_n and ν_n positive is taken in computing κ_n from Eq. E.12. Combining the above expressions for $\bar{p}_y(y,\omega)$ and $\bar{p}_x(x,\omega)$ for all n leads to

$$\bar{p}(x,y,\omega) = \sum_{n=1}^{\infty} \bar{\eta}_n(\omega)\ \psi_n(y)\ e^{-\kappa_n x} \tag{E.14}$$

Substitution of Eq. E.14 into the boundary condition Eq. E.1 results in

$$\sum_{n=1}^{\infty} \bar{\eta}_n(\omega)\ \psi_n(y)\ \kappa_n = \frac{w}{g}\, a_x(y) \tag{E.15}$$

By multiplying Eq. E.15 by $\psi_n(y)$ and integrating from $y = 0$ to H (using Eq. E.10), $\bar{\eta}_n(\omega)$ is found as

$$\bar{\eta}_n(\omega) = \frac{w}{g}\ \frac{2\lambda_n^2}{H(\lambda_n^2 - \omega^2 q^2) + i\omega q}\ \frac{I_n}{\kappa_n} \tag{E.16}$$

where $I_n = \int_0^H a_x(y)\ \psi_n(y)\ dy$. Substitution of Eq. E.16 into Eq. E.14 leads to

$$\bar{p}(x,y,\omega) = \frac{w}{g}\sum_{n=1}^{\infty} \frac{2\lambda_n^2}{H(\lambda_n^2 - \omega^2 q^2) + i\omega q}\,\frac{I_n}{\kappa_n}\,\psi_n(y)\, e^{-\kappa_n x} \qquad \text{(E.17)}$$

$\bar{p}(x,y,\omega)$ is a bounded function of frequency and complex valued for $\omega > 0$.

For $q = 0$, $\lambda_n = (2n-1)\pi/2H$ and $\psi_n(y) = \cos\lambda_n y$ (both real valued and frequency independent). Equation E.17 reduces to

$$\bar{p}(x,y,\omega) = \frac{w}{g}\,\frac{2}{H}\sum_{n=1}^{\infty} \frac{I_n}{\kappa_n}\cos\lambda_n y\, e^{-\kappa_n x} \qquad \text{(E.18)}$$

where $I_n = \int_0^H a_x(y)\cos\lambda_n y\,dy$. For $\omega < \lambda_n C$, $\kappa_n = \mu_n$; and for $\omega > \lambda_n C$, $\kappa_n = i\nu_n$. Thus, $\psi_n(y)$ either decays exponentially with increasing x at $e^{-\mu_n x}$ $(\omega < \lambda_n C)$ or is an undecaying harmonic $e^{-i\nu_n x}$ $(\omega > \lambda_n C)$. Also, for an eigenfrequency $\omega_n^i = \lambda_n C$, $\kappa_n = 0$ and the amplitude of $\psi_n(y)$ is infinite. The part of the amplitude that approaches infinity is real below ω_n^i and imaginary above.

E.2 Second B.V.P.

The problem of Fig. E.1b is one-dimensional in the y coordinate. The hydrodynamic pressure $\bar{p}(y,\omega)$ arising from the acceleration a_y^i of the reservoir floor is governed by the one-dimensional Helmholtz equation:

$$\frac{d^2\bar{p}}{dy^2} + \frac{\omega^2}{C^2}\,\bar{p} = 0 \tag{E.19}$$

subject to boundary conditions

$$\frac{d\bar{p}}{dy}\,(0,\omega) = -\,\frac{W}{g}\,a_y^{\,i} + i\omega q\;\bar{p}(0,\omega) \tag{E.20}$$

$$\bar{p}(H,\omega) = 0 \tag{E.21}$$

The general solution to Eq. E.19 is

$$\bar{p}(y,\omega) = A_n(\omega)\;e^{-i\,\frac{\omega}{C}\,y} + B_n(\omega)\;e^{i\,\frac{\omega}{C}\,y} \tag{E.22}$$

Application of the boundary conditions of Eqs. E.20 and E.21 and some algebraic manipulation results in

$$\bar{p}(y,\omega) = \frac{W}{g}\,\frac{C}{\omega}\,a_y^{\,i}\,\frac{\sin\frac{\omega}{C}\,(H-y)}{\cos\frac{\omega}{C}\,H + iCq\,\sin\frac{\omega}{C}\,H} \tag{E.23}$$

$\bar{p}(y,\omega)$ can also be determined using an eigenfunction expansion employing the complex valued and frequency dependent eigenvalues λ_n and eigenfunctions $\psi_n(y)$ resulting from the associated eigenproblem of the first B.V.P. $\bar{p}(y,\omega)$ is expressed as

$$\bar{p}(y,\omega) = \sum_{n=1}^{\infty} \bar{\beta}_n(\omega)\ \psi_n(y) \tag{E.24}$$

where the coefficients $\bar{\beta}_n(\omega)$ are evaluated to satisfy the boundary condition of Eq. E.20. This is possible through a variational approach which requires minimization of a functional $\chi(\bar{p})$ defined by

$$\chi(\bar{p}) = \int_0^H \frac{1}{2}\left(\left(\frac{d\bar{p}}{dy}\right)^2 - \frac{\omega^2}{C^2}\,\bar{p}^2\right) dy - \frac{w}{g}\,a_y^{\mathcal{i}}\ \bar{p}(0,\omega) + \frac{1}{2}\ i\omega q\left(\bar{p}(0,\omega)\right)^2 \tag{E.25}$$

Substituting Eq. E.24 into Eq. E.25 and setting to zero the derivative of $\chi(\bar{p})$ with respect to $\bar{\beta}_n(\omega)$ results in

$$\bar{\beta}_n(\omega) = \frac{w}{g}\,a_y^{\mathcal{i}}\ \frac{2\lambda_n^2}{H(\lambda_n^2 - \omega^2 q^2) + i\omega q}\ \frac{1}{\lambda_n^2 - \dfrac{\omega^2}{C^2}} \tag{E.26}$$

Substitution of Eq. E.26 into Eq. E.24 leads to

$$\bar{p}(y,\omega) = \frac{w}{g}\,a_y^{\mathcal{i}} \sum_{n=1}^{\infty} \frac{2\lambda_n^2}{H(\lambda_n^2 - \omega^2 q^2) + i\omega q}\ \frac{1}{\lambda_n^2 - \dfrac{\omega^2}{C^2}}\ \psi_n(y) \tag{E.27}$$

$\bar{p}(y,\omega)$ is a bounded function of frequency and complex valued for $\omega > 0$.

For $q = 0$, Eq. E.27 reduces to

$$\bar{p}(y,\omega) = \frac{w}{g}\frac{2}{H} a_y^{i} \sum_{n=1}^{\infty} \frac{1}{\lambda_n^2 - \frac{\omega^2}{C^2}} \cos \lambda_n y \qquad \text{(E.28)}$$

where $\lambda_n = (2n-1)\pi/2H$ and where $\cos \lambda_n y$ is the eigenfunction $\psi_n(y)$, as in the first B.V.P. The amplitude of $\psi_n(y)$ is real valued and is unbounded at the eigenfrequency $\omega_n^{i} = \lambda_n C$ with opposite sign on each side.

APPENDIX F. COMPUTATIONAL DETAILS

All computations of this report were carried out on a CDC 7600 computer with the Fortran program EADFS (14). In this program, subspace iteration (17), modified for consistent mass matrices (1), is employed to solve the eigenproblem of the dam (Eq. 2.4/6.3) for the first J natural frequencies ω_j and mode shapes $\underline{\phi}_j$.

The computer program can handle either finite fluid domains or infinite fluid domains of irregular geometry through solution of Eq. 3.6/7.6 or Eq. 3.39/7.26 with the accelerations stated in Secs. 3.5 and 7.5. These equations are stored by a compacted, column-wise scheme and solved by modified Crout reduction (18). If water compressibility is included but fluid-foundation interaction neglected $(q = 0)$, then the fluid domain equations have only real valued terms except in the diagonal matrix $\underline{K}$ of Eq. 3.39/7.26 whose nth diagonal term κ_n is imaginary if $\omega > \omega_n^{\ell}$. Arithmetic for complex valued numbers is used only where necessary in solving Eq. 3.39/7.26. If fluid-foundation interaction is included $(q > 0)$, then solutions to the fluid domain equations are carried out entirely with complex arithmetic. The N eigenvalues λ_n and eigenvectors $\underline{\psi}_n$ of Eq. 3.39/7.26 are independent of excitation frequency ω if $q = 0$; in which case, they are determined from a single solution of the real-valued eigenproblem Eq. 3.18/7.15 by the determinant search method (17). For $q > 0$, the eigenproblem is frequency dependent and is complex valued except at $\omega = 0$ where the above solution is applicable. The λ_n and $\underline{\psi}_n$ at successively higher frequencies are computed by inverse vector iteration with shifting (19) using the λ_n from the previous frequency to

Preceding page blank

compute the shifts and the previous ψ_n as trial vectors. The incompressible water, rigid foundation solutions to Eq. 3.6/7.6 or Eq. 3.39/7.26 are independent of excitation frequency; the compressible water solution at $\omega = 0$ is employed.

Table F.1 lists the Central Processor times on the CDC 7600 to compute frequency response functions of J dam modes for the concrete gravity dam with both the finite fluid domain and the infinite fluid domain with sloped floor (Figs. 4.1b and c) and for symmetric and antisymmetric cases of Morrow Point Dam with infinite fluid domain (Fig. 8.1). If the reservoir is empty, then solution of the eigenproblem of the dam accounts for nearly all the computational effort. C.P. times are listed in Table F.1a.

With compressible water, nearly all the computational effort is spent to solve Eq. 3.6/7.6 or to solve Eq. 3.39/7.26 (along with the eigenproblem Eq. 3.18/7.15 if $q > 0$) for the range of excitation frequencies. Average C.P. times per frequency, both neglecting and including fluid-foundation interaction, are listed in Table F.1b. The total C.P. times also listed are based on the numbers of frequencies indicated which are sufficient to define the frequency response functions for J dam modes. Fewer frequencies are required when fluid-foundation interaction is included because of the smoother response curves.

From Table F.1, the total C.P. times when the reservoir is empty are small compared to those when compressible water is included. Solution times with incompressible water would also be small because only one solution of the fluid domain equations is required. The inclusion of fluid-foundation interaction increases the total computational effort about 60% for the concrete gravity dam and about 600% for Morrow Point Dam. The relatively large computational effort for Morrow Point Dam when fluid-foundation interaction is included is due to the time consuming solution of the complex valued, frequency dependent eigenproblem Eq. 3.18/7.15 which accounts for most of the computational effort.

Dam	Number DOF	J	C.P. Seconds for Eigensolution	Components of Ground Motion	Total C.P. Seconds
concrete gravity	126	6	2.	x,y	2.
Morrow Point (symmetric case)	220	12	14.	x,y	14.
Morrow Point (antisymmetric case)	210	12	13.	z	13.

a. NO WATER

Dam	Fluid Domain	Number Group 1 DOF	Number Group 2 DOF	N	Components of Ground Motion	Fluid-Foundation Interaction	Average C.P. Seconds per Frequency	Number Frequencies	Total C.P. Seconds
concrete gravity	finite	120	-	-	x,y	neglected	.0687	400	27.
						included	.2181	200	44.
concrete gravity	infinite, sloped floor	64	8	8	x,y	neglected	.0611	300	18.
						included	.1797	150	27.
Morrow Point (symmetric case)	infinite	105	52	31	x,y	neglected	.2553	400	102.
						included	3.860	200	772.
Morrow Point (antisymmetric case)	infinite	90	42	27	z	neglected	.1775	400	71.
						included	2.478	200	496.

b. COMPRESSIBLE WATER, NEGLECTING AND INCLUDING FLUID-FOUNDATION INTERACTION

TABLE F.1 SAMPLE SOLUTION TIMES FOR COMPUTING FREQUENCY RESPONSE FUNCTIONS OF J DAM MODES

EERC REPORT LISTING

Preceding page blank

EARTHQUAKE ENGINEERING RESEARCH CENTER REPORTS

NOTE: Numbers in parenthesis are Accession Numbers assigned by the National Technical Information Service; these are followed by a price code. Copies of the reports may be ordered from the National Technical Information Service, 5285 Port Royal Road, Springfield, Virginia, 22161. Accession Numbers should be quoted on orders for reports (PB --- ---) and remittance must accompany each order. Reports without this information were not available at time of printing. Upon request, EERC will mail inquirers this information when it becomes available.

EERC 67-1 "Feasibility Study Large-Scale Earthquake Simulator Facility," by J. Penzien, J.G. Bouwkamp, R.W. Clough and D. Rea - 1967 (PB 187 905)A07

EERC 68-1 Unassigned

EERC 68-2 "Inelastic Behavior of Beam-to-Column Subassemblages Under Repeated Loading," by V.V. Bertero - 1968 (PB 184 888)A05

EERC 68-3 "A Graphical Method for Solving the Wave Reflection-Refraction Problem," by H.D. McNiven and Y. Mengi - 1968 (PB 187 943)A03

EERC 68-4 "Dynamic Properties of McKinley School Buildings," by D. Rea, J.G. Bouwkamp and R.W. Clough - 1968 (PB 187 902)A07

EERC 68-5 "Characteristics of Rock Motions During Earthquakes," by H.B. Seed, I.M. Idriss and F.W. Kiefer - 1968 (PB 188 338)A03

EERC 69-1 "Earthquake Engineering Research at Berkeley," - 1969 (PB 187 906)A11

EERC 69-2 "Nonlinear Seismic Response of Earth Structures," by M. Dibaj and J. Penzien - 1969 (PB 187 904)A08

EERC 69-3 "Probabilistic Study of the Behavior of Structures During Earthquakes," by R. Ruiz and J. Penzien - 1969 (PB 187 886)A06

EERC 69-4 "Numerical Solution of Boundary Value Problems in Structural Mechanics by Reduction to an Initial Value Formulation," by N. Distefano and J. Schujman - 1969 (PB 187 942)A02

EERC 69-5 "Dynamic Programming and the Solution of the Biharmonic Equation," by N. Distefano - 1969 (PB 187 941)A03

EERC 69-6 "Stochastic Analysis of Offshore Tower Structures," by A.K. Malhotra and J. Penzien - 1969 (PB 187 903)A09

EERC 69-7 "Rock Motion Accelerograms for High Magnitude Earthquakes," by H.B. Seed and I.M. Idriss - 1969 (PB 187 940)A02

EERC 69-8 "Structural Dynamics Testing Facilities at the University of California, Berkeley," by R.M. Stephen, J.G. Bouwkamp, R.W. Clough and J. Penzien - 1969 (PB 189 111)A04

EERC 69-9 "Seismic Response of Soil Deposits Underlain by Sloping Rock Boundaries," by H. Dezfulian and H.B. Seed 1969 (PB 189 114)A03

EERC 69-10 "Dynamic Stress Analysis of Axisymmetric Structures Under Arbitrary Loading," by S. Ghosh and E.L. Wilson 1969 (PB 189 026)A10

EERC 69-11 "Seismic Behavior of Multistory Frames Designed by Different Philosophies," by J.C. Anderson and V. V. Bertero - 1969 (PB 190 662)A10

EERC 69-12 "Stiffness Degradation of Reinforcing Concrete Members Subjected to Cyclic Flexural Moments," by V.V. Bertero, B. Bresler and H. Ming Liao - 1969 (PB 202 942)A07

EERC 69-13 "Response of Non-Uniform Soil Deposits to Travelling Seismic Waves," by H. Dezfulian and H.B. Seed - 1969 (PB 191 023)A03

EERC 69-14 "Damping Capacity of a Model Steel Structure," by D. Rea, R.W. Clough and J.G. Bouwkamp - 1969 (PB 190 663)A06

EERC 69-15 "Influence of Local Soil Conditions on Building Damage Potential during Earthquakes," by H.B. Seed and I.M. Idriss - 1969 (PB 191 036)A03

EERC 69-16 "The Behavior of Sands Under Seismic Loading Conditions," by M.L. Silver and H.B. Seed - 1969 (AD 714 982)A07

EERC 70-1 "Earthquake Response of Gravity Dams," by A.K. Chopra - 1970 (AD 709 640)A03

EERC 70-2 "Relationships between Soil Conditions and Building Damage in the Caracas Earthquake of July 29, 1967," by H.B. Seed, I.M. Idriss and H. Dezfulian - 1970 (PB 195 762)A05

EERC 70-3 "Cyclic Loading of Full Size Steel Connections," by E.P. Popov and R.M. Stephen - 1970 (PB 213 545)A04

EERC 70-4 "Seismic Analysis of the Charaima Building, Caraballeda, Venezuela," by Subcommittee of the SEAONC Research Committee: V.V. Bertero, P.F. Fratessa, S.A. Mahin, J.H. Sexton, A.C. Scordelis, E.L. Wilson, L.A. Wyllie, H.B. Seed and J. Penzien, Chairman - 1970 (PB 201 455)A06

EERC 70-5 "A Computer Program for Earthquake Analysis of Dams," by A.K. Chopra and P. Chakrabarti - 1970 (AD 723 994)A05

EERC 70-6 "The Propagation of Love Waves Across Non-Horizontally Layered Structures," by J. Lysmer and L.A. Drake 1970 (PB 197 896)A03

EERC 70-7 "Influence of Base Rock Characteristics on Ground Response," by J. Lysmer, H.B. Seed and P.B. Schnabel 1970 (PB 197 897)A03

EERC 70-8 "Applicability of Laboratory Test Procedures for Measuring Soil Liquefaction Characteristics under Cyclic Loading," by H.B. Seed and W.H. Peacock - 1970 (PB 198 016)A03

EERC 70-9 "A Simplified Procedure for Evaluating Soil Liquefaction Potential," by H.B. Seed and I.M. Idriss - 1970 (PB 198 009)A03

EERC 70-10 "Soil Moduli and Damping Factors for Dynamic Response Analysis," by H.B. Seed and I.M. Idriss - 1970 (PB 197 869)A03

EERC 71-1 "Koyna Earthquake of December 11, 1967 and the Performance of Koyna Dam," by A.K. Chopra and P. Chakrabarti 1971 (AD 731 496)A06

EERC 71-2 "Preliminary In-Situ Measurements of Anelastic Absorption in Soils Using a Prototype Earthquake Simulator," by R.D. Borcherdt and P.W. Rodgers - 1971 (PB 201 454)A03

EERC 71-3 "Static and Dynamic Analysis of Inelastic Frame Structures," by F.L. Porter and G.H. Powell - 1971 (PB 210 135)A06

EERC 71-4 "Research Needs in Limit Design of Reinforced Concrete Structures," by V.V. Bertero - 1971 (PB 202 943)A04

EERC 71-5 "Dynamic Behavior of a High-Rise Diagonally Braced Steel Building," by D. Rea, A.A. Shah and J.G. Bouwkamp 1971 (PB 203 584)A06

EERC 71-6 "Dynamic Stress Analysis of Porous Elastic Solids Saturated with Compressible Fluids," by J. Ghaboussi and E. L. Wilson - 1971 (PB 211 396)A06

EERC 71-7 "Inelastic Behavior of Steel Beam-to-Column Subassemblages," by H. Krawinkler, V.V. Bertero and E.P. Popov 1971 (PB 211 335)A14

EERC 71-8 "Modification of Seismograph Records for Effects of Local Soil Conditions," by P. Schnabel, H.B. Seed and J. Lysmer - 1971 (PB 214 450)A03

EERC 72-1 "Static and Earthquake Analysis of Three Dimensional Frame and Shear Wall Buildings," by E.L. Wilson and H.H. Dovey - 1972 (PB 212 904)A05

EERC 72-2 "Accelerations in Rock for Earthquakes in the Western United States," by P.B. Schnabel and H.B. Seed - 1972 (PB 213 100)A03

EERC 72-3 "Elastic-Plastic Earthquake Response of Soil-Building Systems," by T. Minami - 1972 (PB 214 868)A08

EERC 72-4 "Stochastic Inelastic Response of Offshore Towers to Strong Motion Earthquakes," by M.K. Kaul - 1972 (PB 215 713)A05

EERC 72-5 "Cyclic Behavior of Three Reinforced Concrete Flexural Members with High Shear," by E.P. Popov, V.V. Bertero and H. Krawinkler - 1972 (PB 214 555)A05

EERC 72-6 "Earthquake Response of Gravity Dams Including Reservoir Interaction Effects," by P. Chakrabarti and A.K. Chopra - 1972 (AD 762 330)A08

EERC 72-7 "Dynamic Properties of Pine Flat Dam," by D. Rea, C.Y. Liaw and A.K. Chopra - 1972 (AD 763 928)A05

EERC 72-8 "Three Dimensional Analysis of Building Systems," by E.L. Wilson and H.H. Dovey - 1972 (PB 222 438)A06

EERC 72-9 "Rate of Loading Effects on Uncracked and Repaired Reinforced Concrete Members," by S. Mahin, V.V. Bertero, D. Rea and M. Atalay - 1972 (PB 224 520)A08

EERC 72-10 "Computer Program for Static and Dynamic Analysis of Linear Structural Systems," by E.L. Wilson, K.-J. Bathe, J.E. Peterson and H.H.Dovey - 1972 (PB 220 437)A04

EERC 72-11 "Literature Survey - Seismic Effects on Highway Bridges," by T. Iwasaki, J. Penzien and R.W. Clough - 1972 (PB 215 613)A19

EERC 72-12 "SHAKE-A Computer Program for Earthquake Response Analysis of Horizontally Layered Sites," by P.B. Schnabel and J. Lysmer - 1972 (PB 220 207)A06

EERC 73-1 "Optimal Seismic Design of Multistory Frames," by V.V. Bertero and H. Kamil - 1973

EERC 73-2 "Analysis of the Slides in the San Fernando Dams During the Earthquake of February 9, 1971," by H.B. Seed, K.L. Lee, I.M. Idriss and F. Makdisi - 1973 (PB 223 402)A14

EERC 73-3 "Computer Aided Ultimate Load Design of Unbraced Multistory Steel Frames," by M.B. El-Hafez and G.H. Powell 1973 (PB 248 315)A09

EERC 73-4 "Experimental Investigation into the Seismic Behavior of Critical Regions of Reinforced Concrete Components as Influenced by Moment and Shear," by M. Celebi and J. Penzien - 1973 (PB 215 884)A09

EERC 73-5 "Hysteretic Behavior of Epoxy-Repaired Reinforced Concrete Beams," by M. Celebi and J. Penzien - 1973 (PB 239 568)A03

EERC 73-6 "General Purpose Computer Program for Inelastic Dynamic Response of Plane Structures," by A. Kanaan and G.H. Powell - 1973 (PB 221 260)A08

EERC 73-7 "A Computer Program for Earthquake Analysis of Gravity Dams Including Reservoir Interaction," by P. Chakrabarti and A.K. Chopra - 1973 (AD 766 271)A04

EERC 73-8 "Behavior of Reinforced Concrete Deep Beam-Column Subassemblages Under Cyclic Loads," by O. Küstü and J.G. Bouwkamp - 1973 (PB 246 117)A12

EERC 73-9 "Earthquake Analysis of Structure-Foundation Systems," by A.K. Vaish and A.K. Chopra - 1973 (AD 766 272)A07

EERC 73-10 "Deconvolution of Seismic Response for Linear Systems," by R.B. Reimer - 1973 (PB 227 179)A08

EERC 73-11 "SAP IV: A Structural Analysis Program for Static and Dynamic Response of Linear Systems," by K.-J. Bathe, E.L. Wilson and F.E. Peterson - 1973 (PB 221 967)A09

EERC 73-12 "Analytical Investigations of the Seismic Response of Long, Multiple Span Highway Bridges," by W.S. Tseng and J. Penzien - 1973 (PB 227 816)A10

EERC 73-13 "Earthquake Analysis of Multi-Story Buildings Including Foundation Interaction," by A.K. Chopra and J.A. Gutierrez - 1973 (PB 222 970)A03

EERC 73-14 "ADAP: A Computer Program for Static and Dynamic Analysis of Arch Dams," by R.W. Clough, J.M. Raphael and S. Mojtahedi - 1973 (PB 223 763)A09

EERC 73-15 "Cyclic Plastic Analysis of Structural Steel Joints," by R.B. Pinkney and R.W. Clough - 1973 (PB 226 843)A08

EERC 73-16 "QUAD-4: A Computer Program for Evaluating the Seismic Response of Soil Structures by Variable Damping Finite Element Procedures," by I.M. Idriss, J. Lysmer, R. Hwang and H.B. Seed - 1973 (PB 229 424)A05

EERC 73-17 "Dynamic Behavior of a Multi-Story Pyramid Shaped Building," by R.M. Stephen, J.P. Hollings and J.G. Bouwkamp - 1973 (PB 240 718)A06

EERC 73-18 "Effect of Different Types of Reinforcing on Seismic Behavior of Short Concrete Columns," by V.V. Bertero, J. Hollings, O. Küstü, R.M. Stephen and J.G. Bouwkamp - 1973

EERC 73-19 "Olive View Medical Center Materials Studies, Phase I," by B. Bresler and V.V. Bertero - 1973 (PB 235 986)A06

EERC 73-20 "Linear and Nonlinear Seismic Analysis Computer Programs for Long Multiple-Span Highway Bridges," by W.S. Tseng and J. Penzien - 1973

EERC 73-21 "Constitutive Models for Cyclic Plastic Deformation of Engineering Materials," by J.M. Kelly and P.P. Gillis 1973 (PB 226 024)A03

EERC 73-22 "DRAIN - 2D User's Guide," by G.H. Powell - 1973 (PB 227 016)A05

EERC 73-23 "Earthquake Engineering at Berkeley - 1973," (PB 226 033)A11

EERC 73-24 Unassigned

EERC 73-25 "Earthquake Response of Axisymmetric Tower Structures Surrounded by Water," by C.Y. Liaw and A.K. Chopra 1973 (AD 773 052)A09

EERC 73-26 "Investigation of the Failures of the Olive View Stairtowers During the San Fernando Earthquake and Their Implications on Seismic Design," by V.V. Bertero and R.G. Collins - 1973 (PB 235 106)A13

EERC 73-27 "Further Studies on Seismic Behavior of Steel Beam-Column Subassemblages," by V.V. Bertero, H. Krawinkler and E.P. Popov - 1973 (PB 234 172)A06

EERC 74-1 "Seismic Risk Analysis," by C.S. Oliveira - 1974 (PB 235 920)A06

EERC 74-2 "Settlement and Liquefaction of Sands Under Multi-Directional Shaking," by R. Pyke, C.K. Chan and H.B. Seed 1974

EERC 74-3 "Optimum Design of Earthquake Resistant Shear Buildings," by D. Ray, K.S. Pister and A.K. Chopra - 1974 (PB 231 172)A06

EERC 74-4 "LUSH - A Computer Program for Complex Response Analysis of Soil-Structure Systems," by J. Lysmer, T. Udaka, H.B. Seed and R. Hwang - 1974 (PB 236 796)A05

EERC 74-5 "Sensitivity Analysis for Hysteretic Dynamic Systems: Applications to Earthquake Engineering," by D. Ray 1974 (PB 233 213)A06

EERC 74-6 "Soil Structure Interaction Analyses for Evaluating Seismic Response," by H.B. Seed, J. Lysmer and R. Hwang 1974 (PB 236 519)A04

EERC 74-7 Unassigned

EERC 74-8 "Shaking Table Tests of a Steel Frame - A Progress Report," by R.W. Clough and D. Tang - 1974 (PB 240 869)A03

EERC 74-9 "Hysteretic Behavior of Reinforced Concrete Flexural Members with Special Web Reinforcement," by V.V. Bertero, E.P. Popov and T.Y. Wang - 1974 (PB 236 797)A07

EERC 74-10 "Applications of Reliability-Based, Global Cost Optimization to Design of Earthquake Resistant Structures," by E. Vitiello and K.S. Pister - 1974 (PB 237 231)A06

EERC 74-11 "Liquefaction of Gravelly Soils Under Cyclic Loading Conditions," by R.T. Wong, H.B. Seed and C.K. Chan 1974 (PB 242 042)A03

EERC 74-12 "Site-Dependent Spectra for Earthquake-Resistant Design," by H.B. Seed, C. Ugas and J. Lysmer - 1974 (PB 240 953)A03

EERC 74-13 "Earthquake Simulator Study of a Reinforced Concrete Frame," by P. Hidalgo and R.W. Clough - 1974 (PB 241 944)A13

EERC 74-14 "Nonlinear Earthquake Response of Concrete Gravity Dams," by N. Pal - 1974 (AD/A 006 583)A06

EERC 74-15 "Modeling and Identification in Nonlinear Structural Dynamics - I. One Degree of Freedom Models," by N. Distefano and A. Rath - 1974 (PB 241 548)A06

EERC 75-1 "Determination of Seismic Design Criteria for the Dumbarton Bridge Replacement Structure, Vol. I: Description, Theory and Analytical Modeling of Bridge and Parameters," by F. Baron and S.-H. Pang - 1975 (PB 259 407)A15

EERC 75-2 "Determination of Seismic Design Criteria for the Dumbarton Bridge Replacement Structure, Vol. II: Numerical Studies and Establishment of Seismic Design Criteria," by F. Baron and S.-H. Pang - 1975 (PB 259 408)A11 (For set of EERC 75-1 and 75-2 (PB 259 406))

EERC 75-3 "Seismic Risk Analysis for a Site and a Metropolitan Area," by C.S. Oliveira - 1975 (PB 248 134)A09

EERC 75-4 "Analytical Investigations of Seismic Response of Short, Single or Multiple-Span Highway Bridges," by M.-C. Chen and J. Penzien - 1975 (PB 241 454)A09

EERC 75-5 "An Evaluation of Some Methods for Predicting Seismic Behavior of Reinforced Concrete Buildings," by S.A. Mahin and V.V. Bertero - 1975 (PB 246 306)A16

EERC 75-6 "Earthquake Simulator Study of a Steel Frame Structure, Vol. I: Experimental Results," by R.W. Clough and D.T. Tang - 1975 (PB 243 981)A13

EERC 75-7 "Dynamic Properties of San Bernardino Intake Tower," by D. Rea, C.-Y. Liaw and A.K. Chopra - 1975 (AD/A008 406) A05

EERC 75-8 "Seismic Studies of the Articulation for the Dumbarton Bridge Replacement Structure, Vol. I: Description, Theory and Analytical Modeling of Bridge Components," by F. Baron and R.E. Hamati - 1975 (PB 251 539)A07

EERC 75-9 "Seismic Studies of the Articulation for the Dumbarton Bridge Replacement Structure, Vol. 2: Numerical Studies of Steel and Concrete Girder Alternates," by F. Baron and R.E. Hamati - 1975 (PB 251 540)A10

EERC 75-10 "Static and Dynamic Analysis of Nonlinear Structures," by D.P. Mondkar and G.H. Powell - 1975 (PB 242 434)A08

EERC 75-11 "Hysteretic Behavior of Steel Columns," by E.P. Popov, V.V. Bertero and S. Chandramouli - 1975 (PB 252 365)A11

EERC 75-12 "Earthquake Engineering Research Center Library Printed Catalog," - 1975 (PB 243 711)A26

EERC 75-13 "Three Dimensional Analysis of Building Systems (Extended Version)," by E.L. Wilson, J.P. Hollings and H.H. Dovey - 1975 (PB 243 989)A07

EERC 75-14 "Determination of Soil Liquefaction Characteristics by Large-Scale Laboratory Tests," by P. De Alba, C.K. Chan and H.B. Seed - 1975 (NUREG 0027)A08

EERC 75-15 "A Literature Survey - Compressive, Tensile, Bond and Shear Strength of Masonry," by R.L. Mayes and R.W. Clough - 1975 (PB 246 292)A10

EERC 75-16 "Hysteretic Behavior of Ductile Moment Resisting Reinforced Concrete Frame Components," by V.V. Bertero and E.P. Popov - 1975 (PB 246 388)A05

EERC 75-17 "Relationships Between Maximum Acceleration, Maximum Velocity, Distance from Source, Local Site Conditions for Moderately Strong Earthquakes," by H.B. Seed, R. Murarka, J. Lysmer and I.M. Idriss - 1975 (PB 248 172)A03

EERC 75-18 "The Effects of Method of Sample Preparation on the Cyclic Stress-Strain Behavior of Sands," by J. Mulilis, C.K. Chan and H.B. Seed - 1975 (Summarized in EERC 75-28)

EERC 75-19 "The Seismic Behavior of Critical Regions of Reinforced Concrete Components as Influenced by Moment, Shear and Axial Force," by M.B. Atalay and J. Penzien - 1975 (PB 258 842)A11

EERC 75-20 "Dynamic Properties of an Eleven Story Masonry Building," by R.M. Stephen, J.P. Hollings, J.G. Bouwkamp and D. Jurukovski - 1975 (PB 246 945)A04

EERC 75-21 "State-of-the-Art in Seismic Strength of Masonry - An Evaluation and Review," by R.L. Mayes and R.W. Clough 1975 (PB 249 040)A07

EERC 75-22 "Frequency Dependent Stiffness Matrices for Viscoelastic Half-Plane Foundations," by A.K. Chopra, P. Chakrabarti and G. Dasgupta - 1975 (PB 248 121)A07

EERC 75-23 "Hysteretic Behavior of Reinforced Concrete Framed Walls," by T.Y. Wong, V.V. Bertero and E.P. Popov - 1975

EERC 75-24 "Testing Facility for Subassemblages of Frame-Wall Structural Systems," by V.V. Bertero, E.P. Popov and T. Endo - 1975

EERC 75-25 "Influence of Seismic History on the Liquefaction Characteristics of Sands," by H.B. Seed, K. Mori and C.K. Chan - 1975 (Summarized in EERC 75-28)

EERC 75-26 "The Generation and Dissipation of Pore Water Pressures during Soil Liquefaction," by H.B. Seed, P.P. Martin and J. Lysmer - 1975 (PB 252 648)A03

EERC 75-27 "Identification of Research Needs for Improving Aseismic Design of Building Structures," by V.V. Bertero 1975 (PB 248 136)A05

EERC 75-28 "Evaluation of Soil Liquefaction Potential during Earthquakes," by H.B. Seed, I. Arango and C.K. Chan - 1975 (NUREG 0026)A13

EERC 75-29 "Representation of Irregular Stress Time Histories by Equivalent Uniform Stress Series in Liquefaction Analyses," by H.B. Seed, I.M. Idriss, F. Makdisi and N. Banerjee - 1975 (PB 252 635)A03

EERC 75-30 "FLUSH - A Computer Program for Approximate 3-D Analysis of Soil-Structure Interaction Problems," by J. Lysmer, T. Udaka, C.-F. Tsai and H.B. Seed - 1975 (PB 259 332)A07

EERC 75-31 "ALUSH - A Computer Program for Seismic Response Analysis of Axisymmetric Soil-Structure Systems," by E. Berger, J. Lysmer and H.B. Seed - 1975

EERC 75-32 "TRIP and TRAVEL - Computer Programs for Soil-Structure Interaction Analysis with Horizontally Travelling Waves," by T. Udaka, J. Lysmer and H.B. Seed - 1975

EERC 75-33 "Predicting the Performance of Structures in Regions of High Seismicity," by J. Penzien - 1975 (PB 248 130)A03

EERC 75-34 "Efficient Finite Element Analysis of Seismic Structure - Soil - Direction," by J. Lysmer, H.B. Seed, T. Udaka, R.N. Hwang and C.-F. Tsai - 1975 (PB 253 570)A03

EERC 75-35 "The Dynamic Behavior of a First Story Girder of a Three-Story Steel Frame Subjected to Earthquake Loading," by R.W. Clough and L.-Y. Li - 1975 (PB 248 841)A05

EERC 75-36 "Earthquake Simulator Study of a Steel Frame Structure, Volume II - Analytical Results," by D.T. Tang - 1975 (PB 252 926)A10

EERC 75-37 "ANSR-I General Purpose Computer Program for Analysis of Non-Linear Structural Response," by D.P. Mondkar and G.H. Powell - 1975 (PB 252 386)A08

EERC 75-38 "Nonlinear Response Spectra for Probabilistic Seismic Design and Damage Assessment of Reinforced Concrete Structures," by M. Murakami and J. Penzien - 1975 (PB 259 530)A05

EERC 75-39 "Study of a Method of Feasible Directions for Optimal Elastic Design of Frame Structures Subjected to Earthquake Loading," by N.D. Walker and K.S. Pister - 1975 (PB 257 781)A06

EERC 75-40 "An Alternative Representation of the Elastic-Viscoelastic Analogy," by G. Dasgupta and J.L. Sackman - 1975 (PB 252 173)A03

EERC 75-41 "Effect of Multi-Directional Shaking on Liquefaction of Sands," by H.B. Seed, R. Pyke and G.R. Martin - 1975 (PB 258 781)A03

EERC 76-1 "Strength and Ductility Evaluation of Existing Low-Rise Reinforced Concrete Buildings - Screening Method," by T. Okada and B. Bresler - 1976 (PB 257 906)A11

EERC 76-2 "Experimental and Analytical Studies on the Hysteretic Behavior of Reinforced Concrete Rectangular and T-Beams," by S.-Y.M. Ma, E.P. Popov and V.V. Bertero - 1976 (PB 260 843)A12

EERC 76-3 "Dynamic Behavior of a Multistory Triangular-Shaped Building," by J. Petrovski, R.M. Stephen, E. Gartenbaum and J.G. Bouwkamp - 1976 (PB 273 279)A07

EERC 76-4 "Earthquake Induced Deformations of Earth Dams," by N. Serff, H.B. Seed, F.I. Makdisi & C.-Y. Chang - 1976 (PB 292 065)A08

EERC 76-5 "Analysis and Design of Tube-Type Tall Building Structures," by H. de Clercq and G.H. Powell - 1976 (PB 252 220) A10

EERC 76-6 "Time and Frequency Domain Analysis of Three-Dimensional Ground Motions, San Fernando Earthquake," by T. Kubo and J. Penzien (PB 260 556)A11

EERC 76-7 "Expected Performance of Uniform Building Code Design Masonry Structures," by R.L. Mayes, Y. Omote, S.W. Chen and R.W. Clough - 1976 (PB 270 098)A05

EERC 76-8 "Cyclic Shear Tests of Masonry Piers, Volume 1 - Test Results," by R.L. Mayes, Y. Omote, R.W. Clough - 1976 (PB 264 424)A06

EERC 76-9 "A Substructure Method for Earthquake Analysis of Structure - Soil Interaction," by J.A. Gutierrez and A.K. Chopra - 1976 (PB 257 783)A08

EERC 76-10 "Stabilization of Potentially Liquefiable Sand Deposits using Gravel Drain Systems," by H.B. Seed and J.R. Booker - 1976 (PB 258 820)A04

EERC 76-11 "Influence of Design and Analysis Assumptions on Computed Inelastic Response of Moderately Tall Frames," by G.H. Powell and D.G. Row - 1976 (PB 271 409)A06

EERC 76-12 "Sensitivity Analysis for Hysteretic Dynamic Systems: Theory and Applications," by D. Ray, K.S. Pister and E. Polak - 1976 (PB 262 859)A04

EERC 76-13 "Coupled Lateral Torsional Response of Buildings to Ground Shaking," by C.L. Kan and A.K. Chopra - 1976 (PB 257 907)A09

EERC 76-14 "Seismic Analyses of the Banco de America," by V.V. Bertero, S.A. Mahin and J.A. Hollings - 1976

EERC 76-15 "Reinforced Concrete Frame 2: Seismic Testing and Analytical Correlation," by R.W. Clough and J. Gidwani - 1976 (PB 261 323)A08

EERC 76-16 "Cyclic Shear Tests of Masonry Piers, Volume 2 - Analysis of Test Results," by R.L. Mayes, Y. Omote and R.W. Clough - 1976

EERC 76-17 "Structural Steel Bracing Systems: Behavior Under Cyclic Loading," by E.P. Popov, K. Takanashi and C.W. Roeder - 1976 (PB 260 715)A05

EERC 76-18 "Experimental Model Studies on Seismic Response of High Curved Overcrossings," by D. Williams and W.G. Godden - 1976 (PB 269 548)A08

EERC 76-19 "Effects of Non-Uniform Seismic Disturbances on the Dumbarton Bridge Replacement Structure," by F. Baron and R.E. Hamati - 1976 (PB 282 981)A16

EERC 76-20 "Investigation of the Inelastic Characteristics of a Single Story Steel Structure Using System Identification and Shaking Table Experiments," by V.C. Matzen and H.D. McNiven - 1976 (PB 258 453)A07

EERC 76-21 "Capacity of Columns with Splice Imperfections," by E.P. Popov, R.M. Stephen and R. Philbrick - 1976 (PB 260 378)A04

EERC 76-22 "Response of the Olive View Hospital Main Building during the San Fernando Earthquake," by S. A. Mahin, V.V. Bertero, A.K. Chopra and R. Collins - 1976 (PB 271 425)A14

EERC 76-23 "A Study on the Major Factors Influencing the Strength of Masonry Prisms," by N.M. Mostaghel, R.L. Mayes, R. W. Clough and S.W. Chen - 1976 (Not published)

EERC 76-24 "GADFLEA - A Computer Program for the Analysis of Pore Pressure Generation and Dissipation during Cyclic or Earthquake Loading," by J.R. Booker, M.S. Rahman and H.B. Seed - 1976 (PB 263 947)A04

EERC 76-25 "Seismic Safety Evaluation of a R/C School Building," by B. Bresler and J. Axley - 1976

EERC 76-26 "Correlative Investigations on Theoretical and Experimental Dynamic Behavior of a Model Bridge Structure," by K. Kawashima and J. Penzien - 1976 (PB 263 388)A11

EERC 76-27 "Earthquake Response of Coupled Shear Wall Buildings," by T. Srichatrapimuk - 1976 (PB 265 157)A07

EERC 76-28 "Tensile Capacity of Partial Penetration Welds," by E.P. Popov and R.M. Stephen - 1976 (PB 262 899)A03

EERC 76-29 "Analysis and Design of Numerical Integration Methods in Structural Dynamics," by H.M. Hilber - 1976 (PB 264 410)A06

EERC 76-30 "Contribution of a Floor System to the Dynamic Characteristics of Reinforced Concrete Buildings," by L.E. Malik and V.V. Bertero - 1976 (PB 272 247)A13

EERC 76-31 "The Effects of Seismic Disturbances on the Golden Gate Bridge," by F. Baron, M. Arikan and R.E. Hamati - 1976 (PB 272 279)A09

EERC 76-32 "Infilled Frames in Earthquake Resistant Construction," by R.E. Klingner and V.V. Bertero - 1976 (PB 265 892)A13

UCB/EERC-77/01 "PLUSH - A Computer Program for Probabilistic Finite Element Analysis of Seismic Soil-Structure Interaction," by M.P. Romo Organista, J. Lysmer and H.B. Seed - 1977

UCB/EERC-77/02 "Soil-Structure Interaction Effects at the Humboldt Bay Power Plant in the Ferndale Earthquake of June 7, 1975," by J.E. Valera, H.B. Seed, C.F. Tsai and J. Lysmer - 1977 (PB 265 795)A04

UCB/EERC-77/03 "Influence of Sample Disturbance on Sand Response to Cyclic Loading," by K. Mori, H.B. Seed and C.K. Chan - 1977 (PB 267 352)A04

UCB/EERC-77/04 "Seismological Studies of Strong Motion Records," by J. Shoja-Taheri - 1977 (PB 269 655)A10

UCB/EERC-77/05 "Testing Facility for Coupled-Shear Walls," by L. Li-Hyung, V.V. Bertero and E.P. Popov - 1977

UCB/EERC-77/06 "Developing Methodologies for Evaluating the Earthquake Safety of Existing Buildings," by No. 1 - B. Bresler; No. 2 - B. Bresler, T. Okada and D. Zisling; No. 3 - T. Okada and B. Bresler; No. 4 - V.V. Bertero and B. Bresler - 1977 (PB 267 354)A08

UCB/EERC-77/07 "A Literature Survey - Transverse Strength of Masonry Walls," by Y. Omote, R.L. Mayes, S.W. Chen and R.W. Clough - 1977 (PB 277 933)A07

UCB/EERC-77/08 "DRAIN-TABS: A Computer Program for Inelastic Earthquake Response of Three Dimensional Buildings," by R. Guendelman-Israel and G.H. Powell - 1977 (PB 270 693)A07

UCB/EERC-77/09 "SUBWALL: A Special Purpose Finite Element Computer Program for Practical Elastic Analysis and Design of Structural Walls with Substructure Option," by D.Q. Le, H. Peterson and E.P. Popov - 1977 (PB 270 567)A05

UCB/EERC-77/10 "Experimental Evaluation of Seismic Design Methods for Broad Cylindrical Tanks," by D.P. Clough (PB 272 280)A13

UCB/EERC-77/11 "Earthquake Engineering Research at Berkeley - 1976," - 1977 (PB 273 507)A09

UCB/EERC-77/12 "Automated Design of Earthquake Resistant Multistory Steel Building Frames," by N.D. Walker, Jr. - 1977 (PB 276 526)A09

UCB/EERC-77/13 "Concrete Confined by Rectangular Hoops Subjected to Axial Loads," by J. Vallenas, V.V. Bertero and E.P. Popov - 1977 (PB 275 165)A06

UCB/EERC-77/14 "Seismic Strain Induced in the Ground During Earthquakes," by Y. Sugimura - 1977 (PB 284 201)A04

UCB/EERC-77/15 "Bond Deterioration under Generalized Loading," by V.V. Bertero, E.P. Popov and S. Viwathanatepa - 1977

UCB/EERC-77/16 "Computer Aided Optimum Design of Ductile Reinforced Concrete Moment Resisting Frames," by S.W. Zagajeski and V.V. Bertero - 1977 (PB 280 137)A07

UCB/EERC-77/17 "Earthquake Simulation Testing of a Stepping Frame with Energy-Absorbing Devices," by J.M. Kelly and D.F. Tsztoo - 1977 (PB 273 506)A04

UCB/EERC-77/18 "Inelastic Behavior of Eccentrically Braced Steel Frames under Cyclic Loadings," by C.W. Roeder and E.P. Popov - 1977 (PB 275 526)A15

UCB/EERC-77/19 "A Simplified Procedure for Estimating Earthquake-Induced Deformations in Dams and Embankments," by F.I. Makdisi and H.B. Seed - 1977 (PB 276 820)A04

UCB/EERC-77/20 "The Performance of Earth Dams during Earthquakes," by H.B. Seed, F.I. Makdisi and P. de Alba - 1977 (PB 276 821)A04

UCB/EERC-77/21 "Dynamic Plastic Analysis Using Stress Resultant Finite Element Formulation," by P. Lukkunapvasit and J.M. Kelly - 1977 (PB 275 453)A04

UCB/EERC-77/22 "Preliminary Experimental Study of Seismic Uplift of a Steel Frame," by R.W. Clough and A.A. Huckelbridge 1977 (PB 278 769)A08

UCB/EERC-77/23 "Earthquake Simulator Tests of a Nine-Story Steel Frame with Columns Allowed to Uplift," by A.A. Huckelbridge - 1977 (PB 277 944)A09

UCB/EERC-77/24 "Nonlinear Soil-Structure Interaction of Skew Highway Bridges," by M.-C. Chen and J. Penzien - 1977 (PB 276 176)A07

UCB/EERC-77/25 "Seismic Analysis of an Offshore Structure Supported on Pile Foundations," by D.D.-N. Liou and J. Penzien 1977 (PB 283 180)A06

UCB/EERC-77/26 "Dynamic Stiffness Matrices for Homogeneous Viscoelastic Half-Planes," by G. Dasgupta and A.K. Chopra - 1977 (PB 279 654)A06

UCB/EERC-77/27 "A Practical Soft Story Earthquake Isolation System," by J.M. Kelly, J.M. Eidinger and C.J. Derham - 1977 (PB 276 814)A07

UCB/EERC-77/28 "Seismic Safety of Existing Buildings and Incentives for Hazard Mitigation in San Francisco: An Exploratory Study," by A.J. Meltsner - 1977 (PB 281 970)A05

UCB/EERC-77/29 "Dynamic Analysis of Electrohydraulic Shaking Tables," by D. Rea, S. Abedi-Hayati and Y. Takahashi 1977 (PB 282 569)A04

UCB/EERC-77/30 "An Approach for Improving Seismic - Resistant Behavior of Reinforced Concrete Interior Joints," by B. Galunic, V.V. Bertero and E.P. Popov - 1977 (PB 290 870)A06

UCB/EERC-78/01 "The Development of Energy-Absorbing Devices for Aseismic Base Isolation Systems," by J.M. Kelly and D.F. Tsztoo - 1978 (PB 284 978)A04

UCB/EERC-78/02 "Effect of Tensile Prestrain on the Cyclic Response of Structural Steel Connections, by J.G. Bouwkamp and A. Mukhopadhyay - 1978

UCB/EERC-78/03 "Experimental Results of an Earthquake Isolation System using Natural Rubber Bearings," by J.M. Eidinger and J.M. Kelly - 1978 (PB 281 686)A04

UCB/EERC-78/04 "Seismic Behavior of Tall Liquid Storage Tanks," by A. Niwa - 1978 (PB 284 017)A14

UCB/EERC-78/05 "Hysteretic Behavior of Reinforced Concrete Columns Subjected to High Axial and Cyclic Shear Forces," by S.W. Zagajeski, V.V. Bertero and J.G. Bouwkamp - 1978 (PB 283 858)A13

UCB/EERC-78/06 "Inelastic Beam-Column Elements for the ANSR-I Program," by A. Riahi, D.G. Row and G.H. Powell - 1978

UCB/EERC-78/07 "Studies of Structural Response to Earthquake Ground Motion," by O.A. Lopez and A.K. Chopra - 1978 (PB 282 790)A05

UCB/EERC-78/08 "A Laboratory Study of the Fluid-Structure Interaction of Submerged Tanks and Caissons in Earthquakes," by R.C. Byrd - 1978 (PB 284 957)A08

UCB/EERC-78/09 "Model for Evaluating Damageability of Structures," by I. Sakamoto and B. Bresler - 1978

UCB/EERC-78/10 "Seismic Performance of Nonstructural and Secondary Structural Elements," by I. Sakamoto - 1978

UCB/EERC-78/11 "Mathematical Modelling of Hysteresis Loops for Reinforced Concrete Columns," by S. Nakata, T. Sproul and J. Penzien - 1978

UCB/EERC-78/12 "Damageability in Existing Buildings," by T. Blejwas and B. Bresler - 1978

UCB/EERC-78/13 "Dynamic Behavior of a Pedestal Base Multistory Building," by R.M. Stephen, E.L. Wilson, J.G. Bouwkamp and M. Button - 1978 (PB 286 650)A08

UCB/EERC-78/14 "Seismic Response of Bridges - Case Studies," by R.A. Imbsen, V. Nutt and J. Penzien - 1978 (PB 286 503)A10

UCB/EERC-78/15 "A Substructure Technique for Nonlinear Static and Dynamic Analysis," by D.G. Row and G.H. Powell - 1978 (PB 288 077)A10

UCB/EERC-78/16 "Seismic Risk Studies for San Francisco and for the Greater San Francisco Bay Area," by C.S. Oliveira - 1978

UCB/EERC-78/17 "Strength of Timber Roof Connections Subjected to Cyclic Loads," by P. Gülkan, R.L. Mayes and R.W. Clough - 1978

UCB/EERC-78/18 "Response of K-Braced Steel Frame Models to Lateral Loads," by J.G. Bouwkamp, R.M. Stephen and E.P. Popov - 1978

UCB/EERC-78/19 "Rational Design Methods for Light Equipment in Structures Subjected to Ground Motion," by J.L. Sackman and J.M. Kelly - 1978 (PB 292 357)A04

UCB/EERC-78/20 "Testing of a Wind Restraint for Aseismic Base Isolation," by J.M. Kelly and D.E. Chitty - 1978 (PB 292 833)A03

UCB/EERC-78/21 "APOLLO - A Computer Program for the Analysis of Pore Pressure Generation and Dissipation in Horizontal Sand Layers During Cyclic or Earthquake Loading," by P.P. Martin and H.B. Seed - 1978 (PB 292 835)A04

UCB/EERC-78/22 "Optimal Design of an Earthquake Isolation System," by M.A. Bhatti, K.S. Pister and E. Polak - 1978 (PB 294 735)A06

UCB/EERC-78/23 "MASH - A Computer Program for the Non-Linear Analysis of Vertically Propagating Shear Waves in Horizontally Layered Deposits," by P.P. Martin and H.B. Seed - 1978 (PB 293 101)A05

UCB/EERC-78/24 "Investigation of the Elastic Characteristics of a Three Story Steel Frame Using System Identification," by I. Kaya and H.D. McNiven - 1978

UCB/EERC-78/25 "Investigation of the Nonlinear Characteristics of a Three-Story Steel Frame Using System Identification," by I. Kaya and H.D. McNiven - 1978

UCB/EERC-78/26 "Studies of Strong Ground Motion in Taiwan," by Y.M. Hsiung, B.A. Bolt and J. Penzien - 1978

UCB/EERC-78/27 "Cyclic Loading Tests of Masonry Single Piers: Volume 1 - Height to Width Ratio of 2," by P.A. Hidalgo, R.L. Mayes, H.D. McNiven and R.W. Clough - 1978

UCB/EERC-78/28 "Cyclic Loading Tests of Masonry Single Piers: Volume 2 - Height to Width Ratio of 1," by S.-W.J. Chen, P.A. Hidalgo, R.L. Mayes, R.W. Clough and H.D. McNiven - 1978

UCB/EERC-78/29 "Analytical Procedures in Soil Dynamics," by J. Lysmer - 1978

UCB/EERC-79/01 "Hysteretic Behavior of Lightweight Reinforced Concrete Beam-Column Subassemblages," by B. Forzani, E.P. Popov, and V.V. Bertero - 1979

UCB/EERC-79/02 "The Development of a Mathematical Model to Predict the Flexural Response of Reinforced Concrete Beams to Cyclic Loads, Using System Identification," by J.F. Stanton and H.D. McNiven - 1979

UCB/EERC-79/03 "Linear and Nonlinear Earthquake Response of Simple Torsionally Coupled Systems," by C.L. Kan and A.K. Chopra - 1979

UCB/EERC-79/04 "A Mathematical Model of Masonry for Predicting Its Linear Seismic Response Characteristics," by Y. Mengi and H.D. McNiven - 1979

UCB/EERC-79/05 "Mechanical Behavior of Lightweight Concrete Confined by Different Types of Lateral Reinforcement," by M.A. Manrique, V.V. Bertero and E.P. Popov - 1979

UCB/EERC-79/06 "Static Tilt Tests of a Tall Cylindrical Liquid Storage Tank," by R.W. Clough and A. Niwa - 1979

UCB/EERC-79/07 "The Design of Steel Energy Absorbing Restrainers and Their Incorporation Into Nuclear Power Plants for Enhanced Safety: Volume 1 - Summary Report," by P.N. Spencer, V.F. Zackay, and E.R. Parker - 1979

UCB/EERC-79/08 "The Design of Steel Energy Absorbing Restrainers and Their Incorporation Into Nuclear Power Plants for Enhanced Safety: Volume 2 - The Development of Analyses for Reactor System Piping," "Simple Systems" by M.C. Lee, J. Penzien, A.K. Chopra, and K. Suzuki "Complex Systems" by G.H. Powell, E.L. Wilson, R.W. Clough and D.G. Row - 1979

UCB/EERC-79/09 "The Design of Steel Energy Absorbing Restrainers and Their Incorporation Into Nuclear Power Plants for Enhanced Safety: Volume 3 - Evaluation of Commerical Steels," by W.S. Owen, R.M.N. Pelloux, R.O. Ritchie, M. Faral, T. Ohhashi, J. Toplosky, S.J. Hartman, V.F. Zackay, and E.R. Parker - 1979

UCB/EERC-79/10 "The Design of Steel Energy Absorbing Restrainers and Their Incorporation Into Nuclear Power Plants for Enhanced Safety: Volume 4 - A Review of Energy-Absorbing Devices," by J.M. Kelly and M.S. Skinner - 1979

UCB/EERC-79/11 "Conservatism In Summation Rules for Closely Spaced Modes," by J.M. Kelly and J.L. Sackman - 1979

UCB/EERC-79/12 "Cyclic Loading Tests of Masonry Single Piers Volume 3 - Height to Width Ratio of 0.5," by P.A. Hidalgo, R.L. Mayes, H.D. McNiven and R.W. Clough - 1979

UCB/EERC-79/13 "Cyclic Behavior of Dense Coarse-Grained Materials in Relation to the Seismic Stability of Dams," by N.G. Banerjee, H.B. Seed and C.K. Chan - 1979

UCB/EERC-79/14 "Seismic Behavior of Reinforced Concrete Interior Beam-Column Subassemblages," by S. Viwathanatepa, E.P. Popov and V.V. Bertero - 1979

UCB/EERC-79/15 "Optimal Design of Localized Nonlinear Systems with Dual Performance Criteria Under Earthquake Excitations," by M.A. Bhatti - 1979

UCB/EERC-79/16 "OPTDYN - A General Purpose Optimization Program for Problems with or without Dynamic Constraints," by M.A. Bhatti, E. Polak and K.S. Pister - 1979

UCB/EERC-79/17 "ANSR-II, Analysis of Nonlinear Structural Response, Users Manual," by D.P. Mondkar and G.H. Powell - 1979

UCB/EERC-79/18 "Soil Structure Interaction in Different Seismic Environments," A. Gomez-Masso, J. Lysmer, J.-C. Chen and H.B. Seed - 1979

UCB/EERC-79/19 "ARMA Models for Earthquake Ground Motions," by M.K. Chang, J.W. Kwiatkowski, R.F. Nau, R.M. Oliver and K.S. Pister - 1979

UCB/EERC-79/20 "Hysteretic Behavior of Reinforced Concrete Structural Walls," by J.M. Vallenas, V.V. Bertero and E.P. Popov - 1979

UCB/EERC-79/21 "Studies on High-Frequency Vibrations of Buildings I: The Column Effects," by J. Lubliner - 1979

UCB/EERC-79/22 "Effects of Generalized Loadings on Bond Reinforcing Bars Embedded in Confined Concrete Blocks," by S. Viwathanatepa, E.P. Popov and V.V. Bertero - 1979

UCB/EERC-79/23 "Shaking Table Study of Single-Story Masonry Houses, Volume 1: Test Structures 1 and 2," by P. Gülkan, R.L. Mayes and R.W. Clough - 1979

UCB/EERC-79/24 "Shaking Table Study of Single-Story Masonry Houses, Volume 2: Test Structures 3 and 4," by P. Gülkan, R.L. Mayes and R.W. Clough - 1979

UCB/EERC-79/25 "Shaking Table Study of Single-Story Masonry Houses, Volume 3: Summary, Conclusions and Recommendations," by R.W. Clough, R.L. Mayes and P. Gülkan - 1979

UCB/EERC-79/26 "Recommendations for a U.S.-Japan Cooperative Research Program Utilizing Large-Scale Testing Facilities," by U.S.-Japan Planning Group - 1979

UCB/EERC-79/27 "Earthquake-Induced Liquefaction Near Lake Amatitlan, Guatemala," by H.B. Seed, I. Arango, C.K. Chan, A. Gomez-Masso and R. Grant de Ascoli - 1979

UCB/EERC-79/28 "Infill Panels: Their Influence on Seismic Response of Buildings," by J.W. Axley and V.V. Bertero - 1979

UCB/EERC-79/29 "3D Truss Bar Element (Type 1) for the ANSR-II Program," by D.P. Mondkar and G.H. Powell - 1979

UCB/EERC-79/30 "2D Beam-Column Element (Type 5 - Parallel Element Theory) for the ANSR-II Program," by D.G. Row, G.H. Powell and D.P. Mondkar

UCB/EERC-79/31 "3D Beam-Column Element (Type 2 - Parallel Element Theory) for the ANSR-II Program," by A. Riahi, G.H. Powell and D.P. Mondkar - 1979

UCB/EERC-79/32 "On Response of Structures to Stationary Excitation," by A. Der Kiureghian - 1979

UCB/EERC-79/33 "Undisturbed Sampling and Cyclic Load Testing of Sands," by S. Singh, H.B. Seed and C.K. Chan - 1979

UCB/EERC-79/34 "Interaction Effects of Simultaneous Torsional and Compressional Cyclic Loading of Sand," by P.M. Griffin and W.N. Houston - 1979

UCB/EERC-80/01 "Earthquake Response of Concrete Gravity Dams Including Hydrodynamic and Foundation Interaction Effects," by A.K. Chopra, P. Chakrabarti and S. Gupta - 1980

UCB/EERC-80/02 "Rocking Response of Rigid Blocks to Earthquakes," by C.S. Yim, A.K. Chopra and J. Penzien - 1980

UCB/EERC-80/03 "Optimum Inelastic Design of Seismic-Resistant Reinforced Concrete Frame Structures," by S.W. Zagajeski and V.V. Bertero - 1980

UCB/EERC-80/04 "Effects of Amount and Arrangement of Wall-Panel Reinforcement on Hysteretic Behavior of Reinforced Concrete Walls," by R. Iliya and V.V. Bertero - 1980

UCB/EERC-80/05 "Shaking Table Research on Concrete Dam Models," by A. Niwa and R.W. Clough - 1980

UCB/EERC-80/06 "Piping With Energy Absorbing Restrainers: Parameter Study on Small Systems," by G.H. Powell, C. Oughourlian and J. Simons - 1980

UCB/EERC-80/07 "Inelastic Torsional Response of Structures Subjected to Earthquake Ground Motions," by Y. Yamazaki - 1980

UCB/EERC-80/08 "Study of X-Braced Steel Frame Structures Under Earthquake Simulation," by Y. Ghanaat - 1980

UCB/EERC-80/09 "Hybrid Modelling of Soil-Structure Interaction," by S. Gupta, T.W. Lin, J. Penzien and C.S. Yeh - 1980

UCB/EERC-80/10 "General Applicability of a Nonlinear Model of a One Story Steel Frame," by B.I. Sveinsson and H. McNiven - 1980

UCB/EERC-80/11 "A Green-Function Method for Wave Interaction with a Submerged Body," by W. Kioka - 1980

UCB/EERC-80/12 "Hydrodynamic Pressure and Added Mass for Axisymmetric Bodies," by F. Nilrat - 1980

UCB/EERC-80/13 "Treatment of Non-Linear Drag Forces Acting on Offshore Platforms," by B.V. Dao and J. Penzien - 1980

UCB/EERC-80/14 "2D Plane/Axisymmetric Solid Element (Type 3 - Elastic or Elastic-Perfectly Plastic) for the ANSR-II Program," by D.P. Mondkar and G.H. Powell - 1980

UCB/EERC-80/15 "A Response Spectrum Method for Random Vibrations," by A. Der Kiureghian - 1980

UCB/EERC-80/16 "Cyclic Inelastic Buckling of Tubular Steel Braces," by V.A. Zayas, E.P. Popov and S.A. Mahin - June 1980

UCB/EERC-80/17 "Dynamic Response of Simple Arch Dams Including Hydrodynamic Interaction," by C.S. Porter and A.K. Chopra - July 1980

UCB/EERC-80/18 "Experimental Testing of a Friction Damped Aseismic Base Isolation System with Fail-Safe Characteristics," by J.M. Kelly, K.E. Beucke and M.S. Skinner - July 1980

UCB/EERC-80/19 "The Design of Steel Energy-Absorbing Restrainers and their Incorporation into Nuclear Power Plants for Enhanced Safety (Vol 1B): Stochastic Seismic Analyses of Nuclear Power Plant Structures and Piping Systems Subjected to Multiple Support Excitations," by M.C. Lee and J. Penzien - 1980

UCB/EERC-80/20 "The Design of Steel Energy-Absorbing Restrainers and their Incorporation into Nuclear Power Plants for Enhanced Safety (Vol 1C): Numerical Method for Dynamic Substructure Analysis," by J.M. Dickens and E.L. Wilson - 1980

UCB/EERC-80/21 "The Design of Steel Energy-Absorbing Restrainers and their Incorporation into Nuclear Power Plants for Enhanced Safety (Vol 2): Development and Testing of Restraints for Nuclear Piping Systems," by J.M. Kelly and M.S. Skinner - 1980

UCB/EERC-80/22 "3D Solid Element (Type 4-Elastic or Elastic-Perfectly-Plastic) for the ANSR-II Program," by D.P. Mondkar and G.H. Powell - 1980

UCB/EERC-80/23 "Gap-Friction Element (Type 5) for the ANSR-II Program," by D.P. Mondkar and G.H. Powell - 1980

UCB/EERC-80/24 "U-Bar Restraint Element (Type 11) for the ANSR-II Program," C. Oughourlian and G.H. Powell - 1980

UCB/EERC-80/25 "Testing of a Natural Rubber Base Isolation System by an Explosively Simulated Earthquake," by J.M. Kelly 1980

UCB/EERC-80/26 "Input Identification from Structural Vibrational Response," by Y. Hu - 1980

UCB/EERC-80/27 "Cyclic Inelastic Behavior of Steel Offshore Structures," by V.A. Zayas, S.A. Mahin and E.P. Popov - 1980

UCB/EERC-80/28 "Shaking Table Testing of a Reinforced Concrete Frame with Biaxial Response," M.G. Oliva and R.W. Clough 1980

UCB/EERC-80/29 "Dynamic Properties of a Twelve-Story Prefabricated Panel Building," by J.G. Bouwkamp, J.P. Kollegger and R.M. Stephen - 1980

UCB/EERC-80/30 "Dynamic Properties of a Eight-Story Prefabricated Panel Building," by J.G. Bouwkamp, J.P. Kollegger and R.M. Stephen - 1980

UCB/EERC-80/31 "Predictive Dynamic Response of Panel Type Structures Under Earthquakes," by J.P. Kollegger and J.G. Bouwkamp 1980

UCB/EERC-80/32 "The Design of Steel Energy-Absorbing Restrainers and their Incorporation into Nuclear Power Plants for Enhanced Safety: Vol 3, Testing of Commercial Steels in Low-Cycle Torsional Fatigue," by P. Spencer, E.R. Parker, E. Jongewaard and M. Drory - 1980

UCB/EERC-80/33 "The Design of Steel Energy-Absorbing Restrainers and their Incorporation into Nuclear Power Plants for Enhanced Safety: Vol 4, Shaking Table Tests of Piping Systems with Energy-Absorbing Restrainers," by S.F. Stiemer and W.G. Godden - 1980

UCB/EERC-80/34 "The Design of Steel Energy-Absorbing Restrainers and their Incorporation into Nuclear Power Plants for Enhanced Safety: Vol 5, Summary Report," by P. Spencer 1980

UCB/EERC-80/35 "Experimental Testing of an Energy Absorbing Base Isolation System," by J. Kelly, M.S. Skinner and K.E. Beucke - 1980

UCB/EERC-80/36 "Simulating and Analyzing Artificial Non-Stationary Earthquake Ground Motions," by R.F. Nau, R.M. Oliver and K.S. Pister - 1980

UCB/EERC-80/37 "Stochastic Seismic Analysis of Nuclear Power Plant Structures and Piping Systems Subjected to Multiple Support Excitations," by M.C. Lee and J. Penzien - 1980

UCB/EERC-80/38 "Inelastic Seismic Analysis of Large Panel Buildings," by V. Schricker and G.H. Powell - 1980

UCB/EERC-80/39 "Dynamic Response of Embankment, Concrete-Gravity and Arch Dams Including Hydrodynamic Interaction," by J.F. Hall and A.K. Chopra - 1980